SAPIENZA UNIVERSITÁ DI ROMA

Ph.D. in Information and Communication Technologies

Curriculum: Radar and Remote Sensing

Cycle XXIX

Ph.D. Dissertation

THERMOGRAVIMETRIC TECHNIQUE FOR VOLATILES DETECTION IN PLANETARY AND SPACE ENVIRONMENTS

Candidate

Fabrizio Dirri

Tutor

Prof. Frank Silvio Marzano

Dr. Ernesto Palomba

Academic Year 2015-2016

Fabrizio Dirri

Abstract

Introduction. The PhD work has been performed at Institute of Astrophysics and Space Planetology (IAPS-INAF) in the framework of the two projects VISTA (Volatile In-Situ Thermogravimeter Analyser) and CAM (Contamination Assessment Microbalance), funded by Italian Space Agency and European Space Agency, respectively, both aiming at developing a microbalance sensor for space mission applications, i.e. to study the minor bodies of Solar System (i.e., ESA-M5 Missions Call, MarcoPolo-M5, Akon, JEM and Castalia) by measuring in-situ volatiles material of scientific interest (VISTA project) and to assess the contamination issue (CAM project).

VISTA is a miniaturized thermogravimeter (composed by Piezoelectric Crystal Microbalance and the related Proximity Electronics), based on Thermogravimetric Analysis (TGA), i.e. a widely used technique to monitor the processes involving compounds, i.e. absorption/desorption and evaporation/sublimation. Thanks to the variation in the microbalance oscillation frequency it is possible to estimate the sample mass loss/deposited from thermal cycles. VISTA is composed of two sensor heads, i.e. the Sensor Head 1 (SH1) for in-orbit contamination measurements from outgassing processes and Sensor Head 2 (SH2) for planetary in-situ measurements, respectively. The breadboard and the Engineering Model of VISTA SH1 have been developed for ESA Project, i.e. CAM, an Invitation to Tender of European Space Agency (EMITS-ESA) aiming at developing a thermogravimeter for contamination measurements in space, leaded by IAPS-INAF and developed by a consortium of three Italian institutes and one Industry. The VISTA SH2 breadboard has been developed in the framework of MarcoPolo-R Mission, where VISTA was part of the scientific payload.

Objectives. In this work, the VISTA capability to monitor the contamination processes in space environment and for the study of planetary surfaces and atmospheres has been demonstrated as well as the good capability of sensor heads to monitoring and to characterizing a contaminant source and organic compounds by realizing TGA cycles and Effusion Method (EM) to obtain the vapor pressures and enthalpy of sublimation.

Material and Method. The first phase of the work was based on the study of Volatile Organic Compounds (VOCs): 1) in planetary atmospheres including their physical-chemical properties and their connections with the atmospheric aerosol sources (biogenic and anthropogenic); 2) in space, coming from outgassing processes of materials exposed to space environment, and the related instrumentation issues. Thus, organic compounds (found in Carbonaceous Chondrite meteorites and in Earth's VOCs) have been selected to perform deposition processes and TGA cycles obtaining a complete characterization with SH1 and SH2. The vapor pressures and enthalpy of sublimation were identified as those thermochemical parameters able to characterize a kinetics process regarding VOCs in planetary atmosphere and in space. Thus, a laboratory activity was planned and divided in a first design and development phase of two laboratory setup and in a second calibration phase of VISTA sensor heads. A third phase was devoted at performing different tests for contamination study in space (using a contaminant source and SH1 breadboard) and for VOCs characterization in atmosphere (using five dicarboxylic acids and SH2 breadboard). *Results*. The breadboards of VISTA instrument SH1 and SH2 have been developed to monitor the contamination in space (SH1) and to characterize organic compounds (SH2). The main results reached in the PhD work with VISTA SH1 have been: 1) to monitor contamination processes in vacuum chamber simulating the space environment (between $5x10^{-9}$ to $7x10^{-4}$ g/cm^2); 2) the contaminant source characterization by means of TGA cycles (ΔT_{max}~60°C) and retrieval of vapour pressure of compounds (Pi) and the enthalpy of sublimation (ΔH_{sub}) by using the Langmuir and Clausius-Clapeyron relations; 3) the sensor regeneration by means of thermal cycles by using the integrated heaters on crystal surface (with an accuracy within 0.1°C). On the other hand, the main scientific objectives reached with VISTA SH2 have been: 1) the volatiles material measurement deposited on the sensor surface at different temperatures by using the Effusion Method simulating the asteroidal/cometary environment; 2) the characterization of VOCs, i.e. dicarboxylic acids, by calculating the enthalpy of sublimation (ΔH_{sub}) with Van't Hoff relation. *Conclusion*. In this work, the VISTA SH1 and SH2 Breadboards have been designed and developed as well as two different laboratory set-up to verify the capability of SH1 and SH2 to monitor a contamination process and to characterize a pure organic compound, respectively, using TGA cycles and EM. The enthalpies of sublimation results obtained with SH1 from one contaminant source (adipic acid) using TGA and EM, are in agreement within 3.5% while the enthalpies of sublimation obtained for five dicarboxylic acids and using EM, are in agreement within 6% (oxalic, succinic and adipic acids) and 11% (azelaic and suberic acids) with previous works. These results demonstrate the capability of SH1 and SH2 Breadboards to detect organic contaminant and to characterize different organic compounds presents in VOCs terrestrial atmosphere obtaining a good characterization for a pure compound.

Index

Acronym List

AEROSE	AEROSOL AND OCEANOGRAPHIC SCIENCE EXPEDITION
AO	ATOMIC OXYGEN
AOD	AEROSOL OPTICAL DEPTH
ASAP-MS	ATMOSPHERIC SOLIDS ANALYSIS PROBE MASS SPECTROMETRY
ASTM	AMERICAN SOCIETY FOR TESTING MATERIALS
ATHENA	ADVANCED TELESCOPE for HIGH ENERGY ASTROPHYSISCS
AVHRR	ADVANCED VERY HIGH RESOLUTION RADIOMETER
BAM	BETA ATTENUATION MONITORS
BB	BREADBOARD
CALIOP	CLOUD-AEROSOL LIDAR with ORTHOGONAL POLARIZATION
CALIPSO	CLOUD-AEROSOL LIDAR AND INFRARED PATHFINDER SATELLITE OBSERVATIONS
CC	CARBONACEOUS CHONDRITE
CNR	ITALIAN NATIONAL RESEARCH COUNCIL
CQCM	CRYOGENIC QUARTZ CRYSTAL MICROBALANCE
CT	CONTAMINATION TEST
DC	DOUBLE CRYSTAL
DNA	DEOXYRIBONUCLEIC ACID
DS1	DEEP SPACE ONE
DT	DEPOSITION TEST
EM	EFFUSION METHOD
EMITS	ELECTRONIC MAILING INVITATION TO TENDER SYSTEM
EOIM	EVALUATION OF OXYGEN INTERACTION WITH MATERIALS EXPERIMENT
EPA	ENVIRONMENTAL PROTECTION AGENCY
ESA	EUROPEAN SPACE AGENCY
FOV	FIELD OF VIEW
GHS	GLOBAL HEAT SINK
HST	HUBBLE SPACE TELESCOPE
IAPS	INSTITUTE FOR SPACE ASTROPHYSISCS AND PLANETOLOGY
IECM	INDUCED ENVIRONMENT CONTAMINATION MONITOR
IIA	INSTITUTE OF ATMOSPHERIC POLLUTION
INAF	NATIONAL INSTITUTE FOR ASTROPHYSICS
ISS	INTERNATIONAL SPACE STATION
IUPAC	INTERNATIONAL UNION OF PURE AND APPLIED CHEMISTRY
IVM	INTEGRATED VOLUME METHOD
JAXA	JAPAN AEROSPACE EXPLORATION AGENCY
JEM	JOINT EUROPA MISSION
JUICE	JUPITER AND ICY MOONS EXPLORER
KEM	KNUDSEN EFFUSION MASS SPECTROMETRY
KEMS	KNUDSEN EFFUSION MASS-loss
LEO	LOW EARTH ORBIT
MBCs	MAIN BELT COMETs
MEDET	MATERIALS EXPOSURE AND DEGRADATION EXPERIMENT
MEU	MAIN ELECTRONICS UNIT
MISR	MULTI - angle IMAGING SPECTRORADIOMETER
MODIS	MODERATE RESOLUTION IMAGING SPECTRORADIOMETER
MSX	MIDCOURSE SPACE EXPERIMENT
NASA	NATIONAL AERONAUTICS AND SPACE ADMINISTRATION
NEA	NEAR EARTH ASTEROID
NI-DaQ	NATIONAL INSTRUMENT DATA ACQUISITION
NIR	NEAR INFRARED
OGO-6	ORBITING GEOPHYSICAL OBSERVATORY
OLEB	ORIGIN OF LIFE AND EVOLUTION OF BIOSPHERES
OMI	OZON MONITORING INSTRUMENT
PAH	POLYCYCLIC AROMATIC HYDROCARBONS
PCM	PIEZOELECTRIC CRYSTAL MICROBALANCE
PE	PROXIMITY ELECTRONICS

PIC	PLUME IMPINGEMENT CONTAMINATION
PID	PROPORTIANAL INTERGAL DERIVATIVE
PM	PARTICULATE MATTER
POLDER	POLARIZATION AND DIRECTIONALITY OF THE EARTH'S REFLECTANCES
PRCS	PRIMARY REACTION CONTROL SYSTEM
PT	PRELIMINARY TEST
PT-CIMS	PROTON-TRANSFER CHEMICAL IONIZATION MASS SPECTROMETRY
PVC	POLYVINYL CHLORIDE
QCM	QUARTZ CRYSTALS MICROBALANCE
RCS	REACTION CONTROL SYSTEM
REFLEX	RETURN FLUX EXPERIMENT
RTD	RESISTANCE TEMPERATURE DETECTOR
SAGEII	STRATOSPHERIC AEROSOL and GAS EXPERIMENT II
SARE	SOLAR ARRAY RETURN EXPERIMENT
SC	SINGLE CRYSTAL
SEE	ENVIRONMENTS and EFFECT
SEM	SCANNING ELECTRONIC MICROSCOPE
SDS	SMALL DEMONSTRATION SATELLITE
SH	SENSOR HEAD
SMART	SMALL MISSION FOR ADVANCED RESEARCH AND TECHNOLOGIES
SOA	SECONDARY ORGANIC AEROSOL
SPICA	SPACE INFRARED TELESCOPE for COSMOLOGY AND ASTROPHYSICS
SPIRIT	SPATIAL INFRARED IMAGING TELESCOPE
SST	SINGLE SCATTERING ALBEDO
ST	SATURATION TEST
STS	SPACE TRANSPORTATION SYSTEM
SVOC	SEMI-VOLATILE ORGANIC COMPOUND
TCS	TEMPERATURE CONTROL SYSTEM
TDMA	TANDEM DIFFERENTIAL MOBILITY ANALYZER
TDPD	TEMPERATURE PROGRAMMED THERMAL DESORPTION
TEC	THERMO-ELECTRIC COOLER
TDPBMS	TEMPERATURE PROGRAMMED THERMAL DESORPTION METHOD
TG	THERMOGRAVIMETRY
TGA	THERMOGRAVIMETRIC ANALYSIS
TQCM	THERMAL QUARTZ CRYSTAL MICROBALANCE
TPTD	THERMAL DESORPTION PARTICLE BEAM MASS SPECTROMETRY
TRL	TECHNOLOGY READINESS LEVEL
TSMR	THICKNESS SHEAR MODE RESONATOR
UI	USER INTERFACE
Vis	VISIBLE
VISTA	VOLATILE IN-SITU THERMOGRAVIMETER ANALYSER
VOC	VOLATILE ORGANIC COMPOUND
VTDMA	VOLATILITY TANDEM DIFFERENTIAL MOBILITY ANALYSER
VVOC	VERY VOLATILE ORGANIC COMPOUND
WSOC	WATER-SOLUBLE ORGANIC COMPOUNDS
WHO	WORLD HEALTH ORGANIZATION
XMM	X-ray MULTI MIRROR MISSION

Chapter 1. Introduction

The study of minor bodies of the Solar System such as comets and asteroids is fundamental to understand formation and early evolution of Solar System, including scenario of water delivery on the Earth. This because most of the minor bodies are primitive, i.e. preserve information about the ancient solar nebula and the first processes occurred. In particular, study of comets and asteroids received more attention thanks to the recent missions such as the ESA mission Rosetta [Glassmeier 2007], the NASA missions NEAR-Shoemaker [Williams 2001] and Dawn [Russell and Raymond 2011], the JAXA Hayabusa 1[Kubota 2006]. The Rosetta mission flayed over the Asteroid 2867 Šteins e 21Lutetia and studied in detail the comet 67P/Churyumov-Gerasimenko giving some important results about the nucleus, dust and gas composition. The NASA NEAR-Shoemaker Mission which has studied in depth the surface composition and geomorphology of the Asteroid 433 Eros . The NASA Dawn Mission whose targets were the giant asteroids 4Vesta and 1 Ceres. Finally, the JAXA Hayabusa 1 mission mapped the asteroid Itokawa studying its surface geology and mineral composition and returned to Earth fragments of its regolith.

In addition, Sample Return Missions such as JAXA Hayabusa 2 [Tsuda 2013] and NASA Osiris-REx [Barry 2013] are in progress and are addressed to two primitive asteroids, i.e. 101955 Bennu and 162173 Ryugu, respectively. These missions will help the characterization and classification of these bodies and most importantly will return pristine material to the Earth laboratories.

In the last Call for a Medium-size mission opportunity in ESA's Science Program (M5), many missions to minor bodies are proposed: theMarcoPolo-M5 (Sample Return Mission from a primitive asteroid, i.e. 1993 HA), Akon and JEM (Europa target) and Castalia (Main Belt Comets target) will be helpful for the characterization of Asteroids and Comets.

Volatiles detection and characterization is required during the outgassing processes which occur in space environment aboard satellites, spacecraft and space stations (e.g. ISS, Mir) [Soares 2003, Soares and Mikatarian 1994]. Indeed, it is well-known that observed phenomena as surface erosion (e.g. by Atomic Oxygen, AO), weight loss, oxidation and surface bombardment (e.g. thruster firings) can degredates the performance of telescope, optics and other sensible parts of scientific instruments [de Chambure 1997]. On the other hand, volatiles detection in the minor bodies of Solar System and in planetary atmospheres represent a good opportunity to understand the mineralogical history of the processes concerning the evolution and the transformation processes in atmosphere in order to characterize the organic fraction of atmospheric aerosols. Furthermore, specific substances (*markers*) can be identified in order to provide some information on the atmospheric aerosol sources (biogenic or anthropogenic, i.e. on the Earth) [Bacco 2010, Dirri 2016a]. In this sense, the study and monitoring of the thermodynamical and thermochemical processes and parameters useful to characterize a compound or a mix of them should be taken into account.

This work has been performed in the Volatile In-Situ Thermogravimeter Analyser (VISTA) activity framework which aims at developing an instrument to detect volatiles in planetary and space environments [Palomba 2016]. The project is led by IAPS-INAF and developed by a consortium of three Italian institutes and one Industry. This work has take advantage of the collaboration between the VISTA-team members. Two main project are included in these activity: Contamination Assessment Microbalance (CAM), an Electronic Mailing Invitation to Tender System of European Space Agency (EMITS-ESA) Project aiming a development of thermogravimeter for contamination measurements in space and VISTA-MarcoPoloR [Palomba 2012] which aims at develop a thermogravimeter for a planetary in-situ mission on primitive asteroid.

VISTA is a miniaturized thermogravimeter system based on Thermogravimetric Analysis (TGA), a widely used technique to investigate deposition/sublimation and absorption/desorption processes of volatile compounds in different environments: outgassing contamination in space, dehydration and organic decomposition in minerals [Grady and Wright 2003, Fermo 2006]. It measures the change in mass of a sample as a function of temperature and time. The VISTA main innovation introduced is the PCM special design equipped with two built-in resistors, placed on the opposite faces on the crystal, acting as heater and temperature sensor, respectively.VISTA is composed of two sensor heads, i.e. the Sensor Head 1 (SH1) for in-orbit contamination measurements from outgassing processes and Sensor Head 2 (SH2) for planetary in-situ measurements, respectively [Palomba 2016]. Each sensor head includes a sensing piezoelectric crystal and related Proximity Electronics (PE).

A Engineering Model and laboratory breadboard of SH1 were developed in a EMITS-ESA Project, i.e. CAM, which aim to design and develop a instrument for space contamination monitoring for the future ESA payloads. For SH2, a laboratory breadboard has been developed, too.

VISTA can accomplish the following scientific goals:

a. measurement of the abundance of volatiles and organics in the asteroid regolith and measuring the water content in the hydrate minerals;
b. measurement the cometary activity or the possible cometary-like activity;
c. monitoring sampling operations by measuring the flux of dust raised;
d. monitoring a contaminant source, simulating an outgassing process in space environment;
e. characterizing a contaminant source by realizing TGA cycles to obtain the vapor pressures and enthalpy of sublimation;
f. evaluating the degradation of the instrumentation performance by means of the measured mass deposited on the crystal surface.

A first phase of the work was based on Volatile Organic Compounds (VOCs) study in planetary atmospheres including their physical-chemical properties and their connections with the atmospheric aerosol sources.

Simultaneously, a study of VOCs detection in space come from outgassing processes of materials exposed to space environment and the related instrumentation issues was studied in depth.
Successively, a complete study of TGA and thermochemical processes as well as a complete review for Quartz Crystal Microbalance (QCM) sensors used for contamination in space were performed. Thus, vapor pressures and enthalpy of sublimation were identified as those thermochemical parameters able to characterize a kinetics process regarding VOCs in planetary atmosphere and in space. A laboratory activity was divided in a first design and development phase of two laboratory setup and in a second calibration phase of VISTA sensor heads. A third phase was devoted to performing different tests for contamination study in space (using a contaminant source and SH1 breadboard) and for VOCs characterization in atmosphere (using five dicarboxylic acids and SH2 breadboard). The dicarboxylic acids have been chosen due to their high sublimation rates starting from 25-30°C which make them a good contaminant source and due to their presence in the organic materials of CC (come from primitive asteroids) and in Secondary Organic Aerosol (SOA) of terrestrial atmosphere.

The work of the thesis is divided in seven chapters. The first chapter aims to introduce the work performed while the second chapter gives a description about VOCs and their detection in terrestrial atmospheric SOA (as organic fraction) and in space (as contaminant), especially focusing the attention on dicarboxylic acid compounds and their chemical-physical properties.

In the third chapter, the thermochemical relations, the physical-chemical quantity for organic compounds characterization are introduced. The basic concept of Thermogravimetry, the working principle of microbalance system for laboratory-use and VISTA sensor heads (SH1 and SH2) are explained in detail.

The fourth chapter gives a description of the two experimental setups designed, developed and tested for contamination tests performed with the SH1 breadboard and for atmospheric organic compounds characterization with the SH2 breadboard. Thermal tests, User Interface (UI) to manage the SH1 and SH2, vacuum system and experimental procedures are described.

The fifth chapter describes the contamination and saturation tests performed with SH1 breadboard, the data analysis and the experimental procedure performed using a contamination source with a sufficient sublimation rates from 25-30°C, i.e. the adipic acid. Different TGA cycles are performed (with the built-in heaters) to regenerate the crystals and obtaining a characterization of the source by means of the enthalpy of sublimation using the Langmuir equation. The results has been discussed and compared with previous works.

In the sixth chapter, in preparation for organic compounds characterization with SH2, the TGA data set obtained with SH1 have been used to obtain the vapor pressures and the enthalpy of sublimation using Clausius-Clapeyron equation. Thus, the SH2 experimental activity, i.e. deposition tests obtained with the

Effusion Method (EM) are introduced. Calibration test, experimental procedure and data analysis are described as well as the results of deposition rates and enthalpy of sublimation obtained (with Van't Hoff equation) for five compounds, i.e. oxalic acid, succinic acid, adipic acid, suberic acid and azelaic acid. The results have been discussed and compared with previous works. In particular, the enthalpy of sublimation obtained with Langmuir and Clausius-Clapeyron equation and SH1 breadboard (TGA method) have been compared with enthalpy average value obtained with Van't Hoff equation and SH2 breadboard (EM).

In the seventh chapter, the laboratory work and the results (deposition rates and enthalpy of sublimation) obtained with different methods (TGA and EM) and breadboards (SH1 and SH2) are summarized. A complete list of future applications, i.e. for Space Missions (ESA-M5) and Transfer Technological Application (terrestrial atmosphere, farming business, pharmaceutical area etc.) relating to VISTA sensor heads following the results of this thesis are described.

Chapter 2. VOCs in terrestrial atmosphere and space

2.1 Introduction

Volatile Organic Compounds (VOCs) in terrestrial atmosphere and in space detection including their physical-chemical processes are introduce in this chapter.

The different types of atmospheric aerosols and VOCs are described as well as the importance of their detection in atmosphere because of their influence on the climate. In particular, markers for the Secondary Organic Aerosol (SOA) characterization, i.e. dicarboxylic acid are identified and their chemical-physical properties are introduced.

VOCs detection in space originate from material outgassing processes exposed to vacuum environment and high temperature variations are also introduced. The instrumentation issues related to the contamination processes and a review of contamination measurement performed on ISS and Mir Station and aboard satellites and spacecraft are illustrated.

The detection of volatile materials in the planetary bodies, i.e. from comets and asteroids and their connection with analogue materials are discussed (in particular, focusing the attention on dicarboxylic acid compounds related to these analogue materials).

2.2. Terrestrial atmospheric aerosols

Aerosol system is a liquid and/or solid particles (diameter from 10^{-9} to 10^{-4} m) in a carrier gas. It is generally defined as a solid suspension of liquid or solid particles in a gas able to scatter and absorb sunlight if sufficient large [Rozaini 2012]. Aerosols interact both directly and indirectly with the Earth's radiation budget (the aerosols scatter sunlight directly back into space) having a direct effect on climate. Because of the large number of aerosol species in atmosphere and physical-chemical processes which occur to create/destroy compounds, a complete characterization and monitoring of them is a tricky task. Thus, it is necessary to identify a specific substances or a class of substances (i.e. "*markers*") able to provide information about the sources (biogenic or anthropogenic) which generates the Particulate Matter (PM) (microscopic solid or liquid particles suspended in atmosphere) in the aerosol and their permanence in atmosphere [Bacco 2010]. Because of aerosols change their characteristics very slowly, they can be used as tracers for atmospheric motions and generally to understand how the Earth's atmosphere moves [NASA 1996]. For example, atmospheric aerosols have been used to study the dynamics of the polar regions and the exchange of air between the troposphere and stratosphere. Three types of aerosols are mainly present at Earth's atmosphere and affect the climate:

1. *Background aerosol (aged accumulation mode aerosol, i.e. volcanic aerosol)*, which forms a layer in the stratosphere after volcanic eruptions (sulfur dioxide gas).

2. *Maritime aerosol*, a main component of which is sea salt.

3a. *Continental aerosol, i.e. desert dust*, minute grains of dirt blown from the desert surface (clay minerals dust).

3b. *Continental aerosol, human-made aerosol*, coming from process as rock erosion, smoke from burning tropical forests (*rural aerosol*) and from human vehicles, industries etc. (*urban aerosols*, these particles can affect the heart and lungs and cause serious health effects. Generally, urban and rural aerosols are also identified as "*primary atmospheric aerosol*".

PM distinction can be done due to the presence of complex mixture of organic and inorganic substances suspended in the air existing in different size range. The PM sources can be human-made or natural and having impacts on climate and on human health. The US. Environmental Protection Agency (EPA) refers to different groups of particulates which includes (Fig. 2.1):

- Suspended Particulate Matter (SPM)
- Thoracic and respirable particles
- Inhalable coarse particle, with a diameter between 2.5 and 10 µm
- Fine particles with a diameter of 2.5 µm or less
- PM_{10} and $PM_{2.5}$
- Ultrafine particles

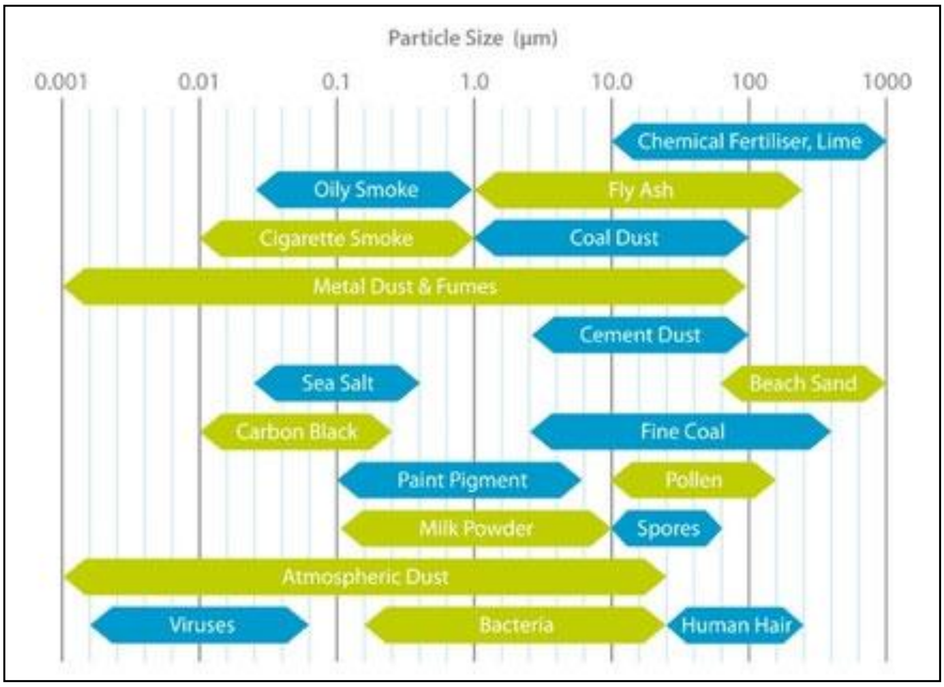

Figure 2.1 (Air filter information, GlobalSpec Engineering). PMs sizes and their classification.

A significant contribution to atmospheric aerosol particles is the product formation of low volatility and chemically processed Volatile Organic Compound (VOCs). By means of photochemical and oxidation processes, VOCs are transformed to less volatile contributing to Secondary Organic Aerosol (SOA) [Salo 2010]. The physical pathways and identification of the low-volatility products originating from oxidation of VOCs are not fully understood even though it is know that typical class of products from atmospheric oxidation processes yielding SOA are the carboxylic acids class which includes a subclass: dicarboxylic acids.

The atmospheric aerosol study has a scientific relevance due to connection between the public health and to the particulate exposition, in particular the ultra-thin organic component of $PM_{2.5}$ and PM_{10} [Ladji 2007]. The origin of atmospheric pollutants source becoming more important on the basis of current EU Directive of 2008 on ambient air quality and cleaner air for Europe explicitly states that: "*emissions of harmful air pollutants should be avoided, prevented or reduced and appropriate objectives set for ambient air quality taking into account relevant World Health Organization standards, guidelines and programmes*" [EU 2008]. Table 2.1 shows the maximum annual concentration of $PM_{2.5}$ and PM_{10} allowed by EU Directive and by WHO (World Health Organization) air quality guidelines [EEA 2014] according to 1999 and 2008 normative, respectively.

Table 2.1 [EEA 2014]. Particulate matter concentration limits regulated by European Union directives.

European Directive	Annual average concentration allowed of PM10 ($\mu g/m^3$) EU-Dir	Annual average concentration allowed of PM10 ($\mu g/m^3$) WHO-Dir	Annual average concentration allowed of PM2.5 ($\mu g/m^3$) EU-Dir	Annual average concentration allowed of PM10 ($\mu g/m^3$) WHO-Dir
1999	40	10	25	20
2008	20	--	10	--

The influence of the aerosol on climate is difficult to measure, especially with respect to aerosol microphysical properties and the evaluation of anthropogenic aerosol effect. Currently, there are many satellite missions studying aerosol distribution in the terrestrial atmosphere, such as MISR/Terra, OMI/Aura, AVHRR, MODIS/Terra and Aqua, CALIOP/CALIPSO managed by Space Agencies [NASA 1996] while several new missions are planned, e.g. Ukrainian project Aerosol-UA designed for remote sensing of the aerosol microphysics and cloud properties on a global scale [Milinevsky 2015].

2.2.1. VOC and SOA

The EPA definition of VOC means any compound of carbon, excluding carbon monoxide, carbon dioxide, carbonic acid, metallic carbides or carbonates and ammonium carbonate, which participates in atmospheric photochemical reactions, except those designated by EPA as having negligible photochemical reactivity [EPA 2016].

VOCs are those organic compounds whose composition makes it possible for them to evaporate under normal indoor atmospheric conditions of temperature and pressure. The volatility of organic compounds are defined and classified by their boiling points because the volatility generally increase when boiling point temperature is lower (VOC have a boiling point less than 250°C at 101.3 kPa) [EPA 2016]. VOCs are sometimes categorized by the ease they will be emitted. For example, WHO categorizes the indoor organic pollutants [WHO 1987] as:

- Very volatile organic compounds (VVOCs)
- Volatile organic compounds (VOCs)
- Semi-volatile organic compounds (SVOCs)

For higher volatility (i.e., lower the boiling point in air, or sublimation point in vacuum), more emission will be produced into the air. SVOCs constitute an important class that includes phthalate esters, brominated flame-retardants, polychlorinated biphenyls, nonionic surfactants and pesticides. Many SVOCs are produced from chemicals used in plastics, detergents, furniture, building material components [Xu 2011]. Instead, VVOCs compounds are difficult to measure and are found almost entirely as gases in the air rather than in materials or on surfaces. VVOC, VOC and SVOC compounds with boiling point are described in table 2.2.

Table 2.2 [adapted from WHO 1987]. Classification of Inorganic Organic Pollutants.

Description	Abbreviation	Boiling Point Range (°C)	Example Compounds
VVOCs (gaseous)	VVOC	<0 to 50-100	Propane, butane, methyl chloride
VOCs	VOC	50-100 to 240-260	Formaldehyde, d-Limonene, toluene, acetone, ethanol (ethyl alcohol) 2-propanol (isopropyl alcohol), hexane
SVOCs	SVOC	240-260 to 380-400	Pesticides (DDT, chlordane, plasticizers (phthalates), fire retardants (PCBs, PBB)

VOCs oxidation leads to the formation of intermediate organics species [Aumont 2005] typically more functionalized than their precursor compounds. These secondary species typically have lower saturation vapor pressures allowing a gas particle partitioning, leading a SOA formation.

SOA is mainly composed of fine particles, i.e. lower than 1-2µm, [Salzen and Schlűnzen 1999] from photo-oxidation reactions with compounds in Earth's atmosphere, in particular hydroxyl radical, ozone and nitrate radical. For example, hydrocarbons are enriched carboxyl (-COOH), carbonyl (-CO) or hydroxyl (-OH) functional groups are transformed in ketones or carboxylic acid after several reactions. SOA formation involves a multitude of Semi-Volatile Organic Compounds (SVOC) having complex molecular structures. SVOC formation is suspected to be more complex with the possibility of multiple oxidation steps [Kroll and Seinfeld 2005].

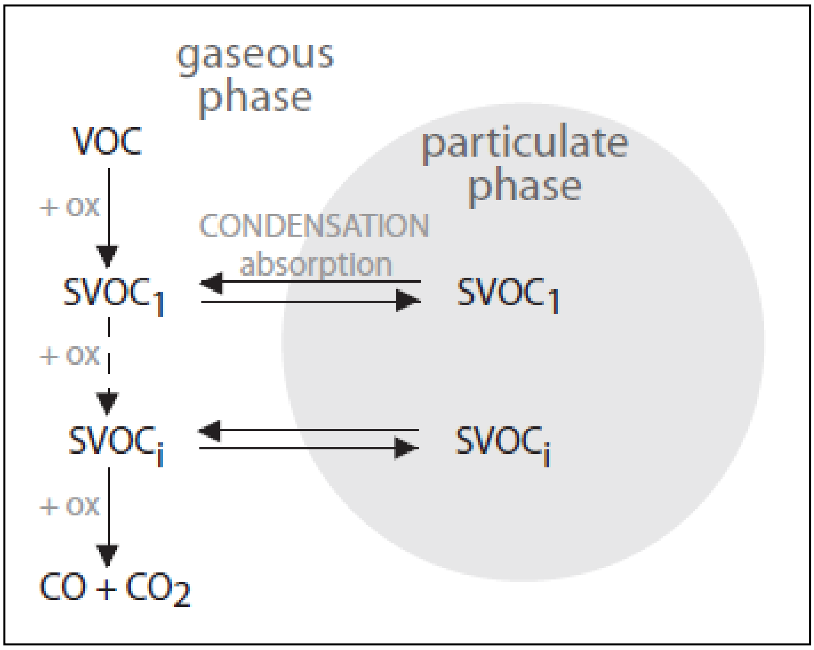

Figure 2.2 [Camredon et al. 2007]. Schematic diagram of SOA formation. The number "*1*" was referred to 1-octene oxidation studied.

SVOC production might require many successive oxidation steps which provide minor individual contribution to the organic budget. In particular, the model assumed for SOA formation includes the production of "*i*" species by means of single oxidation step from parent hydrocarbons and a specific thermodynamic module for condensation (Fig. 2.2). The oxidation scheme up to CO_2 production has been developed using the self-generation approach of Aumont (2005) and assuming a basic thermodynamic absorption process [Pankow 1994] for gas/particles partitioning of low volatility species.

2.2.2. Organic fraction of VOC and SOA

Generally, a lot of aerosols transformation processes occur in the terrestrial atmosphere. Aerosols are largely composed by inorganic species but a significant fraction of the total particulate matter is composed of organics. These substances are typically mixed to inorganic compounds and has been determined that organics usually constitute 20-50% of fine aerosol mass over the continental U.S. [Brown 2013]. Organics may also constitute a significant fraction of atmospheric aerosol even at high altitudes, which may be important for ice formation in clouds [Salo 2010] showing an important role on atmospheric aerosol formation and growth (due to its hygroscopic characteristic, toxicity and radiation absorption). Rogge (1993) identified more than 80 organic compounds in atmospheric particles, including Dicarboxylic acids (identified in cloud water samples). The occurrence of Polycyclic Aromatic Hydrocarbons (PAH), could be cause of concern, due to their carcinogenic effects. Generally, organic compounds are related to species contains between 5 and 10 carbon atoms (C_5-C_{10}), since the species with higher carbon atoms have low concentrations, low molecular weight and high vapor pressure [Barthelmie 1997]. The organic fraction of SOA can be formed by biogenic (80% of VOC) and anthropogenic precursor: species as O_3 and H-O (hydroxyl radical) can transform group contains hydrocarbon in carboxylic group (-COOH) and carbonyl group (-CO) or hydroxyl (OH) compounds enriched. These reaction lead to formation of ketones, carboxylic acids etc. Furthermore, in different samples of urban, rural and sea aerosol have been identify alkanes longer chain, ketones, different salts, dicarboxylic acid and PAH.

2.2.3. Marker substances in SOA

Because of the wide number of VOCs transformation processes it is crucial to know the chemical-physical properties (i.e. enthalpy, entropy, free energy) in order to characterize the organic fraction of the atmospheric aerosol [Dirri 2016a]. In detail, specific substances (*markers*) or class of substances should be identified in order to provide some information on the atmospheric aerosol sources, e.g. evaluating the transformation degree of the organic compound and their release by primary sources [Pietrogrande 2014]. Carbohydrates and dicarboxylic acids with low molecular weight (these latter subclass of carboxylic acids) are among the most important groups of molecules identified in the atmospheric aerosol: they have been collected in several sample campaigns, i.e. in the mountain range in central Europe, north Pacifica [Kawamura 1993], in urban areas [Kawamura 2005, Yu and Fraser 2004] and Artic regions [Kawamura 2012] (oxalic acid was the most prevalent, followed by malonic and succinic acids). Low molecular weight dicarboxylic acids are produced in automobile exhaust, as emissions from meat cooking, and as emissions from pyrolysis of plants and other organic material.

Photochemical reactions are also an important source of atmospheric dicarboxylic acids and probably is the dominant pathway of their formation as measured in Los Angeles urban area [Kawamura 1993]. Dicarboxylic acids show relatively low vapor pressures and are sufficiently soluble to be present in the water soluble fraction of atmospheric particles. Thus, it could be useful to consider these substances as molecular tracers ("markers") providing information on the aerosol origin (biogenic or anthropogenic), i.e. on the emission source and on the processes that the organic substances undergo in the atmosphere [Dirri 2016a].

2.2.4. Continental and background aerosols monitoring

Although the aerosol measurement and monitoring is improved during the last decades, many questions are already open about the competing impacts of aerosols. For example, measuring the particles within clouds remains challenging because of different types of particles can clump together to form hybrids that are difficult to distinguish. During the last years, the scientist have used an array of satellite, aircraft, and ground-based instruments to monitor aerosols, e.g. the radiometer instruments which are able to quantify the amount of electromagnetic radiation. Some properties such as Aerosol Optical Depth (AOD), i.e. a measure of the amount of light that aerosols scatter and absorb in the atmosphere or Single Scattering Albedo (SSA), i.e. the fraction of light that is scattered compared to the total are the main quantities measured [NASA Earth Observatory 2016]. Satellites to monitor the AOD and in the Visible (Vis) and Near-Infrared (NIR) spectrum, i.e. the Advanced Very High Resolution Radiometer (AVHRR) and to view and study aerosols at more angles and wavelengths, i.e. the Multi-angle Imaging Spectroadiometer (MISR) and the Moderate Resolution Imaging Spectroradiomer (MODIS) have been used [Mishchenko 2007, Remer 2008]. Other instruments such as the Cloud Aerosol Lidar and Infrared Pathfinder Satellite Observer (CALIPSO) and the Polarization and Directionality of the Earth’s Reflectances (POLDER) are able to measure in detail the vertical profiles of aerosol (in the plumes and clouds) and the orientation (or polarization) of light waves and their movement through the atmosphere, respectively [NASA Earth Observatory 2016].

In particular, the studying on *continental aerosol* due to desert dust (e.g. Saharan dust) it's important to understand the microphysical evolution of thin particles from the source regions with reactive gas phase species during the long distance transport [Effiong 2011]. These properties could change the chemistry of the troposphere influencing the radiative transfer and optical properties [Otto 2007].

The PCM sensors, in particular the Quartz Crystal Microbalance (QCM) can be used for atmospheric monitoring, e.g. AEROSE mission. The objective of Aerosol and Oceanographic Science Expedition (AEROSE) was to provide measurements about the dust Sahara storm and on the influence of dust particles on atmospheric and oceanographic properties during trans-Atlantic transport. QCMs were used as deposition surface for different types of particles ($PM_{2.5}$ and PM_{10}), in order to realize in situ real time measurement sample in various portion of the dust plume that occurred over the tropical Atlantic Ocean [Effiong 2011].

Two QCM’s have been placed inside the Howard University Van located at 8 m above mean sea level on an Oceanographic ship. By means of Scanning Electron Microscope (SEM) analysis has been shown that they are able to obtain a smaller samples with an high resolution in its measurements that view the size fraction of 0.15, 0.3, 0.6, 1.2 and 5.0 μm. In figure 2.3 (at *Right*) it is possible to observe the size particles distribution before the dust storm (QCM data1) and the evolution (at *Left*) of the particles during the storm exposure (QCM data2, March 5-7, 2004).

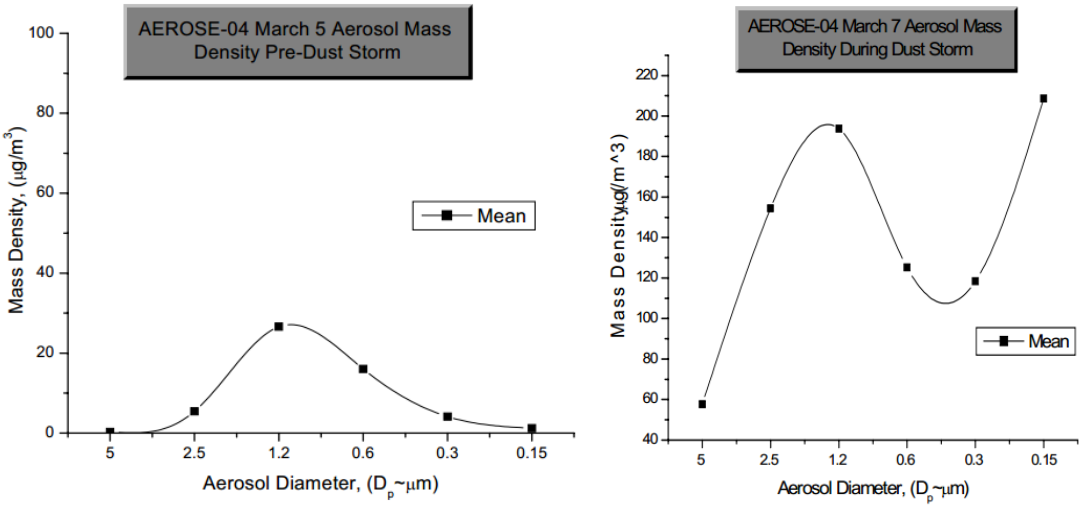

Figure 2.3 [Morris and Roldan 2005]. *Left*: atmospheric PM before the dust storm. The particulate was between 2.5 and 0.3 µm with the peak at 1.2 µm. *Right*: evolution of the PM detected by QCM2; the PM detected are $PM_{2.5}$ and $PM_{1.2}$ with a peak near 0.3 µm.

Beforehand dust storm, the aerosol dust density (March 5th) had a peak in the 1.2 micron size range while during the storm (March 7th) a double distribution was observed in the 1.2 and 0.5 micron size range.

By means of a QCMs the flux of PM_{10} and $PM_{2.5}$ were measured (in µg/m^3) during the AEROSE campaigns. SEM analysis confirmed the results and the capability of the QCM to reveal the different particulate. Then, the AEROSE team encountered several dust event and completed the different measurements, giving a unique and valuable open ocean data set, obtaining a data on the aerosol properties during and after the event [Morris and Roldan 2005].

On the other hand, the *background aerosol (i.e. volcanic aerosol)* deposited into stratosphere during several decades is also largely studied due to change the chemistry and reducing the amount of energy reaching the lower atmosphere and the Earth's surface, cooling them. Data from satellites such as the NASA Langley Stratospheric Aerosol and Gas Experiment II (SAGE II) have enabled scientists to better understand the effects of volcanic aerosols on our atmosphere [NASA 1996].

The study of volcanic solid particles present in atmosphere and the composition of volatile outgassed species before and after a strong volcanic eruptions could be useful to provide information about the time evolution of the volcanic activity [Casadevall 1984].

Currently, the substances monitoring emitted in volcanic areas is based on accumulation chambers which collect the gaseous mixture coming from underground, while systems aimed at detecting volcanic particulate are not available. The major producers of these systems are LI-COR BIOSCIENCES (USA), WEST SYSTEM (Italy), PASI (Italy), ADC BioScientific (UK) (with costs range: from 4000 up to 10000€). In this framework, a PCM device can be used with a coated material (i.e. metals) in order to reveal the volcanic gases which can be corrode the metal (e.g. gold). In addition, PCM would allow the continuous measurement of PM, too while the small dimensions makes it easy to install in different places of the volcanic area.

Generally, the aim of the scientists for the next future is to reduce the quantitative uncertainties on the amount of aerosol (especially on the aerosol properties). Indeed, thermochemical properties will help to know the aerosols behavior in the terrestrial atmosphere providing a critical information to understand the aerosol impacts into climate models (thanks to sophisticated computer modeling) and to reduce the uncertainties about how the climate is influenced by aerosols.

2.3. VOC detection in space

Spacecraft contamination from volatile desorption is one the main problem that engineers have to take into account when developing a new satellites. Indeed, the solar radiation and instantaneously thermal variation induced a difference behavior of materials which results as outgassing processes. By several decades, one of the aim of National Aeronautics and Space Administration (NASA) and European Space Agency (ESA) was to monitor the outgassing properties of aerospace materials based on ground and testing the outgassing effects on spacecraft in flight [Green 2001].

During the next decades, the contamination around Satellite and Space Shuttle missions have been monitored. In fact, when spacecrafts proceeds from Earth environments to space environment, the major part of the satellite components can degas and major flux of contaminant can deposited on the spacecraft surfaces or on the sensitive component of instruments (e.g. optics). In addition, the cabin leakage, thruster firings and the solar effects complicate the contamination detecting and data analysis on ground.

Generally, for contamination detection, QCM's have been used on spacecrafts and satellites (for on-orbit measurements of contaminations level), in various Shuttle mission (STS) and in new technologies interest missions, e.g. Midcourse Space Experiment (MSX). The first task to avoid contamination was to accumulate data from facilities using QCMs to measure the outgassing rates for satellite materials. Specially, the American Society for Testing Materials (ASTM) E-1559 standard method (established procedure in 1993) [Garrett 1995] has been used to evaluate the satellite materials outgassing. This test method allows the total mass loss to be determined through the use of 2 to 4 quartz crystal microbalances cooled to various temperatures [Green 2001]. In particular, two procedures (A and B) can be used for determining the outgassing kinetics. Method A can use a standard effusion cell temperatures and three QCMs cooled at 90, 160, and 298K while the source temperature was 125°C [Garrett 1995]. The geometries provide a standard view factors form the QCMs to the effusion cell orifice (Fig. 2.4). The B procedure, shows a considerable flexibility considering the experimental parameters, in particular the set-point temperatures and test geometry. Basically, the user can perform a custom test using specific parameters or modified apparatus [Green 2001].

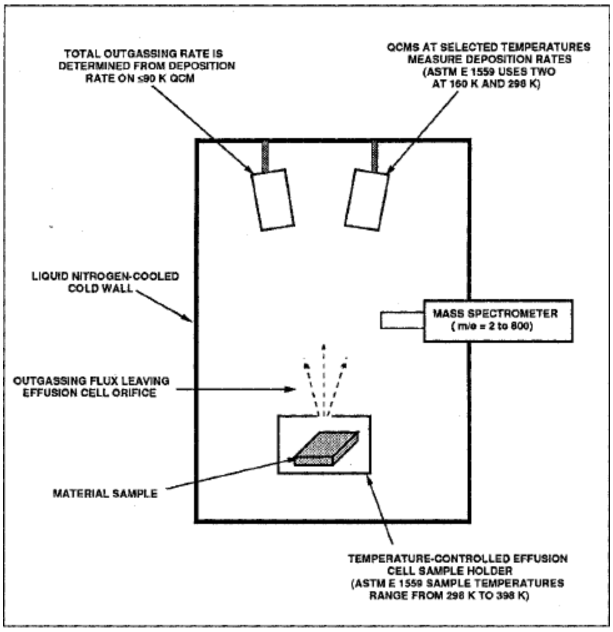

Figure 2.4 [Garrett 1995]. Schematic view of QCM collection measurement with ASTM E-1559 method. The QCMs are optically polished with resonant frequency of 10 to 15 MHz and are angled of 10° from their axis. The intersection point (the effusion cell orifice exit plane) is at 150 mm from the crystal surface. The liquid nitrogen reservoirs is able to cool the QCMs down to 90K.

A database of outgassing kinetics parameters have been created and managed by NASA's Space Environments and Effect (SEE) Program Office located a t the Marshall Space Flight Center in Huntsville, Alabama [Green 2001].

2.3.1. Outgassing process and instrument issues

Generally, the gassing and outgassing are recognized as gas controlled processes in high and ultra-high vacuum system. The mechanisms contributing to outgassing processes are [De Segovia 1999] (Fig. 2.5):

1. Thermal desorption
2. Gas permeation through the wall
3. Gas diffusion from the bulk and subsequent desorption
4. Gas permeation (adsorption) through the wall
5. Vaporization of materials

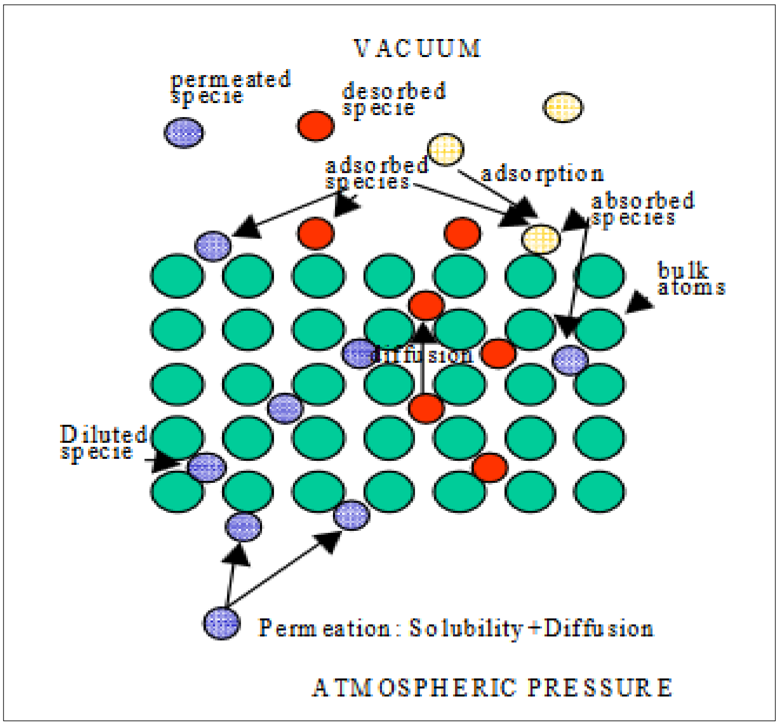

Figure 2.5 [De Segovia 1999]. Surface and bulk phenomena in vacuum.

In order to reduce these mechanisms the following procedure should be adopted:

1. Thermal desorption: reduce the surface concentration.
2. Gas permeation through the wall: adopt a barrier layer on surface.
3. Gas diffusion from the bulk and subsequent desorption: reduce dissolved hydrogen, induce trapping states (bulk or surface) reduce or increase grain boundary density.
4. Gas permeation (adsorption) through the wall: reduce the binding sites.
5. Vaporization of materials: reduce the surface mobility by introducing surface trapping sites.

In table 2.3 and 2.4 are reported the outgassing rates of different materials used in space instrumentations. These materials have been tested in vacuum using a long heating cycle in order to evaluate the molecular outgassing. In particular, the best materials are the stainless steel and teflon: the latter, does not present an outgassing rate after a heating cycle at 100°C for 16 hours (Tab. 2.3).

Table 2.3 [Peacock 1980]. Outgassing rates of unbaked and baked polymers in torr l s^{-1}.

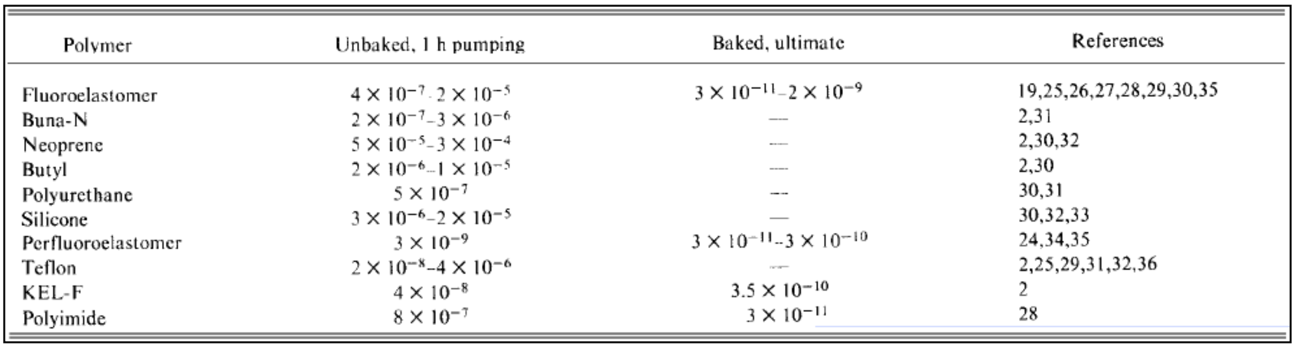

Polymer	Unbaked, 1 h pumping	Baked, ultimate	References
Fluoroelastomer	4×10^{-7}–2×10^{-5}	3×10^{-11}–2×10^{-9}	19,25,26,27,28,29,30,35
Buna-N	2×10^{-7}–3×10^{-6}	—	2,31
Neoprene	5×10^{-5}–3×10^{-4}	—	2,30,32
Butyl	2×10^{-6}–1×10^{-5}	—	2,30
Polyurethane	5×10^{-7}	—	30,31
Silicone	3×10^{-6}–2×10^{-5}	—	30,32,33
Perfluoroelastomer	3×10^{-9}	3×10^{-11}–3×10^{-10}	24,34,35
Teflon	2×10^{-8}–4×10^{-6}	—	2,25,29,31,32,36
KEL-F	4×10^{-8}	3.5×10^{-10}	2
Polyimide	8×10^{-7}	3×10^{-11}	28

Table 2.4 [Patrick 1973]. Outgassing rates of some materials used in space instrumentations.

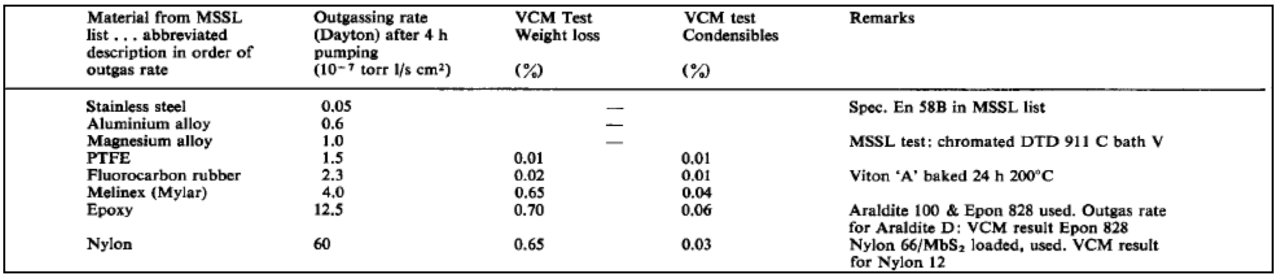

Material from MSSL list . . . abbreviated description in order of outgas rate	Outgassing rate (Dayton) after 4 h pumping (10^{-7} torr l/s cm^2)	VCM Test Weight loss (%)	VCM test Condensibles (%)	Remarks
Stainless steel	0.05	—		Spec. En 58B in MSSL list
Aluminium alloy	0.6	—		
Magnesium alloy	1.0	—		MSSL test: chromated DTD 911 C bath V
PTFE	1.5	0.01	0.01	
Fluorocarbon rubber	2.3	0.02	0.01	Viton 'A' baked 24 h 200°C
Melinex (Mylar)	4.0	0.65	0.04	
Epoxy	12.5	0.70	0.06	Araldite 100 & Epon 828 used. Outgas rate for Araldite D: VCM result Epon 828
Nylon	60	0.65	0.03	Nylon 66/MbS_2 loaded, used. VCM result for Nylon 12

Because of not all the materials show low outgassing rates, a self-contamination aboard spacecraft and deposition of molecular films onto surfaces induced from PVC cables, plastic, silicon and other polymers occur and potentially limiting the performance of instruments. In particular, the most sensitive surfaces to contamination as solar voltaic power sources and optical solar reflectors for thermal control or solar dynamic power generation are subjected to a degradation during several years (i.e., ISS) [Arnold and Hall 1988]. Moreover, the contamination can be further enhanced by solar radiation which can photo-polymerize materials deposited on a surface). Other source of erosions and contaminations are the Atomic Oxygen (AO), which can cause erosion of some surfaces and oxidation of sensitive materials increasing the particles release [Inguimbert 2008], cabin leakage and thruster firings [Soares 2003].

The contamination requirements are stringent due to the problems described before. For example, for International Space Station (ISS) the proposed NASA was a requirement for 30 years performance, because the contamination could potentially change the requirements considered. Instead, for telescope optics, i.e. Athena missions, SPICA and XMM, different contamination limit are required due to sensitive part of the instruments (Tab. 2.5). The range of deposited mass measurable spans from ng/cm^2 to hundreds of μg/cm^2. This large range fully includes the molecular cleanliness requirements of many scientific payloads, such as the XMM optics (200 ng/cm^2) [de Chambure 1997], the SPICA telescope (200 ng/cm^2), the Herschel telescope (4μg/cm^2) or the ATHENA X-ray spectrometer (4 μg/cm^2).

Table 2.5. The Space Station and spacecraft contamination limits.

Spacecraft/Satellites	**Instrument**	**Contamination limit (ng/cm^2)**
ISS	Solar panel, reflectors	0.9 per day
Mir	Hardware component	0.9 per day
XMM	Optics	200
SPICA	Telescope	200
ATHENA	X-ray Spectrometer	4000
Herschel	Telescope	4000

2.3.2. Contamination measurement on ISS, Mir, STS and Satellites

Because of the large instruments components aboard of Space Stations (Mir and ISS) and satellites and possible degradation, contamination measurement have been performed by means of QCM's, near the flimsy instruments at various locations. The QCM's have flown as far back aboard the Shuttle Columbia (November 1981) and more recently in STS-82 flight onboard the Shuttle Discovery (February 1997) to measure the contamination near the Hubble Space Telescope (HST). QCM’s flown on the following NASA Shuttle programs (STS):

2 **IECM** (Induced Environment Contamination Monitor) - [Miller 1982]
9 **IECM** (Induced Environment Contamination Monitor) - [Miller 1984, McKeown 1999]
46 **EOIM 3** (Evaluation of Oxygen Interaction with Materials Experiment) - [Green 2001, Stuckey 1993]
72 **REFLEX** (REturn *FLux* EXperiment) - [Benner 1998, Green 2001]
74 **PIC** (Plume Impingement Contamination) - [Soares 2003]
82 **HST** (Hubble Space Telescope) - [Hansen 1994, Green 2001]

QCM’s data experiments are summarized in table 2.6. Considering the Induced Environment Contamination Monitor (IECM), the QCM's used were developed by NASA and flown on flights STS 2,3,4,9 and in Plume Impingement Contamination-I (PIC-I, on STS 74), whereas Plume Impingement Contamination-II (PIC-II, SMART-2 mission) is already under study and development.

Table 2.6. Comparison between QCM's used in several Shuttle flights. For each mission two configurations are possible: DC=double crystal or SC=single crystal (SC has not been used in the listed experiments). The QCM supplier and the experimental characteristics (i.e. warm-up rate, regeneration temperature and the coating) are also given. Empty cell means not available data (e.g. HST).

Experiment on STS	**EIOM-3 (STS-46)**	**IECM (STS-2)**	**IECM (STS-9)**	**REFLEX (STS-72)**	**HST (STS-82)**	**PIC (STS-74)**
Configuration	DC	DC	DC	DC	--	DC
QCM frequency (MHz)	10	15	15	15	15	10
QCM Producer	QCM Research	Faraday Lab. Inc.	Faraday Lab. Inc.	Faraday Lab. Inc.	--	QCM Research (MK 16)
Mass sensitivity (g/Hz×cm^2)	4.42×10^{-9}	1.56×10^{-9}	1.56×10^{-9}	1.56×10^{-9}	--	4.42×10^{-9}
Operative temperature (°C)	minimal temperature of each orbit - no specified	-50/+30 (CQCM) +30/0/-30/-60 (TQCM)	-10/-40 (CQCM) and -60 to 80 (TQCM)	+16/+18	+20 CQCM 0 TQCM	+25
Resolution f (Hz)	--	±1	±1	±1	--	±2
Max mass loading (g/cm^2)	--	3×10^{-4}	3×10^{-4}	--	--	measured
T resolution (°C)	--	±1	±1	±1	--	--
Warm-up rate	NO	0,008 °C/s (cooling and warm up)	0,33 °C/s (cooling) 0,77°C/s (warm up)	NO	--	0.02°C/min
Coating	ZnS - In_2O_3	NO	NO	Graphite-Kapton	NO	NO
ΔF (Hz) and ΔT(°C) for solar pulse	400-700 Hz --	Observed but no received	Observed but no received	500-800 Hz 2°C	-- --	Correction data for the temperature contribution
Regeneration T(°C)	--	80	80	--	--	>50

Typical contamination events (Fig. 2.6, *Left*) has been measured during PIC experiment where several thrusting firings have been monitored using QCMs. Damage are caused by refractory materials (particles size <20μm) (Fig. 2.6, *Right*) produced from thrusters and analysed with SEM.

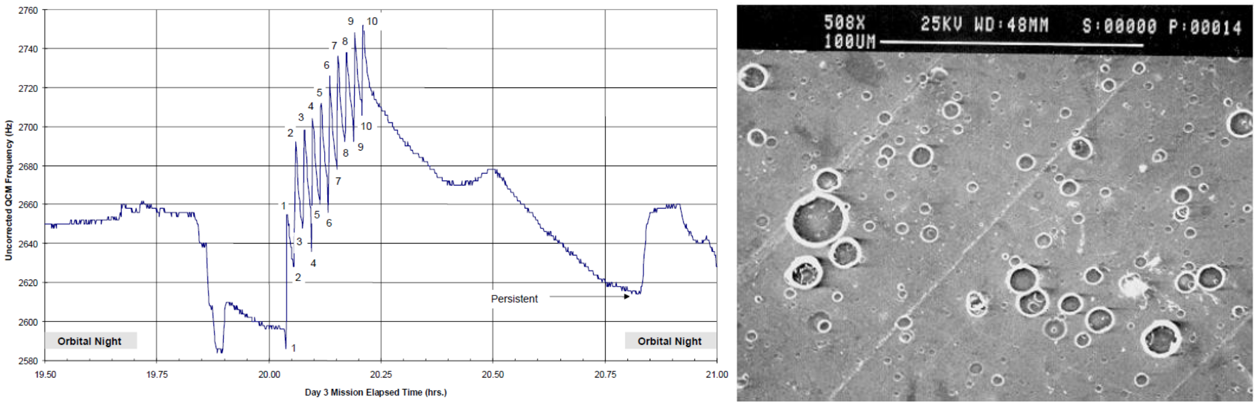

Figure 2.6 [Soares 2003]. *Left*: the figure shows the ten spikes (100 ms pulses) that correspond to ten cycles of the thrusters firings. The final trend shows the persistent materials (refractory) after the regeneration. *Right*: droplet impact features on Kapton sample and the craters that are the result of impingement of chemically reactive liquid drops.

The QCM for STS are mainly used to monitor contamination and return flux particles on the spacecraft, as well as to estimate the AO erosion in the upper terrestrial atmosphere. The QCMs used on STS have shown:

- in the EIOM-3 experiment the contamination an increase in weight and a mass deposition of 0.2 μg/cm^2 in 424 days;
- in IECM, a mass deposition of 39 μg/cm^2 (X direction), 16.4 μg/cm^2 (-Y direction) 1.6 μg/cm^2 (-X direction) and 1.2 μg/cm^2 (-X and Z directions) in 244 hours;
- in the PIC experiment, a deposition of 2.56 μg/cm^2 was measured on the Mir Station, 130-N Russian due to contaminants containing 7.5% of refractory materials and 80% of volatiles sublimating at 52°C; and a mass deposition of 0.384 μg/cm^2 was measured by the thrusters firings of the Orbiter PRCS (only 2% of refractory materials).

By means of SEM analyses, contaminants have been found to have different composition: Carbon and Silicon particles (EIOM-3); Silicon, Aluminum, Magnesium, Zinc, Sulfur, Titanium and Chlorine (between 1 μm and 2 μm in size for aluminum and up to 370 μm for Zinc particles) (IECM experiment); and thruster firings particles (PIC).

Table 2.7. Characteristics of QCMs used in satellite mission. Empty cell means not available data. The crystal configuration can be double crystal (DC) or single crystal (SC) (see chapter 3) and the QCM supplier are QCM Research, Faraday Laboratory and Meisei Electric.

Satellite Mission	**SDS-4 (2012)**	**SMART-2 (2015)**	**SMART-1 (2003)**	**MSX (1996)**	**Deep Space1 (1998)**	**OGO-6 (1969)**	**MEDET (2008)**
Configuration	SC	DC	DC	DC	DC	DC	SC
QCM frequency (MHz)	9	10	10	10 TQCM 15 CQCM	10	10	10-11
QCM Supplier	Meisei Electric Co.	QCM Research (MK 17)	QCM Research (MK 17)	QCM Research (MK 16, MK 10)	QCM Research (MK 16)	Faraday Lab. Inc. (Mckeown)	Variation of commercially QCM
Mass sensitivity (g/Hz×cm^2)	1 ng (T=const) 100 ng (over T range)	4.4×10^{-9}	4.4×10^{-9}	4.42×10^{-9} TQCM 1.96×10^{-9} CQCM	4.43×10^{-9}	3.5×10^{-9}	4.42×10^{-9}
Operative Temperature(°C)	from -40 to+65	from -50 to 120	from -50 to 120	-253 for CQCM -40/-50 for TQCM	from -43°C to +80°C	from -50°C to 100°C	Temperature of RAM direction
Resolution f(Hz)	--	0.1	0.1	±2	--	±1	--
Max mass loading (g/cm^2)	--	--	--	3.5×10^{-6} CQCM 3.3×10^{-6} TQCM	$>10^{-4}$	10^{-5}	--
T resolution (°C)	--	--	--	±0.25	<±0.2	10^{-4}	--
Warm-up rate (°C/min)	--	--	NO	2.5	--	NO	NO
Coating	Carbon	NO	NO	NO	NO	MgFl	Carbon
ΔF(Hz) and ΔT(°C) for solar pulse	--	--	--	300-450 Temperatures are not available	<250 Temperatures are not available	Decrease of contamination due to solar exposure	--
Regeneration T(°C)	85	--	--	60	75	100	Present

In the last case, the image obtained with the SEM showed the damage produced on a small Kapton sample: small (<4 μm), medium (5-10 μm) and large craters (11-20 μm) in the sample. During these experiments, the Sun radiation on the crystal surface induced a frequency variation, ascribed to the temperature change. The frequency variation with temperature is different for the EIOM-3, REFLEX and IECM experiments, and depends on the crystal coating and on the incidence angle.

QCM's have been also applied in satellite missions, in order to test and monitoring new technologies aboard on the spacecraft. QCM's supplier, characteristics and performances in seven satellite mission of JAXA (SDS-4), NASA (DS1, MEDET, OGO-6, MSX) and collaborations with ESA (SMART 1 and 2) are summarized in Tab.2.7. The main goals of QCMs have been:

- to estimate the erosion due to AO (MEDET, SDS4);
- to measure the contamination from the solar panels of the spacecraft (OGO-6);
- to control the contamination induced from the Propulsion System of the spacecraft (DS1);
- to monitor the contamination and the degradation near the scientific instruments, i.e. solar cell, telescope (MSX, SMART1);
- to monitor the frequency trend, when the QCMs are exposed to full or partial sunlight (MSX).

In SDS-4 satellite, a frequency increase of 200 Hz was observed in the launch phase, due to the erosion of coating materials of the QCM surface. In MEDET experiment the carbon-coated QCM showed a frequency increase of 60 Hz (after two weeks), which indicated a linear decrease of carbon mass, due to AO erosion.
The main contamination sources is often generated by the Solar panels of the spacecraft. OGO-6 experiment measured a contamination of 10^{-5} g/cm^2 during full exposition to Sun (Solar panels temperature of 72°C) and 9×10^{-6} g/cm^2 during the maximum eclipse (30% in the Earth's shadow and Solar panels temperature of 60°C).The mass loss was due to the fact that the lower flux from the solar panel did not balance the contaminant desorbed from the crystal surface.
During the launch phase of DS1 mission, QCMs were used to monitor the ion propulsion induced contamination. A total contaminant mass of 0.8 μg/cm^2 has been measured. This mass has been removed when the DS1 has been rotated to Sun. Otherwise, in MSX experiment, a CQCM placed near the SPIRIT3 telescope revealed oxygen and argon (film thickness deposition of approximately 200 Angstrom), whereas four TQCM's placed in different locations measured a total thickness (since launch) of 134, 144, 13, and 63 Angstrom, respectively. In this scenario TQCM's have the disadvantage of being sensitive to incident solar flux. The frequency showed a negative shift of 240-450 Hz depending on full or partial exposure to Sun conditions. The regeneration temperature never exceeded the 100°C (OGO-6) in all the experiments (i.e.

75°C for DS1, 52°C for PIC, 60°C in MSX, figure 2.7, and 85°C in SDS-4 satellite mission) even if higher temperatures could be considered to remove all the refractory contaminants.

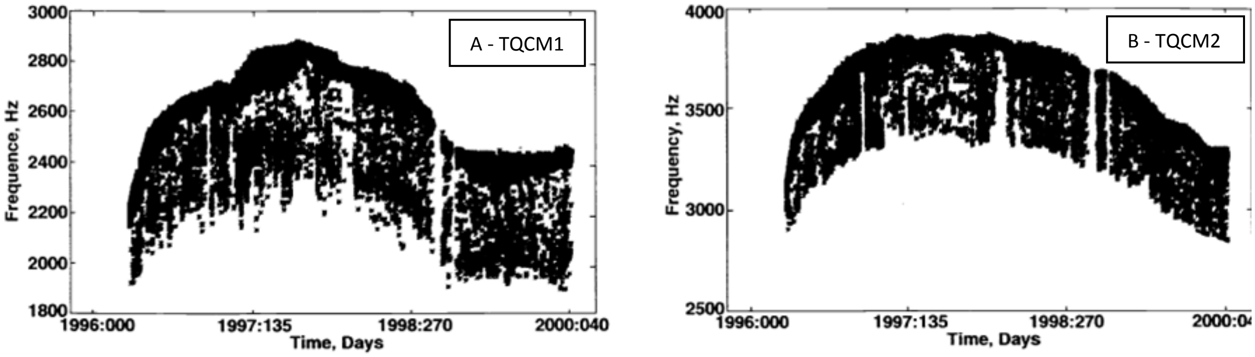

Figure 2.7 [Wood 2000]. A: facing in the (+Y, -X) direction and viewing the solar panels (ΔF_{sun}=300-450 Hz); B: TQCM2, facing into RAM (the side that points in the direction of the satellite's motion) direction (+Z) and also having the solar panel in its FOV (ΔF_{sun}=300-450 Hz)

A series of external contamination measurement have been performed aboard Mir Space Station in order to evaluate the impact of Russian Segment on ISS. Mir contamination observations includes results from a series of flight experiments: CNES Comes-Aragatz, retrieved NASA camera bracket, Euro-Mir 1995 ICA, retrieved NASA Trek blanket, Russian Astra-II, Mir Solar Array Return Experiment (SARE).

The outgassing rates observed from this experiment were estimated between 4.1×10^{-12} and 1.2×10^{-10} g/cm^2/sec (camera brackets, organic silicon based paint would be the contamination source). Another silicone contamination source, is AK-573 (organic silicone based paint) and the PVC cable insulation and the BF-4 impregnated mesh (arrays) also contribute to contamination, but these are hydrocarbon contamination sources. Low amount of AO and high amount of UV have been measured by Comes-Aragatz experiment while higher rate inferred from the camera bracket contaminant deposit layer is consistent with the higher source temperatures due to the Mir solar cycle [Soares and Mikatarian 1994]. As a result, modifications in Russian materials selection and/or usage were implemented to control contamination and mitigate risk to ISS [Soares and Mikatarian 1994], for example:

1. Cable insulation on ISS Russian segment: Teflon instead of PVC.

2. Replace high-outgassing KO-5191 and AK-573 with AK-512.

3. Solar array lubricant: fluorocarbon instead of silicone.

2.4. Volatiles reservoirs in planetary bodies detectable by TGA

The chemical and mineralogical analysis on asteroidal and cometary samples will help the classification of these minor bodies of Solar System (thanks to Sample Return Mission, e.g. Stardust, Hayabusa1 etc.). In order to know the mineralogical composition of these bodies, a study related to Chondrite meteorites (asteroids analogues) that are classified in Carbonaceous, Ordinary and Enstatites (which show different organics content inside, Tab. 2.8) should be done. In particular, the asteroids span very different mineralogical compositions: some of them appear to be completely unprocessed while other ones are composed by processed materials. In order to understand the mineralogical history of the processes concerning asteroids evolution, all the thermodynamical and thermochemical processes should be taken into account. In particular, the asteroids represent a great opportunity to study a possible cometary-like activity and to exactly determine the desorption rate and even to discern the refractory/volatile ratio. Mainly, the thermodynamical processes are related to ejection (sublimation or vaporization) of a mixture of gas or dust. Gas molecule rates are easily monitored at sublimation temperature at which the process occurs. For example, the water in space can be collected at $T<77\ K$ [Tribble 1996] while for tiny dust particles it is also important to monitor the ejection speeds.

Table 2.8 [Grady and Wright 2003, Sephton 2002, Schaefer and Fegley Jr. 2006, Stalder and Skogby 2002]. Carbon, organic compounds and water abundance in the three families of chondrites.

Chondrite Class	*Carbon content*	*Organic content*	*Water content*
Carbonaceous	0.1-5 %	0-4%	0-20 %
Ordinary	300-6000 ppm	~ 0.1%	~ 0.3%
Enstatites	1500-7000 ppm	-	~ 1000 ppm

On the other hand, the Carbonaceous Chondrites (CC) (related to primitive asteroid, the most thermodynamically and chemically processed), are divided in groups showing different volatile content (see Tab.2.9) which can be used as a marker for asteroid types. The CI, CM, CR groups form the first ensemble with similar organic and water content. The other CC are included in the second ensemble, which is characterized by very low volatile (water, organic) content.

Table 2.9 [Grady and Wright 2003, Remusat 2008]. Carbon, organic and water content in carbonaceous chondrites.

CC Group	Carbon content	Organic content	Water content
CI	2-5 %	1-4 %	18-22 %
CM, CR	2-5 %	1-4 %	2-16 %
CO	0.1-1.1 %	< 1 %	0.3-3 %
CV	0.1-1.1 %	-	0.3-3 %
CK	0.1-1.1 %	-	-
CH, CB	0.2-1 %	-	0.3-3 %

Table 2.10. Combustion temperatures of Chondrites components.

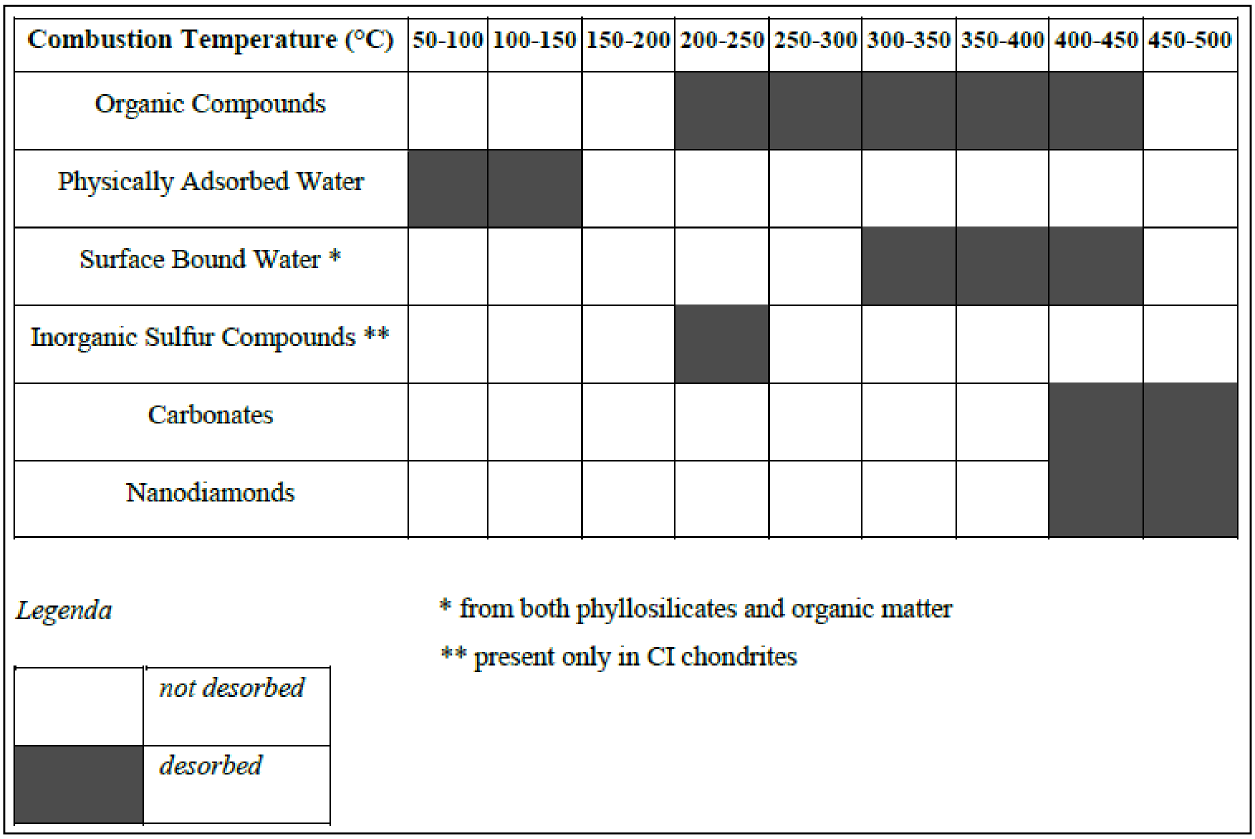

Combustion Temperature (°C)	**50-100**	**100-150**	**150-200**	**200-250**	**250-300**	**300-350**	**350-400**	**400-450**	**450-500**
Organic Compounds				■	■	■	■	■	
Physically Adsorbed Water	■	■							
Surface Bound Water *						■	■	■	
Inorganic Sulfur Compounds **				■					
Carbonates								■	■
Nanodiamonds								■	■

Legenda

□	*not desorbed*
■	*desorbed*

* from both phyllosilicates and organic matter

** present only in CI chondrites

Thus, QCM-based device equipped with built-in heater can be used to perform heating cycles up to 400°C on Chondrites samples in order to study the decomposition processes of materials at different temperatures (Tab. 2.10). The decomposition processes will be:

1. organics degassing between 200°C and 400°C [Grady 2002, Sephton 2002, Halbout 1986];
2. water desorption. A distinguishing between *physically adsorbed water* (loosely bound molecules held by Van der Waals' forces), that desorbs to lower temperatures (up to 160 °C), and *surface bounded water* (molecules more tightly bounded, attached to basal clay surfaces), that desorbs at higher temperatures (above 300°C) have to be done. Surface bounded water can be detached from organic materials or from phyllosilicates [Bruckenthal and Singer 1987, Halbout 1986];
3. inorganic sulphur compounds, present only in CI chondrites, that desorbs between 200-250 °C [Halbout 1986];
4. carbonates and nanodiamonds, that are decomposed above 400 °C [Sephton 2002].

From table 2.10 a thermal trend is defined:

- *T< 160°C (433 K)*: in this range only *physically adsorbed water* is released.
- *200°C (473 K)< T < 300°C (573 K)*: organic matter decomposition starts at 200 °C and up to 300 °C is the only compound to be decomposed. If sample composition is similar to CI's, in addition to the organic matter we can detect the inorganic sulphur decomposition too, even if its abundance is not larger than about 12 % of the organic [Halbout 1986].
- *300°C (573 K)< T < 450°C (723 K):* at 300°C even surface bounded water begins to desorbs and partly is desorbed from organic compounds. In this range, the desorption of both water and organics is observed.
- *T>450°C (723 K):* neither organics and water evaporate, but only carbonates and nanodiamonds.

TGA can be used to study the thermodynamical processes as well as to detect *surface bound water, carbonates, organics*. In particular, QCM can measure [Palomba 2011]:

- *dust settling rate and ice content:* VISTA instrument can operate in accumulation mode revealing the ice falls by applying a heating cycle few degrees above the water frost point, while the dust remains onto the crystal. This operation allows also the determination of the water frost temperature and (knowing the actual pressure) of the atmospheric humidity;
- *humidity*: measurements of water vapor local abundance (Langmuir equation);
- *physically adsorbed water* in the dust heating up to 240 K, the mass difference at the beginning and at the end of the cycle gives the adsorbed water mass;

2.5. Dicarboxylic acids

Dicarboxylic acids are organic compounds with a general chemical formula:

$$HOOC(CH_2)_{n-2}COOH$$

where *n* is the number of carbon atoms. According to IUPAC nomenclature, dicarboxylic acids are named by adding the suffix *dioic*-acid to the name of the hydrocarbon with the same number of carbon atoms, e.g., nonanedioic acid for $n = 7$. The dicarboxylic acid contain two carboxylic acid functional groups and are used to prepare copolymers and polyamides and polyesters [Dirri 2016b].

Dicarboxylic acids the most abundant class between the organic components of PM [Rogge 1993] and are present in various concentrations in different terrestrial environments, e.g. marine, rural, urban [Kawamura 2005, Yu and Fraser 2004, Limbeck 2001]. Their formation in atmosphere is likely due to photochemical reactions in gaseous phase involving VOC (in particular aliphatic and aromatic hydrocarbons) of biogenic and anthropogenic origin. By means of the mass spectrum of atmospheric aerosols, we can considered the Dicarboxylic acids as "markers" of SOA [Schuetzle 1975]. Typical concentrations of dicarboxylic acids in ambient air are a few nanograms per cubic meter and thus contribute to a large fraction of the total identifiable resolved organic mass in fine aerosols [Dirri 2016a].

These compounds play an important role on physical-chemical reactions involving aerosol particles, that may be gathered in agglomerates (sub-micron sized), and represent an important component of the atmospheric aerosol particles, both in remote and urban areas [Rohrl and Lammel 2001].

Concentrations of longer-chain diacids (C_6–C_9) varied in different seasons and size fractions with suberic acid (C_8) being the most abundant in the wet season in $PM_{2.5}$, adipic acid (C_6) and azelaic acid (C_9) in the dry season in $PM_{2.5}$ and C_9 in both seasons in PM_{10} [Mkoma and Kawamura 2013].

The oxalic acid is the most abundant dicarboxylic acid in the tropospheric aerosol and comprises 41-67 percent of the total diacids [Sorooshian 2006, Kawamura and Keplan 1983] whereas the succinic and malonic acids are less abundant and reach peaks of 4-8.7 percent during the summer [Kawamura and Ikushima 1993]. Adipic and succinic acids have been identified in laboratory studies as SOA products (reaction of O_3 and cyclohexene) [Hatakeyama 1985]. The Adipic acid is related to N_2O emission, a greenhouse gas that causes stratospheric ozone depletion [EPA 2016] whereas the succinic acid origins probably from biogenic sources, and is an important compound in biochemistry due to its role in the citric acid cycle (Krebs cycle). The azelaic acid is considered a photon-induced oxidation's product, deriving from biogenic unsaturated fatty acid, presenting one or more double bond in their chain [Kawamura and Keplan, 1983]. Succinic and oxalic acids had been proven to be part of the organic materials that contribute to form condensation nuclei of atmospheric clouds [Kerminen 2000, Prenni 2001] and it has been suggested that the ratio between oxalic and succinic acid is a good marker of the atmospheric aerosol oxidation state

[Kawamura and Ikushima 1993]. On the other hand, adipic-azelaic ratio could be an indicator of anthropogenic sources, considering that adipic acid derives from cycle-hexane's oxidation [Dirri 2016a].

Dicarboxylic acids have been found also in carbonaceous chondrites [Andersen 2005, Briscoe 1993], meteorites associated to the primitive asteroids; and hence could give information about chemical and mineralogical composition of the early Solar System. Chemical analyses on carbonaceous chondrites revealed a variety of organic compounds, including amino acids, aliphatic and aromatic hydrocarbons, mono-carboxylic acids and some dicarboxylic acids, such as succinic acid and adipic acid in small quantities (5.9 µg/g and 0.7 µg/g, respectively). In this scenario, the presence of the succinic acid is consistent with a synthesis from hydrogen cyanide and ammonia. In particular the succinic acid/β-Alanine (amino acid) ratio makes it possible to estimate the relative period of synthesis of organic compounds on the Murchison meteorite parent body [Peltzer 1984].

Carboxylic acids have been found in water samples (i.e. indoor contamination) acquired during few STS missions. In particular, the chemical constituent includes contaminants released into the cabin air, come from crew activities, such as by product of metabolism, food preparation and hygiene activities (including the use of cleaners and disinfectants); from revitalization system and from hardware off-gassing, from payload experiments. In this way, the humidity condensate is an important source of indoor water contamination (and probably most variable) and collected by the cabin heat exchanger, which is controlled by the spacecraft's air revitalization system. Different samples have been collected during the STS missions and many organic compounds were identified including: alcohols, amines, carboxylic acids, ethers, esters, ketones, phenols and thiourea. In 1991 and 1992, samples were collected from STS-40, STS-42, STS-47 and STS-50 even if the long delay after landing until samples could be collected could affected their chemical composition [National Research Council 2000]. Besides, the assessment of atmospheric quality aboard Shuttle mission have revealed the presence of organic compounds that appeared in the humidity condensate. Additional samples have been collected from STS-68 and from Mir station [James 1994].

Thus, assuming the carboxylic acids implication in the humidity condensate aboard STS mission and Mir Station, a characterization of these compound and specifically of dicarboxylic acids would be useful for samples analysis on ground, to understand the toxicity level of these compounds in the STS internal atmosphere.

2.5.1. Physical properties

Organic compounds are characterized by molecular lattice whose molecules are arranged to form crystals.
The thermal reactions of organic compounds in the solid state depend on their interatomic relations and cohesive forces acting between their crystals [Muraishi and Suzuki 1994]. Generally, dicarboxylic acid which are originate from combustion of fossil fuels [Kawamura and Kaplan 1983] and biomass burning

[Narukawa 1999] are subjected to thermal breakdown of crystalline organic compounds, which is both a physical and chemical process [Muraishi and Suzuki 1994].

Dicarboxylic acids are colorless, odorless crystalline substances at standard conditions. In table 2.11 are listed the major physical properties of some saturated aliphatic dicarboxylic acids with carbon number from 2 to 10 atoms [Rozaini 2012]. As shown, the acids density decrease steadily with increasing chain length whereas melting point and water solubility show an alternate order: acids with an even number of carbon atoms have higher melting points than the next higher odd-numbered dicarboxylic acid [Rozaini 2012]. The water solubility is higher for odd-numbered C atoms and lower for even-numbered C atoms.

In the range: *n* = 6 – 10, dicarboxylic acids show a lower solubility than those in the range: *n* = 2 – 5. As chain length increases, the influence of the hydrophilic carboxyl groups diminishes; from *n* = 5 (pimelic acid) onward, solubility in water decreases rapidly.

Table 2.11 [Rozaini 2012]. Physical characteristic of dicarboxylic acids. The bold acid names are those analysed in this work.

IUPAC name	Acid name	C	Chemical Structure	Molecular weight (g/mol)	Density at 25°C (g/cm3)	Solubility (mol/kg)	Boiling point	Melting point
Ethanedioic	**Oxalic**	**2**	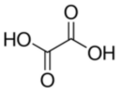	90.03	1.653	1.131	-	189.5
Propanedioc	Malonic	3	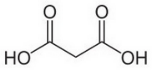	104.06	1.619	16.03	-	135
Butanedioic	**Succinic**	**4**	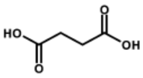	118.08	1.572	0.748	235	188
Pentanedioic	Glutaric	5	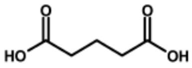	132.11	1.424	8.468	200	99
Hexanedioic	**Adipic**	**6**	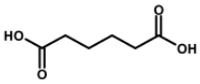	146.14	1.360	0.171	265	153
Heptanedioic	Pimelic	7	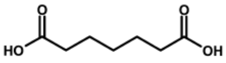	160.17	1.329	0.423	272	106
Octanedioic	**Suberic**	**8**	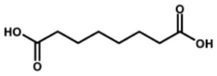	174.19	1.266	0.0139	279	144
Nonanedioic	**Azelaic**	**9**	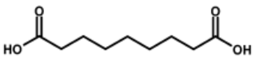	188.22	1.225	0.00946	287	108
Decanedioic	Sebacic	10	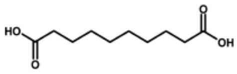	202.25	1.207	0.00012	-	134.5

2.5.2. Chemical properties

The chemical behavior of dicarboxylic acids is determined by their function groups, e.g. the carbonyl or hydroxyl group. Certain chemical reactions of dicarboxylic acids lead to unusual results as compared with those of monocarboxylic acids because there are two carboxyl groups in each molecule [Muraishi and Suzuki 1994].

Thermal decomposition of dicarboxylic acids gives different products depending on the chain length, i.e. acids with an even number of carbon atoms require higher decarboxylation temperatures than the next higher odd-numbered homologues; lower dicarboxylic acids decompose more easily than higher ones. With the exception of oxalic acid, dicarboxylic acids are resistant to oxidation. Furthermore, the thermal behavior of malonic acid and sebacic acid (dicarboxylic acids), may be expected to differ from formic and acetic acid (monocarboxylic acids), because of the separation of the two carboxylic acid groups by CH, which reduces the spatial restriction in bonding [Rozaini, 2012]. The main thermal and chemical properties of dicarboxylic acid are summarized as follow:

- *Oxalic acid*: heating this compound above 190 °C, a decompositions to carbon monoxide, carbon dioxide, and water occurs.

- *Malonic acid*: at temperatures above 150°C, this compound is decarboxylated to acetic acid HOOC-(CH2)n-COOH-CH3COOH + CO2. When malonic acid is heated in the presence of P_2O_5 at 150 °C, small amounts of carbon suboxide (C3O2) are also formed.

- *Succinic and glutaric acid*: it is possible to have cyclic anhydrides on heating (Fig. 2.8). Besides, when the ammonium salt is distilled rapidly from succinic, succinimide is formed, with the release of water and ammonia.

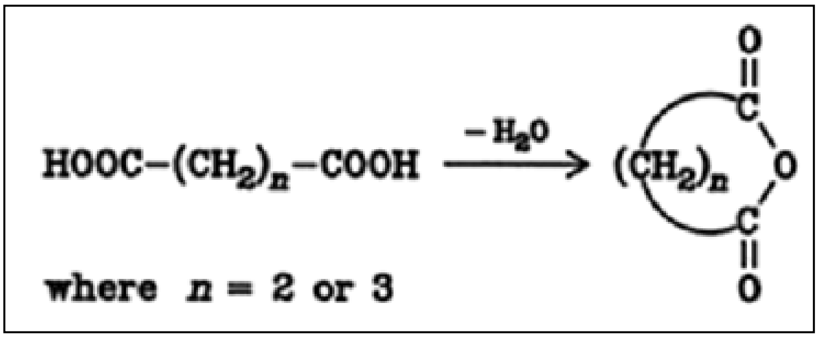

Figure 2.8 [Rozaini, 2012]. Succinic and glutaric acids are converted into cyclic anhydrides on heating.

- *Adipic, Pimelic and Suberic acids* (*n* from 4 to 6): a split off carbon dioxide and water to form cyclic ketones has been possible, i.e. $HOOC\text{-}(CH_2)n\text{-}COOH \longrightarrow (CH_2)_n\ C{=}O+CO_2+H_2O$.

- *Azelaic acid*: heating this compound at *P* standard, starts to decay at 360°C.

Dicarboxylic acids are mainly used as intermediates in the manufacture of esters and polyamides. Esters derived from monofunctional alcohols serve as plasticizers or lubricants. Polyesters are obtained by reaction with dialcohols. In addition, dicarboxylic acids are employed in the manufacture of hydraulic fluids, agricultural chemicals, pharmaceuticals, dyes, complex agents for heavy-metal salts, and lubricant additives (as metal salts) [Rozaini, 2012].

2.5.3. Bio-markers compounds

The dicarboxylic acid are an important group of Water-Soluble Organic Compounds (WSOC) in the atmospheric aerosols [Kawamura and Ikushima 1993, Rogge 1993]. Because of the low vapor pressures and high water solubility, these compounds have received much attention due of their potential roles in affecting the global climate.

The most abundant is oxalic acid followed by malonic and succinic [Kerminen 2000]. The percentage of diacids content is about 1-3% of the total particulate carbon in the urban areas and even above 10 % in the remote marine environment [Kawamura and Ikushima 1993, Kerminen 2000]. In particular, the concentration ratios of these diacids of linear sequence, i.e. C_3/C_4 and C_6/C_9 mass ratio, help to know the ratio between anthropogenic and biogenic source and their precursors in the atmosphere [Kawamura and Ikushima 1993, Ho 2006, Ray and McDow 2005]. It has been suggested that the ratio C_3/C_4 from vehicular emission (0.25-0.44 in urban aerosol and lager than unity for rural aerosols) [Kawamura 1996] could provide the oxidation signature of anthropogenic aerosols because of the succinic acid, after several photochemical processes, can be the precursor element of malonic and oxalic acids. On the other hand, because of the azelaic acid and adipic acid have been proposed as one of the reaction products of ozonolysis of biogenic unsaturated fatty acids [Kawamura and Keplan 1983] and the product of anthropogenic cyclohexene respectively [Kawamura and Ikushima 1993], the ratio C_6/C_9 could be used as an indicator of biogenic sources.

In this work, five dicarboxylic acids with lower molecular weight (C number from 2 to 9) are analysed, founding the thermodynamical properties described in chapter 3. In figure 2.9 are shown the chemical structure of these compounds.

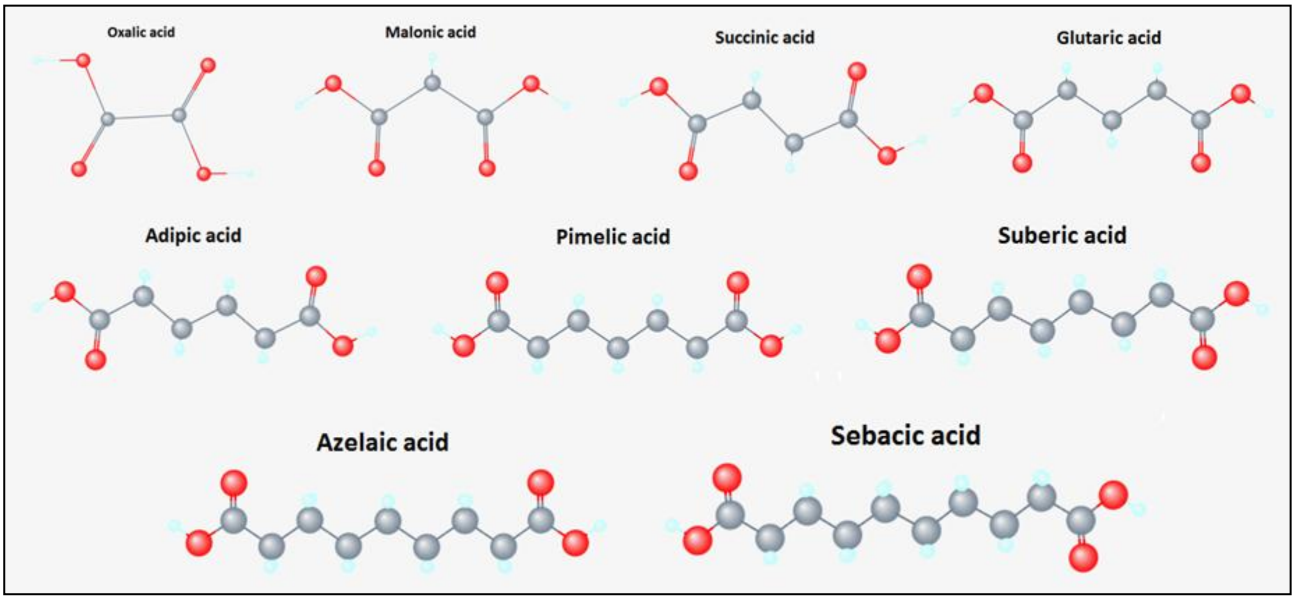

Figure 2.9 [PubChem database, 2016]. Chemical structure of C_2 to C_{10} dicarboxylic acids are shown. Red and gray atoms are the oxygen and carbon respectively while the light blue atoms are hydrogens.

Chapter 3. Thermo-physics and Thermogravimetry: basic concept

3.1. Introduction

The chemical-physical and thermodynamic properties of materials/compounds (i.e. vapor pressure, enthalpy, entropy and Gibbs free energy) are fundamental to know their behaviour in different environment (e.g. terrestrial atmosphere, space etc.) with different external conditions, i.e. pressure and temperature. Thus, thermochemical relations, i.e. Clausius-Clapeyron, Langmuir and Van't Hoff equation and physical-chemical quantities for organic compounds characterization are introduced as well as the thermodynamic quantity as vapor pressure and the enthalpy of phase change which help to identify a compound.

The basic concept of Thermogravimetric Analysis (TGA) and the working principle of microbalance are explained. The Quartz Crystal Microbalance (QCM), Sauerbrey equation and the applications QCM-TGA are discussed in preparation to experimental procedure and results explained in chapters 5-6.

Finally, VISTA instrument (QCM-based device) and the two sensor heads, i.e. Sensor Head 1 (SH1) and Sensor Head 2 (SH2) breadboards are introduced and explained in depth considering all the sub-system units. The Engineering Model of SH1 is also explained. Furthermore, the main innovations, the measurement capability and the scientific goals of SH1 and SH2 are described.

3.2. Thermochemical processes

3.2.1. Phase change thermodynamic processes

The matter phases are class of various molecular motions existed at particular temperatures: at low temperatures, the molecular motion is restricted so that molecules are bounded with strong intermolecular forces while at high temperatures, the molecular motion is due to the translational energy of molecules (the intermolecular forces are ignored). At intermediate temperatures, molecules are in translation mode and bounded with each other.

According to the intermolecular forces between molecules, the matter phases are classified into three different aggregation states: solid, liquid and gas and in rare case, plasma. In order to change the aggregation state it is necessary to change the intensity of the cohesion force between molecules, i.e. varying the kinetic energy. In fact, a thermodynamic phase change is followed by heat variation between compound and external environment. Generally, when heats is provided a liquid or gaseous states are promoted (the molecules are less bounded). On the other hand, if heats is subtracted the inverse phase change is promoted [Levine 1978].

Basically, the thermodynamical phases show a difference in molecules kinetic energy: the solid to liquid change takes place at the melting point of solid while the liquid to gas change is takes place at boiling point. Conversely, if pressure increase, the vapor phase to liquid phase change and liquid to solid state phase changing are promoted. If pressure decrease, the inverse phase change is facilitated. The transitions between the solid, liquid and gaseous phase of a single component, due to the effects of temperature and/or pressure are: solidification (liquid to solid), sublimation (solid to vapor), deposition (vapor to solid), condensation (vapor to liquid) and evaporation/boiling (liquid to vapor).

3.2.2. Activation energy, vapor pressures and enthalpy of phase change

A compound can be characterized by identifying its thermodynamical properties. For example, the knowledge of pure component vapor pressures is essential for calculations of gas/particle partitioning of compounds forming terrestrial atmospheric aerosols [Booth 2009] as well as the knowing of the enthalpy and entropy of sublimation which is different for each compound [Dirri 2016a].

A chemical-physical process happens when the molecules (with a correct orientations) velocity is high enough so that kinetic energy of collision is higher than the minimum energy barrier. The activation energy is the minimum required energy to have collisions: E_a is measured in kilojoules per mole (kJ/mol). During a chemical reaction, if the kinetic energy is higher than the minimum energy it is possible to have the new products formation. Different E_a values are shown in figure 3.1.

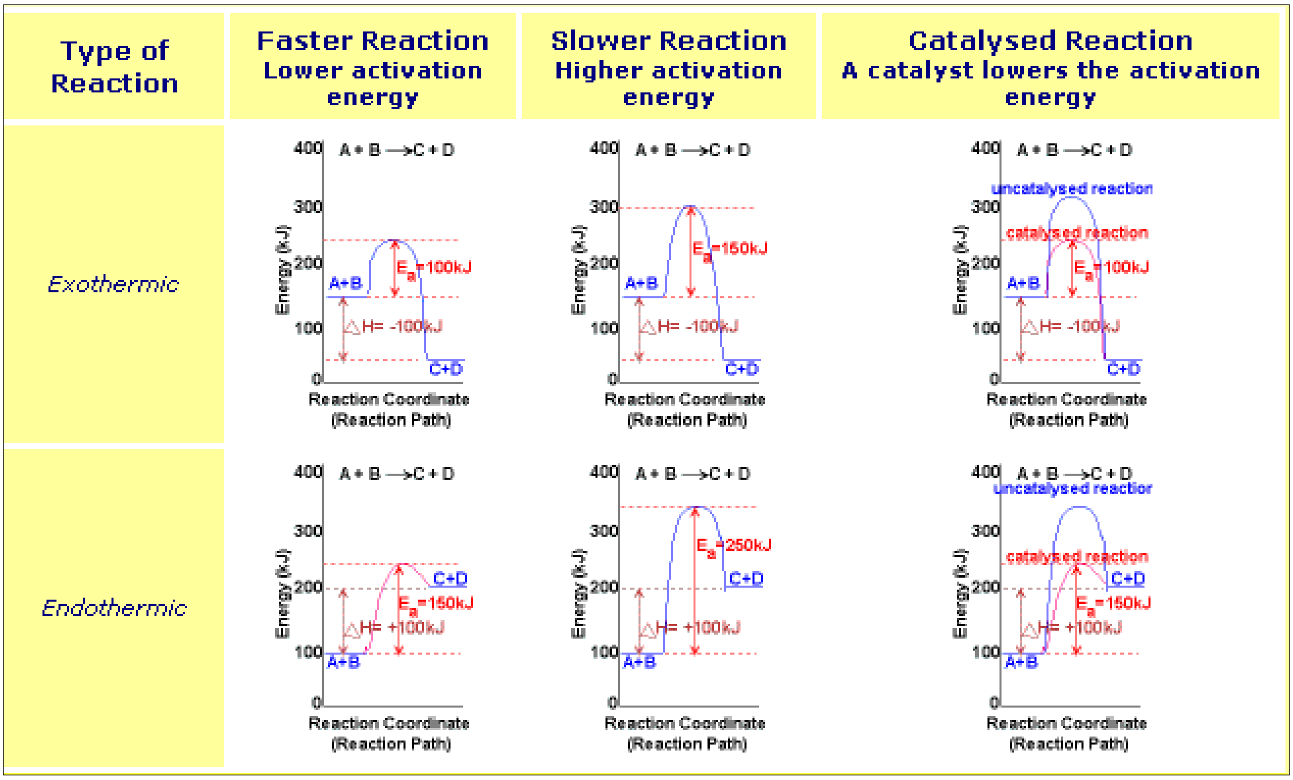

Figure 3.1. Activation energy for exothermic and endothermic reactions. The maximum energy point is called "transition state" which representing a chemical transitory species (due to the energy levels which are higher than products and reagents).

Thus, the activation energy, i.e. E_a *(kJ/mole)* is connected to the temperature *T(K)* and rate constant *k* by means of the Arrhenius equation:

$$k = Ae^{\left(-\frac{RT}{E_a}\right)} \tag{3.1}$$

where $A=const$, proportional to the collision frequency and expressed as (1/s) and R, the gas constant (kJ mol^{-1} K^{-1}). E_a can be retrieved by plotting $ln(k)$ vs. $1/T$. The slope of the straight line obtained will equal to -E_a /R. Generally, the most of chemical reaction show E_a values between 40 and 150 kJ/mol while at T_{amb} up to 80 kJ/mol the reaction proceed quickly.

Enthalpy is a typical thermodynamic quantity that can used to characterizes the organic compounds; specifically the enthalpy of sublimation. When thermodynamic process occurs at constant pressure, the heat evolved in thermochemical process (either released or absorbed) is equal to change in enthalpy. Enthalpy (H) is the sum of the internal energy (U) and the product of pressure and volume (PV):

$$H = U + PV \tag{3.2}$$

Enthalpy is a state function which depends entirely on the state functions T, P and U. It is possible to express the enthalpy as change in enthalpy (ΔH) between initial and final states:

$$\Delta H = \Delta U + \Delta PV \tag{3.3}$$

considering constant pressure the heat flow (q) for the process is equal to the change in enthalpy:

$$\Delta H = q \tag{3.4}$$

ΔH and q relationship can be determined by looking exothermic or endothermic reactions. If the heat is absorbed the reaction will be endothermic (the heat from the surrounding environment is consumed: $q>0$). At constant temperature and pressure, with $q>0$, ΔH is also positive. If the heat is released the reaction will be exothermic (the heat is emitted to surrounding environment: $q<0$). If $q<0$, ΔH will be also negative [Atkins and de Paula 2006]. The enthalpy can be represented at the standard state ($P=1$ bar) as ΔH_o, which is the enthalpy of a phase transition (e.g. ice to liquid water) that require or absorb a particular amount of standard enthalpy:

- Standard enthalpy of vaporization ($\Delta H_{o,\ vap}$) is the energy that must be supplied as heat at constant pressure per mole for vaporization (liquid to gas).

- Standard enthalpy of fusion ($\Delta H_{o,\ fus}$) is the energy that must be supplied as heat at constant pressure per mole of molecules for melting (solid to liquid).

- Standard enthalpy of sublimation ($\Delta H_{o,\ sub}$) is the energy that must be supplied as heat at constant pressure per mole for sublimation.

Considering the Hess law, in a chemical reaction the thermal effects (at $P=const$) depends only to initial and final state of the system. Thus, the enthalpy variation can be calculated by means of the sum of different partial enthalpies:

$$\varDelta H_{0,sub} = \varDelta H_{0,fus} + \varDelta H_{0,vap} \tag{3.5}$$

i.e. for sublimation process, the final enthalpy is the sum of the enthalpy of fusion and vaporization. Applying different thermal cycles to compounds it is possible to calculate the enthalpy of vaporization and the enthalpy of fusion each one, verifying that the difference is the enthalpy of fusion [Price 2001]. In particular, it can be assumed that enthalpy of condensation is the reverse of the enthalpy of vaporization and the enthalpy of freezing is the reverse of the enthalpy of fusion. The enthalpy variation of complete process is the sum of the enthalpy changes for each of the phase transitions [Petrucci 2007].
In this work, different sublimation processes have been monitored (at $P=10^{-6}$ mbar) and the enthalpy of sublimation, i.e. the enthalpy change accompanying the conversion to one mole of solid substance directly into vapor phase at a given temperature [Tyagi 2006], has been inferred for five different crystalline pure organic compounds. The enthalpy of sublimation can be also inferred by means of Clausius-Clapeyron equation that characterizes a phase transition. The vapor pressure can be obtained at each temperature *Ti* and the enthalpy variation from vapor pressure at two different temperatures:

$$\frac{dp}{dt} = \frac{\varDelta H}{T\varDelta V} \tag{3.6}$$

being $\varDelta H$ the specific latent heat of the process (sublimation, vaporization, or fusion), p the vapor pressure and $\varDelta V$ the difference between volumes of gaseous and solid/liquid (sublimation/vaporization) phase, respectively. If the products are in gaseous phase and at temperatures much smaller than their critical one, they can be approximated as ideal gases, i.e. $\Delta V \sim V_{gas}=RT/p$. Replacing in the equation 3.6, we have the differential form:

$$\frac{dlnp}{dT} = \frac{\Delta H}{RT^2} \tag{3.7}$$

In order to characterize a pure substance, the thermogravimetry can be used to determine the vapor pressure, by recurring at Langmuir equation for free kinetic sublimation/evaporation in vacuum [Langmuir 1913]:

$$p = \frac{\sqrt{2\pi R}}{\alpha} \frac{dm}{dt} \sqrt{\frac{T}{M_i}} \tag{3.8}$$

where p is the vapor pressure of the gas, dm/dt is mass loss rate per unit area (the area of the PCM's electrode) is the deposition rate experimentally measured, Mi the molecular weight, R the gas constant, T the absolute temperature and α the vaporization coefficient, assumed to be 1 in vacuum environment (Price 2001). Replacing eq. (3.7) in eq. (3.8), it is possible to obtain the enthalpy of sublimation (multiplied by a constant) as slope of the curve $\ln(dm/dt)T^{1/2}$ versus T^{-1}

$$ln\frac{dm}{dt}T^{1/2} = lnC - \frac{\Delta H}{RT} \tag{3.9}$$

where C is the term $(2\pi R/\alpha Mi)^{1/2}$ that remains constant during all the measurement. The enthalpy of sublimation/evaporation can be also obtained by means of the Van't Hoff equation [Benson 1968], i.e. by measuring at two different temperatures T_1 and T_2 and the respective rate constants k_1 and k_2 (the deposition rates on the PCM):

$$\Delta H = R\left[\left(\frac{T_1T_2}{T_2 - T_1}\right) ln\left(\frac{k_1\sqrt{T_1}}{k_2\sqrt{T_2}}\right)\right] \tag{3.10}$$

Then, the Van't Hoff equation (eq. 3.10) can be used to monitor the enthalpy variation in a temperature range in order to monitor the state functions (e.g. enthalpy, Gibbs energy, and entropy) in a transition phase [Dirri 2016a]. According to this relation, for an endothermic process (i.e. $T_1 > T_2$ and $\Delta H > 0$): $k_1 > k_2$, i.e. the temperature is directly proportional to rate constant.

3.2.3. Entropy and Gibbs free energy: spontaneous and non-spontaneous reactions

Generally, the thermodynamic quantity called entropy (S) measures the degree of the disorder of the system. The entropy of system increases as the disorder of the system also increase. This thermodynamic parameter is a state function such that is possible to define the entropy variation as the difference between the initial and final states:

$$\Delta S = S_f - S_i \tag{3.11}$$

The entropy variation for fusion process will be: $\Delta S > 0$ because the disorder degree increase. Entropy can be transferred in two forms: heat transfer (to a system) and mass flow (from a system). If the thermodynamic process happens at equilibrium conditions (reversible), the ratio of the heat transfer Q/T (absolute temperature) is called entropy flow or entropy transfer:

$$\Delta S = \frac{q}{T} \tag{3.12}$$

Since $T(K)$ is always positive, the direction of the entropy transferred is the same of the heat transfer direction. Defining the entropy as heat of reaction, if the heat transfer between two phase is reversible and the process are on equilibrium at temperature: T_{trasf}, we can define $q = \Delta H_{trasf}$ while ΔS is given to:

$$\Delta S = \frac{\Delta H_{trasf}}{T_{trasf}} \tag{3.13}$$

Thus, we can have three different scenario:

If $\Delta S_{system} > 0$, then the system is at equilibrium.
If $\Delta S_{system} = 0$, the system is at equilibrium.
If $\Delta S_{system} < 0$, then the reverse process is spontaneous.

In order to determine spontaneity, it would be better to have a function depending to the system only, i.e. the Gibbs free energy (G). This is a thermodynamic quantity that can be used to retrieve the maximum work performed by a thermodynamic system at a constant temperature and pressure (isothermal, isobaric). The Gibbs free energy is defined as:

$$G = H - TS \tag{3.14}$$

Because of H, S, T are state functions as well as *G*, for thermodynamic process (initial to final stage) it is possible to define the Gibbs free energy as ΔG in order to determine the spontaneity of chemical reaction at *T, P= const*. In these conditions, ΔG can be rewritten as:

$$\Delta G = \Delta H - T\Delta S \tag{3.15}$$

ΔG is mainly composed by two contributions: energetic, i.e. ΔH and entropic, i.e. $T\Delta S$. The exothermic reactions are facilitated ($\Delta G<0$) with $\Delta H<0$ (Fig. 3.2, *Left*) and a positive entropy variation ($\Delta S>0$). Generally, ΔH contribution is higher than ΔS thus, the sign of ΔG is determines by ΔH. When ΔH contribution is small, $T\Delta S$ can determine the ΔG sign: the endothermic reaction can occurs spontaneously if

$$\Delta S > 0 \;\; and \;\; T\Delta S > \Delta H$$

The quantity $T\Delta S$ became more important in this reaction when the temperature increase. During a fusion processes (evaporation and sublimation): $\Delta H_{fus} > 0$ e $\Delta S_{fus} > 0$, which means that when the temperature increase, also $T\Delta S_{fus}$ increases while for $T > T_{fus}$ we have $\Delta G_{fus} < 0$ (the fusion process in spontaneous).

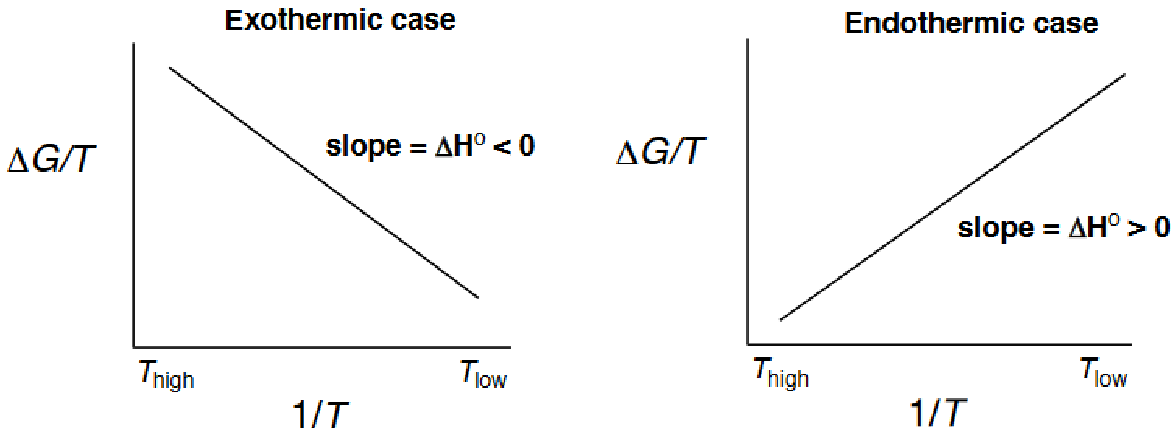

Figure 3.2. *Left*: Gibbs-Helmholtz plot for an endothermic reactions. *Right*: Gibbs-Helmholtz plot for an exothermic reactions.

For exothermic reactions, the slope for the Gibbs equation is negative (Fig. 3.2, *Left*). When the temperature increases the Gibbs free energy variation increases: $T_{final} < T_{initial}$, $\Delta G_{final} > \Delta G_{initial}$.
Instead, for endothermic reactions the slope of the Gibbs equation (Fig. 3.2, *Right*) is positive. Thus, when the temperature increases the Gibbs free energy change decreases: if $T_{final} > T_{initial}$, $\Delta G_{final} < \Delta G_{initial}$. When Gibbs free energy variation is negative at $T_{initial}$ (spontaneous process), increasing the temperature further decreases the Gibbs free energy variation *(ΔG).*

From equation (3.15) it is simple to verify the reaction spontaneity related to ΔH and ΔS signs. Being T positive, the following criteria of spontaneity is adopted:

$$\Delta G < 0 \;\; to\, T, P\; constant$$

considering P,T = *const.*, the different reactions are provided:

- $\Delta H<0$ e $\Delta S>0$ always spontaneous
- $\Delta H<0$ e $\Delta S<0$ spontaneous if $T\Delta S<\Delta H$ *or* $T\Delta S>\Delta H$
- $\Delta H>0$ e $\Delta S>0$ spontaneous if $T\Delta S<\Delta H$
- $\Delta H>0$ e $\Delta S<0$ never spontaneous

3.2.4. Enthalpy and Entropy of sublimation from Gibbs free energy

The enthalpy of sublimation can be also obtained combined the Gibbs free energy equation (3.16) which include the quantities: ΔG and ln(k), where k is defined as the reaction rate:

$$\Delta G = -RTlnk \tag{3.16}$$

and the ΔG *vs.* T dependence:

$$\Delta G = \Delta H - T\Delta S \tag{3.17}$$

which gives the final expression as:

$$lnk = -\frac{\Delta H}{RT} + \frac{\Delta S}{R} \tag{3.18}$$

In this case the *A* constant is: *ΔS/R* which can be obtained plotting *ln* of the constant rate with 1/T. From the slope of the curve it is possible to obtain: *ΔH/R*, while the quantity *ΔS/R* can be obtained by the intercept (*ΔS* is the entropy of thermodynamic process). Generally, the reaction rates "k" is assumed as the sublimation/condensation rates from/on specific surface (i.e. PCM surface in this work). In this way, obtaining the deposition rates of compound it is possible to determine the entropy and enthalpy variation in a temperatures range. Gibbs free energy can be also obtained in order to know the spontaneity or not of the reaction. In particular, the phase change from solid to liquid and liquid to solid are characterized by an increase of disorder: for solid-gas transition (sublimation) *ΔS* increases, i.e. $\Delta S>0$ e $\Delta H>0$ (endothermic process).

3.3. Thermogravimetry: basic concept

Thermogravimetry (TG) or Thermogravimetric Analysis (TGA) is a technique used in research and development of various compounds and materials in order to obtain information about thermal stability and composition and to monitor different processes, e.g. thermal processes namely sublimation, desorption or frosting etc. TGA technique measures the amount and change in weight rate of material as a function of temperature or time in a controlled environment (vacuum, air etc.). The TGA analysis has been frequently used to monitor the deposition/sublimation and absorption/desorption processes of volatiles compounds in different environments: outgassing rates from degassing in space [Wood 1996], dehydration and organics decomposition in minerals [Serpaggi 1999] and the fate of various materials in atmospheric environments [Elder 1997]. These kind of measurements are used to determine the composition of materials (volatiles and refractory materials can be distinguished) and to predict their thermal stability at temperatures up to 1000-1600°C [Sundberg 2004, ELTRA 2016]. By means of TGA, the following processes can be monitored:

- Thermal Stability
- Oxidative Stability
- Composition of Multi-component systems
- Estimated Lifetime of a product
- Decomposition Kinetics
- The Effect of Reactive or Corrosive Atmospheres on materials
- Moisture and Volatiles Content

The materials can be characterize by means of the weight loss and weight gain giving several information about kinetic processes. Considering the weight loss the following processes can be examine in depth:

1. Decomposition: breaking apart of chemical bonds
2. Evaporation: loss of volatiles with elevated temperature with their evaporation rates
3. Reduction: interaction of sample to a reducing atmosphere (hydrogen, ammonia, etc)
4. Desorption: volatiles or low-volatiles desorption rates

On the other hand, with the weight gain it is possible to study:

1. Oxidation: interaction of sample with an oxidizing atmosphere
2. Absorption: VOC molecules adsorbed
3. Deposition: VOC molecules condensed on a cooled surface

The change in mass measurement can be obtained with a frequency change in time of a microbalance system while a heating of the microbalance itself (with an integrated heater which allow to control the sample temperature within 0.1°C) allows to have the desorbed volatiles from deposited sample. Therefore, the sample is heated and simultaneously weighted and cooled with different thermal cycles. Arranging the microbalance and the sample in a specific environment (vacuum chamber, laboratory etc.), the temperature and pressure can be controlled by a separate system. TGA is often coupled with other analytical techniques as mass spectroscopy in order to obtain the molecular composition of loss volatiles from mineral [Grady and Wright 2003, Fermo 2006].

In figure 3.3 are shown two typical processes monitored with QCM: desorption and sublimation processes. In this study, several organic acids have been characterized using microbalance sensor equipped with an integrated heater in order to study the deposition and desorption processes.

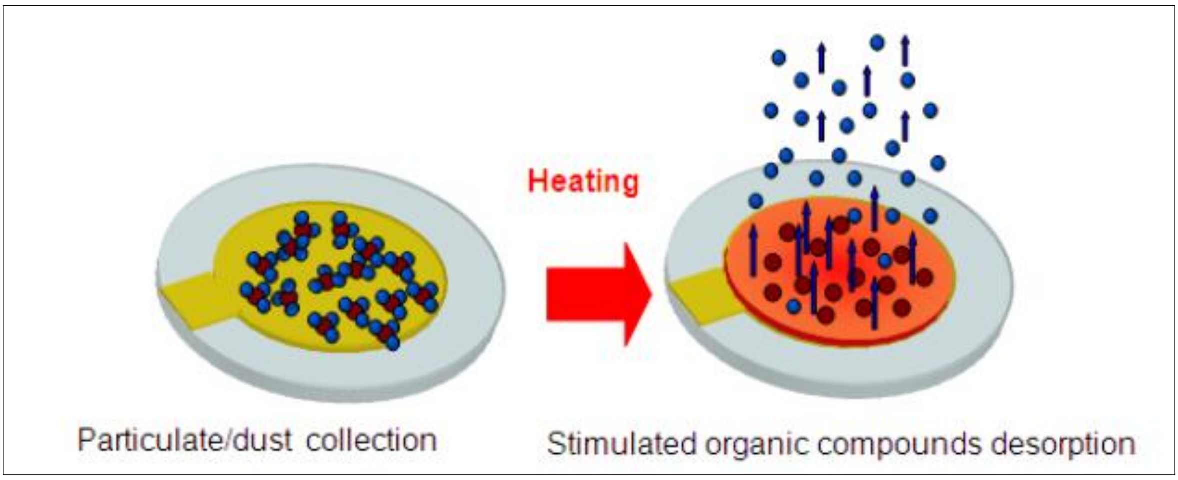

Figure 3.3. Organic material heating by means of microbalance built-in heater. The lighter material is able to sublime from crystal's surface whereas the refractory material (heavier) stand on microbalance surface. By means of frequency variation the mass change can be inferred.

3.3.1. Introduction to transduction mass sensors

The Quartz (SiO_2) is the second abundant mineral in the Earth crust and main constituent of magmatic and sedimentary rocks. In 1880, Jacques and Pierre Curie discovered that a mechanical deformation applied on some crystals, e.g. Tourmaline and Quartz, were able to determine an electric polarization, proportional to the applied deformation. This phenomena, i.e. the "direct piezoelectricity" effect which produces a shift of the electric charges when a mechanical stress is applied. Conversely, the "inverse piezoelectricity" effect, produces a mechanical deformation when an electric field is applied. The crystal which not show a centre of symmetry is able to take advantage from this effect. In dielectric materials (crystals, ceramics, polymers) without centre of symmetry, electric polarization can be generated by a mechanical stress application. The main important piezoelectric materials are listed below:

- Ceramics: Pb (ZrTi), O3 (PZT), PbTiO3 (PT), etc.
- Single crystals: Quartz, LiTaO3, LiNbO3, PZN-PT,etc
- Polymers: PVDF and copolymers, nylon, etc.
- Composites: PZT-polymer 0-3, 2-2, 1-3 composites, etc.
- Thin/thick films: PZT, PT, ZnO and AlN films

Quartz Crystal Microbalance (QCM) and Surface Acoustic Wave (SAW) sensors and chemically reactive materials have been realized using piezoelectric transductors. When piezoelectric device are used as sensors, it is possible to monitor the frequency and temperature for a thermochemical process by means of oscillator circuit. QCM is often used as device for mass monitoring thanks to small film deposition on electrode area which cause the variation of several characteristics of the sensors, i.e. the frequency. Thus, the electric magnitude monitored is the resonant frequency due to interaction between environmental molecules and the sensor. The microbalance is useful to monitor the deposition rates of thin films and the affinity between some fundamental molecules (as proteins) with a specific functionality surfaces (which helps their identification) in vacuum environment and liquid environment respectively.

3.3.2. Microbalance working principle

QCM is able to take advantage of piezoelectric effect thanks to the different SiO_2 cut which make it the most material used in this Sensoristic field. The crystal is composed by two different atomic species connected to ionic bonds. At equilibrium phase, the barycenter of positive and negative charges is coincident while when an external force is applied, the barycenter charges is unbalanced and a crystal deformation is obtained. The consequence will be a moment of dipole which polarize the external surface of the crystal. Thus, in the piezoelectric effect the electrical and mechanical deformations are completely connected.

Quartz Crystal Microbalance (or TSMR: Thickness Shear Mode Resonator, 0.8 - 40 MHz) has been the first piezoelectric device used for chemical reaction processes monitoring in biomedical and industries fields as well as for environmental applications where the mass, density, viscosity change in time were required. The QCMs are also used to monitor the absorption/desorption processes and materials corrosion. The piezoelectric crystal bends in different ways at different frequencies. This bending are called: vibration modes. The crystal can be assembled in different shapes to achieve different vibration modes. Several modes have been developed to operate over several frequency ranges: from low kHz range up to the MHz range. Figure 3.4 shows the vibration modes and the frequencies over which they can work.

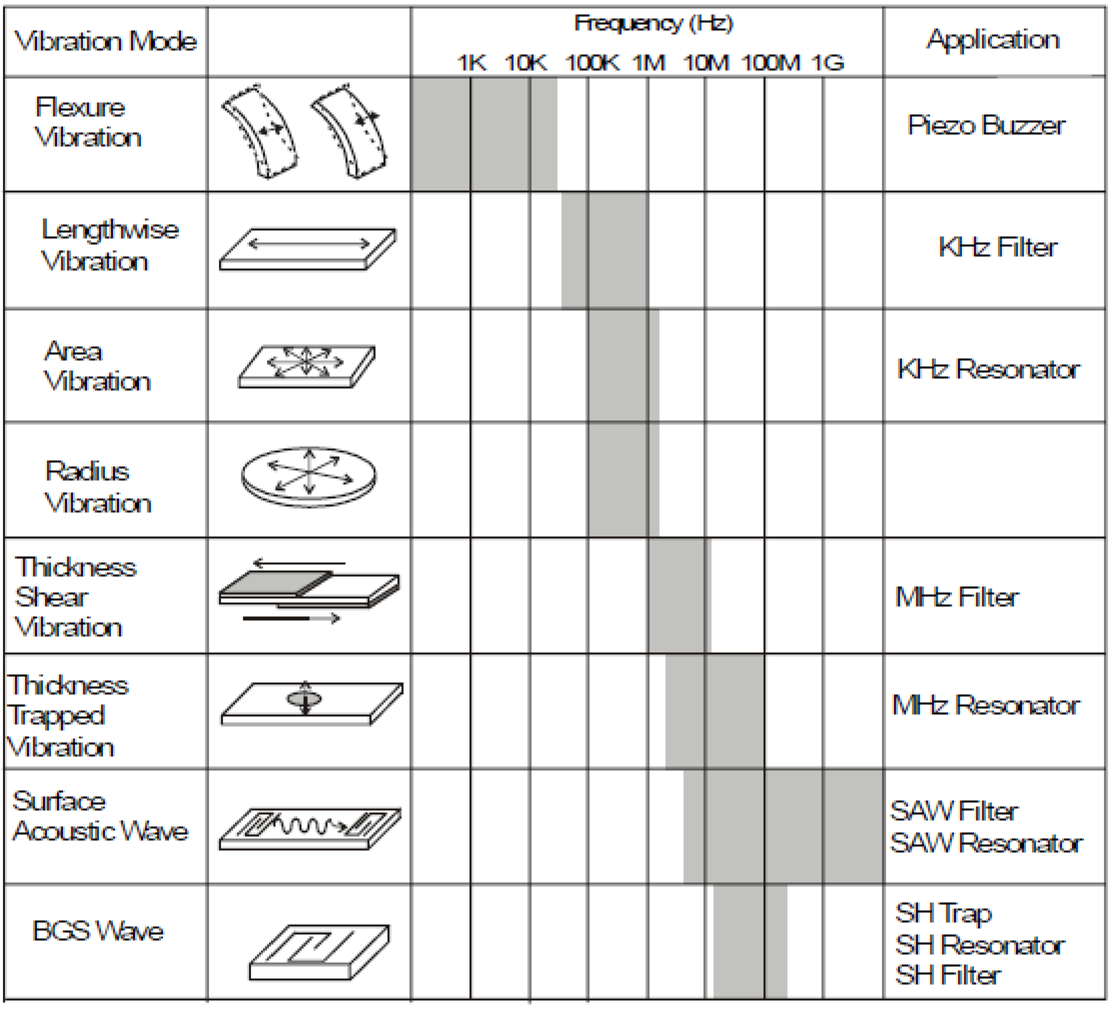

Figure 3.4. The possible Vibration Modes with Piezoelectric Ceramics. In particular, the QCM used here are Thickness Shear Mode Resonator type.

These sensors are composed by AT cut quartz plate (the material deformation act as scrolling of parallel planes) and metal foil (gold, chrome, platinum) whose goal is to spread out the acoustic wave generated by electrodes polarization (Fig. 3.5). Thus, the aim of the quartz is to convert the electric power provided by metal transduction into acoustic waves which are the material reticular vibrations. The generated acoustic waves are in transverse mode with a perpendicular propagation on the surface. Thus, the particles movement is parallel to the surface (Fig. 3.6). Considering the AT cut quartz crystal, the even (n) vibration mode which satisfy the relation are:

$$f = \frac{v_t n}{2l} \tag{3.19}$$

where v_t is the wave velocity in quartz plate (which is 3320 m/s for AT cut) while l is the plate thickness and n the harmonic order.

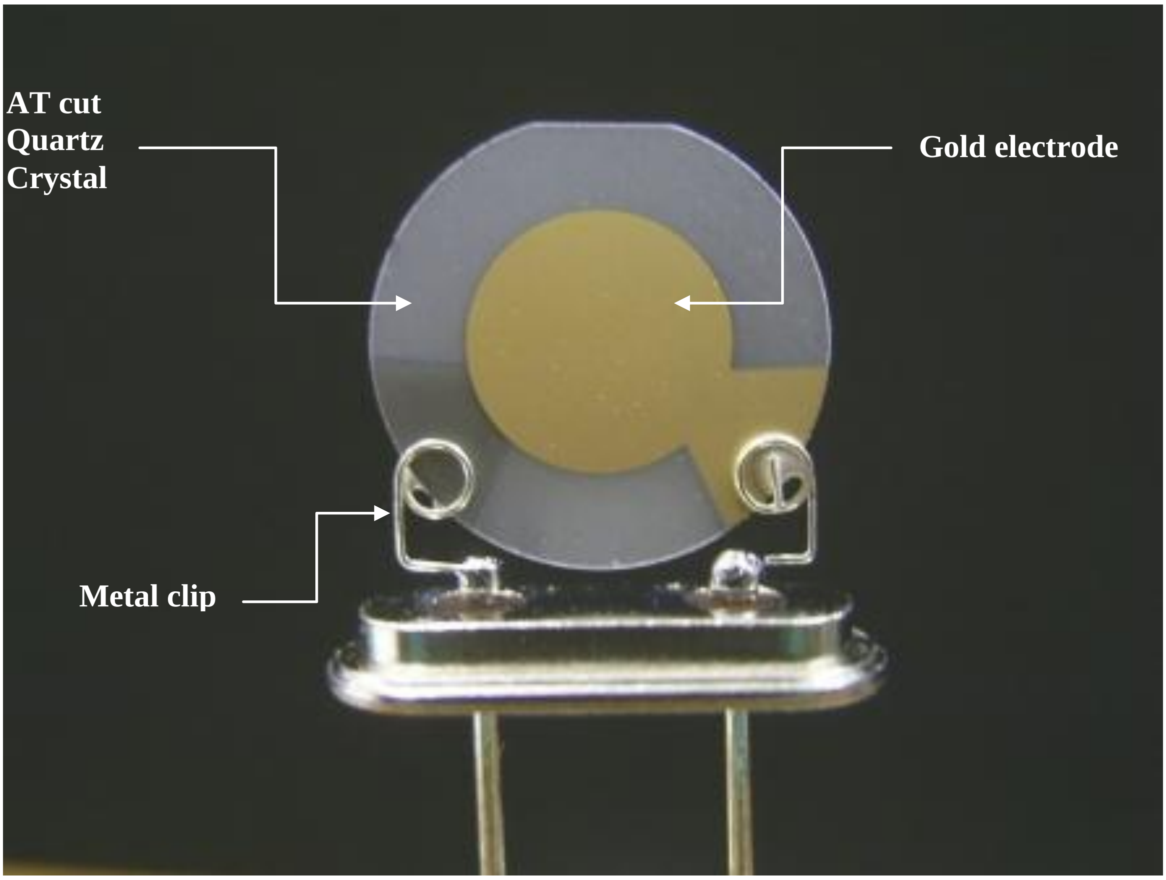

Figure 3.5. Quartz Crystal Microbalance (*from TamaDevice, Solution and Development*). In particular, quartz plate (transparent surface) and electrode (gold area) are shown. The crystal is supported by two metal clips.

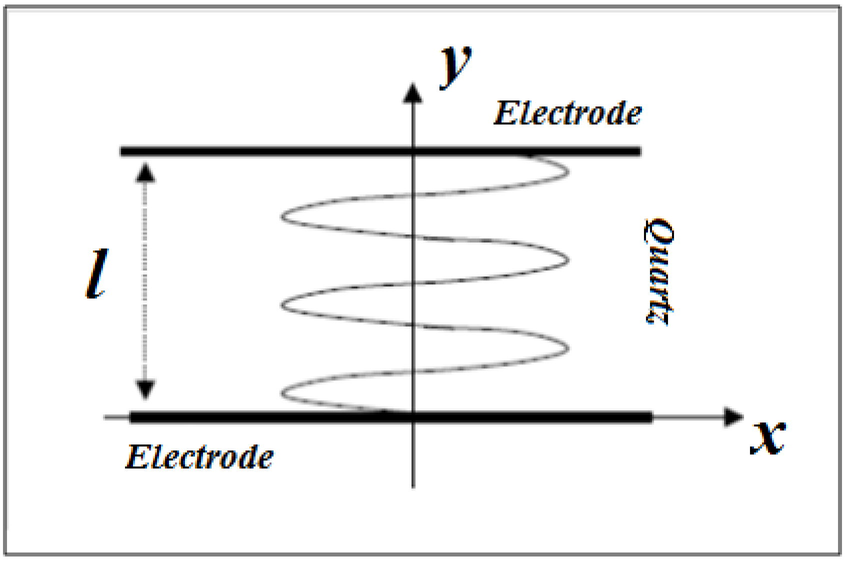

Figure 3.6. Waves propagation in QCM. The acoustic waves generated are transversal while their propagation is perpendicular to the surface.

The most important parameter is "*l*": the thickness of the crystal. In fact, varying "*l*" it is possible to have different resonant frequency of the crystal.

In order to perform TGA measurement, microbalance can be also provided by (integrated or external) heater and temperature sensor (a thermistor) (Fig. 3.7). The heater and the thermistor allow to monitor the desorption process of deposited material on the sensor, i.e. temperatures up to 200-250°C can be reached with thermal cycles to analyze the volatiles substance. In this case, the organic molecular bonds may break or leak and the desorption material can be quantify by means of the mass variation provided by the sensor.

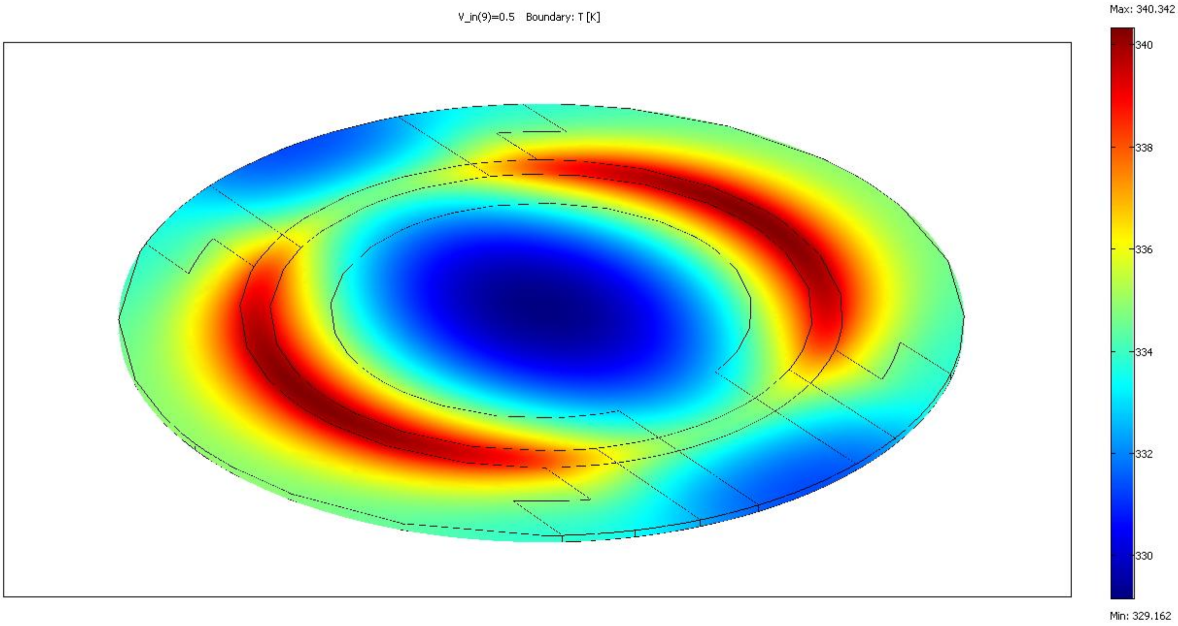

Figure 3.7. The areal temperature distribution results on QCM equipped with integrated built-in heater from thermal simulations. In the present design the heater and thermistor are placed onto the QCM opposite faces.

Figure 3.7 shows a thermal cycle that comes from thermal simulation results for a voltage of 1V, I=50 mA and a power of 50 mW in air. The experimental tests have been shown as the material deposited on blue areas is exposed to unvarying temperature. The temperature difference between built-in heater and built-in thermistor (blue and red areas) is about 10°C.

The microbalance system are sensors able to measure mass variation, Δm, from frequency variation, Δf, using AT cut crystals which vibrates transversely in the cut orthogonal direction. The propagation of the transverse acoustic wave happen through the crystal thickness: the waves are back reflected to crystal separation area. When a sensitive material is deposited on the quartz surface (e.g. gold), the wave will cross the interface (between the quartz and layer) propagating itself over the layer. Considering the same quartz properties for this deposited material, a thickness variation ("l" parameter) have to be considered. Taking into account the equation (3.1), it is possible to obtain the variation in the frequency, Δf, due to the thickness variation of the crystal, Δl:

$$\Delta f = -f\frac{\Delta l}{l} \tag{3.20}$$

the quartz mass is connected to the thickness:

$$m=\rho A l \tag{3.21}$$

where ρ is the density (2.65 g/cm^3) while A is the quartz area. By replacing the mass variation to thickness variation in the expression (3.20)

$$\Delta f = -\frac{f}{l}\frac{\Delta m}{\rho A} \tag{3.22}$$

Using the equation (3.19), the frequency variation can be calculated, obtaining the Sauerbrey equation:

$$\Delta f = -\frac{2f^2}{\nu_t}\frac{\Delta m}{\rho A} = -S_t \Delta m \tag{3.23}$$

where ν_t is the propagation velocity of the acoustic wave of AT cut resonator while "f" is defined as fundamental resonant frequency of QCM before layer deposition. In this case, S_t is the sensibility or Sauerbrey constant (a function of fundamental frequency square) which allow to connect linearly Δf with Δm. In particular, QCM sensibility is defined as the ratio between the frequency variation and deposited mass:

$$S_t = \frac{\Delta f}{\Delta m} = 2{,}26 \cdot 10^6 \frac{f^2}{A} \; Hz\, g^{-1} cm^2 \tag{3.24}$$

From eq. 3.24 it is possible to state that sensor sensibility will be higher reducing the electrode area and increasing the resonant frequency. The deposited mass will be detected the on electrode surface whereas the deposited mass outside the electrode will be not revealed. For these reasons, 3D distribution of the electrode mass sensibility is close to be a Gaussian curve as verified by Sauerbrey: it is maximum in the center and minimum at electrode boundaries. In figure 3.8, QCM mass distribution is shown. The eq. 3.24 is efficient for volatiles condensation on crystal surface. Indeed, assuming the deposited molecules as a film which vibrates at the same quartz resonant frequency, it is possible to consider these molecules as an additional substrate of crystal layer.

On the other hand, a solid grain (refractory particles) won't be completely integrated with the crystal' surface and will have a few contact points. These characteristics confirm the importance of this sensor to study the microscopic processes.

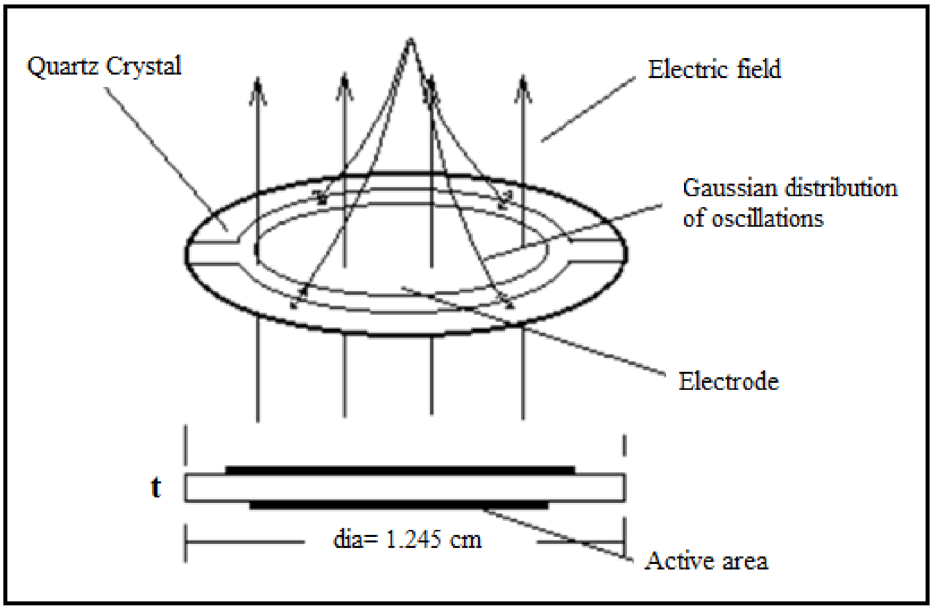

Figure 3.8. QCM sensibility distribution. This distribution is similar to Gaussian curve.

The quality factor (Q) provides information about the quartz resonator quality and is useful to compare the different piezoelectric materials. This parameter represent the ratio between the collected energy and dissipated energy: the value is high into quartz resonator (10^4 - 10^5). The product Q-f depends on material constant:

$$Q = 1{,}6 \cdot 10^{13} \left(\frac{1}{f}\right) s^{-1} \tag{3.25}$$

This relation provides an upper limit for Q which does not reach this value due to crystal defections (related to the impurity and production process). In table 3.1 the sensibilities of quartz resonators (which depends to the crystal frequency) are listed (from 1 to 25 MHz).

Table 3.1. QCM sensibilities for difference resonant frequencies.

QCM resonant frequency (MHz)	Sensitivity (Hz g^{-1} cm^{-2})
1	2.26×10^6
2	9.05×10^6
5	5.66×10^7
10	2.26×10^8
15	5.09×10^8
20	9.05×10^8
25	1.41×10^9

3.3.3. QCM and TGA application

In order to characterized a compound and to predict the impact of contamination on spacecraft and satellites (described in Par. 2.3), QCMs system can be used to obtain information about the temperature-dependent material and outgassing-deposition kinetics data. Generally, QCMs are usually used to measure the deposition rates of molecular species on a surface [Garrett 1994, Albyn, 2004] or to obtain typical thermodynamic properties of VOC's [Dirri 2016a, Freedman 2008]. The official method used for contamination monitoring is ASTM-E 1559 standard [Garrett 1994] for measuring outgassing and deposition kinetics by means of temperature-controlled source. The source term, which is representative of the

material's outgassing rate, can be used as input for computer programs that predict the rate of deposition of the emitted or outgassed material on another surface [Albyn 2004]. In ASTM-E 1559, the outgassing process is controlled by means of two polished QCMs with a sensitivity of at least 10^{-8} g/cm^2 Hz at 25°C with a natural frequency of 10-15 MHz. The QCMs are angled at 10° for the vertical so their axes intersect at a point 150 mm from the crystal surface. This intersection point is where the effusion cell orifice exit plane is positioned. QCMs are cooled at T≤193 °C by means of liquid nitrogen reservoir while the effusion cell (a cylindrical container 65±5 mm) is heated from 25 to 125°C with a precision of ±0.5°C or better. The cell orifice is at 150±1 mm from the surface of the sensing crystals [Garrett 1994].
In this work, a PCM provided by PE has been used in a similar way (as condensation point at -72°C) obtaining the deposition rates and the enthalpy of sublimation at different temperature steps. A PCM provided by built-in heaters has been also used to perform TGA cycles and obtaining vapor pressure and enthalpy of sublimation of analysed compounds (chapters 5 and 6).

3.4. VISTA instrument

VISTA (Volatile In Situ Thermogravimeter Analyser) is a μ-thermogravimeter system, developed by a consortium of Italian institutes, which aims to perform planetary in situ measurements [Palomba 2016]. The instrument is based on thermogravimetric analysis (TGA) and measures the change in mass of a sample as a function of temperature and time. VISTA is based on a lab-on-chip miniaturized sensor philosophy, since it has very small mass/volume and power requirements and needs a quite small amount of material for the analysis, i.e. less than 1 mg.

The VISTA head sensor consists of a PCM and the related Proximity Electronics (PE). The main innovation introduced is the PCM special design equipped with two built-in resistors, placed on the opposite faces on the crystal, acting as heater and temperature sensor, respectively (Fig. 3.9). Considering the built-in heater and built-in thermistor design (the resistances configuration: heater - thermistor are in parallel) the power budget and total resistance required to produce a temperature difference is even half. Thus, the presence of the built-in heater reduces the power needed to reach high temperatures. Thus, it is possible to measure the actual temperature of the PCM sensing crystal by means of a calibration: temperature sensor resistance as a function of the crystal temperature.

VISTA is composed of two sensor heads, i.e. the Sensor Head 1 (SH1) for in-orbit measurements and Sensor Head 2 (SH2) for in-situ measurements, respectively. Each sensor head includes a sensing piezoelectric crystal and related proximity electronics. The VISTA Main Electronic Unit can be shared with other sensors. This allows VISTA to contribute to the total payload mass with the sensor heads, only, being less than 100 grams a sensor head. The VISTA block diagram is shown in Fig. 3.10.

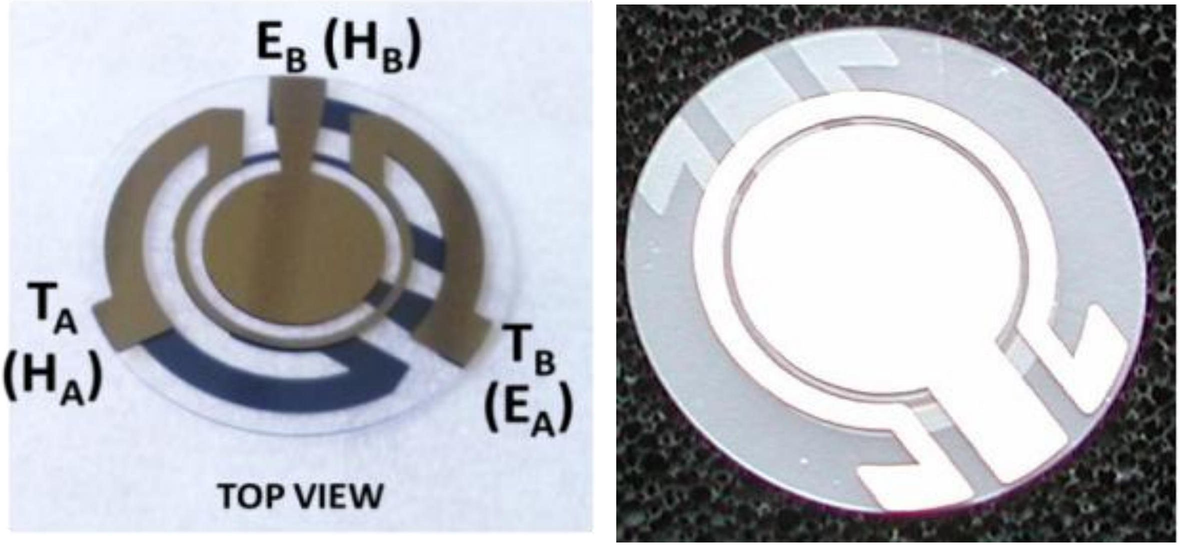

Figure 3.9 [Palomba 2016]. Picture of a crystal used for VISTA, produced at the IIA-CNR Facility Center. The central area is occupied by the electrode, the sensitive area of the crystal. The Omega-shape element surrounding the electrode is a built-in resistor acting either as heater or temperature sensor. This configuration, i.e. electrode surrounded by built-in resistor, is replicated on the opposite face of the crystal. *Left*: quartz crystal used in SH1 breadboard. *Right*: $GaPO_4$ crystal in SH2 breadboard.

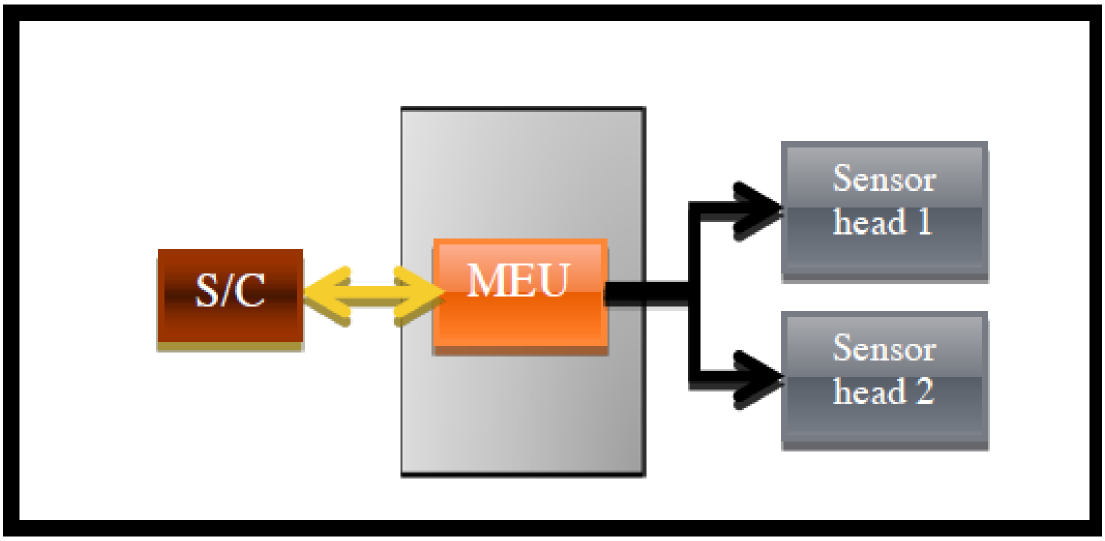

Figure 3.10. VISTA instrument composed by SH1 and SH2. The MEU manage the sensor heads both and can be shared with other device.

In order to study the scientific performance of VISTA instrument, one Engineering Model (EM) and laboratory breadboard have been developed for SH1 whereas a laboratory breadboard have been realized for SH2. Following the ESA Technical Readiness Level (TRL), i.e. Fig. 3.11, which is generally used to define the progress level reached for scientific instrument based on technological ripeness, the SH1-EM is at 5/6 level while the SH2-breadboard is at 4/5 level.

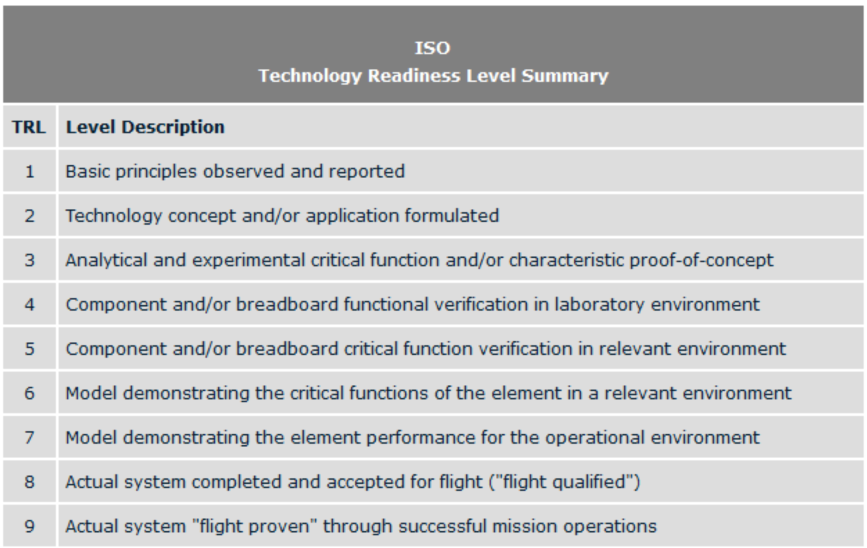

Technology Readiness Levels. *Credit: ESA*

ISO Technology Readiness Level Summary	
TRL	**Level Description**
1	Basic principles observed and reported
2	Technology concept and/or application formulated
3	Analytical and experimental critical function and/or characteristic proof-of-concept
4	Component and/or breadboard functional verification in laboratory environment
5	Component and/or breadboard critical function verification in relevant environment
6	Model demonstrating the critical functions of the element in a relevant environment
7	Model demonstrating the element performance for the operational environment
8	Actual system completed and accepted for flight ("flight qualified")
9	Actual system "flight proven" through successful mission operations

Figure 3.11. ISO standard 16290 Space systems. Definition of the Technology Readiness Levels (TRLs) and their criteria assessment. Instruments and spacecraft sub-systems technical maturity with respect to a specific space application are classified according to a "Technology Readiness Level" (TRL) on a scale of 1 to 9.

Each sensor head (Fig. 3.12) includes a piezoelectric sensing crystal, a frequency reference (a crystal or a digital oscillator) and related proximity electronics. The piezoelectric material is quartz for SH1 and $GaPO_4$ for SH2: this selection is justified by the fact that SH1 works at temperature up to the ice sublimation (i.e. 180 K) and quartz has better thermal stability in this temperature interval, whereas SH2 works up to organics temperature desorption (i.e. 470-570 K), where $GaPO_4$ maintains its piezoelectric properties differently than quartz. Each crystal is equipped with a built-in heater, in order to perform thermogravimetric analyses, and a built-in temperature sensor capable of measuring the crystal temperature with an accuracy of ±0.1°C.

Figure 3.12. VISTA instrument. *Left*: SH1 Engineering Model (double crystal configuration, explained in subpar. 3.4.1). *Right*: SH2 breadboard (single crystal configuration, subpar. 3.4.2).

Proximity Electronics are composed of an oscillator and a beating circuit. The oscillator circuit converts the electromechanical oscillation of crystals into sine wave signals having frequencies equal to the crystal resonance frequencies. The beating circuit gives in output the beating between the sensing crystal frequency and frequency reference (to have a frequency difference in output allows to minimize the noise occurring for transmission for high frequency signals).

Table 3.2. The resources, operating conditions and some performance parameters of VISTA sensor heads.

Unit	Sensor Head 1	Sensor Head 2
Sensor type	Quartz Crystal Microbalance	$GaPO_4$ Crystal Microbalance
Resonant Frequency [Hz]	10	5.8
Mass [g]	90	90
Volume [mm]	50x50x38	50x50x38
Power [W] (peak/mean)	1.0 / 0.12	0.62 / 0.37
Data rate	30 bit/measure	30 bit/measure
Operating Temperatures [K]	<180	<550
TRL	6	4
Sensitivity	4.4 ng cm^{-2} s	100 ppm

VISTA has been selected for MarcoPolo and MarcoPolo-R (M3-ESA mission study), a sample return mission [Barucci 2011] which aims to bring to Earth samples (100g) of a primitive Near-Earth Asteroid (NEA), i.e. 2008EV5. VISTA has been included in the MarcoPolo-R scientific package [Palomba 2012]. VISTA has been also studied for Phase A of JUICE (JUpiter and ICy moons Explorer), in order to perform in-situ measurements on the Europa and Ganymede surfaces. Their main scientific objectives were: the composition of non-ice materials, discriminations between water ice and clathrate hydrates, detection of organics) [Gowen 2011]. VISTA has found application for in-situ mission on Mars (dust and ice settling rate, water content, humidity) [Palomba 2011], on the Moon (water ice detection, water/organics content in regolith) [Longobardo 2013], on Venus (dew point of cloud condensable species, composition of refractory component of clouds) [Wilson 2011] and on Titan (methane dew point and organics content in near-surface aerosols) [Salt 1987].

3.4.1. VISTA Sensor Head 1 for *VOCs monitoring in space*

VISTA SH1 allow to monitor the contamination which occur on materials during in-orbit space missions. This kind of measurement (Par. 2.3) are fundamental since the contaminants outgassing can degrade critical surfaces, such as optical systems, solar panels, thermal radiators and thermal management systems. A experimental breadboard (Fig. 3.13, *Left*) has been used to demonstrates the capability of SH1 to monitor the contamination in space. Laboratory tests have been performed and well described in chapter 5. SH1 shows a low mass (less than 200 grams), low volume (smaller than 5x5x5 cm^3) and low power consumption (never larger than 1.5 W). The main innovative characteristics of SH1 compared to QCM-based sensors used in previous space missions are:

1. *Temperature accuracy*: by means of a resistive element built-in on both sides of the crystal surface and resistance-temperature calibration of these elements it is possible to reach a good temperature accuracy (0.1°C or lower, which will facilitate the characterization of the deposited contaminant).
2. *Regeneration temperature range:* built-in resistive elements can act also as heaters, allowing the crystals' regeneration, in order to clean them from refractory contaminants. The use of integrated heaters extends the SH1 temperature operative ranges at temperatures up to 130°C or while the lower limit of the temperature operative range is -80°C. Moreover, a Thermo-Electric Cooler (TEC) is located under the reference crystal and is able to cool the temperature crystal down to 30°C less than the environmental temperature.
3. *Temperature control :* the presence of built-in heaters allows to maintain the crystals' temperature at a given set-point (within 0.5°C) even when temperature variations of external environment occur.
4. *Measurable mass range:* the range of deposited mass measurable spans from ng/cm^2 to hundreds of $\mu g/cm^2$. This large range fully includes the molecular cleanliness requirements of many scientific payloads, such as the XMM optics (200 ng/cm^2) [de Chambure 1997], the SPICA telescope (200 ng/cm^2), the Herschel telescope (4$\mu g/cm^2$) or the ATHENA X-ray spectrometer (4 $\mu g/cm^2$). In case of hundreds of $\mu g/cm^2$ are deposited on the crystal surface, a saturation should be obtained (the expected beat frequency trend is "zero"). Thus, a regeneration of the crystals is possible with the built-in heaters.
5. *Frequency resolution:* of 0.1 Hz (corresponding to 0.44 ng/cm^2).

VISTA SH1 is composed by the Temperature Control System (TCS) and PE, the harness and the User Interface (UI) developed in LabVIEW software, which is able to control the sensor head operations and read the output data. The sensor head is the instrument core and is composed of three separate sub-units packaged in a shielded enclosure (Fig. 3.13, *Right*):

- *1st sub-unit:* it is composed of two crystals, mounted in a sandwich-like configuration (or double crystal configuration), the *sensing crystal* (top crystal), exposed to the external environment and collects the outgassing material and the *reference crystal* (bottom crystal). The output signal is the beating frequency (the difference in oscillation of the reference and sensing crystals), not affected by temperature effects.
- *2nd sub-unit*: it is the Temperature Control System (TCS), which can drive and regulate the crystals' temperature of ±30°C with respect to the temperature of the external environment in the range from -80 to 130°C. It is composed by built-in resistors on the crystals (i.e. the two heaters and the two temperature sensors) and the Thermo-Electric Cooler (TEC), used to cool the crystals and placed under the reference crystal.
- *3rd sub-unit:* it is the Proximity Electronics (PE), including an oscillator and a beating module. The two QCMs' signals are sent to the beating module, which provides in output the beating frequency between sensing and reference crystal.

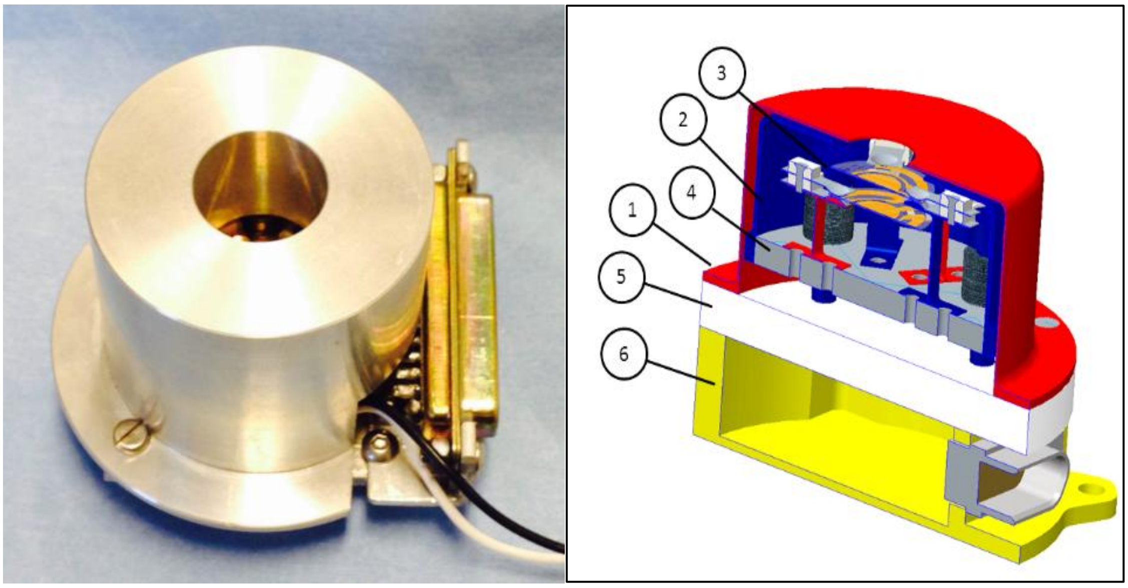

Figure 3.13. *Left*: SH1 breadboard used for laboratory experiments. *Right*: image of SH1 Engineering Model (EM).

The output signal from the sensor head is read out by MEU and monitored in real time by UI. MEU used for laboratory tests was composed of a NI-Compact DaQ Chassis and 3 different modules reading the RTD resistances (acquired and converted in temperatures) and the beat frequency from PE. MEU also drives the TEC and heater powers by means of three different PIDs implemented in the UI core. The harness is composed of shielded wires connecting MEU to PE. The UI allows reading and monitoring in real time the beat frequency, the electrical resistances, the temperatures of RTDs and heaters, the PE and metal case. A summary of technical characteristics of the different SH1 units is given in table 3.3.

Table 3.3. Technical characteristics of SH1 sensor head units and MEU. The regeneration temperature (up to 100°C) is reached by means of the built-in heaters of the crystals. In the passive temperature range (from -80 to -150°C) the TCS is not active but the temperature and mass deposited can be recorded. A saturation mass (or mass limit of the *sensing* crystal) of 734 μg/cm^2 has been measured during the performance test (see Chapter 5).

Sub-system	Mass (g)	Volume (mm)	Mass range (g/cm2)	Saturation mass (μg/cm2)	T range (°C)	Tstability (°C)	T accuracy (°C)	T resolution (°C)
Crystal	0.07	13.95x13.95x0.15	5×10^{-9} to 5×10^{-4}	734	-80 to 130	±0.5	0.1	0.01
PE	7.5	24x34x12	-	-	-40 to 85	±0.5	-	-
TEC	4.27	6.3x6.3x0.03	-	-	-50 to 130	±0.5	-	-

3.4.2. VISTA Sensor Head 2 for *atmospheric VOCs characterization*

Measurement techniques able to analysed different organic species have been raised during the last decade, improving the methods and procedure. These improvements have led to calculate the chemical and thermodynamical properties of the organic fraction of aerosol particles.

Moreover, organic materials, i.e. amino acids, nucleobases and carboxylic acids, have been proposed as complex organic molecules belonging to carbonaceous chondrites, being able to triggering the prebiotic synthesis of biochemical compounds in the early Earth [Andersen 2005, Briscoe 1993]. For these reasons, chemical-physical parameters are fundamental to know in order to have a complete characterization of a specific class of substances or mix of them.

In particular, different methods based on measurement of the evaporation rates and calculation of the enthalpy of sublimation/evaporation have been used to analysed the dicarboxylic acids: Thermal Desorption Particle Beam Mass Spectrometry (TPTD) method [Chattopadhyay and Ziemann 2005], Knudsen Effusion Mass-loss (KEM) [da Silva 2001], Knudsen Effusion Mass Spectrometry (KEMS) [Booth 2009], Tandem Differential Mobility Analyzer (TDMA) technique [Bilde 2003] and effusion method [Davies and Thomas, 1960, Granovskaya 1948]. Discrepancies between results obtained by the different methodologies were found to be up to two orders of magnitude, and this makes the acids characterization even more difficult [Dirri 2016a].

In the framework of VISTA, in order to show the capability of SH2 breadboard to characterize pure compounds, a PCM can be used with a new experimental setup (described in chapter 4). SH2 breadboard consists of PCM and the related PE (single crystal configuration). The sensible part of the crystal (the electrode) used for the experiment is shown in figure 3.14 (*Left*) while the experimental setup is shown in figure 3.14 at right and explained in depth in chapter 4.

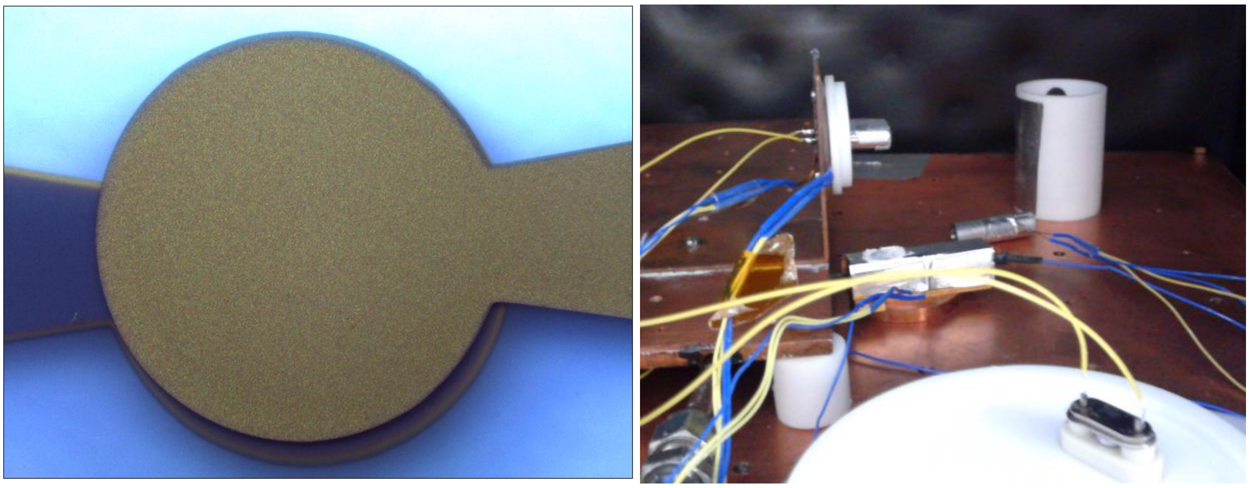

Figure 3.14. VISTA instrument. *Left*: PCM electrode. *Right*: SH2 breadboard well explained in chapter 4.

3.4.3. Aim of the work

In the VISTA framework, the aim of the work is to verify the capability of Sensor Head 1 and Sensor Head 2 breadboards to monitor the contamination processes in space environment and to characterize a compound (or a mix of them) in planetary environments, respectively.

In order to reach these goals, two experimental setups are designed and developed (chapter 4) while contamination and saturation tests are performed using SH1 breadboard (chapter 5) able to monitor the deposition processes from a contaminant source (organic compound). The capability of VISTA-SH1 to perform TGA cycles with the built-in heaters and to obtain some thermodynamic quantities, i.e. the vapor pressure and the enthalpy of sublimation will be verified and discussed. The results will be compared with results come from other methods of analysis (EM, KEMS, TDPD) (chapter 5 and 6).

On the other hand, different organic compounds are characterized using SH2 breadboard in order to demonstrate the capability of VISTA-SH2 to monitor a deposition process at low temperatures (i.e. asteroidal environment) and to characterize a compound by means of the Effusion Method (EM). Each compounds analysed will be characterized more precisely by retrieving its enthalpy of sublimation by measuring the sample deposition rates at different temperatures. The results will be discussed and compared with previous works (chapter 6).

Laboratory tests on SH1 and SH2 and data analysis on VOCs analysed aim to verify the capability of VISTA SH1 to monitor the outgassing processes in space and VISTA-SH2 to perform in-situ measurement and to accomplish several scientific objectives (i.e. compound/s identification) for the study of minor bodies of our Solar System and in planetary atmospheres.

Chapter 4. Laboratory set-up development

4.1. Introduction

In this chapter, the laboratory setup, the mechanical structure and flux calibration are explained. In particular, the design, development and testing of SH1 and SH2 experimental setup are introduced.

The processes monitored, i.e. contamination and TGA (for SH1 breadboard) and deposition processes (for SH2 breadboard) are described.

The breadboard design, the experimental setup design and the thermal test performed with SolidWorks software are explained. Thus, a calibration phase for SH1 and SH2 is introduced in order to discuss:

- the contaminant flux deposition at different temperature set-point (SH1 calibration);
- the PID parameters able to manage the built-in heaters during the TGA cycles (SH1 calibration);
- the molecules flux deposition using an effusion method in particular focusing the attention on the distance source-microbalance cycles (SH2 calibration);
- the fluctuations of sample temperature which may cause a flux instability during the deposition process (SH2 calibration).

The User Interface (UI) developed with LabView software to manage the breadboards, the experimental procedures and to monitor the vacuum system are also explained.

4.2. Monitored processes and method

In order to characterized a pure organic compounds, QCMs can be also used (after many deposition processes) performing TGA cycles by means of built-in heaters. Summarizing, in this work two different QCM methods have been used in order to monitor (described in paragraphs 4.3 and 4.4):

1. condensation processes for gaseous molecules in a controlled environment (deposition rates and enthalpies of sublimation are obtained using an effusion method, i.e. heating a cell with the sample);
2. a contamination process: a condensation and re-evaporation processes performed by means of TGA cycles in a controlled environment (deposition, sublimation rates and enthalpies of sublimation are obtained).

The enthalpy of sublimation can be obtained for both methods. Because of the importance of these laboratory measurement for outgassing monitoring and atmospheric aerosol characterization, the enthalpies of sublimation obtained have been compared (see chapter 7) with those obtained by previous works.

4.3. SH1 setup for VOCs monitoring in space

The SH1 breadboard with a double Quartz Crystal Microbalance (QCMs) configuration is used to help the characterization of materials and to monitor an outgassing process in space. A set-up has been built to test the VISTA SH1 capability to detect contaminant depositions at low temperatures in vacuum chamber (CRV, described in Par. 4.5).

The beat frequency is monitored together with other external parameters (chamber temperature, supply voltage and power consuming) in order to relate possible frequency changes with the variations of the these parameters.

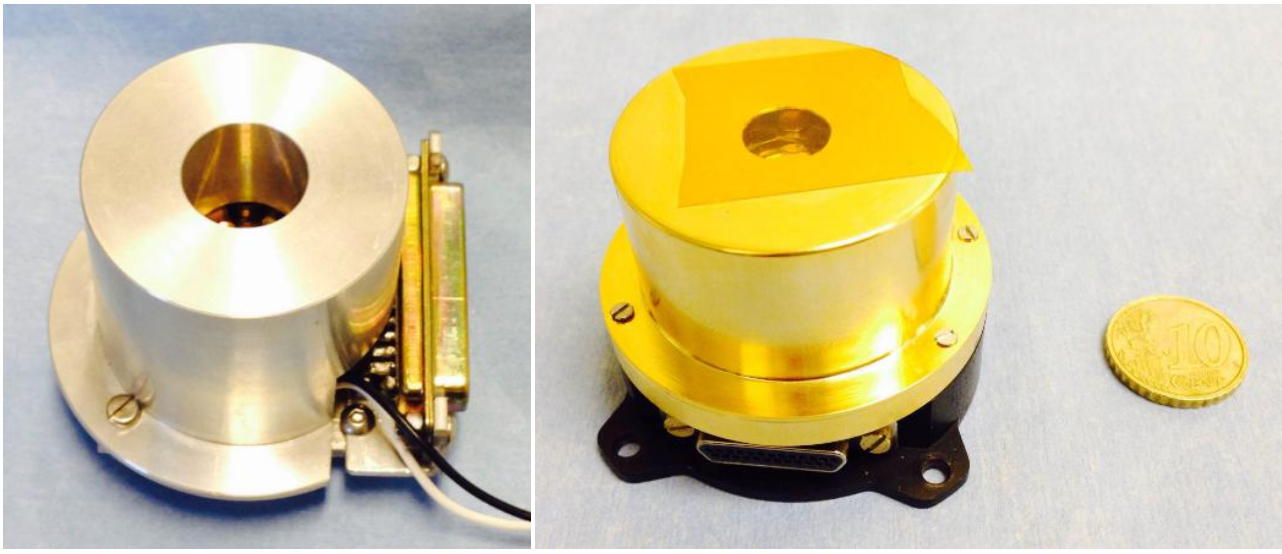

Figure 4.1. VISTA Sensor Head 1 (breadboard and engineering model) used for contamination tests (composed by condensation and TGA processes). *Left*: SH1 Breadboard. The metal cover whose mechanical structure is devoted to help the system thermalization is provided for cell entrance. *Right*: SH1 engineering model. The engineering model has been miniaturized, in particular the metal cover and micro-connector with 25 pin output have been used. In contamination set-up, the engineering model and breadboard are interchangeable.

The sensor head (Fig. 4.1) (engineering model and breadboard are used in the same conditions) is mounted on a copper S-shape in contact with the Global Heat Sink (GHS) or cold finger which can be heated or cooled by means of a Nitrogen circuit. An effusion cell containing 13-20 mg (contamination tests) and 50 mg (saturation test) of an organic volatile acid (adipic acid) has been used as contamination source.

The sensor head has been positioned on a S-shape support (copper material, thickness of 2 mm), in contact with GHS and shielded by an aluminum cover of cylindrical form (perforated in correspondence of the top crystal, Fig. 4.2 and Fig. 4.3). The metal cover favors the crystals thermalization at -80°C avoiding flux dispersion outside of the crystal area. The effusion cell containing the contaminant has been placed in the field of view (FOV) of the top crystal, which acts as mass attractor.

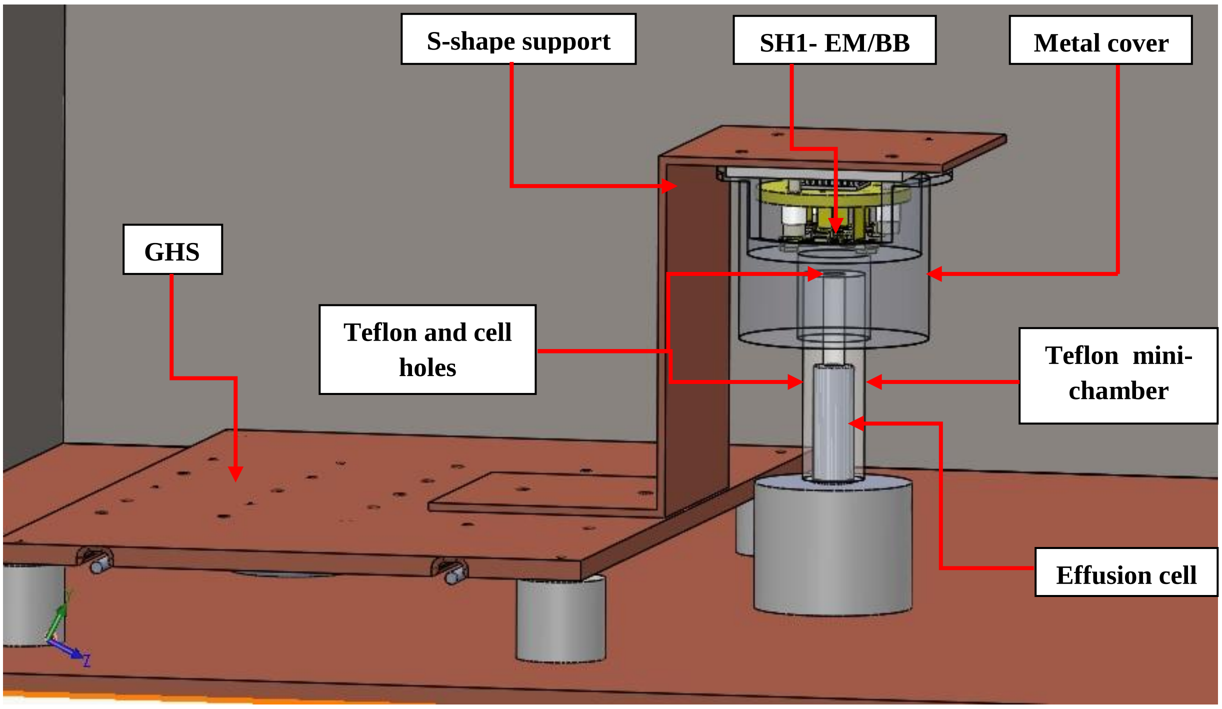

Figure 4.2 *(from simulations with SolidWorks software)***.** Setup for contamination test.

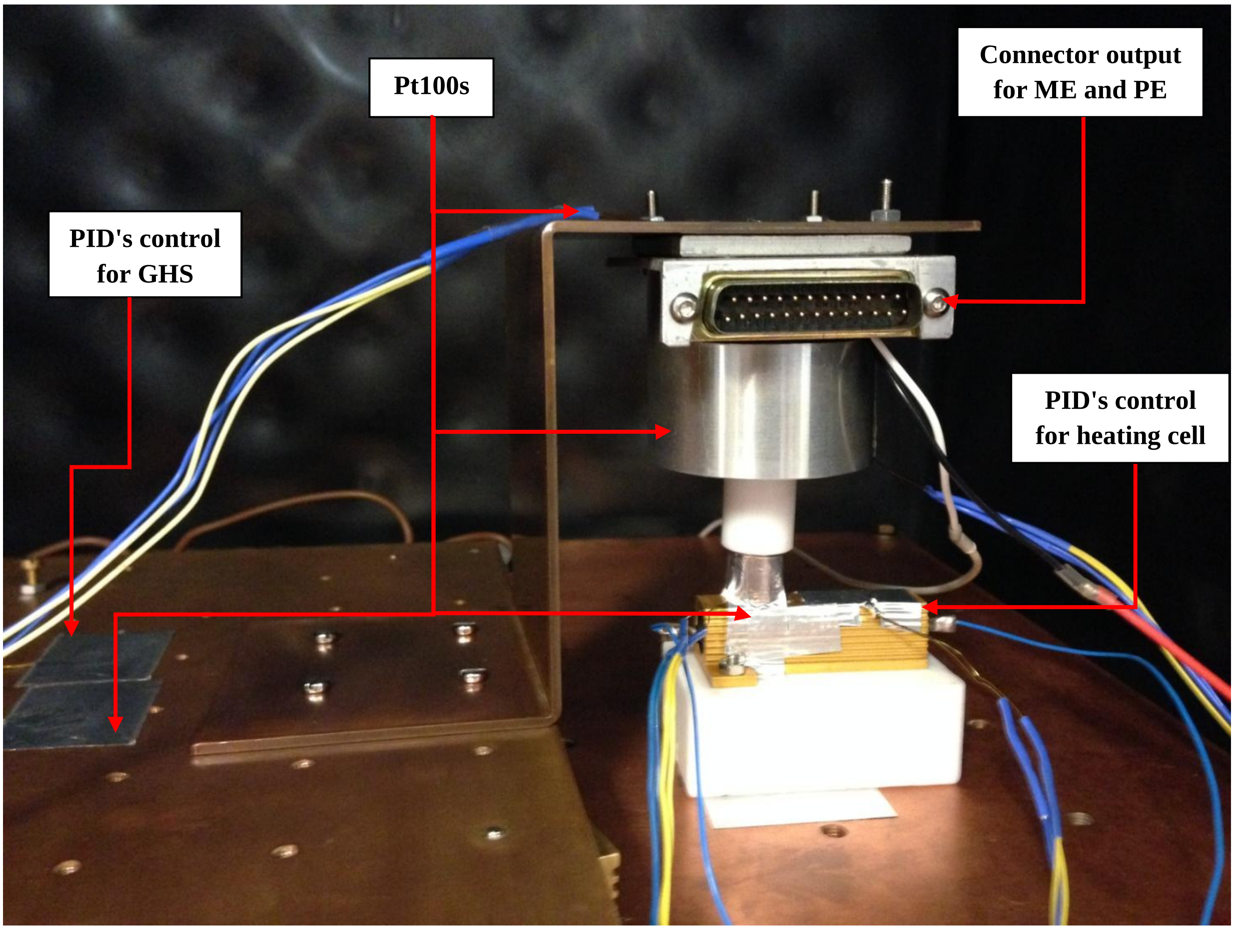

Figure 4.3. Engineering model and breadboard for SH1 used for contamination tests. Pt100s to measure temperature of S-shape, metal cover, effusion cell, aluminum base and GHS have been used.

Moreover, the effusion cell it is directly connected to resistor (25Ω) that heats the system from 25°C up to 120°C (saturation test). The effusion cell is managed by an external PID (Hengstler, Grado 901 type) (subpar. 4.3.3), the same used for the copper plate cooling. After PID's calibration by means of heating cycles similar to those applied in the experiment, we obtained a stability of the effusion cell temperature of ±0.3°C. This allowed us to obtain different fluxes at each set-point temperature from 25°C up to 120°C.
The cell has been placed in a teflon guide (with double stage of depth) and the contaminant can come out in gaseous form from a 5.3 mm diameter hole and focuses on the SH1 sensing crystal (top). The distance between the cell's hole and teflon guide's hole was 1.2 cm whereas the distance between the sample and top crystal was 2 cm (Fig. 4.2). In this manner the contaminant flux will be focused on SH1 sensing crystal (top) with the possibility to change the distance between effusion cell and top crystal (increasing or decreasing the volume of combustion micro-chamber). Thus, the setup composed of:

1. Global Heat Sink (GHS) provided by Nitrogen serpentine
2. Local Heat Sink (LHS) (aluminum base)
3. Teflon guide and support
4. Effusion cell
5. SH1 sensor head
6. Resistance (25Ω)
7. Platinum temperature sensors (Pt100)
8. Cylindrical aluminium case
9. OMRON device for temperature control
10. SH1 software and ME (NI DaQ-9178)

The measurement procedure shows the GHS cooled down to -80°C in order to have the sensor head at -72°C as shown by thermal simulations (described in subpar. 4.3.1) while the organic sample is heated with temperature step of 5/10°C from 25°C up to 120°C. After deposition steps, the effusion cell is switched off and TGA cycles are performed with built-in heaters in the temperature range from -70 up to +80°C. The temperature slope used were of 3.5 and 10 °C/min (for a ΔT=30°C) with stabilization time of 3-5 min per step.

During contamination and saturation tests (chapter 5), beat frequency, crystals' temperatures, Local Heat Sink (LHS) temperature and temperatures managed by PIDs control (GHS and effusion cell) have been monitored. The material deposited on top crystal have been measured during the effusion cell heating at different temperatures steps, whereas the desorption fluxes have been measured during the crystals' heating.

In order to evaluate the capability of SH1 to measure contamination fluxes at different set-point temperatures, the enthalpy of sublimation of the adipic acid (ΔH_{sub}) has been calculated by using the Langmuir method during the desorption processes.

The Langmuir equation [Langmuir 1913] makes it possible to obtain the enthalpy of sublimation (multiplied for a constant) as slope of the curve $ln(dm/dt)T^{1/2}$ *vs.*T^{-1} $[K^{-1}]$

$$ln\frac{dm}{dt}T^{1/2} = lnC - \frac{\Delta H}{RT} \tag{3.9}$$

where T is the temperature of top crystal (where the acid is deposited) whereas the frequency rates 'df/dt' are converted in mass rates 'dm/dt' obtained during the crystals’ heating.

By using Thermogravimetric Analysis (TGA), the enthalpy of sublimation has been obtained and compared with previous works [Booth 2009, Chattopadhyay and Ziemann 2005, Albyn 2004, Dirri 2016a] described in chapter 5.

4.3.1 Thermal simulations

The mechanical structure as described in paragraph 4.1 shows the GHS cooled by means of a thermal contact with a LiN_2 serpentine while the sensor head is mounted on a S-shaped copper support (thickness of 2 mm), in contact with the heat sink and shielded by an aluminum cover (perforated in correspondence of the top crystal, Fig. 4.2).

Thermal simulations performed with SolidWorks software (is a solid modeling computer-aided design (CAD) and computer aided engineering (CAE) software program) have been accomplished in order to estimate the time to reach -80°C on the crystals surface. In order to perform the thermal simulations, the breadboard and the crystals configuration (built-in heater and thermistors, Fig. 4.4, *Left*) has been design and developed following the initial design developed by consortium of institutes. The mechanical structure, including the mechanical supports (aluminum base and clothes pegs) have been considered to have an accurate thermal analysis (Fig. 4.4, *Right*). Each contact between the crystals and the clothes pegs has been verified by means of the software program verification.

Besides, a setup configuration including a copper plate (cold finger), a copper S-shape (for breadboard supporting) and a cover which can help the thermalization of the crystals have been designed and developed (Fig. 4.5, *Right*, bottom side).

In this simulation all the thermal contacts have been considered, i.e. between sensor head and copper S-shape and between the cover and aluminum base of sensor head (Fig. 4.2). The SH1 set-up has been perfectly built with SolidWorks software considering all the components: crystals, TEC, aluminum base (LHS) and cold finger (GHS) and their connections (clothes pegs).

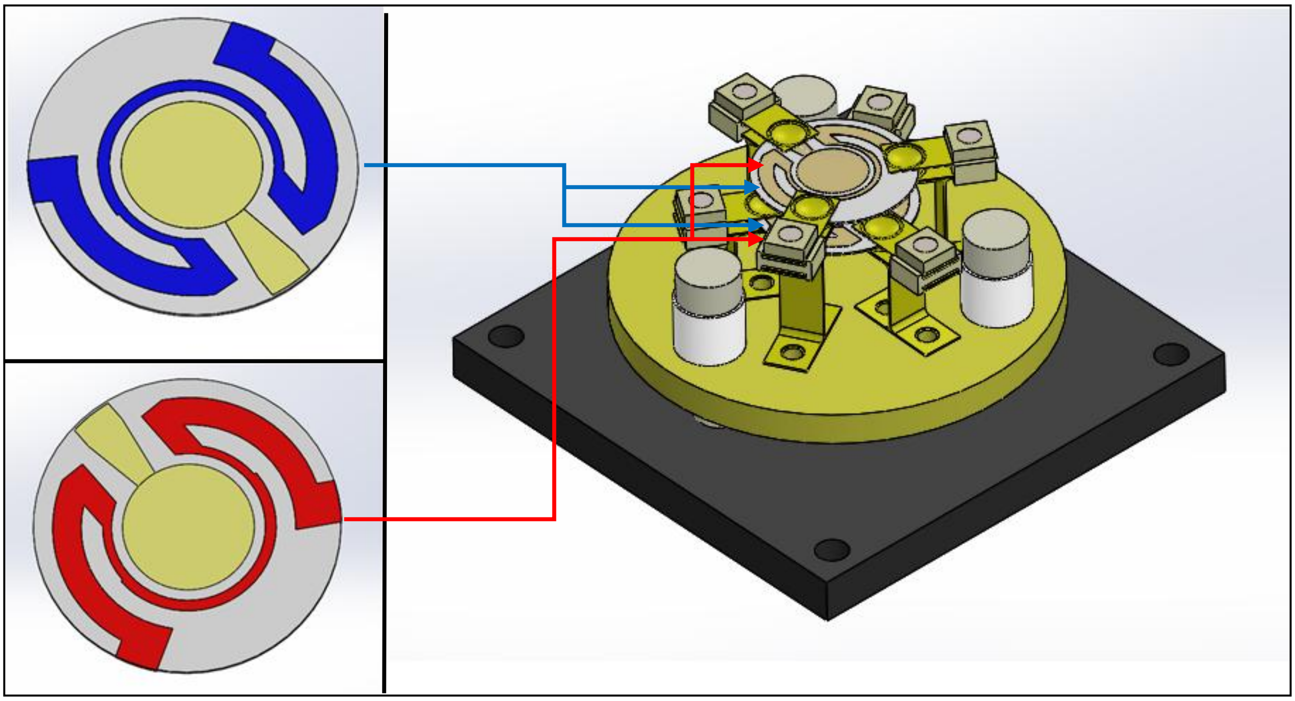

Figure 4.4. *(from SolidWorks Software). Left*: crystal configuration. The built-in heater (red) and the temperature sensor (blue) are placed in the opposite side of the crystal. With this configuration, the sample on gold electrode can be heated and the temperature monitored. *Right*: the breadboard configuration including the mechanical support and the metal clips for the crystals.

Temperature constraints have been considered for thermal simulation, i.e. the liquid nitrogen serpentine has been set at -80°C (the set-point temperature managed by a PID during the experimental phase) while the S-shape, BB, copper plate and effusion cell were set at 20°C. Besides, a thermal contact between a thermo-conductive glue and copper plate has been also considered into our simulations (real configuration). The thermal contact between the serpentine and plate, plate and S-shape, S-shape and SH1 breadboard have been considered to simulate the heat conduction.

In order to avoid the weigh down the simulation, the S-shape and basement plate irradiation were not considered on effusion cell (stable at 20°C). For the same reason, only one resistive element is considered on our simulation. In this manner, knowing the real resistance configuration on the crystal surface during the simulation process, we are able to measure its temperature by means a guide.

Copper material has been used in this thermal simulation for serpentine, plate and S-shape while aluminum material has been used for effusion cell and the BB components, i.e. metal cover, base and clothes pegs, excluding the small cylindrical supports for the clothes pegs, i.e. ceramics material. Teflon material has been considered for the copper plate supports and effusion cell base (Fig. 4.5).

In particular, the simulation has been analyzed in 6 different steps: from 300 s to 1800 s. Results for 300 s, 900 s and 1800 s are compared in Fig. 4.5. The temperature trends of S-shape, copper plate, crystals and metal cover are shown in Fig. 4.6.

Simulation results show that the crystals are able to reach -71°C after 30 minutes. At 1800 s the heat sink temperature is -79.6°C while the metal cover is at -74.5°C.

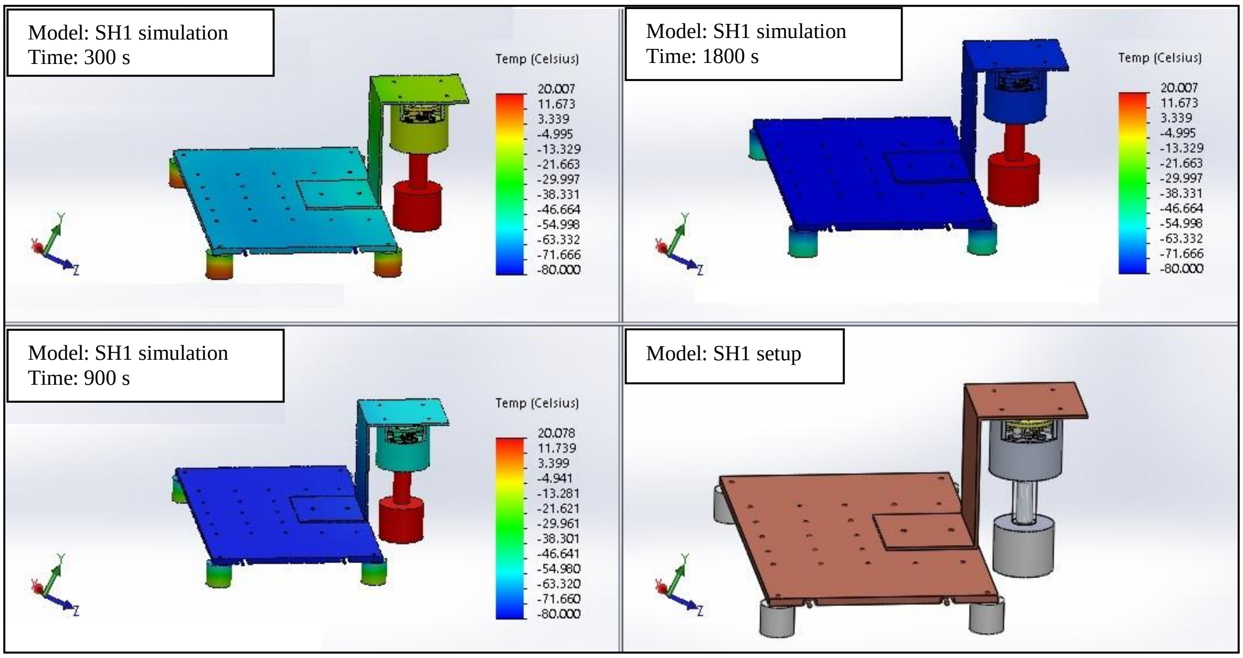

Figure 4.5 *(from SolidWorks Software).* Thermal simulation at 300 s, 900 s and 1800 s. After 1800 s, the copper plate is able to reach -80°C.

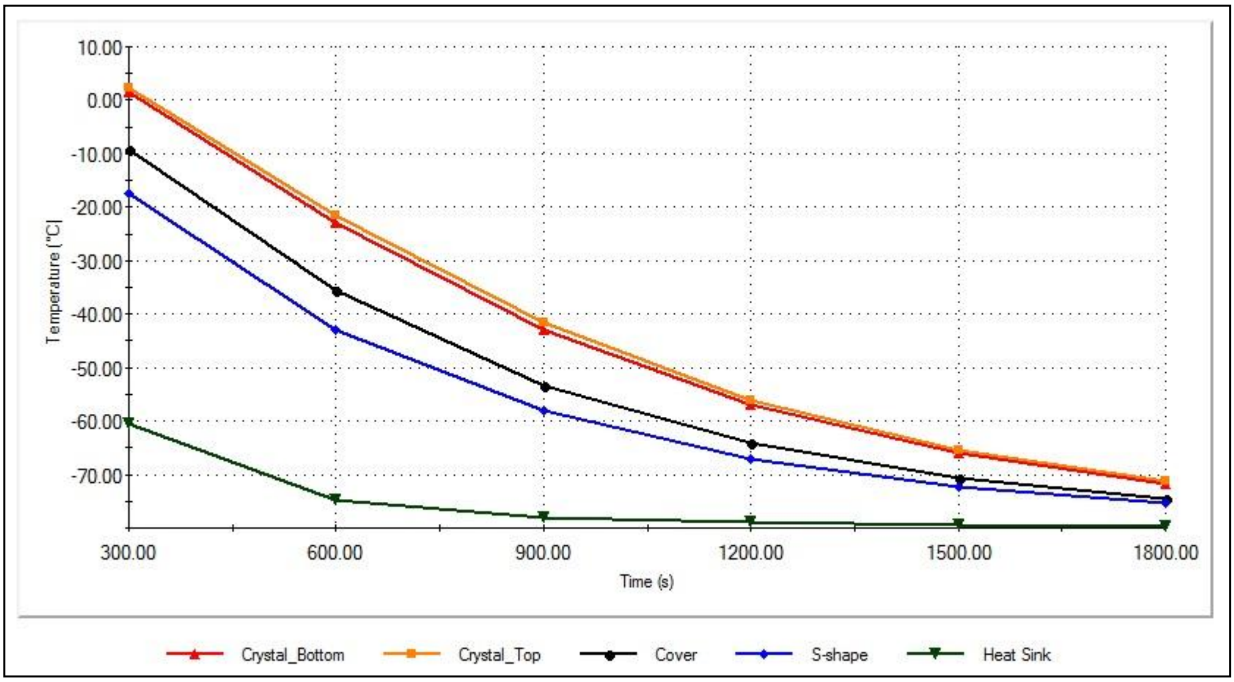

Figure 4.6. Thermal analysis (6 phases between 300 s to 1800 s) with serpentine of liquid nitrogen set to -80°C. The crystals temperature is of -71°C/-72°C after 1800 s.

Another result is that the difference between the crystals is 0.9°C at 300 s (1.3°C and 2.2°C, Bottom/Top crystal respectively), 1.3°C at 900 s (-43°C and -41.7°C, Bottom/Top crystal respectively), 0.5°C at 1800 s (-71.6°C and -71.1°C, Bottom/Top crystal respectively).

In order to obtain -80°C for crystals temperature a long stabilization time is required as shown in figure 4.6. From this plot, we can observe a slope change in the Temperature vs. Time curve, due to a slow stabilization at -71/-72°C.

After the cooling to -80°C, the effusion cell will be heated at different temperatures up to the sublimation of the adipic acid. The heating system will be managed by separate PID in order to control the resistance element within 0.5°C for every cell set point.

4.3.2. User Interface and Main Electronics

The User Interface (UI) is developed with LabVIEW software in order to manage and monitor the contamination and functionality tests of SH1. LabView has been used to develop a program for the acquisition data, the instrumentation control by means of integrated PIDs that manage the system, temperature control and data reading. LabView (Laboratory Virtual Instrument Engineering Workbench) is a system-design platform and development environment for a visual programming from National Instrument. The developed UI provide the data acquisition and managing, controlling the instrumentation (TEC and crystals), the data reading and data writing on file.

The UI is able to monitor and control:

1. the environment pressure (~10^{-6} mbar)
2. the built-in heaters of sensing and reference crystals and TEC by means of Proportional-Integral-Derivative (PID) cycles
3. the GHS, LHS, crystals, TEC temperatures
4. the frequency data (kHz or MHz) and the deposited mass
5. the effusion cell temperature
6. Data saving

The UI is divided into four panels (Fig. 4.7) devoted to:

1. PIDs control and settings (SETUP panel in Fig. 4.7);
2. temperatures and pressure control (CONTROL panel in Fig. 4.7);
3. temperatures controlling and frequency plots (PLOTS panel in Fig. 4.7);
4. contamination process monitoring (CONTAMINATION CONTROL panel in Fig. 4.7).

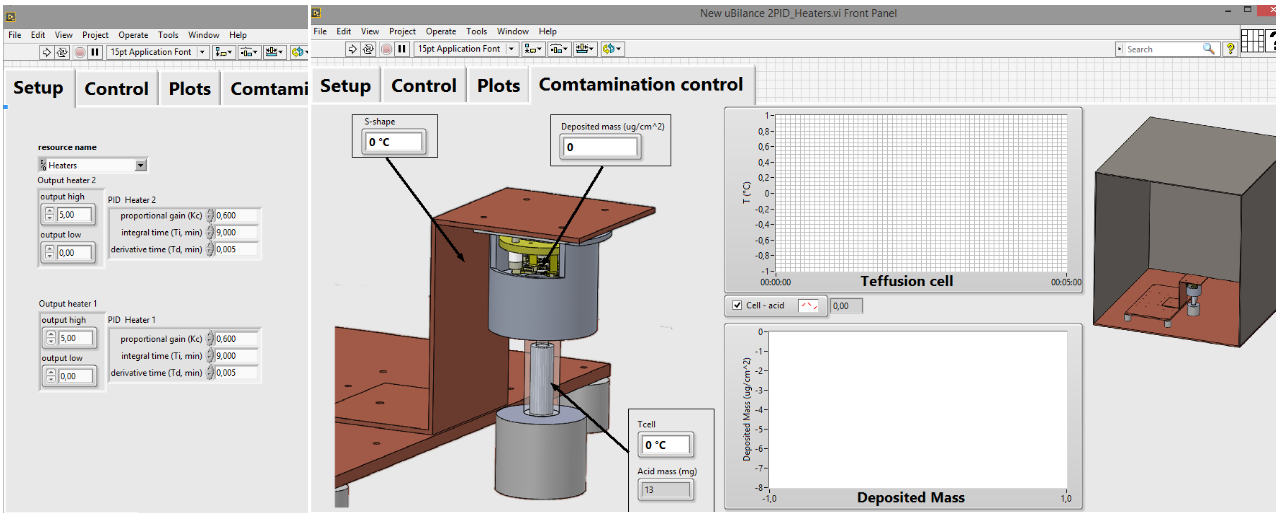

resource name: Heaters
Output heater 2
output high: 5,00
output low: 0,00
PID Heater 2
proportional gain (Kc): 0,600
integral time (Ti, min): 9,000
derivative time (Td, min): 0,005
Output heater 1
output high: 5,00
output low: 0,00
PID Heater 1
proportional gain (Kc): 0,600
integral time (Ti, min): 9,000
derivative time (Td, min): 0,005

S-shape: 0 °C
Deposited mass (ug/cm^2): 0
Tcell: 0 °C
Acid mass (mg): 13
☑ Cell - acid: 0,00

Figure 4.7. UI control panels. *Left*: the *SETUP* panel is devoted to manage the TEC and heaters PIDs (the calibration can be performed by settings the PID parameters). *Right*: *CONTAMINATION CONTROL* panel is able to monitor the deposited mass and organic source temperature.

The core of the program is shown in figure 4.8. The core program is divided in for main different section which are devoted: communicate with the instrumentation (breadboard, power suppliers for the heaters and TEC) and to have data reading and data saving on file (.tdms format), to assign the different channels for the acquisition and data saving, to manage the PIDs of heaters and TEC using different VI which contains the description about the functions that manage the heating/cooling cycles and to plot the trend of frequency and temperatures recorder by the system.

Summarizing the four sections, the LabVIEW core is divided in:

1. variable input and power supply VI communications (section 1 in Fig. 4.8);
2. channels data reading and saving (section 2 in Fig. 4.8);
3. PIDs control (section 3 in Fig. 4.8);
4. plots trend monitoring (section 4 in Fig. 4.8).

The PC/laptop is connected, via USB cable, to the power supply units for heaters and TEC elements. In order to be able to execute the User Interface software it is mandatory to assign the following labels to the three National instrument boards composing the Main Electronics:

- NI-9174 (4 slot USB Chassis)
- N°1 acquisition modules for resistors (NI-9217)
- N°1 acquisition modules for Pt100/Pt1000 (NI-9219)
- N°1 input/output module or digital (NI-9401)

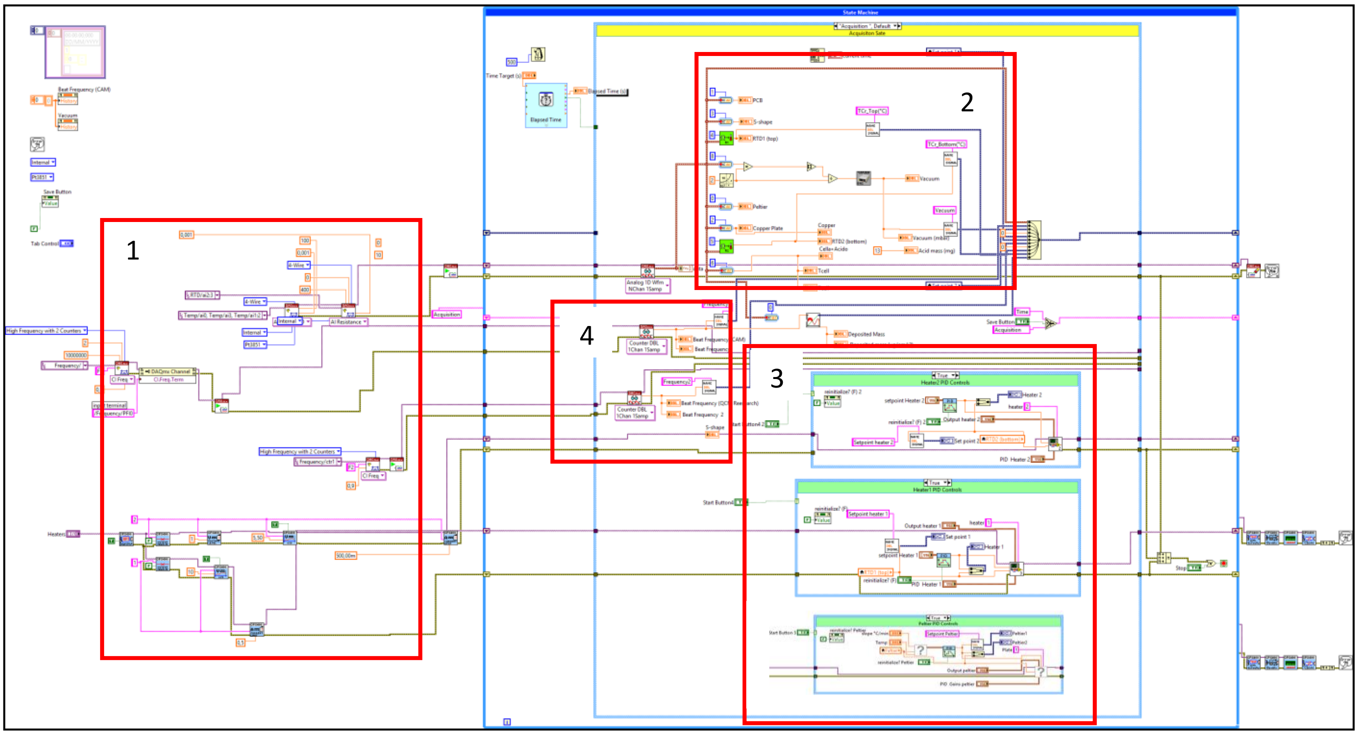

Figure 4.8. LabVIEW core program. Basically, four main section to control, data reading and writing, communications with external instrumentations (power supply for heaters and TEC) can be identified.

Figure 4.9. Main Electronics of Sensor Head 1. *Left*: NI-9174 Chassis. *Right*: NI boards used. The module NI9410 is devoted to frequency monitoring while the two modules NI9217 are devoted to heaters, TEC, PE and QCM cover temperatures control. In figure 4.9 are shown the NI9174 chassis and the three NI modules. The cables coming out from NI boards are shielded by teflon guide and coupled each other.

4.3.3. PIDs parameters and flux calibration

As results of calibration phase, PID (Proportional-Integrated-Derivative) controllers allowing to select temperatures and heating/cooling rate of heat sink and crystal have been implemented. PIDs parameters are fundamental to control and manage the effusion cell temperatures for desorption processes and the built-in heaters for TGA cycles. Three integrated sub-systems (Fig. 4.8, subpar. 4.3.2) have been developed with a LabVIEW software in order to:

- manage heating or cooling cycles (with slope of 1°C/min or less) to reach set-point temperatures with built-in heaters and Thermo Electric Cooler (TEC);
- performing PIDs calibration obtaining the Proportional, Integral and Derivative parameters.

The first and second sub-systems are devoted to control the heating cycles performed with built-in heaters taking in input the initial temperatures and the final temperatures set-point of heaters (in °C) and the total time (in seconds) of heating cycle. The third sub-system is devoted to control the cooling cycles by means of TEC taking in input the initial temperature and the final temperature set-point of TEC (in °C) and the total time (in seconds) of cooling cycle. The slopes of the cycles are automatically calculated inside the LabVIEW Virtual Instrument files (VIs) while the Proportional-Integrated-Derivative parameters can be set-up in the SETUP panel of LabVIEW front panel (Fig. 4.7, *Left*).

An external PID (Hengstler, Grado 901 type), is able to control the effusion cell temperature (in this case, the PID parameters have been also configured with a different calibration).

The Proportional (P) parameter regulates the answer time of the system to reach the set-point step by step: when P is high, a risk of instability is probable (in our case, 0.6 has been chosen). The Integral parameter (I) produces the effect to damp the typical oscillation produced by P parameter. A high value of I slows the system and consequently attenuates the oscillations (in our case, a value from 5 to 9 has been chosen). The derivative value (D) is used to obtain a faster answer in order to reduce the difference between the set point and the temperature of the heaters/TEC (a low value, i.e. 0.05).

In the first phase of PID calibration, a high value of P parameter (i.e. 1) has been set to check the answer of the heaters to reach a specific set-point temperature (e.g., 20 to 50°C). Then, in a second phase the P parameter has been reduced down to 0.6 in order to regulate the heaters. Successively, in order to make smaller the oscillations produced from P, the I parameter (i.e. 1) has been set for PID control. At later time, this value has been increased up to 9 in order to attenuate the oscillations.

In the end, in order to control and reduce the difference between heaters temperature and the final set point temperature, the derivative parameter has been set to 1 and at later set to smaller values, i.e. 0.05.

Thus, the built-in heaters are able to reach an accuracy within 0.1°C at each set point temperature (Fig. 4.10) while the effusion cell has been also able to reach a stability within ±0.3°C (Fig. 4.11).

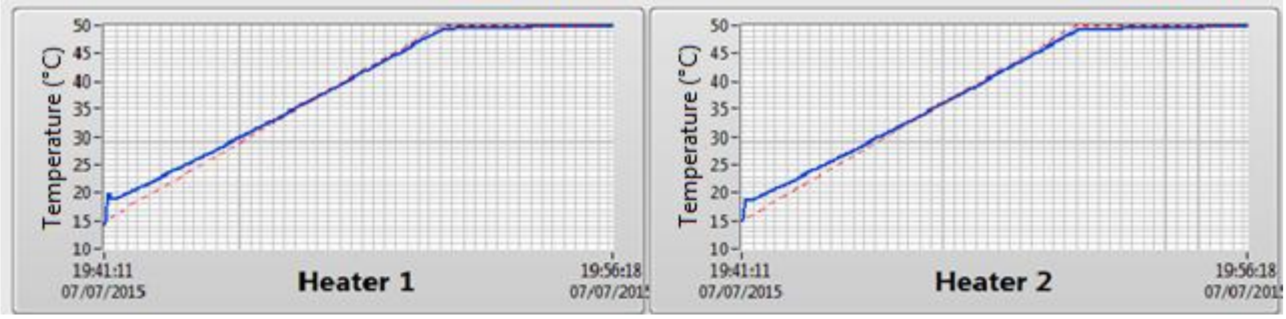

Figure 4.10. LabVIEW PLOT panel for built-in heaters calibration. *Left*: sensing crystal heater characterization in a temperature range between 20 and 50°C (slope 1°C/min). *Right*: reference crystal heater characterization in a temperature range between 20 and 50°C (slope 1°C/min).

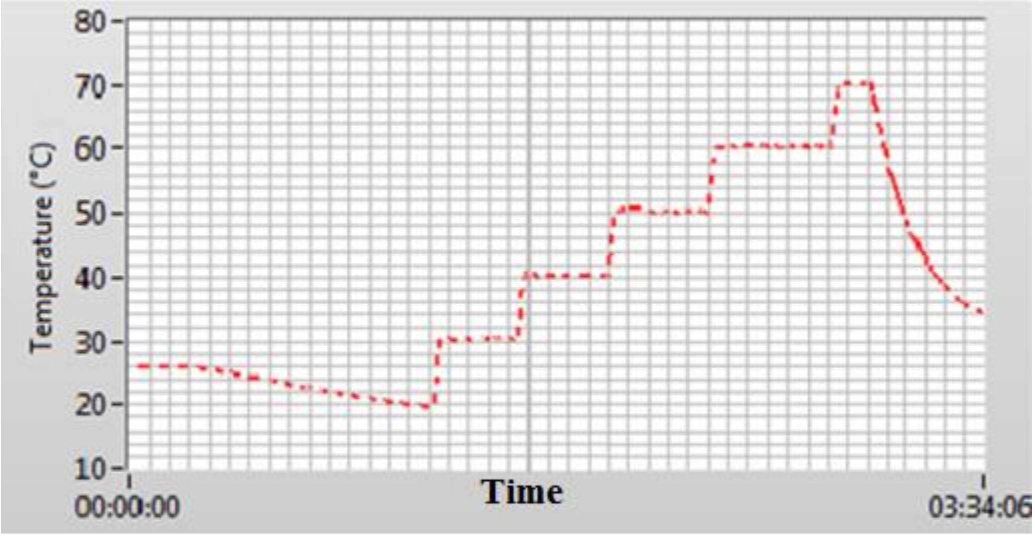

Figure 4.11. LabVIEW PLOT panel for effusion cell calibration at different temperature steps, i.e. from 30 to 70°C.

Taking into account the behavior which influence the molecules flux (well explained in subpar. 4.4.2 for the SH2 calibration), a distance of 2 cm between source and sensor head is used. Thus, performing a heating cycle calibration in the temperature range from 30 to 70°C (Δt= 20 min.) the molecules deposition is about 2.6 kHz up to 70°C (Fig. 4.12).

Using the linear regression analysis the frequency slope in addition to a linear regression coefficient for 40°C temperature step are obtained. The frequency data show a linear trend with r^2 coefficient >0.99 which make them valid for deposition measurement (Fig. 4.13).

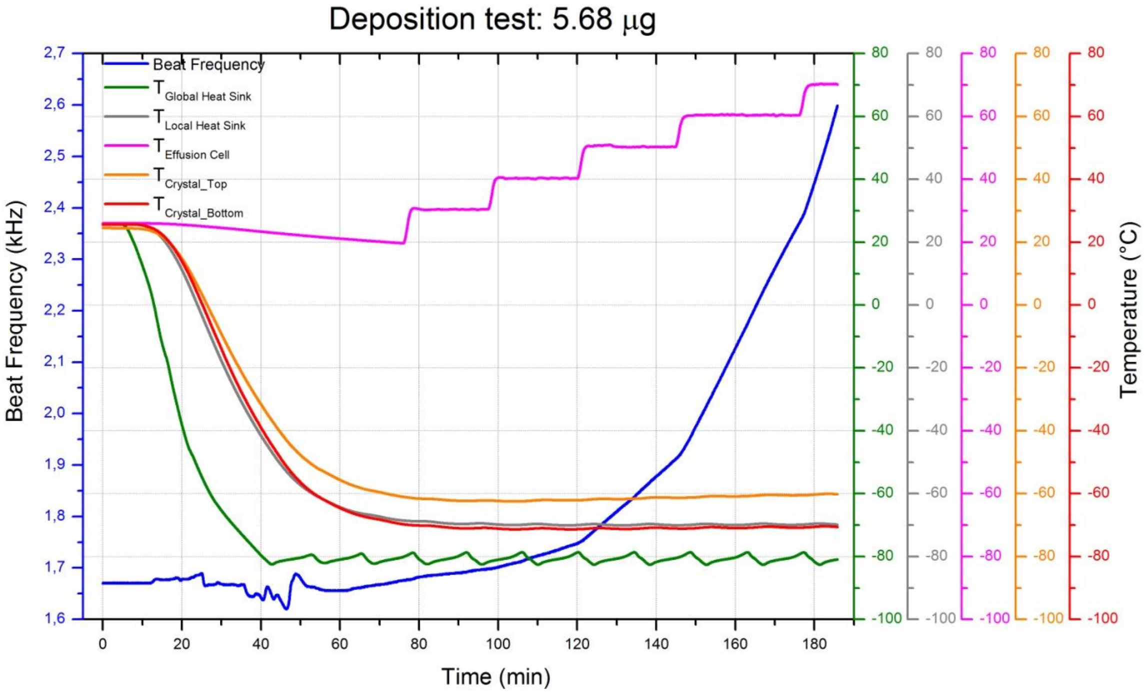

Figure 4.12. Molecules flux calibration with a distance source-sensor head of 2 cm. This configuration shows that the organic compound is going to deposited on the sensing crystal (the beat frequency increase).

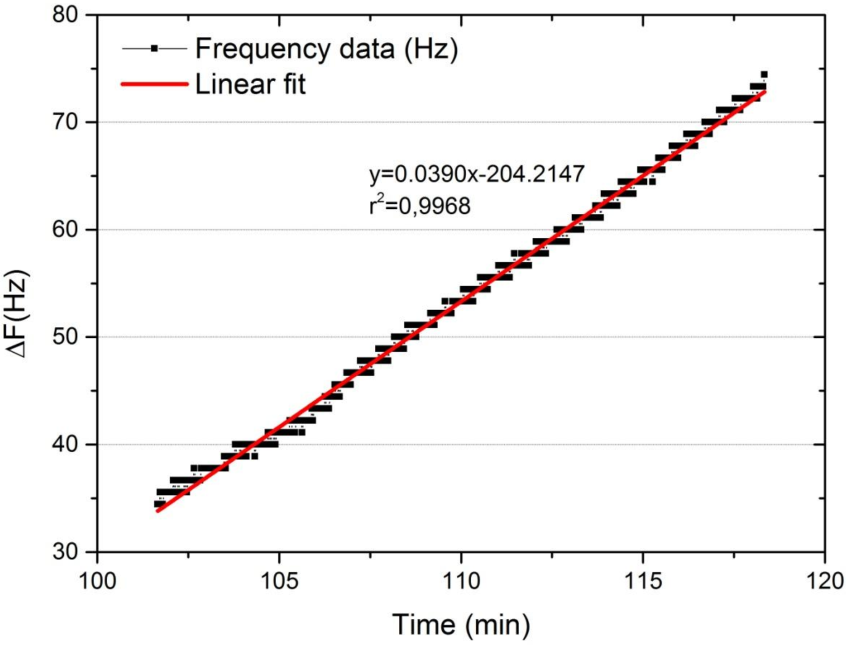

Figure 4.13. Linear regression coefficient for adipic acid temperature step at 40°C for contamination measurement. The acquisition data is performed every 2 sec. with time interval of 20 minutes. The r^2 test demonstrates that the data are valid for deposition measurement.

4.4. SH2 setup for atmospheric VOCs characterization

In the framework of VISTA sensor head 2, a single Quartz Crystal Microbalance (QCM) is used as condensation point cooled down to -72°C by means of a cold finger. The sample (organic compound) is positioned in effusion cell and heated up to sublimation. The setup is placed in vacuum in order to avoid water vapor condensation and to facilitate the sublimation process (occurring between 25°C and 80°C), whereas the cooled crystal works as mass attractor for VOC's molecules. This configuration allowed to measure the deposition rate of the VOC samples on the QCM at different temperatures and to infer the corresponding enthalpy of sublimation. A preliminary test to measure the enthalpy of sublimation by means of QCM was performed focusing and upgrading the thermal contact between QCM and the cold sink, by increasing the difference between sensor effusion cell temperature and QCM, improving the efficiency of QCM as mass attractor. This made it possible to measure deposition fluxes even at two close temperatures (e.g. $\Delta T=5°C$). However, a very small frequency variation (3 kHz) was observed, due to the low deposition of acid molecules (adipic acid), and the retrieved enthalpies of sublimation were different from previous works by about 20 percent [Chattopadhyay and Ziemann 2005]. The preliminary test results shown in subpar. 4.4.2 demonstrate how the temperature control at each temperature set point have to be improved whereas the distance between the sample and QCM have to be decrease to have a reliable fluxes to calculate the enthalpy of sublimation. In this work our accuracy has been improved as described in chapter 6.

4.4.1. Experimental configuration and measurement procedure

A Quartz Crystal Microbalance (resonance frequency of 10 MHz) has been used to monitor the transition phase (solid→gas) of some dicarboxylic acids in a controlled environment in order to obtain their enthalpy of sublimation.

The microbalance is composed of a quartz crystal having a diameter of 14 mm and a thickness of 0.2 mm. The electrode, the sensible area of the crystal, is located in the central part and has a diameter of 4 mm (Fig. 4.14). The microbalance is connected to its PE, including a frequency counter and an oscillation circuit, powered by USB-PC input.

In order to use the microbalance as an efficient mass attractor, the quartz crystal should be cooled with respect to the surrounding environment and in addition the VOC molecular flux should be focused onto the crystal. The QCM cooling is performed by means of a conductive connection to a copper plate in thermal contact with a coil containing liquid nitrogen. Finally, the QCM is enclosed in a metal case, acting as thermal shield and avoiding the QCM heating by irradiation of internal wall of the vacuum chamber, which are at ambient temperature (see Fig. 4.15).

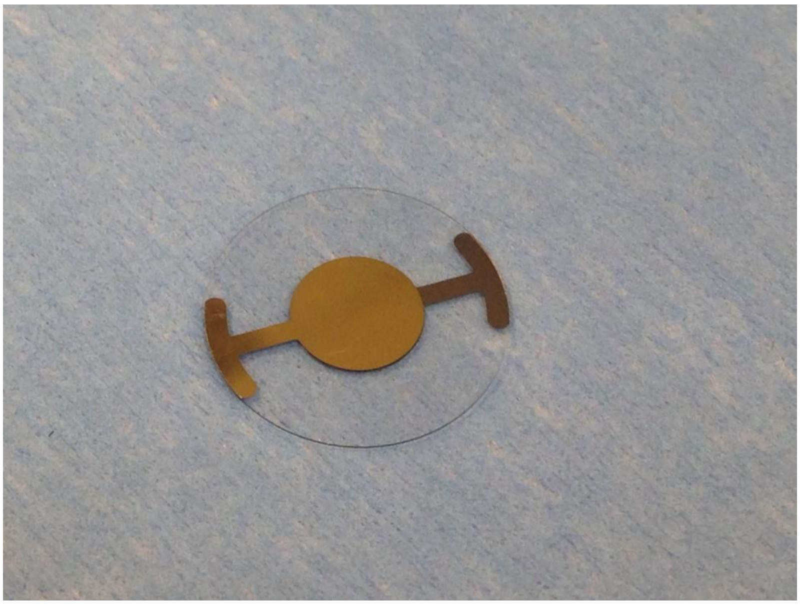

Figure 4.14. Quartz Crystal Microbalance: quartz crystal (transparent plate) and gold electrode in the centre. On the right side and left side are the contact points for the PE.

Then QCM and effusion cell are placed in a *sublimation micro-chamber*, i.e. a controlled environment of cylindrical form (located inside the vacuum chamber) made of insulating material (teflon), which further minimises thermal dispersion and avoids VOC's loss into the microbalance surrounding area (Fig. 4.15, *Right*). The effusion cell is inserted in a hole in the cylinder's base. The main setup components are:

1. Cold finger (copper L-shape)
2. Micro-sublimation chamber
3. Effusion cell
4. QCM and PE
5. Heater (R=25Ω)
6. Platinum temperature sensors (Pt100)
7. Metal case

The organic source are the dicarboxylic acids while a separate heater (a resistance) is used to control the effusion cell heating. QCM is cooled down to -72°C while the acid sample is placed in a small cylinder case (effusion cell) 6 mm wide and 10 mm deep. This configuration allows to monitor the VOC's deposition rates from about 10^{-13} mol cm^{-2}s^{-1} up to 10^{-10} molcm^{-2}s^{-1}, two orders of magnitude better than the results obtained during the preliminary test.

The sample is heated from room temperature (i.e. 25°C-30°C) up to high temperatures (i.e. 75°C-80°C) by means a heater of 20Ω (resistance) in thermal contact with the effusion cell. In figure 4.16 a schematic representation of the set-up is shown.

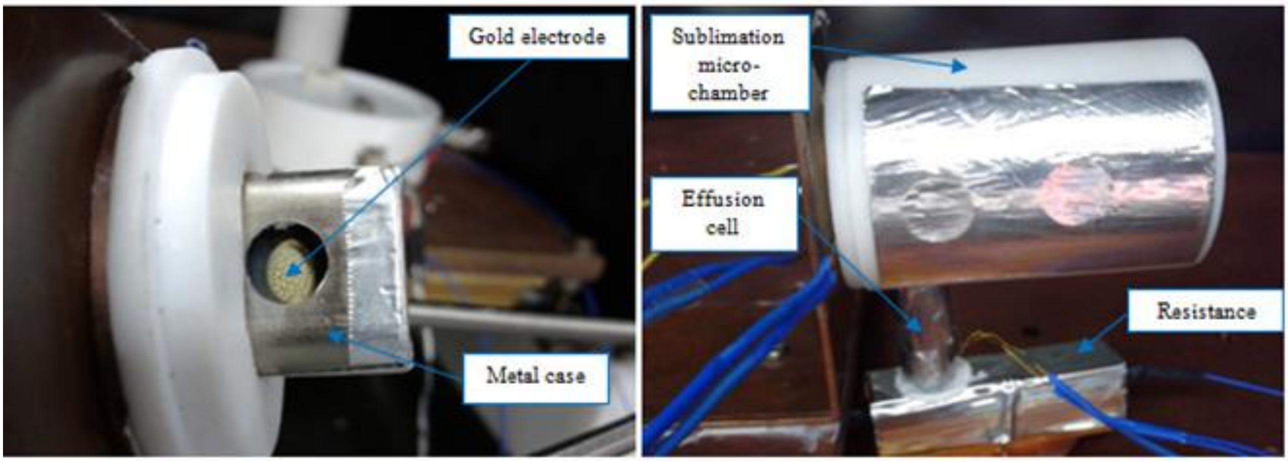

Figure 4.15. Experimental set-up. *Left*: QCM inserted in the metal case. VOC molecules deposited on the QCM's electrode are visible and correspond to the white spots on the crystal area. *Right*: the sublimation micro-chamber containing the QCM and the outgassing material. It is made of insulating material (teflon) in order to limit sublimation and thermal dispersion. The contacts are instead made of grease vacuum.

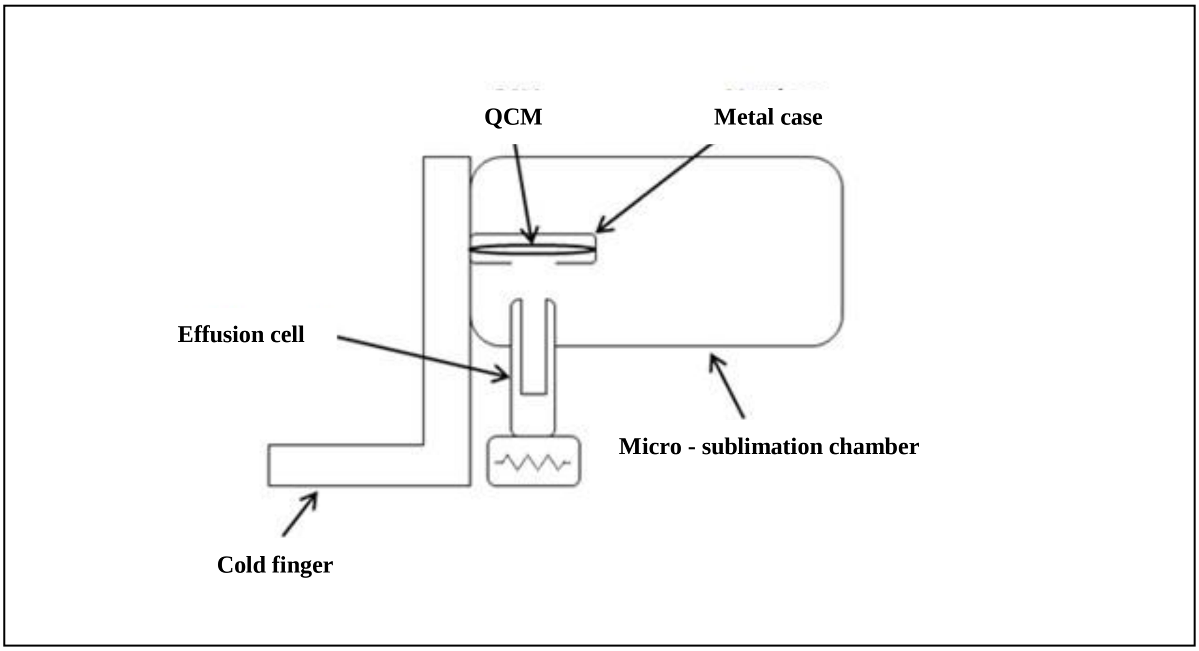

Figure 4.16. Schematic representation of the experimental set-up. The sample is placed in the effusion cell and heated by a resistance. QCM (cooled by a cold finger) is positioned in a metal case perforated in the centre to allow the VOC deposition. The deposition rates are monitored by QCM frequency, whereas the sample temperature is monitored (5°C for each step) by a resistance temperature with PT100 sensor. In order to avoid flux dispersion, the QCM and effusion cell are located in an isolated micro-chamber and the whole set-up is placed in a vacuum chamber. The resistance is separated by a cold finger in order to obtain a first sublimation step from 25 to 30°C.

4.4.2. Molecules flux calibration and preliminary test

Because of the efficiency of the deposition process on QCM increasing as the deposition surface temperature becomes increasingly colder than the temperature of the outgassing material, the intensity of the flux is directly influenced [Albyn 2004]. Thus, QCMs have to be necessarily cooled down at low temperature (-72°C) by means of a cold finger (-90°C).

Besides, in order to maximize the VOC flux, the microbalance is placed in front of the effusion cell. This configuration strongly improves the flux collimation, increasing the amount of the collected molecules. The metal case has a temperature similar or even slightly smaller of the crystal and if the effusion cell is too far away from the QCM, the molecular flux could condense preferably on the metal case rather than the crystal, lowering the deposition rate too much (Fig. 4.15, *Left*). Moreover, reaching low QCM temperatures (i.e. -72°C) by improving the thermal contact with QCM and cold finger, it is possible to increase the incident flow of molecules on the microbalance (avoiding molecules dispersion in the surrounding environment).

The assumption that the deposited material on crystal remains on the surface and that all the condensed species have the same affinity for the deposition surface is often considered valid (the sticking material coefficient is assumed to be even though this assumption is not always true. Indeed, during a deposition process some deposited material may be lost or re-evaporated, from the deposition surface while the majority of the condensate remains on the deposition surface. Generally, the re-evaporation usually occurs at a significantly lower rate than the measured deposition rate and varies with the deposition surface temperature and composition [Albyn 2004]. This behavior can be ascribed to:

1. the distance source-QCM (which has to be low in order to have a sufficient flux to obtain a reliable value or ΔH_{sub});
2. the fluctuations of sample temperature (managed by separate temperature control system) during the deposition process;
3. the small variations in the deposition surface temperature;
4. the disturbances of metal case temperature which induce a less pronounced flux on crystal surface.

In order to have a good statistical analysis, a number of sufficient data during each measurement should be acquired. Generally, we considered 1 acquisition data per 2/10 seconds for each temperature step of 30/20 minutes: this provide an adequate amount of data with good resolution for deposition calculations. During the first attempt (QCM at -72°C, distance QCM-sample: d>2cm), only 3 kHz of frequency variation was observed due to the low molecules deposition. Besides, due to the temperature fluctuations of effusion cell and the slight fluctuations of the deposition surface temperature, the frequency fluctuations have been recorded (Fig. 4.17).

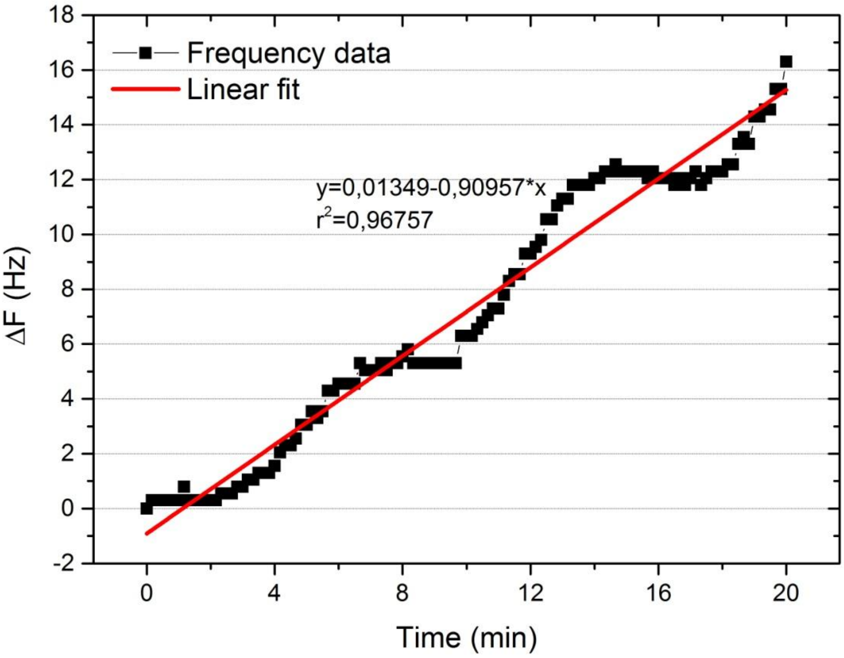

Figure 4.17. Linear regression coefficient for adipic acid step at 40°C during the first attempt. The acquisition data was performed every 10 sec. in time interval of 20 minutes. The r^2 test shows as the data are not reliable for deposition measurement ($r^2 < 0.99$).

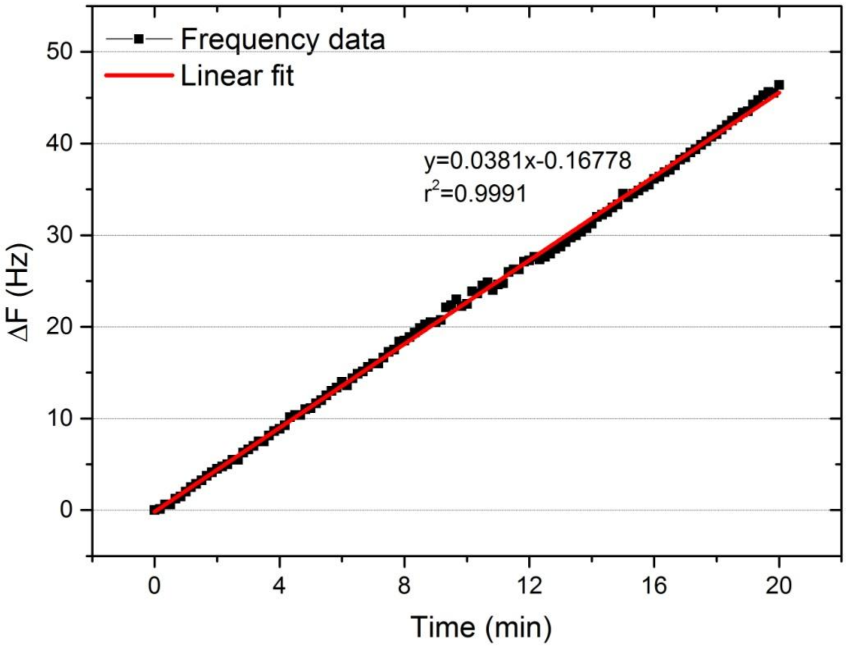

Figure 4.18. Linear regression coefficient for Adipic acid step at 40°C during with condensation set-up (this work). In this case, the acquisition data was performed every 10 sec. in time interval of 20 minutes. The r^2 test (>0.99) shows as the data are valid for deposition measurement.

Linear regression analysis is a good method for the evaluation of frequency data. It provides the slope of the curve (as shown in Fig. 4.17 and 3.18, i.e. 0.013 Hz/s and 0.038 Hz/s, respectively) in addition to a linear regression coefficient. Typically, data with a coefficient of determination[1] $r^2>0.99$ are of high enough quality to produce good deposition data and are adequate for the accurate calculation of the enthalpy of sublimation [Albyn 2001].

In the first attempt, the frequency data show several oscillations with r^2 coefficient <0.99 and are not valid for a deposition measurement (Fig. 4.17).

Improving the set-up (decreasing the distance between QCM and sample: d<2cm) and the temperature control system (the temperature accuracy should be lower than ±0.5°C), the data frequencies are adequate for deposition measurement ($r^2>0.999$, Fig. 4.18).

4.5. Vacuum system and data acquisition system

The whole setup is placed in a vacuum chamber in order to facilitate the transition phase, to avoid the simultaneous condensation on the QCM of other molecules present in the atmosphere at ambient pressure (mainly H_2O) and to avoid convective heat exchange with the atmosphere which would affect QCM and effusion cell temperature. The Vacuum System (Fig. 4.19) is composed by a Rotative pump (CF29PR-Alcatel Society), Turbo Pump (1602450-Elettrorava Society) and a chamber (90 litres), all of them assembled by the Vacuum Centre Representative (CRV S.r.l., Rome, Italy).

Rotative Pump can drive the system down to 10^{-2} mbar whereas the Turbo Pump can lower the pressure down to 10^{-6} - 10^{-7} mbar. Pressure is measured using the TC1 sensor (Varian) up to 10^{-2} mbar and the IG sensor (Varian) or Ionization Gauge up to 10^{-6} - 10^{-7} mbar. During data acquisition the pressure of the system is maintained constant during each experiment (fixed values between 3.5×10^{-6} mbar and 8×10^{-7} mbar).

The temperatures of copper plate, metal case, resistance and effusion cell, have been continuously monitored with platinum sensors (PT100, dimensions of 7.6×7.6×0.7 mm), whose resistance changes linearly with temperature. Temperature controls of the effusion cell (heating system from 25°C to 120°C) and of the copper plate (cooling system, set to -90°C and stable within 0.3 °C) are driven by a Proportional-Integral-Derivative system (PID), which allows a temperature stability of typically ±0.5°C or below and managed by means the LabView (2014) software. The frequencies are acquired by means of the Eureka electronic box powered by a USB of PC2, controlled by the software provided by Bioelectronics and Advanced Genomic Engineering (BioAge S.r.l., Lamezia Terme, Italy).

---

[1] The coefficient of determination, denoted as r^2, gives the proportion of variance (fluctuation) of one variable that is predictable from the other variable. This coefficient is the ration of the explained variation to the total variance, such that $0 \leq r^2 \leq 1$, and denotes the strength of the linear association between *x* and *y*.

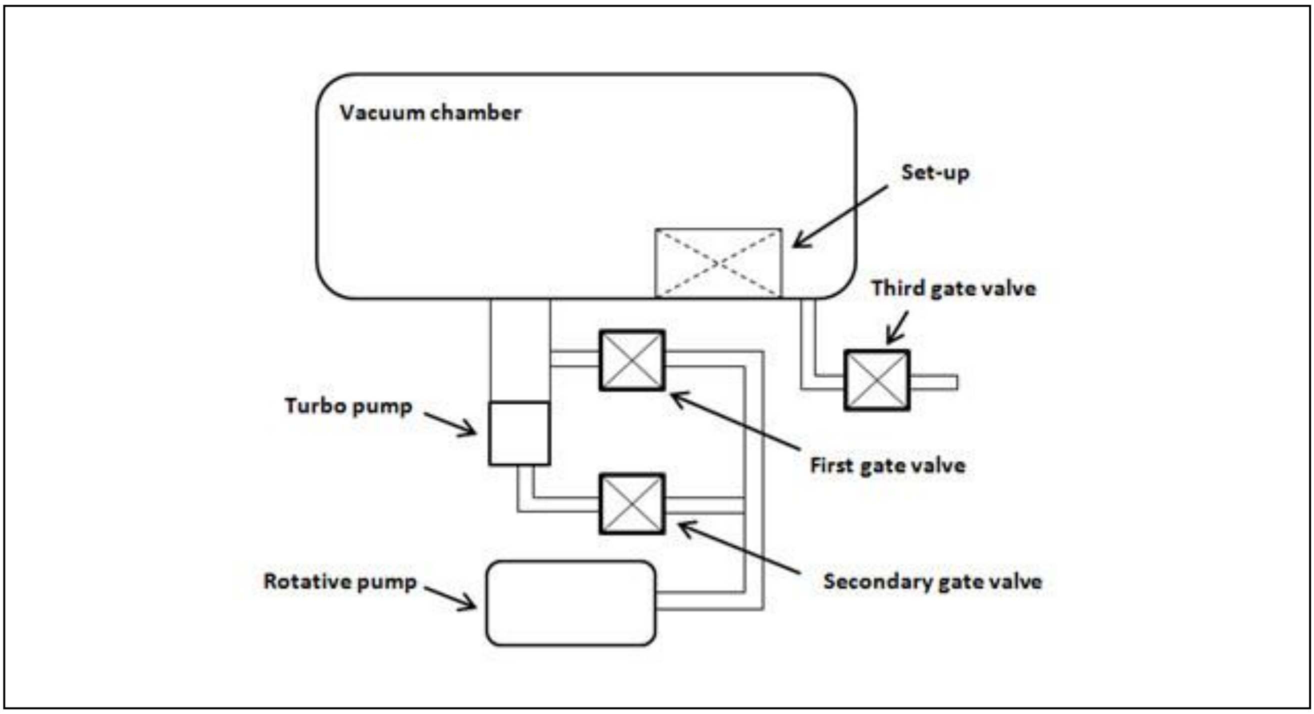

Figure 4.19. The vacuum system, composed of a rotative pump, turbo pump, and a vacuum chamber. Each pump is managed by an electro-valve: in the initial phase, the first valve (rotative) is opened, whereas the second valve is closed (turbo); in the next phase (at pressure of 10^{-2} mbar) the first valve is closed, whereas the second valve is opened (down to 10^{-6} mbar). The third valve is used to apply the re-entry in air at the end of each experiment.

4.6. Setup and measurement procedures summary

Two different setup have been developed to monitor the contamination at different temperatures set point performing TGA cycles (Fig. 4.20, *Left*) and to monitor a condensation processes by heating a pure compounds (Fig. 4.20, *Right*).

The measurement procedures used with these experimental setup are described in table 4.1. Different steps have been considered.

Finally, the enthalpy of sublimation can be obtained using Langmuir equation (eq. 3.9) and Van't Hoff equation (eq. 3.10). In the first case (SH1 procedure), the sublimation rates are obtained by using the TGA cycles in a temperature range from 20 to 50°C (whose results are reported in chapter 5 and 6) whereas in the second case (SH2 procedure) the condensation rates can be obtained from molecules condensation at fixed temperatures set-point (the results are reported in chapter 6).

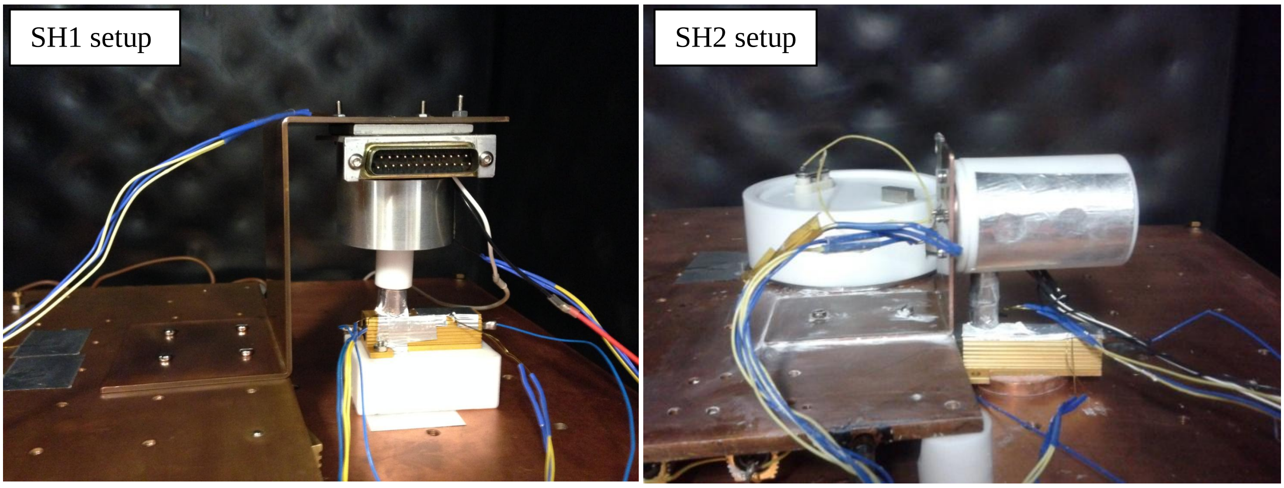

Figure 4.20. *Left*: SH2 setup for contamination monitoring and TGA cycles. The effusion cell is surrounded by a teflon guide while the sensor head is supported by copper S-shape. *Right*: SH1 setup for condensation process monitoring. This setup includes a micro-sublimation chamber (teflon material) while the QCM is surrounded by metal case to help the thermalization. The mechanical structure is different (L-shape support instead of S-shape support) because of the different sensor head 1 mechanical structure.

Table 4.1. The measurement procedures are described. In particular, the time stability at each temperature set-point for SH1 setup are 20 minutes instead of 30 minutes because of the larger temperature range monitored. The equation used are different because of the different method used for these analysis, i.e. using SH1 the condensation and sublimation rates (from sensing crystal surface) are obtained whereas using SH2, only the condensation rates are obtained.

General procedure	Step	SH1 setup	SH2 setup
Cooling the system (EM, BB)	1	-80°C	-90°C
Source heating (acid sample)	2	from 25 to 120°C	from 25 to 80°C
Temperature step	3	5/10°C	5°C
Set-point stability	4	20 min.	30 min.
Acquisition data rate	5	every 2 sec.	every 2/10 sec.
Deposition rates measured	6	YES	YES
TGA cycles	7	YES	NO
Equation used	8	Langmuir	Van't Hoff
Enthalpy of sublimation	9	YES	YES

Chapter 5. SH1 for contamination monitoring in space

5.1. Introduction

The long term stability of new and modified spacecraft materials when exposed to space environment continues to be a major area of investigation. From previous space flights (STS, ISS, Satellites etc.) it has been recognized that exposure of a wide variety of materials (organic, inorganic and metallic) has resulted as significant changes in their physical state or properties.

In this framework, a breadboard and Engineering Model of VISTA SH1 have been developed for ESA project, i.e. Contamination Assessment Microbalance (CAM), which aim is to design and realized a QCM-based instrument able to monitor in-orbit contamination of sensitive surfaces and payloads of future ESA satellites. The laboratory breadboard and the Engineering Model (subpar. 3.4.1) have been developed (following the ESA requirements, ESA Statement of Work) and tested in space conditions (vacuum and low temperatures). Thus, saturation and contamination tests here presented have been performed with SH1 breadboard which structure is based on a double crystal configuration (the output signal is the beat frequency). The test presented are:

1. the contamination tests (to verify the SH1 capability to monitor a contamination process in space conditions);
2. the saturation test (to know the maximum mass loaded by SH1);
3. the TGA cycles (to perform the SH1 regeneration and to characterize a contaminant source using Clausius-Clapeyron and Langmuir equations, i.e. eq. 3.8 and eq. 3.9, respectively).

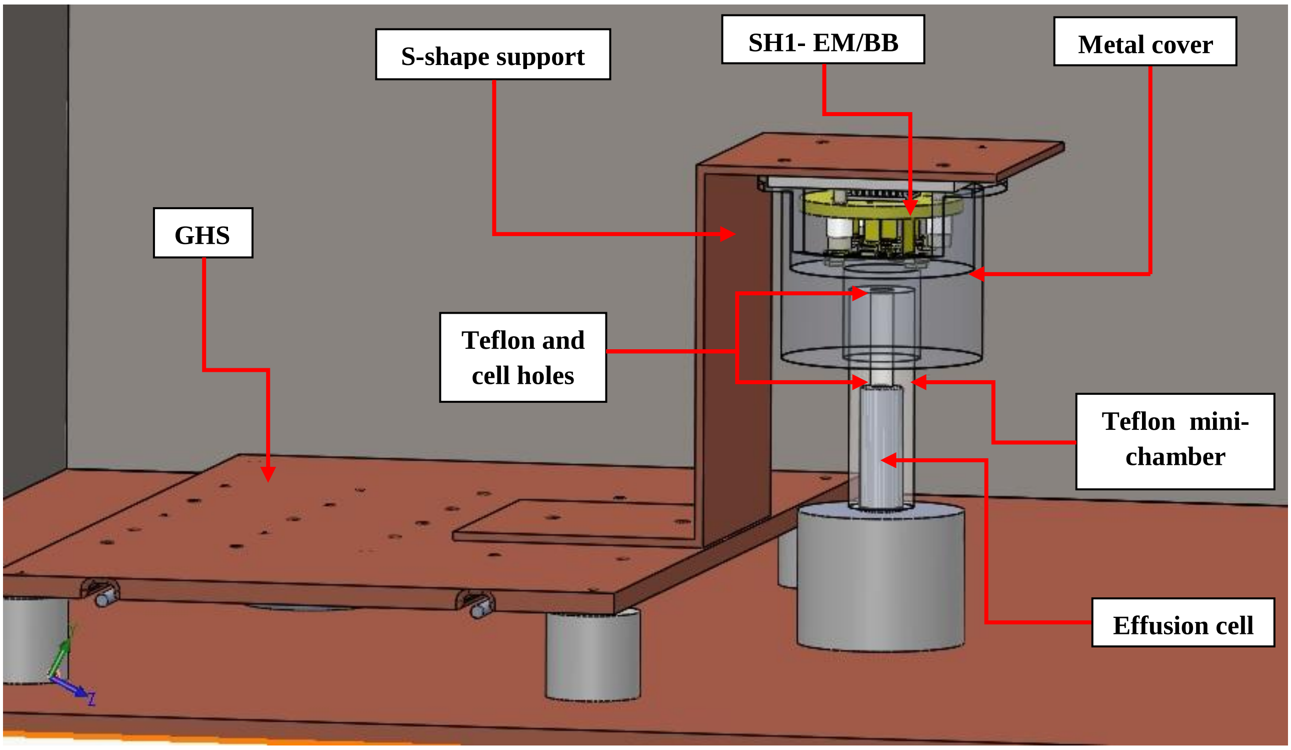

Figure 4.2 *(from simulations with SolidWorks software)*. Setup for contamination test with SH1.

The SH1 breadboard is mounted on a copper S-shape in contact with the Global Heat Sink (GHS) or cold finger which can be heated or cooled by means of a nitrogen circuit (Fig. 4.2).
An effusion cell containing a organic source has been used as contamination source and placed in the FOV of SH1. SH1 breadboard is positioned on a S-shape and shielded by an aluminum cover of cylindrical form which favors the crystals thermalization at -80°C avoiding flux dispersion.

Using TGA cycles after contamination and saturation tests, a thermodynamic quantity, i.e. the enthalpy of sublimation, has been used to characterize the contaminant source (adipic acid). The enthalpy of sublimation obtained has been calculated using Langmuir and Clausius-Clapeyron equations, i.e. $\ln \frac{dm}{dt}T^{1/2} = lnC - \frac{\Delta H}{RT}$, using different TGA data points and the linear fit of $ln \frac{dm}{dt}T^{1/2}$ as a function of *(1000/T)* $[K^{-1}]$ whose slope gives the enthalpy of sublimation. The results are compared with those obtained by previous work using similar method and temperature range [Albyn 2004, Booth 2009, Chattopadhyay and Ziemann 2005, Bilde 2003, Dirri 2016a].

5.2. Contamination tests

Two contamination tests on SH1 sensing crystal have been performed from 25 to 75°C (first experiment, Fig. 5.1) and from 40 to 100°C (second experiment, Fig. 5.2) in order to measure the contaminant's fluxes at different set-point temperatures. This Effusion Method is similar to that used for the organic compounds characterization (described in chapter 6) even though the main goal for SH1 is to monitor the contamination process at different temperature set points obtaining the deposition rates.

5.2.1. Contamination tests: deposition processes

The effusion cell containing the contaminant sample has been heated with different temperature steps of 5-10°C at -80°C, i.e. the temperature of Global Heat Sink (GHS) (the copper plate). The output signal is the beat frequency (between the sensing, i.e. top crystal and reference, i.e. bottom crystal, *1st sub-unit* explained in subpar. 3.4.1) which increases at increasing contaminant deposition on the sensing crystal surface.

In figure 5.1 and 5.2 it is possible to observe the increasing of the difference between the two crystals temperature during the deposition process, due to irradiation of the effusion cell on the top crystal, which is most effective on the sensing crystal (increase of 4.5°C in the first experiment and 5.4°C in the second one) than on the bottom crystal (temperature increase 2.5°C and 2.2°C, respectively).

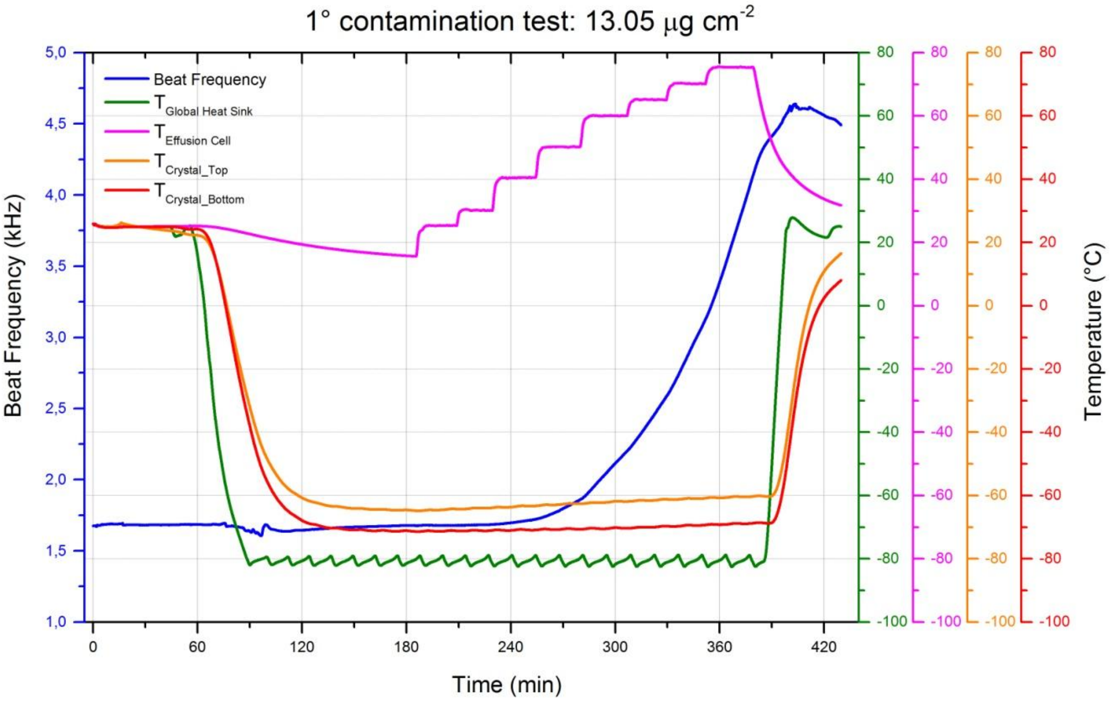

Figure 5.1. First contamination test performed by varying the effusion cell temperature from 25 to 75°C. Deposition rates increased up to 0.65 Hz/s with a total collected material of 13.05 μgcm^{-2}.

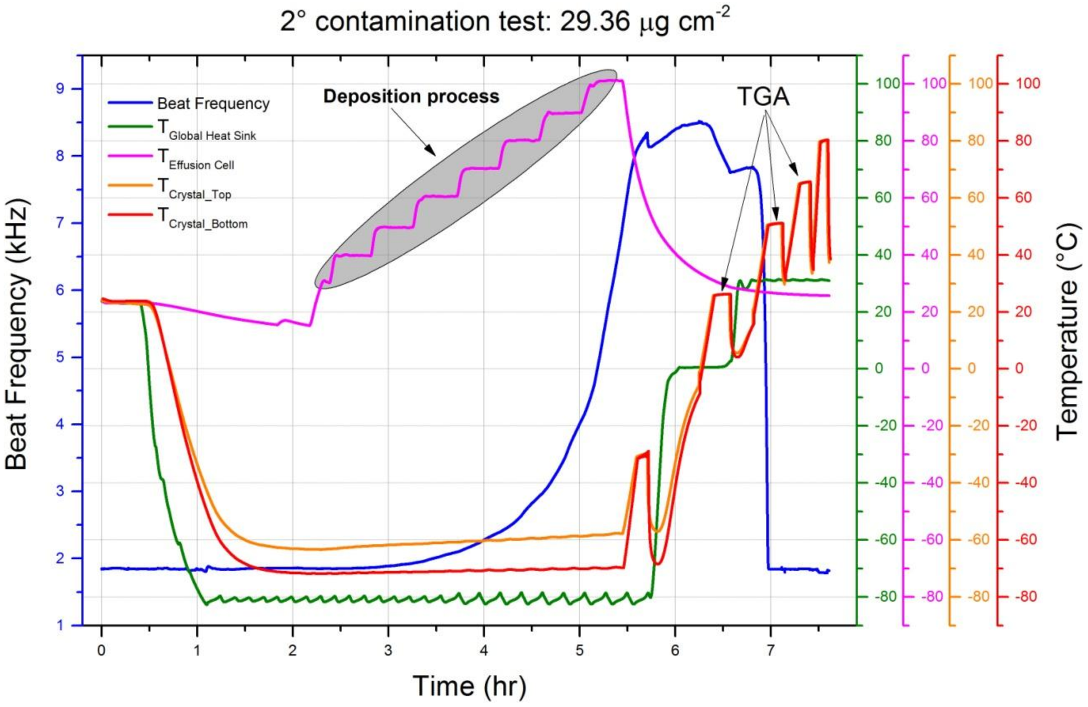

Figure 5.2. Second contamination test performed from 40°C to 100°C for effusion cell temperature. Deposition rates increased up to 2.2 Hz/s with a total collected material of 29.36 μg cm^{-2}.

The first experiment shows low deposition rates up to 75°C (0.6 Hz/s) whereas the second experiment shows higher deposition rates up to 100°C (2.2 Hz/s). The enthalpy of sublimation has been calculated by means of TGA cycles (Fig. 5.3) performed in the second experiment by using Langmuir equation (eq. 3.9). Details of the two tests are summarized in Tab. 5.1.

Table 5.1. Details of the two deposition experiments performed. The temperature range monitored as well as the crystals temperatures are listed. The deposition rates are higher in the second test.

Deposition test	*I*	*II*
Mass Adipic acid (mg)	13	20
Sublimated mass (mg)	1	3
$\Delta T_{\text{Effusion Cell}}$ (°C)	25-75	40-100
Deposition (µg cm^{-2})	13.05	29.36
Deposition Rates (Hz/s)	from 0.004 to 0.65	from 0.009 to 2.20
$T_{\text{Global Heat Sink}}$ (°C)	-80.7±1.0	-80.9±0.9
$T_{\text{Crystal\_Top}}$(°C)	-62.5±1.3	-60.2±1.4
$T_{\text{Crystal\_Bottom}}$(°C)	-70.3±0.7	-70.7±0.6
$\Delta T_{\text{Crystals}}$ (°C)	7.9	10.4

In VISTA-SH1 framework we are able to obtain sufficiently high fluxes, especially in the second contamination test where a deposition of 2.2 Hz/s has been obtained at 100°C. A total deposition of 7 kHz has been used to perform the TGA cycles by means of the built-in heaters obtaining the enthalpy of sublimation for the contaminant source (subpar. 5.2.2). The sublimation process has been obtained by applying the heaters as shown in Fig 5.2 and in best detail in Fig. 5.3. In particular, by using Langmuir equation it has been possible to calculate the enthalpy of sublimation during the third TGA cycle (Fig. 5.3, from 15 to 50°C of crystals temperatures), where the highest frequency rate due to desorption is recorded.

5.2.2. Contamination tests: TGA cycles

Different TGA cycles have been performed in order to observe contaminant desorption at different temperature steps (Fig. 5.3) as listed in table 5.2.

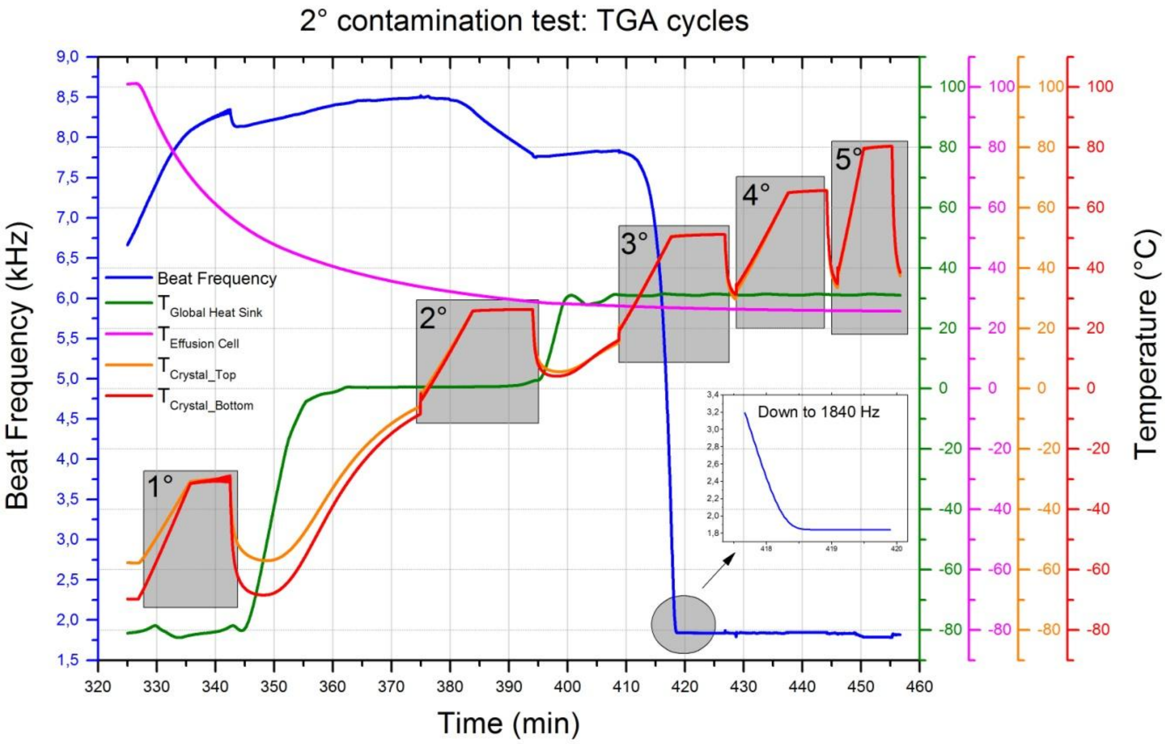

Figure 5.3. Second contamination test: different TGA cycles have been performed with crystals up to 80°C. A material desorption of 29.36 μg occurred after the fifth cycle. As showed in the central box, the beat frequency comes back to its initial value (~1.8 kHz).

The TGA cycles have been performed with the built-in heaters considering a temperature difference of 30°C [ESA Statement of Work 2013]. Details about the heating steps performed are summarized in Table 5.2. Generally, the frequency variation every 2 seconds ("*df/dt*") has been converted in mass variation by multiplying the frequency for the sensitivity of the crystal (i.e. 4.4 $ng\ Hz^{-1} cm^{-2}$).

During the first cycle a mass increase has been observed due to the still high temperatures of the effusion cell. The deposited mass in this phase was 5.8 μg cm^{-2} (Fig. 5.3, min. 325-345).

In the second cycle, the GHS temperature was set at 0°C in order to lead crystals to 25°C (whose initial temperature was -5°C; Fig. 5.3, min. 375). In the last three cycles, GHS temperature has been increased up to 30°C in order to reach higher crystals' temperature (up to 80°C; Fig. 5.3, min.455).

Table 5.2. Starting/final temperatures of top/bottom crystals, T_{GHS} (copper plate temperature), ΔT between two crystals, slope of thermal cycles and stabilization time at different set-point, frequency variation and mass deposited/desorbed (indicated by +/-) for each TGA cycles performed.

TGA cycle	*1°*	*2°*	*3°*	*4°*	*5°*
Starting-Final: $T_{top\_crystals}$ (°C)	-57.7±0.2 -30.1±0.1	-5.8±0.2 26.0±0.1	15.1±0.1 50.9±0.2	30.1±0.2 65.4±0.2	39.1±0.4 80.3±0.1
Starting-Final: $T_{bottom\_crystals}$ (°C)	-69.9±0.5 -30.5±0.2	-8.4±0.2 26.0±0.1	15.9±0.2 50.9±0.2	31.6±0.2 65.4±0.2	39.9±0.4 80.2±0.1
T_{GHS} (°C)	-80.9±1.1	0.2±0.6	31.2±0.2	31.2±0.1	31.2±0.1
$\Delta T_{Crystals\_Set\ Point}$ (°C)	0.44	0.01	0.08	0.01	0.05
Slope (°C/min)	2.8/4	3.5	3.5	3.5	5.5
Δt (min)	10	10	10	8	5
ΔF (kHz)	+1.324	-0.650	-5.986	-0.003	-0.013
Desorbed mass (μg cm^{-2})	+5.8	-2.9	-26.3	-0.01	-0.06

The highest desorption has been obtained during the second cycle (650 Hz) and third cycle (~6 kHz) where the final crystals' temperature were 26°C and 51°C. In particular, the most of contaminant desorbs between 20 and 50°C. During the last two cycles, little changes have been recorded (up to 16 Hz) since frequency already came back to its initial value at the end of third cycle (i.e. the contaminant mass was almost completely sublimated from the crystal area). At end of each cycle (except the first) the temperatures of the two crystals differed no more than 0.08°C, independently of the stabilization time.

Due to high desorption rates and the highest desorbed mass from the sensing crystal a reliable value of the enthalpy of sublimation has been obtained using the Langmuir equation (eq. 3.9) between 25 and 50°C (third cycle). Least squares fit is reported in Fig. 5.4. From the slope of the curve it is possible to infer the enthalpy of sublimation of a specific compound or a mixture of compounds. The enthalpy result for this compound is ΔH_{sub} = (133.8±1.8) [kJ mol^{-1}].

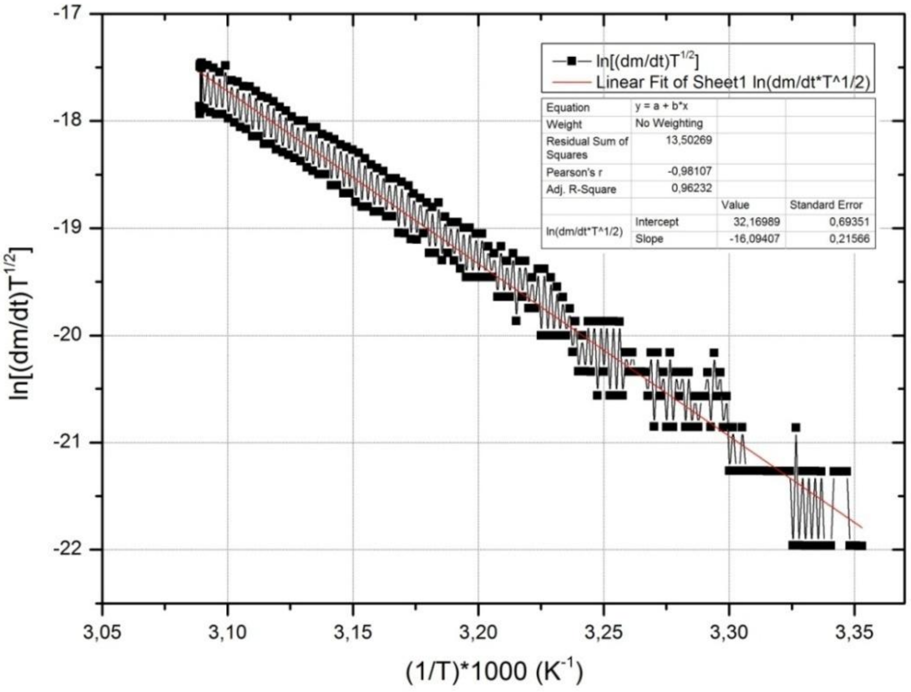

Figure 5.4. Linear fit of $\ln(\frac{dm}{dt}T^{1/2})$ as a function of (1000/T) [K^{-1}] (corresponding to the third TGA cycle), whose slope gives the enthalpy of sublimation.

These results have been also compared with those obtained by Dirri (2016a) by applying the Langmuir equation to data obtained during the deposition due to effusion cell heating. Comparison is shown in table 5.3. The results are in agreement within 3%.

Table 5.3. Enthalpy of sublimation results obtained with Langmuir method are listed. Two different measurements procedure have been used. In the first procedure, the crystals have been heated by means of their integrated heaters whereas in the second procedure the cell has been heated by means one external resistor.

Langmuir equation	*II Contamination test*	*Dirri (2016)*
$\Delta H_{sub} \pm \sigma_{\Delta H}$ (kJ/mol)	133.8±1.8	138.2±1.1
T_{range} (°C)	25-50	30-70
Heating mode	Crystal's heaters	Effusion Cell

5.3. Saturation test

In order to know the maximum loaded mass by SH1, a saturation test (long deposition test up to 120°C) has been performed. Indeed, the aim of this test is to reach the saturation observing the beat frequency behavior. A beat frequency trend to "zero" is expected because of the maximum mass achieved by the sensing crystal (i.e. the mixer element integrated on PE is not able to provide a frequency output).

5.3.1.Saturation test: deposition process

Thus, saturation test with the same compound used for contamination tests has been performed in two steps. The aim of this test is to know the maximum detectable mass by SH1 when a contaminant source is heated at temperature >100°C (simulating the solar pulses on materials in space environment). In the first step, the effusion cell containing 50 mg of contaminant has been heated in order to favour its deposition on the crystal. Therefore, it has been necessary to heat the cell up to 120°C in order to have deposition rates >2 Hz/s and a following saturation (Fig. 5.5). Then, by heating the cell up to 120°C it has been possible to have a flux of 35 Hz s^{-1} (corresponding to 0.15 μm cm^{-2} s^{-1}) which allows a saturation, maintained for about 50 minutes (Fig. 5.5, 285-345 min.), and a total contaminant's deposition of 733.9 μg cm^{-2}.

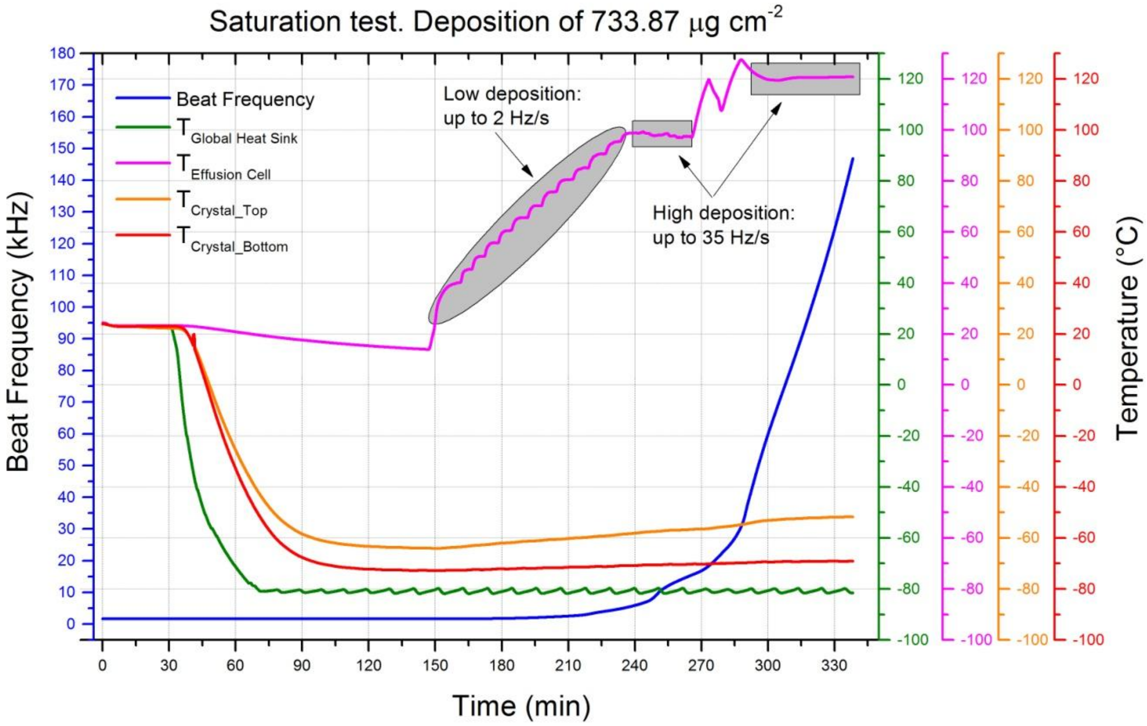

Figure 5.5. Saturation process heating the cell up to 120°C. The contaminants is heated at 120°C for 50 minutes to reach the complete saturation of the sensing crystal.

In the deposition process, a heating of the crystals has been verified: during the cell heating from 100°C up to 120°C, top/bottom crystals increased their temperatures of 6.6°C and 1.8°C respectively, due to the sensor head's FOV. In this manner, top crystal presents a temperature of 4.8°C higher than crystal bottom that corresponds to a difference of 125 Hz, calculated by previous calibrations (28 Hz °C^{-1}).

In the second step, the crystals have been regenerated by applying temperature steps with built-in heaters. After the deposition process, the effusion cell has been switched off while the residual contaminant has been accumulated on the crystal surface (Tab. 5.4, first cycle) due to the high temperature of the cell. This allowed an additional deposition up to 166.5 kHz and a saturation of the crystal. In this case the signal went to 0 Hz (Fig. 5.6, min. 350).

Successively, the setup has been heated up to 20°C and four TGA cycles have been realized by means of integrated heaters (Tab. 5.4). At the end of the last cycle, the total mass of sublimated contaminant has been measured. The sublimated mass was 10 mg.

5.3.2. Saturation test: TGA cycles

Four TGA cycles have been performed in order to reach a complete regeneration of sensing crystal (Fig. 5.6, min. 380-415).

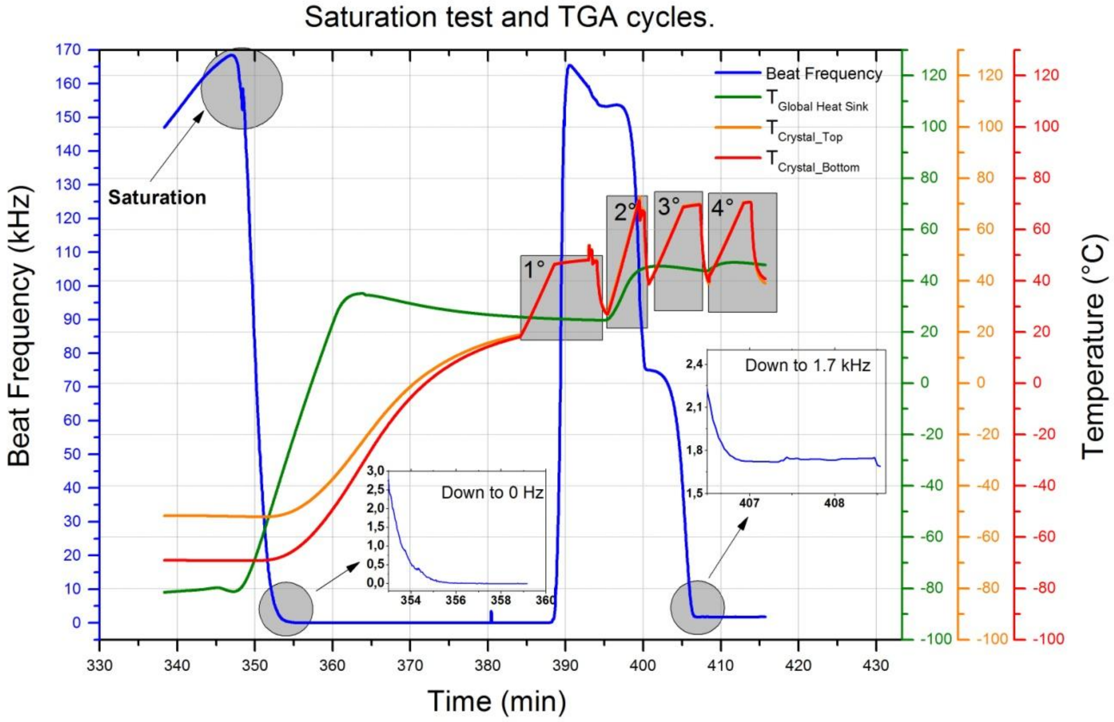

Figure 5.6. Saturation process. Four TGA cycles with crystals up to 70°C have been realized. A total desorption of 733 µg cm^{-2} has been observed. The starting frequency corresponds to frequency at the end of desorption.

During the first test (Fig. 5.6, min. 385-395, from 20 to 50°C) sensor head came out from saturation, occurred at 166.5 kHz, and 12 kHz of material were desorbed.

The second cycle has been performed at higher temperature (Fig. 5.6, min. 395-400, from 30 to 70°C), obtaining a desorption of 79.6 kHz (half of the whole deposition).

The third cycle (Fig. 5.6, min.400-410, from 40 to 70°C) has successfully completed the desorption (beat frequency returns at its initial value of 1.7 kHz, Fig. 5.6, min.410).

Last cycle has been performed from 40 to 70°C and a variation of only 11 Hz was observed. The largest desorption occurred during the second and the third cycle when the crystals were at 50 and 70°C. In these cycles, a short stabilization time is sufficient to obtain the contaminant desorption (for example: 3 minutes have been necessary for a desorption of 73.3 kHz, Tab. 5.4).

Table 5.4. The starting/final temperatures of the crystals top/bottom, T_{GHS}, ΔT between two crystals, slope of thermal cycles and stabilization time at each set-point, frequency variation and mass desorbed for each TGA cycle performed. During the first cycle, an increased mass has been recorded due to still high temperatures of effusion cell.

TGA cycle	***1°***	***2°***	***3°***	***4°***
Starting-Final: $T_{Top\_Crystals}$ (°C)	18.8±0.1 47.6±0.3	27.9±0.1 71.8	39.2 69.6±0.17	39.4 70.6±0.1
Starting-Final: $T_{Bottom\_Crystals}$ (°C)	17.9±0.1 47.5±0.3	27.2±0.2 70.9	39.4 69.4±0.18	40.2 70.5±0.1
T_{GHS} (°C)	25.1±0.3	44.4±0.2	45.4±0.3	46.5±0.8
$\Delta T_{Crystals\_Set\ Point}$ (°C)	0.1	1.1	0.2	0.1
Slope (°C/min)	5	9	5	5
Δt (min)	5	--	3	2
ΔF (kHz)	11.8	78.2	73.3	0.01
Desorbed mass (μg cm^{-2})	51.9	344.1	322.5	0.05

Enthalpy of sublimation has been calculated by applying Langmuir method to the data obtained during the second and the third cycle (Fig. 5.6). Results are listed in Tab. 5.5 and compared with Dirri (2016a) results obtained with Langmuir equation and different heating method applied to different setup. The enthalpies of sublimation in the second and third TGA cycles have been obtained from linear fit in Fig. 5.7.

Table 5.5. Enthalpies of sublimation obtained with Langmuir method. Effusion cell and crystal's heaters have been used.

Langmuir equation	**Saturation test (2° TGA cycle)**	**Saturation test (3° TGA cycle)**	**Dirri (2016)**
$\Delta H_{sub} \pm \sigma_{\Delta H}$ (kJ/mol)	134.3±3.4	138.2±2.2	138.2±1.1
T_{range} (°C)	47-72	44-69	30-70
Heating mode	Crystal's heaters	Crystal's heaters	Effusion Cell

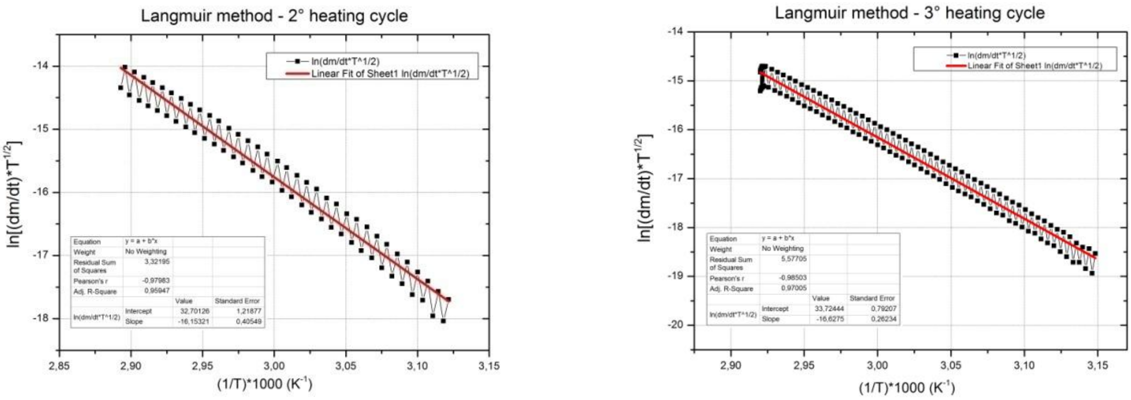

Figure 5.7. Linear fit of $\ln(\frac{dm}{dt}T^{1/2})$ vs. *(1000/T) [K^{-1}]* during the desorption process between 47-72°C (2° cycle in Fig. 5.3) and 44-69°C (3° cycle in Fig. 5.6).

The depositions data obtained from Dirri (2016a) in the temperature range 30-70°C have been used with Langmuir equation to obtain the enthalpy of sublimation from the linear fit of $\ln\frac{dm}{dt}T^{1/2}$ as a function of (1000/T) [K^{-1}]. The results calculated for second and third cycles with Langmuir method are in agreement with results of Dirri (2016a), within 3%.

5.4. Enthalpy of sublimation results comparison

In table 5.6 are listed the enthalpy of sublimation obtained with SH1 by means of TGA cycles. TGA have been performed after the second contamination test and saturation test. In particular, the second and third TGA cycles of Saturation Test (ST) and the fourth TGA cycle of second Contamination Test (IICT) have been used. The enthalpy results are in agreement within 3.5% demonstrating a good capability for TGA method to estimate the enthalpy of sublimation.

Table 5.6. Enthalpies of sublimation obtained with Langmuir equation and TGA method.

Langmuir equation	**ST (2° TGA cycle)**	**ST (3° TGA cycle)**	***II CT (4° TGA cycle)***
$\Delta H_{sub} \pm \sigma_{\Delta H}$ (kJ/mol)	134.3±3.4	138.2±2.2	133.8±1.8
T_{range} (°C)	47-72	44-69	25-50
Method	TGA	TGA	TGA

In table 5.7 a comparison with adipic acid enthalpy measured in different literature works is performed. Deposition and evaporation rates have been obtained with different techniques listed in table 5.7 while different temperatures range have been used to calculate the enthalpy of sublimation. In particular, Booth (2009) and Albyn (2004) experiments (described in Par. 6.6) show the same pressure and high temperature limit as our experiment.

Finally, the result obtained is in agreement with Albyn (2004) and Chattopadhyay (2005) within 5% and within the error with Booth (2009).

Table 5.7. Enthalpy of sublimation obtained in this work and compared with literature results. The weighted average value obtained with Langmuir method from TGA cycles has been considered for this work.

Reference	**$\Delta H_{sub} \pm \sigma_{\Delta H}$ (kJ/mol)**	**T_{range} (°C)**	**Method**
This work	135.4±1.3	25-72	TGA
Albyn (2004)	129.3±2.5	33-55	EM
Booth (2009)	119±26	30-60	KEMS
Chattopadhyay (2005)	140	22-45	TDPD

Chapter 6. Atmospheric VOCs characterization: results

6.1. Introduction

In preparation for the characterization of different organic compounds (i.e. dicarboxylic acids) using the Sensor Head 2, the data set of sublimation rates obtained from TGA tests performed with Sensor Head 1 (double crystal configuration, $f \sim 2\ kHz$) has been used to obtain the vapor pressure by means of Langmuir equation (eq. 3.9) (in particular P_{298K} [Pa], related to the volatility and useful for the compounds characterization) and the enthalpy of sublimation or the organic compound used as contaminant source by means of the Clausius-Clapeyron equation, i.e. $lnP = \frac{\Delta H}{RT} + lnC$. The results have been discussed and compared with previous works in subparagraph 6.2.2.

Then, the experimental activity of Sensor Head 2 (single crystal configuration, i.e. QCM with $f \sim 10\ MHz$) and laboratory tests for different organic samples characterization are introduced in paragraph 6.3. Calibration test, experimental procedure of Effusion Method (EM) used and data analysis are described as well as the results of deposition rates and enthalpy of sublimation (calculated with Van't Hoff equation, i.e. $\Delta H = R\left[\left(\frac{T_1T_2}{T_2-T_1}\right) ln\left(\frac{k_1\sqrt{T_1}}{k_2\sqrt{T_2}}\right)\right]$) of five compounds, i.e. oxalic acid, succinic acid, adipic acid, suberic acid and azelaic acid.

The setup for dicarboxylic acids characterization is composed by a single QCM cooled by a cold finger down to -72°C and positioned in a metal case perforated in the centre to allow VOCs deposition. The organic sample is placed in the effusion cell and heated by a resistance from 25-30°C to 80°C. The sample and QCM are located in an isolated micro-chamber to avoid flux dispersion while the whole setup is under vacuum condition (Fig. 4.16).

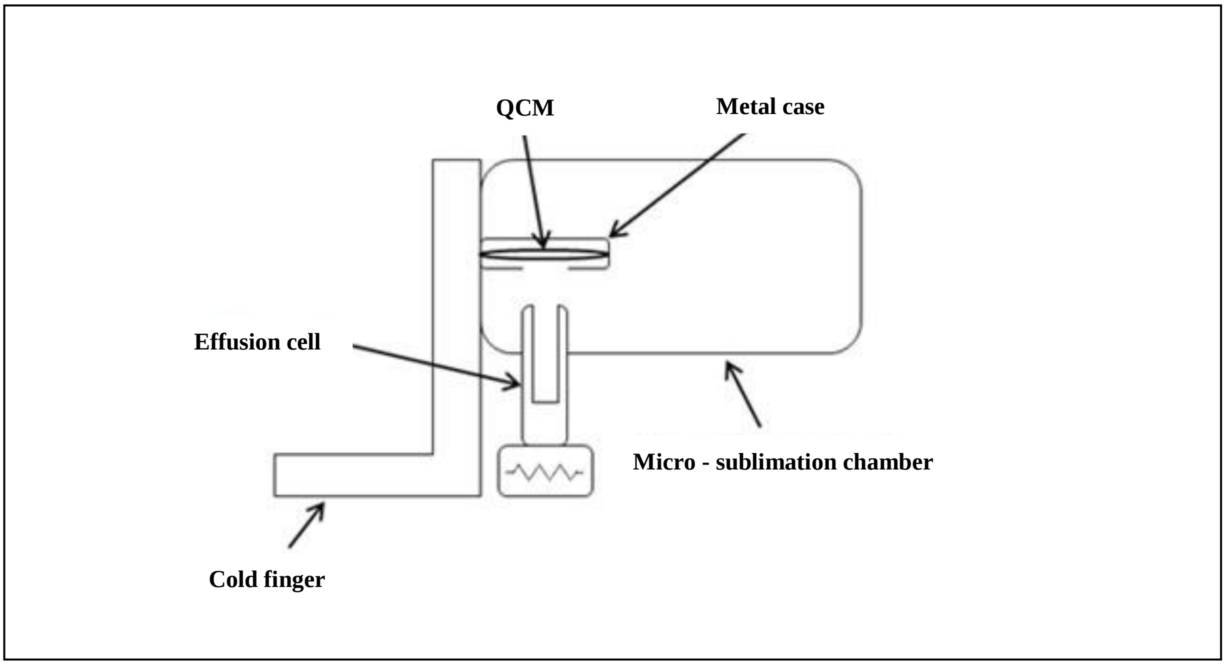

Figure 4.16. Schematic representation of the experimental set-up used for SH2.The Effusion Method is used.

The results obtained with Van't Hoff equation have been discussed and compared with previous works. Furthermore, the enthalpy of sublimation obtained with Langmuir and Clausius-Clapeyron equation (subpar. 5.2.2, 5.3.2 and subpar. 6.2.2) and SH1 breadboard have been compared with enthalpy average value obtained with Van't Hoff equation obtained and SH2 breadboard (par. 6.6).

6.2. SH1 for organic compound characterization (TGA method)

An important property of VOCs in atmosphere is the vapor pressure which gives information about the potential contribution of compounds to the formation and growth of airborne particles (described in subpar. 2.2.1).

As stated by Booth (2009) and Camredon (2007), the vapor pressure are essential to calculate the gas/particle partitioning of compounds forming the atmospheric aerosol and will help to study the SOA formation and characterization (during the in-situ measurement campaigns, less than 20% of the total particulate organic mass is typically identified [Rogge 1993, Puxbaum 2000]. Indeed, the atmospheric models incorporates the assumption that particles grow via equilibrium partitioning of gas phase compounds onto preexisting particles, with a partitioning coefficient that is inversely proportional to vapor pressure [Pankow 1994].

Thus, in order to reach a complete characterization of volatile or a mixture of them, the vapor pressure at different temperatures, enthalpy and entropy of sublimation should be obtained. The equation 3.8, i.e. $p = \frac{\sqrt{2\pi R}}{\alpha}\frac{dm}{dt}\sqrt{\frac{T}{M_i}}$ to calculate the vapor pressure in the temperature range of interest (where the TGA cycles have been performed) and the Clausius-Clapeyron equation [Booth 2009] are used:

$$lnP = \frac{\Delta H_{sub}}{RT} + C \qquad (6.1)$$

where T is the temperature, R is the ideal gas constant, the C a constant of integration (i.e. $\Delta S_{sub}/R$) and ΔH_{sub} and ΔS_{sub} are the enthalpies and entropies of sublimation respectively. By means of the eq. 6.1 it is possible to infer the enthalpy and entropy of sublimation of a pure compound.

As described by Bilde (2015), in order to infer the saturation vapor pressure at 298K for a combined data set (TGA cycles data in this work), a regression linear fit can be applied when high temperature range are monitored. Thus, the results can be compared with vapor pressures at 298K obtained from previous works [Davies and Thomas 1960, Booth 2009, Tao and McMurry 1989, Bilde 2003, Saleh 2008, Salo 2010, Chattopadhyay and Ziemann 2005, Cappa 2007, Bruns 2012].

6.2.1. General fitting method and procedure

The vapor pressure of adipic acid have been obtained by means of the sublimation processes from sensing crystal's surface: three data set of sublimation rates have been analysed in the temperature range: 25-50°C, 47-72°C and 44-69°C. The mass variation *dm/dt* has been used to calculate the vapor pressure using the eq. 3.8 and eq. 6.1 to obtain the enthalpy of sublimation and *C* constant. The saturation vapor pressure (P_i) are referred to a phase transition from solid to gas.

In Fig. 6.1 are plotted the *ln(P) [Pa] vs. 1000×(1/T)* $[K^{-1}]$ of the three TGA cycles data set in the listed temperature range. A linear fit has been performed for each vapor pressure data set obtaining the slope of the curve ($-\Delta H_{sub}/R$) and the intercept ($+\Delta S_{sub}/R$).

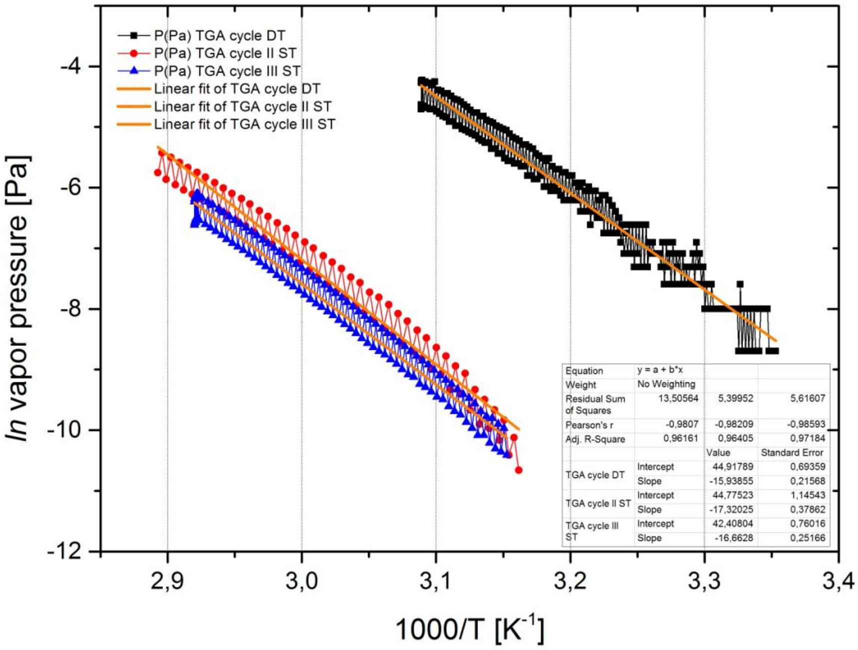

Equation	y = a + b*x		
Weight	No Weighting		
Residual Sum of Squares	13,50564	5,39952	5,61607
Pearson's r	-0,9807	-0,98209	-0,98593
Adj. R-Square	0,96161	0,96405	0,97184
		Value	Standard Error
TGA cycle DT	Intercept	44,91789	0,69359
	Slope	-15,93855	0,21568
TGA cycle II ST	Intercept	44,77523	1,14543
	Slope	-17,32025	0,37862
TGA cycle III ST	Intercept	42,40804	0,76016
	Slope	-16,6628	0,25166

Figure 6.1. Linear fit of vapor pressures obtained in different TGA cycles performed during the Deposition Test (DT) and Saturation Test (ST). From the slope of the curve and the intercept it is possible to obtain the enthalpy and entropy of sublimation of the organic compound used as contamination source.

To calculate vapor pressures at 298K in the second and third TGA cycles, a linear regression has been applied on data within the temperature range listed in table 6.1 was performed. The linear fit are >97% confidence interval of the linear regression. Indeed, for the first TGA cycle we were able to obtain the vapor pressure at 298K directly by measuring the flux with the QCM at that temperature.

Hence, the saturation vapor pressure at 298 K may deviate significantly from the mean of the published data points as shown in next subparagraph [Bilde 2015, Burns 2012]. The results for vapor pressures calculated at 298K are shown in table 6.1.

Table 6.1. Slopes and intercepts data obtained from the fit of *ln(P) [Pa]* vs. *1000/T* $[K^{-1}]$. The vapor pressure calculated at 298K are also reported as well as the temperature range where *Pi* have been calculated. For the second and third cycles, linear regression analysis has been performed to obtain P_{298K} due to higher temperature monitored.

TGA cycles	T_{range} (°C)	P_{298K} (Pa)	$-\Delta H_{sub}/R$ (kJ/mol)	$\Delta S_{sub}/R$ (kJ/mol)
I (DT)	25-50	5.01×10^{-6}	-15.94	44.92
II (ST)	47-72	1.65×10^{-6}	-17.32	44.76
III (ST)	44-69	1.36×10^{-6}	-16.66	42.41

6.2.2. P_i and ΔH_{sub} : results and comparison

In figure 6.2 the plot of the natural log of vapor pressure as a function of (1000/T) are shown for the adipic acid. At left of figure 6.2 are shown the solid-state vapor pressure obtained from different methods (described in par. 6.6) and reviewed from Bilde (2015). At right of figure 6.2, the vapor pressure of adipic acid obtained during three TGA cycles using QCM are shown (this work). In particular, the difference between the black line and red/blue lines plotted are probably due to the different temperature range monitored (25-50°C for black line and 44-72°C for red-blue lines) and to the different test performed.
Indeed, the first test (black line) is referred to the deposition test (DT) with low material deposited on QCM surface (~30 μg cm^{-2}) whereas the second and third tests (blue/red lines) are referred to two different TGA cycles performed after the saturation test (ST) where about 730 μg cm^{-2} of material was deposited on QCM. Therefore, the different mass depositions ($\Delta M_{ST} \cong 25\ \Delta M_{DT}$) can be the cause of the shift between the vapor pressure obtained in the first and second/third tests (black and red/blue trend) (i.e. during the TGA performed in the DT the acids desorbs faster than in TGA performed in ST).

In order to compare our results, the Clausius-Clapeyron equation has been used to extrapolate the vapor pressure at 298 K. The vapor pressures at 298K have been calculated and compared with solid-state vapor pressure obtained in different works concerning the adipic acid. In figure 6.3, the calculated average value (P_{298K} *[Pa]*, red filled square) has been compared with vapor pressure from previous works and with the average value of them (light blue filled circle, Fig. 6.3). The same average values are listed in Tab. 6.2 (bold values) as well as the vapor pressure at 298K obtained using different experimental methods. Generally, there is a variability in the published adipic acid vapor pressure (from 8.4×10^{-6} Pa to 1.4×10^{-5} Pa, Tab. 6.2 Indeed, our average value are different by one order of magnitude in difference with the average value from literature data (1.9×10^{-5} Pa with 2.7×10^{-6} Pa, Tab. 6.2) but in agreement within 2 times the error bars. Besides, our result is comparable with Booth (2010), Cappa (2007) and Bruns (2012).

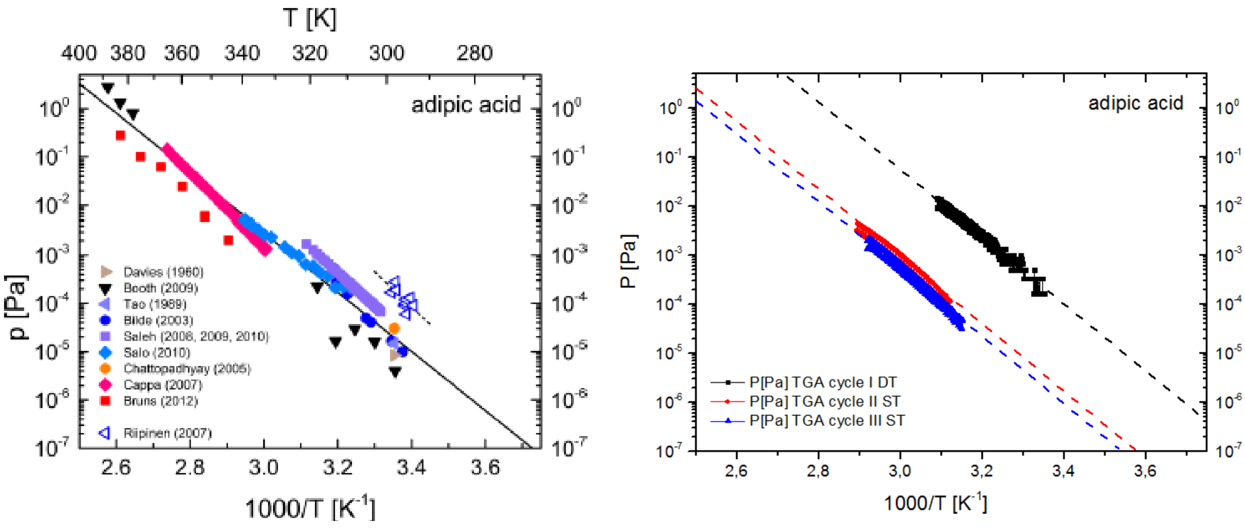

Figure 6.2. Natural log of vapor pressure measurements as a function of temperature: *P [Pa]* è vs. *(1000/T) [K^{-1}]*. The trends obtained in this work and in literatures are shown in the same temperature interval. *Left (from Bilde 2015)*: saturation vapor pressure of the solid-state (filled symbols) and the subcooled liquid state (open symbols) of adipic acid reported in the literatures: Davies and Thomas (1960), Booth (2009), Tao and McMurry (1989), Bilde (2003), Saleh (2008), Saleh (2009), Saleh (2010), Salo (2010), Chattopadhyay and Ziemann (2005), Cappa (2007), Bruns (2012) and Riipinen (2007). The lines represent a linear least-squares fit. Solid-state vapor pressure (black solid line) and subcooled liquid state vapor pressure (black dashed line). *Right (this work)*: the vapor pressure of adipic acid obtained with different TGA cycles (from 298 to 345K) are shown. The linear fit for each vapor pressure data set have been performed and extended (black, red and blue dashed lines) throughout the temperature range. The fit results are listed in table 6.2.

The P_{298K} [Pa] high variability is probably due to the different methods used (temperature range monitored, pressure and heating methods, Par. 6.6). For example, in Bruns (2012), an Atmospheric Solids Analysis Probe Mass Spectrometry (ASAP-MS), a relatively new atmospheric pressure ionization technique, has been used to determine the vapor pressures and heats of sublimation by means of Clausius-Clapeyron equation. The samples were analysed in the temperature range: 71-110°C (completely different from our work) obtaining the data set (consisting of mass spectra as a function of temperature) used to measure the evaporation rates and by means of the kinetic theory of gas, the vapor pressures. The evaporation rates have been also obtained by Saleh (2008) by using the Integrated Volume Method (IVM, easier to implement than the classic TDMA method) to estimate P_{sat} and ΔH_{sub} of lab-generated semi-volatiles organic aerosol (pimelic and adipic acids, aerosol distribution).

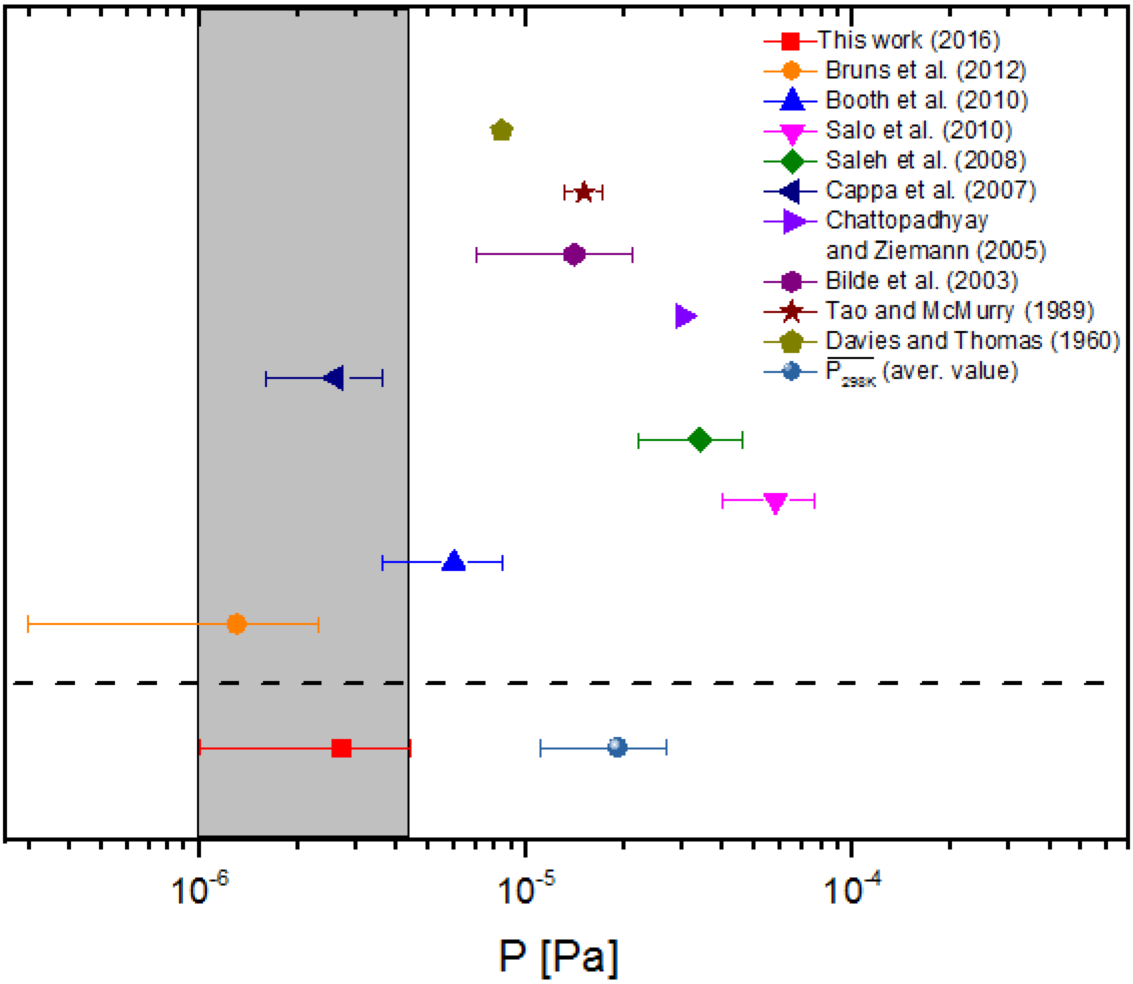

Figure 6.3. Best estimates (based on the fit) for the vapor pressure in the solid-state at 298K (red filled circle) of adipic acid together with the reported vapor pressures at 298 K by the individual experiments shown in figure 6.2. The different colors are referred to previous works: Davies and Thomas (1960), Booth (2009), Tao and McMurry (1989), Bilde (2003), Saleh (2008), Salo (2010), Chattopadhyay and Ziemann (2005), Cappa (2007), Bruns (2012). The average value obtained from previous works is the light blue filled circle: 1.9×10^{-5} Pa. The results have been shifted each one along the "y" axis in order to distinguish the vapor pressure values. The grey rectangle emphasizes the error bars of the average vapor pressure obtained with TGA method.

The method used by Cappa (2007) shared some general similarities to the TPD experiments of Chattopadhyay and Ziemann (2005), however this method allows for direct measurement of temperature-dependent evaporation rates (and therefore vapor pressures) directly from Hertz-Knudsen equation. This method: the Proton-Transfer Chemical Ionization Mass Spectrometry (PT-CIMS) was used for detection of the evaporated molecules. The result obtained by Cappa (2007) suggest that the vapor pressures of the diacids are typically lower than those measured using TDMA [Tao and McMurray 1989, Bilde 2003] or Knudsen cell [Davies and Thomas 1960, da Silva 1999] or other TPD methods [Chattopadhyay and Ziemann 2005] whereas is fully comparable with our average value (TGA method). Generally, our average value, i.e. $\overline{P_{298K}}$, is lower than those obtained with KEMS and EM methods while is higher than the other results (Tab. 6.2). The obtained enthalpy of sublimation (136.5 kJ mol^{-1}) is generally higher than results obtained with other methods excluding the results obtained with TDPBMS, TDMA and PT-CIMS.

Table 6.2. Experimentally derived vapor pressures at 298K, enthalpy of sublimation, i.e. ΔH_{sub} and the integration constant *C* of previous works in different temperature range of adipic acid. The average results of enthalpy of sublimation (bold values) are in agreement within 5%.

Reference	P_{298K} (Pa)	C	$\Delta H_{sub} \pm \sigma_{\Delta H}$ (kJ/mol)	T_{range} (°C)	Method
This work	**$(2.7 \pm 1.7) \times 10^{-6}$**	43.9±0.5	**136.5±1.2**	25-70	TGA
Bruns et al. (2012)	$(1.3 \pm 1) \times 10^{-6}$	41.5±5	136±10	71-110	ASAP-MS
Booth et al. (2010)	$(6 \pm 2.4) \times 10^{-6}$	27.8±0.6	119±18	30-60	KEMS
Salo et al. (2010)	$(5.8 \pm 1.8) \times 10^{-5}$	-	97±8	30-84	VTDMA
Saleh et al. (2008)	$(3.4 \pm 1.2) \times 10^{-5}$	-	135±13	27-40	IVM
Cappa et al. (2007)	$(2.6 \pm 1) \times 10^{-6}$		145±8	55-95	PT-CIMS
Chattopadhyay and Ziemann (2005)	$(3.02) \times 10^{-5}$	21.1	146,2	12-34	TDPBMS
Bilde et al. (2003)	$(1.4 \pm 0.7) \times 10^{-5}$	-	154±6	17-41	TDMA
Tao and McMurry (1989)	$(1.5 \pm 0.2) \times 10^{-5}$	36.3	118	10-50	TDMA
Davies and Thomas (1960)	$(8.4) \times 10^{-6}$	35.6	129±1	86-133	EM
$\overline{P}$, $\overline{\Delta H_{sub}}$ **(Bilde et al. 2015)**	**$(1.9 \pm 0.8) \times 10^{-5}$**	-	**131±18**	-	-

As listed in table 6.2 the enthalpy of sublimation and the integration constant, *C* have been obtained and compared with the average value from literatures data. The results obtained in this work are in agreement within 5% with the mean of the published sublimation enthalpies: $\overline{\Delta H}_{sub,adipic}$ = (131±18) kJ mol^{-1}. Table 6.2 summarizes the vapor pressure measurements as a function of temperature as well as the enthalpies value for the adipic acids. A comparison between our results (red filled square) and literatures data are shown in figure 6.4. The average enthalpy obtained with TGA method is within the errors bar of the calculated average enthalpy from previous works ($\overline{\Delta H}_{sub}$).

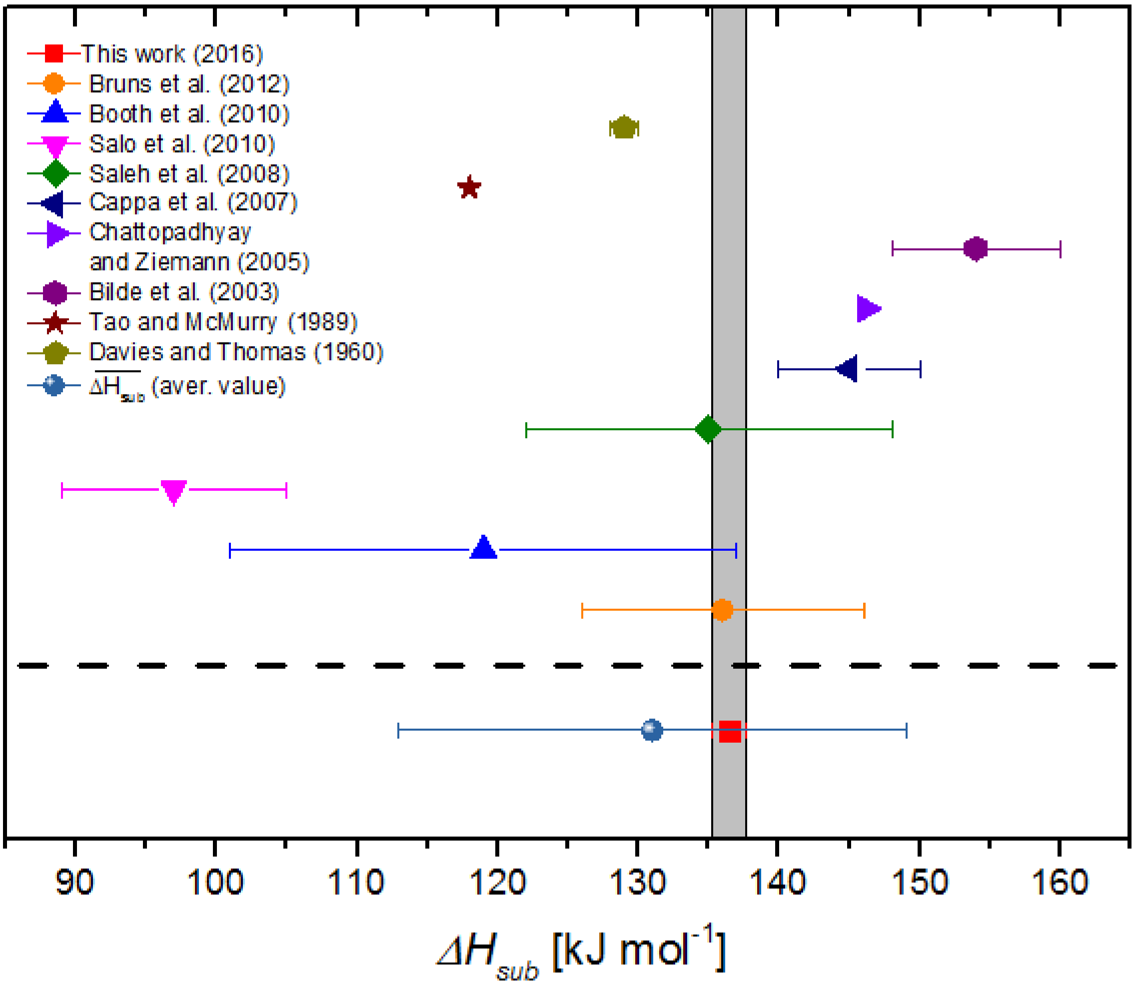

Figure 6.4. Best estimates (based on the fit) for the enthalpy of sublimation (red filled square) of adipic acid together with the reported enthalpy by the individual experiments. The different colors are referred to previous works as shown in figure 6.2. The enthalpy of sublimation obtained are compared with literatures: Davies and Thomas (1960), Booth (2009), Tao and McMurry (1989), Bilde (2003), Saleh (2008), Salo (2010), Chattopadhyay and Ziemann (2005), Cappa (2007), Bruns (2012). The average value obtained from previous works is the light blue filled circle, i.e. $\overline{\Delta H}_{sub}$ = (131±18) kJ mol^{-1}. The results have been shifted each one along the "*y*" axis in order to distinguish the enthalpy values. The grey rectangle emphasizes the error bars for enthalpy of sublimation result obtained with TGA method.

6.3. SH2 for organic compounds characterization (Effusion Method)

The dicarboxylic acid chemical formula is HOOC $(CH2)_{n=2}$COOH where '*n*' is the number of carbon atoms. The considered samples (described in Par. 2.5) are small grains in white crystalline form (odorless solid) with a purity degree of 99%. Considering the sublimation point of these acids and the temperature range available by our set-up (from 25 to 80°C), the studies are focused on acids with '*n*' between 2 and 9 carbon number: Oxalic (*n*=2), Succinic (*n*=4), Adipic (*n*=6), Suberic (*n*=8) and Azelaic (*n*=9) acids. Adipic acid was provided by Sigma Aldrich S.r.l., succinic acid by Institute of Translational Pharmacology (ITF-CNR, Rome, Italy), while azelaic, suberic and oxalic acids were kindly provided by the University of Rome, Sapienza (Department of Chemistry). Some structural and thermodynamic characteristics of the acids utilized in this work are shown in table 6.3.

Table 6.3. (*from* [a]*Afeedy, H.Y., NIST 1998*; [b]*CRC Handbook of Physical Properties of Organic Chemicals*; [c]*CAS Data Base List - Chemical Book*) **.**Thermodynamic properties of the compounds used in experiments at ambient pressure. In particular, the oxalic and succinic acids have a high solubility in water, and are the most present in submicron terrestrial aerosol.

Name	**Oxalic(C_2)**	**Succinic(C_4)**	**Adipic(C_6)**	**Suberic (C_8)**	**Azelaic(C_9)**
Chemical formula[a]	$C_2H_2O_4$	$C_4H_6O_4$	$C_6H_{10}O_4$	$C_8H_{14}O_4$	$C_9H_{16}O_4$
Molecular weight[a]	90.03	118.0880	146.1412	174.1944	188.2209
Water solubility(mg/l) at 25°C	[b]2.2×10^5	[b]8.3×10^4	[b]3.2×10^2	[c]6×10^3	[c]2.28×10^3
Vapor Pressure(torr)[c]	<1 (20°C)	3 (20°C)	1 (160°C)	5 (25°C)	<1 (20°C)
ΔH_{sub}($kJmol^{-1}$)[a]	93-98	118-123	129.3	143.1	156-159
ΔH_{fus}($kJ\ mol^{-1}$)[a]	--	32,9	34,8	28.8	32,6
T_{fusion}(°C)[a]	189.5	188	152.1	142.1	110

6.4. Experimental activity

6.4.1. Measurement procedure and data acquisition method

In order to measure the enthalpy of sublimation, QCM has been used as a mass attractor for the volatile molecules inside the teflon micro-sublimation chamber. Firstly, the crystal in thermal contact with a copper plate was cooled down to -72°C (constant temperature during the heating cycle). Then, each sample (13–20 mg) was placed in an effusion cell and at a later stage was heated by a resistance in a range of temperature from 25–30 to 75–80°C. The stabilization of the VOC's molecular flow at each heating temperature was obtained by keeping the temperature constant for 30 min, while a good distinction between two successive flows at two different temperatures was possible by adopting temperature steps of 5°C. The QCM frequency and temperature were measured every 2 seconds. Then, deposition rates are measured at each temperature set point in $mol\ cm^{-2}\ s^{-1}$ (Tab. 6.6 deposition rates comparison). Finally, in order to infer the enthalpy of sublimation in a well-defined temperature range (from 25–30°C to 75–80°C), different couples of temperatures (T_1 and T_2) are considered for data analysis. By applying the Van 't Hoff equation (eq. 3.10) to each couple of T_1 and T_2 and considering the related deposition rates k_1 and k_2, measured in $Hz\ s^{-1}$, ΔH_{sub} is inferred. The parameters of heating cycles of different acids, i.e. initial mass, pressure, expected enthalpy of sublimation, temperature range, stabilization time at each temperature, are listed in table 6.4.

Table 6.4. Parameters of the experiments involving the different dicarboxylic acids. λ_{Start} and $\lambda_{Sublimated}$ are the initial mass and the sublimated mass of the sample measured before and after the heating process with an electronic balance. Pressure is stable in the range of 10^{-6} - 10^{-7} mbar. T_L is the limit temperature, i.e. the temperature above which a slope change of deposition curve is expected. $T_{Monitored}$ is the temperature interval where the effusion cell was heated. $\Delta t_{Stabilization}$ is the time interval where the frequency and temperature data have been recorded and used for the analysis. $\Delta H_{literature}$ is the average value obtained from the in literature values (for oxalic acid, only the enthalpy of dehydrates form have been considered) which using different methods (see table 6.7)

Name	**Oxalic(C_2)**	**Succinic(C_4)**	**Adipic(C_6)**	**Suberic (C_8)**	**Azelaic(C_9)**
λ_{Start} (mg)	20± 0,5	13.0±0.5	13.0±0.5	18.0±0.5	19± 0.5
P_{work} (mbar)	$3{,}5 \times 10^{-6}$	$6{,}5 \times 10^{-6}$	$5{,}5 \times 10^{-6}$	$3{,}5 \times 10^{-6}$	8×10^{-7}
T_L (°C)	55	55	70	70	60
$T_{Monitored}$ (°C)	25 to 65	30 to75	30 to 75	40 to 75	25 to 80
$\Delta t_{Stabilization}$ (min)	30	30	30	30	20
$\Delta H_{Literature}$	73	118	134	130	149
$\lambda_{Sublimated}$ (mg)	3	1	4	2	3

Our set-up and measurement procedure is similar to Albyn (2001). We can predict that a temperature stability within ±0.5°C (temperature control on effusion cell) should produce an error on the enthalpy of sublimation within ±7%. This value would be a good starting point for the organic compounds analysed in this work. This value is mainly related to the temperature instability of the sample heating and the efficiency of the deposition process [Albyn 2001].

When the crystal is at -72°C and the effusion cell at 30°C, the succinic and oxalic acids already show higher sublimation rates than adipic and azelaic acids. Thus, the enthalpy of sublimation has been calculated considering a maximum temperature of 55°C for oxalic and succinic, lower than those used for adipic acid, i.e. 70°C, suberic acid, i.e. 65°C and azelaic, i.e. 60°C (see table 6.6). Besides, the retrieval of the enthalpy of sublimation can be considered reliable as long as T_2 is quite distinct (≥5°C) from the temperature limit, T_L (Tab. 6.4), where the flows of molecules are not reliable. Choosing $T_2 \sim T_L$, a slope change of deposition curve is expected due to the phase transition or due to the introduction of a new physical–chemical process.

6.4.2. Deposition rates

Molecular or atomic species released from a material during the outgassing-sublimation processes are typically quantified and characterized by means of the total amount of material that is lost through the outgassing-sublimation processes (often referred to as the total mass loss for the material). The material released during these processes is quantified with the measured deposition rates which give information about the condensation rate of outgassed/sublimated materials on the QCM surface.

By means of QCM sensitivity, the measured change in frequency can be converted into a deposition rate.

The deposition rate is typically reported in units of grams per centimeter squared-second and are calculated from the observed change in the frequency with time *(Hz/s).*

Thus, the deposition rates have been calculated from the frequency acquisition. In particular, from two consecutive frequency acquisition, divided by $\Delta t=10$ *sec.*, the deposition rates df/dt have been obtained in *Hz/s*. As shown in figure 6.5, the deposition rates trend increase when the temperature increase. Sure enough at low temperatures also, i.e. 30-35°C, a decrease in frequency has been observed during the calibration phase. In table 6.5, the deposition rates obtained from the preliminary test and second attempt using the adipic acid as calibration source are listed.

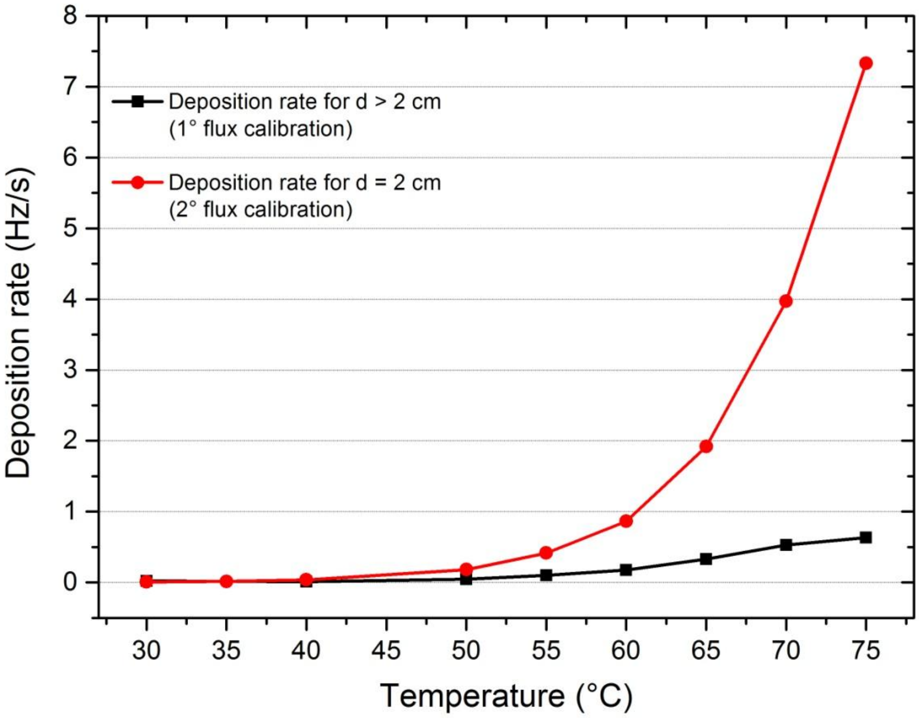

Figure 6.5. Calibration curves performed in different tests: the black curve is the Adipic acid flux for d>2 cm while the red curve is the flux for d=2 cm. Considering different distances (2 cm or more between the source and QCM) it is possible to increase of molecules flux by 10 factor at 75°C.

Table 6.5. Deposition rates observed in the preliminary test and in the second attempt are listed. The difference related to deposition rates is mainly explained in subpar. 4.4.2.

T_{cell} (°C)	***df/dt* (Hz/s)** **preliminary test**	***df/dt* (Hz/s)** **second attempt**
40	0,020	0,037
50	0,073	0,182
55	0,053	0,416
60	0,150	0,863
65	0,250	1,919
70	0,312	3,972
75	0,430	7,330

Taking into account the developed setup it is possible to obtain deposition flux eight times higher than the deposition rates obtained during the preliminary test. In figure 6.5 the deposition events are shown. Deposition rates with $\Delta T=5°C$ and $\Delta t=30$ for each temperature step. The difference behavior of the fluxes is due to the distance between the source and QCM surface (Fig. 6.5 and explained in subpar. 4.4.2).

The frequency and temperatures acquisition have been performed every 2 seconds while the enthalpy of sublimation have been obtained for frequency values every 10 seconds in order to minimize the errors due to frequency oscillations (highest at low temperatures, i.e. 30-40°C). The

6.4.3. Enthalpy of sublimation retrieval

Deposition rates *df/dt* in $Hz\ s^{-1}$ were measured with a sampling rate of 10 seconds. A QCM frequency decrease was observed at increasing temperature due to the larger VOC deposition.
The rates in $Hz\ s^{-1}$ were multiplied for the QCM sensitivity (4.4 $ng\ cm^{-2}\ Hz^{-1}$) and converted into $g\ cm^{-2}\ s^{-1}$. Then, they were divided by the substance molecular weight and converted into $mol\ cm^{-2}\ s^{-1}$ (see table 6.7). Finally, the enthalpy of sublimation and its error were expressed in $kJ\ mol^{-1}$ (Tab. 6.7 and Tab. 6.8). The uncertainty of temperatures and deposition rates has been calculated as standard deviation of the mean, due to the Gaussian distribution of measured values of *df/dt* and temperature distribution (Fig. 6.6 and Fig. 6.7). Indeed, performing the χ^2 test for each frequency variation (*df/dt*) and temperature data set (with a significance level of 5%) we can verify the Gaussian distribution for the each data set. In this case, the standard deviation of the mean can be assumed for the frequency and temperature data whereas the classic stardard deviation has been assumed when our data distrubution is not represented by Gaussian distribution.

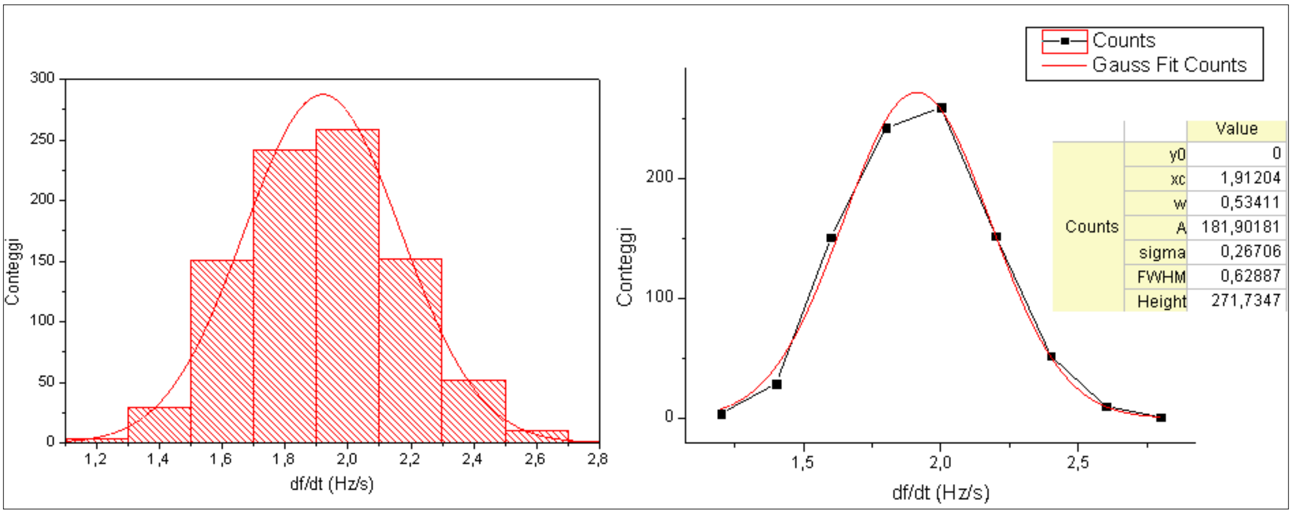

		Value
Counts	y0	0
	xc	1,91204
	w	0,53411
	A	181,90181
	sigma	0,26706
	FWHM	0,62887
	Height	271,7347

Figure 6.6. Deposition rates distribution at T_{cell}= 65°C, of *df/dt* every 10 seconds. *Left*: the histograms shows the distrubution of deposition rates around the medium value of 1.9 *Hz/s*. *Right*: Gaussian fit performed shows that it is possible to assume the standard deviation of the mean on the deposition rates at 65°C.

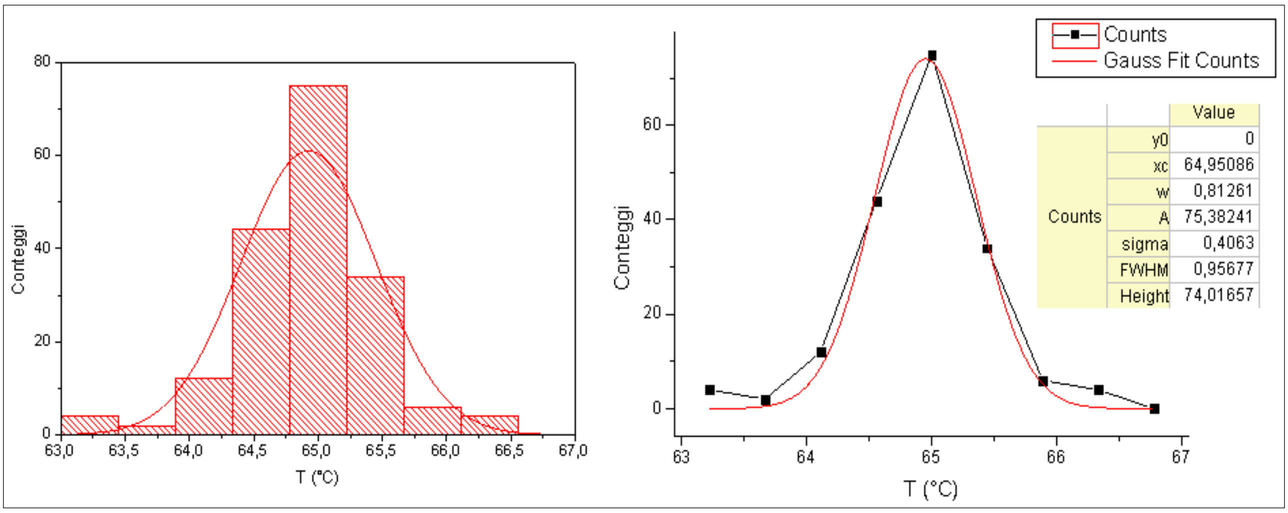

		Value
Counts	y0	0
	xc	64,95086
	w	0,81261
	A	75,38241
	sigma	0,4063
	FWHM	0,95677
	Height	74,01657

Figure 6.7. Temperatures distribution at T_{cell}= 65°C. *Left*: the histograms shows the distrubution of temperatures around the medium value of 65°C. *Right*: Gaussian fit performed shows that it is possible to assume the standard deviation of the mean of temperatures data.

The weight average values (ΔH_{sub}) obtained in this work are reported in table 6.8. These results have been obtained with the weight function:

$$\omega_i = (\frac{1}{\sigma_i^2}) \tag{6.2}$$

where the "i" index expresses the number of data obtained listed in tab.6.7.Thus, ΔH_{sub} can be calculated as:

$$\Delta H_{sub} = [(\Sigma_i \omega_i \Delta H_i)/(\Sigma_i \omega_i)] \tag{6.3}$$

Thus, in order to monitor enthalpy variation over the whole considered temperature range considered, a good choice for T_2 could be a temperature not close to T_L (i.e. from 60 to 70°C for adipic acid, 60-65°C for suberic acid, from 50 to 60°C for azelaic acid, and from 45 to 55°C for succinic acid). Our results were compared with previous works (Tab. 6.8) that use a similar effusion method and theoretical approach, i.e. Albyn (2001), Booth (2009), Ribeiro da Silva (2001) and with works that analyze the same dicarboxylic acids used in our study, i.e. Chattopadhyay and Ziemann (2005), Bilde (2003), Salo (2010), Davies and Thomas (1960), de Wit (1983), Granovskaya (1948), Ribeiro da Silva (1999).

6.5. Data analysis and results

6.5.1. Oxalic acid (C_2)

A total frequency variation of 13 kHz has been observed for the oxalic acid in the whole temperature range monitored (Fig. 6.8): from 25 to 65°C, corresponding to a mass deposition of 9.3 μg. This compound (with short carbon chain, C_2) showed a high volatility even at low temperatures, confirmed by the moderately high deposition rates measured already at 25°C. The deposition rate curve shows a continuous increase up to 60°C, with a constant slope (Fig. 6.8).

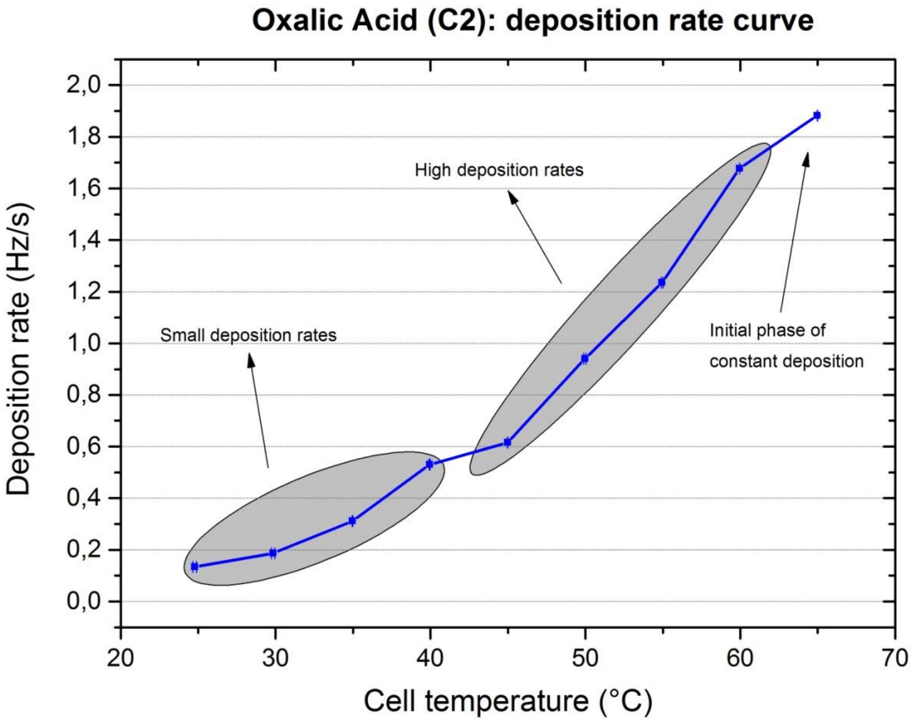

Figure 6.8. Oxalic acid deposition curve. The deposition rates are low from 25 to 40°C, are high from 45 to 65°C whereas at 65°C, shows a different slope due to a change in the desorption process.

The enthalpy of sublimation has been obtained in the temperature range from 25 up to 55°C (Tab. 6.7), due to the instability of the sublimation flows at temperatures larger than 60°C. Moreover, a best agreement is obtained when the difference between T_1 and T_2 is between 15 and 25°C (within 9% compared with the literature values, Tab. 6.8). The oxalic acid presents in its molecular structure two water molecules (dihydrate, monocline structure) which are lost at about 100°C and 1 bar. In this dehydration reaction, its molecular structure changes from monocline to rhombic crystals and becomes anhydrous [Bah l A. and Bahl B.S. 2010].

In our experiment, we considered a monocline dehydrate oxalic acid and the obtained enthalpy results (Tab. 6.8) differ to previous works, relative to the anhydrous form [Booth 2009]. On the contrary, our results, i.e. (62.5±3.5) kJmol^{-1} (Tab. 6.8), agree within 5.5% with values, relative to dehydrate oxalic acid [de Wit 1983, Granovskaya 1948], as it should be. Indeed, as verified by de Wit (1983), a difference for the sublimation enthalpy values between the two anhydrous forms (beta and alpha, obtained by means vacuum sublimation) and the dehydrate state (this work) happens due to the two water molecules' desorption from oxalic acid structure.

6.5.2. Succinic acid (C_4)

In the succinic acid case, the frequency decreases by 10.6 kHz in the whole temperature range monitored (i.e. from 30 to 75°C), corresponding to 5.9 μg. The measured deposition rates are shown in figure 6.9 (orange curve).

During the sublimation process, at temperature larger than 60°C, the deposition rate oscillates around a medium value (Fig. 6.9). The enthalpy of sublimation has been obtained in the temperature range from 30 to 55°C (Tab. 6.7) because of the instability of the flow of molecules from 60°C. Probably, a new chemical–physical process occurred at these temperatures. The results at 75°C have been excluded due to the high temperature oscillations occurred.

Succinic acid (with a short carbon chain, C_4) shows a smaller deposition rates than the oxalic acid, even if it already strongly sublimates at 25°C. The deposition rate curve shows an increase up to 60°C and a slope change beyond this temperature. The succinic acid tends to lose one water molecule easily, becoming succinic anhydride. A good temperature range to monitor enthalpy variation is 30-55°C, far away from the point where succinic acid changes its structure (~137°C) [Vanderzee and Westrum 1970]. In this range, the average enthalpy of sublimation measured is (113.3±1.3) kJ mol^{-1}, in agreement within 5% with the previous works [Chattopadhyay and Ziemann 2005, Davies and Thomas 1960] (Tab. 6.8). Considering the vacuum environment and an upper temperature larger than 55°C, the retrieved enthalpy may not be reliable for the transformation (initial phase) of succinic acid crystalline form (monocline/triclinic prisms) into cyclic anhydride, a ring structure (pyramidal crystal), losing one water molecule [Orchin 2005, Vanderzee and Westrum 1970].

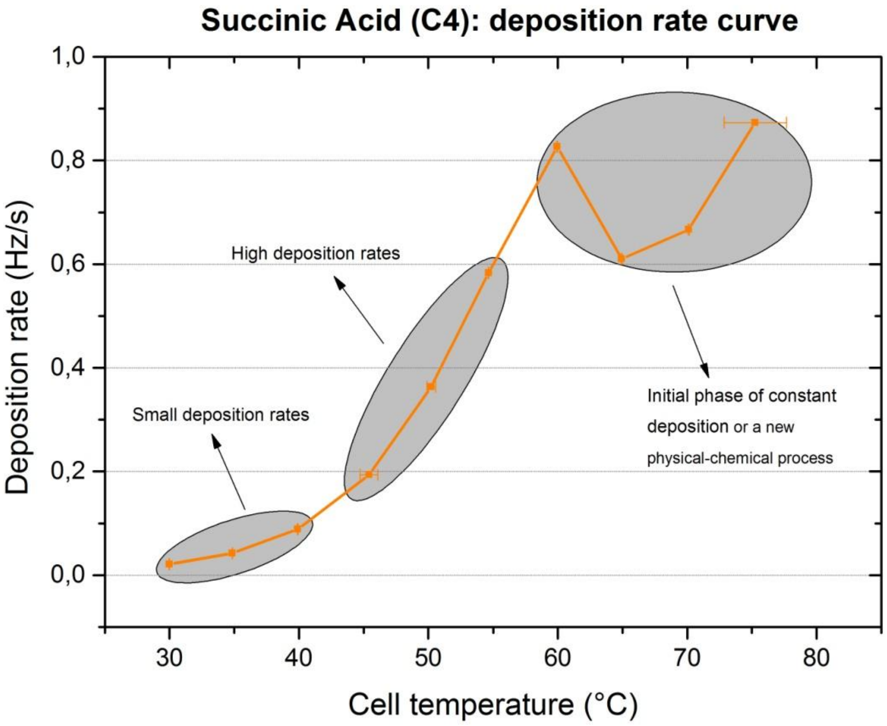

Figure 6.9. Succinic acid deposition curve. The deposition rates are low from 30 to 40°C while increase from 45 to 55°C. At 60°C, the deposition rates show a different slope due to a change in the physical-chemical process.

6.5.3. Adipic acid (C_6)

In the case of adipic acid (long carbon chain, C_6), a total frequency decrease of 28 kHz in the whole temperature range monitored (i.e. from 30 to 75°C, Fig. 6.10 black curve) corresponding to 15.5 μg has been observed. A considerable frequency variation is observed above 50°C, due to the high volatility of the acid at these temperatures. This acid sublimates at low pressure without a decomposition and only at 230–250°C changes its molecular structure, becoming cyclopentanone plus H_2O and CO_2. As a matter of fact, at temperatures lower than 50°C, the variation of deposition rates of adipic acids is only 1.5 and 27% of that measured for oxalic and succinic acid, respectively; this is due to the better stability of its carbon chain at these temperatures. The enthalpy of sublimation of adipic acid has been obtained in the temperature range from 40 to 70°C. The data acquired at 75°C have been excluded from the analysis due to the high temperature oscillations which produce unstable deposition rates. The deposition rates at 30 and 35°C have been also excluded because of the low flows of molecules. At these temperatures, the adipic acid flows are 2 orders of magnitude lower than the oxalic and succinic acids.

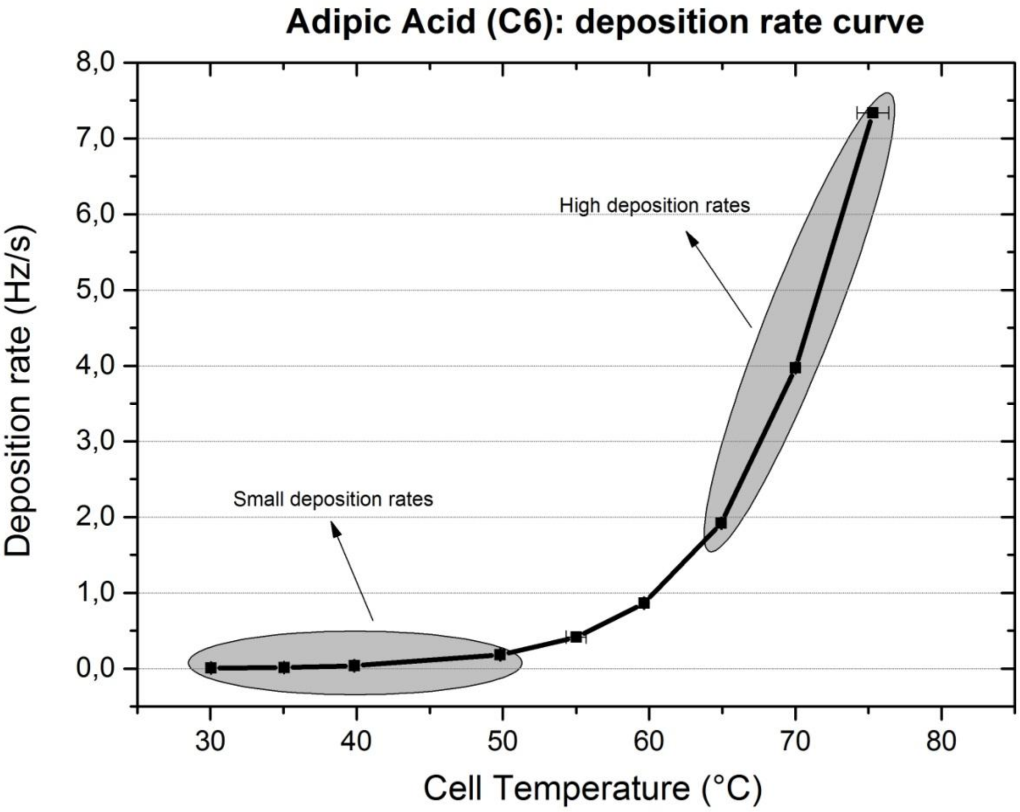

Figure 6.10. Adipic acid deposition curve. In particular, the fluxes at 30 and 35°C and at 75°C have been excluded from the analysis for low deposition and temperature oscillations (at 75°C), respectively. The flux from 60 to 70°C are a good range to calculate the enthalpy of sublimation.

6.5.4. Suberic acid (C_8)

In the case of suberic acid (long carbon chain, C_8), a total frequency decrease of 10 kHz in the whole temperature range monitored (i.e. from 40 to 75°C, Fig. 6.11 violet curve) corresponding to 5.6 μg has been observed. A considerable frequency variation is observed from 55 to 70°C, due to the high volatility of the acid at these temperatures. The frequency variation is very similar to succinic acid experiment while the deposition rates are lower than succinic acid rates from 45 to 60°C. This behavior can be ascribed to the better stability of high-carbon chain at low temperatures (observed also for adipic acid). In particular, the suberic acid, which can split off carbon the dioxide and water to form cyclic ketones, starts to decay from 141°C (melting point).

The enthalpy of sublimation has been obtained in the temperature range from 40 to 65°C. The data acquired at 70-75°C have been excluded from the analysis due to constant rates probably due to metastable phase or to one more new phase change.

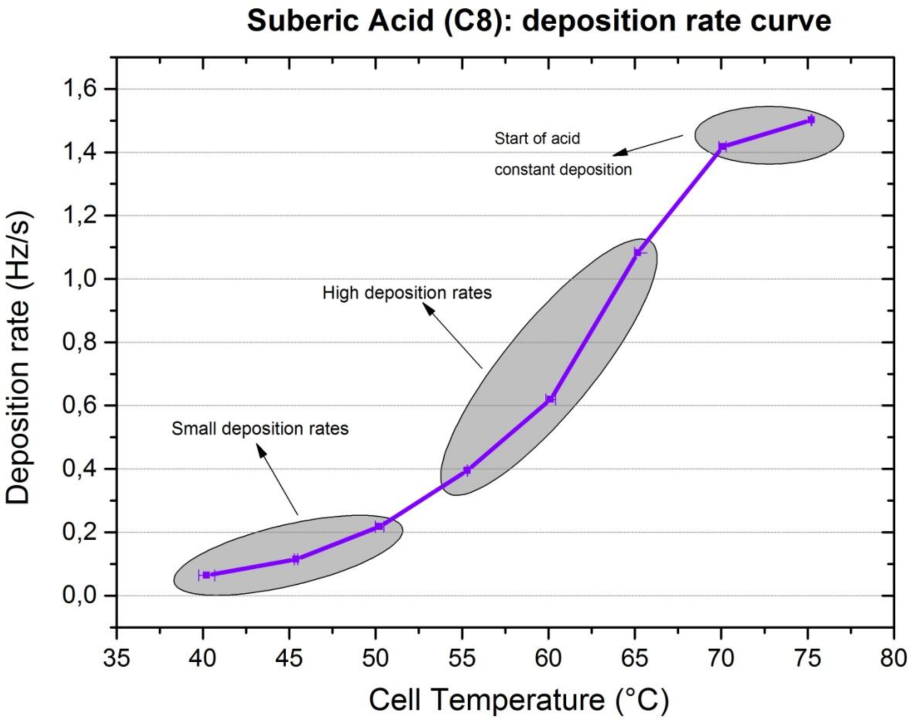

Figure 6.11. Suberic acid deposition curve. The fluxes at 70 and 75°C have been excluded from the analysis while a good temperature range to monitor enthalpy variation is 40-65°C, far away from the point where suberic acid changes its structure (~141°C) [Afeedy 2015]. In this range, the average enthalpy of sublimation measured is (101.4±1.9) kJ mol^{-1}. The best agreement is obtained with Salo (2010) who measures the enthalpy of sublimation of (101±10) kJ mol^{-1} (Tab.6.8) while is in contrast with Chattopadhyay and Ziemann (2005) and Davies and Thomas (1960) due to different temperatures range monitored (see Par. 6.6).

6.5.5. Azelaic acid (C_9)

Azelaic acid shows a larger frequency variation than succinic and oxalic acid, with a total frequency decrease in the whole temperature range monitored (from 35 to 80°C, Fig. 6.12 red curve) of 21 kHz corresponding to 11.6 μg. Azelaic acid presents a very slow sublimation up to 35°C and reaches the maximum deposition rate at 75°C (whereas at 80°C, the deposition rate begins to decrease). The enthalpy of sublimation has been obtained in the temperature range from 35 to 60°C (Tab. 6.7). The enthalpies of sublimation at temperatures higher than 60°C have not been considered reliable due to a decrease of the deposition rates. This compound starts to decay at 360°C (at atmospheric pressure) but in our experiment, the deposition curve shows a slope variation at 80°C and a instability of the deposition flow from 65 to 80°C (not used for the analysis). The reasons for that should be studied in more detail and the temperature range should be increased in order to monitor enthalpy variation at larger temperatures. Probably, monitoring a wider temperature range for the two other acids (oxalic and adipic) we could observe the same trend.

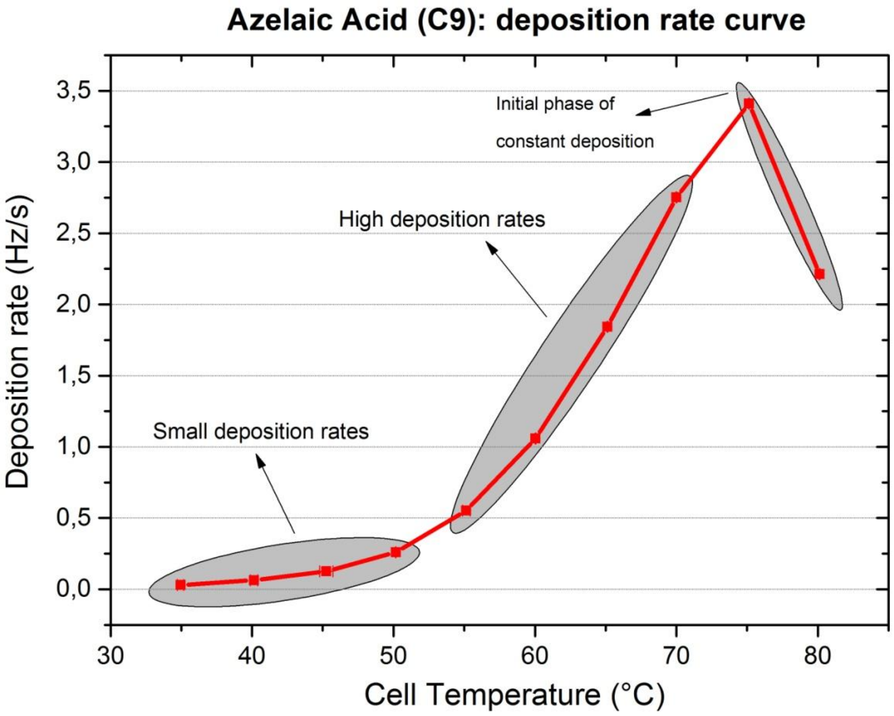

Figure 6.12. Azelaic acid deposition curve. The fluxes from 65 and 80°C have been excluded from the analysis while the enthalpy of sublimation has been calculated from 35 to 60°C.

6.6. Results and discussion

The deposition rates, reported in *Hz/s*, are listed in table 6.6. The long carbon chain samples as adipic (C_6), suberic (C_8) and azelaic (C_9) acids show lower deposition rates from 25 to 50°C than low carbon chain samples, i.e. oxalic (C_2) and succinic (C_4) acids. Indeed, the oxalic and succinic start to sublime from 25°C due to their high desorption behavior at these temperatures.

The enthalpy of sublimation values show also an increasing trend with the carbon atoms number (Tab. 6.8, Fig. 6.14) as demonstrated by previous works [Booth 2009, Davies and Thomas 1960]. As shown in Fig. 6.14, more complex is the molecular structure and higher is the enthalpy of sublimation.

In order to understand better the acid samples desorption in the temperature range: 25-80°C, the deposition rate trends are shown in Fig. 6.13.

Table 6.6. Deposition rates: dicarboxylic acids comparison

T_{cell} (°C)	df/dt (Hz/s) Oxalic acid (C_2)	df/dt (Hz/s) Succinic acid (C_4)	df/dt (Hz/s) Adipic acid (C_6)	df/dt (Hz/s) Suberic acid (C_8)	df/dt (Hz/s) Azelaic acid (C_9)
25	0,13	--	--	--	--
30	0,19	0,02	0,01	--	--
35	0,31	0,04	0,02	--	0,03
40	0,53	0,09	0,04	0,06	0,06
45	0,62	0,19	--	0,11	0,13
50	0,94	0,36	0,18	0,22	0,26
55	1,24	0,58	0,42	0,40	0,55
60	1,68	0,83	0,87	0,62	1,06
65	1,88	0,61	1,92	1,08	1,84
70	--	0,68	3,97	1,42	2,75
75	--	0,87	7,34	1,50	3,41
80	--	--	--	--	2,21

.

In particular, the Oxalic acid (*C=2)*, show higher desorption rates already from 25°C (blue line) while compounds with longer chemical structure $C \geq 6$ (adipic, suberic and azelaic acids) start to be different from zero from 45-50°C and show higher deposition rates starting to 60°C (adipic and azelaic acids). Indeed, at 50°C the deposition rates of succinic and oxalic are 2-4 times higher than the acids with carbon atoms number higher than 5. Calculating the saturation vapor pressures at 25°C it can be possible to study the odd-even acids alternation as stated from Bilde (2015) and discussed at the end of this paragraph.

The enthalpy of sublimation results are listed in Tab. 6.7. From data analysis, three different sources of errors have been identified that give a total uncertainty higher than 8 kJ mol^{-1} on the enthalpy of sublimation:

1. the temperature oscillations of ±0.5°C or larger;
2. the errors on deposition rates (Tab. 6.7 and subpar. 6.4.3);
3. two comparable fluxes obtained at two consecutive temperature T_1 and T_2 (Tab. 6.7).

As listed in Tab. 6.7 and as stated in subpar. 4.4.2, when the temperature oscillations are within ±0.5°C, the errors are ~8 kJ mol^{-1} or less, whereas when the temperatures oscillations are ±0.5°C or larger, the errors on the enthalpy of sublimation are larger than 8 kJ mol^{-1} (succinic, adipic, suberic and azelaic acids, underlined values in Tab. 6.7). In addition, when two deposition rates are similar (at two consecutive temperature T_1 and T_2, e.g. 60 and 65° or 55 and 60°C), the error on the enthalpy of sublimation are larger than ~11 kJ mol^{-1} (italic values in Tab. 6.7).

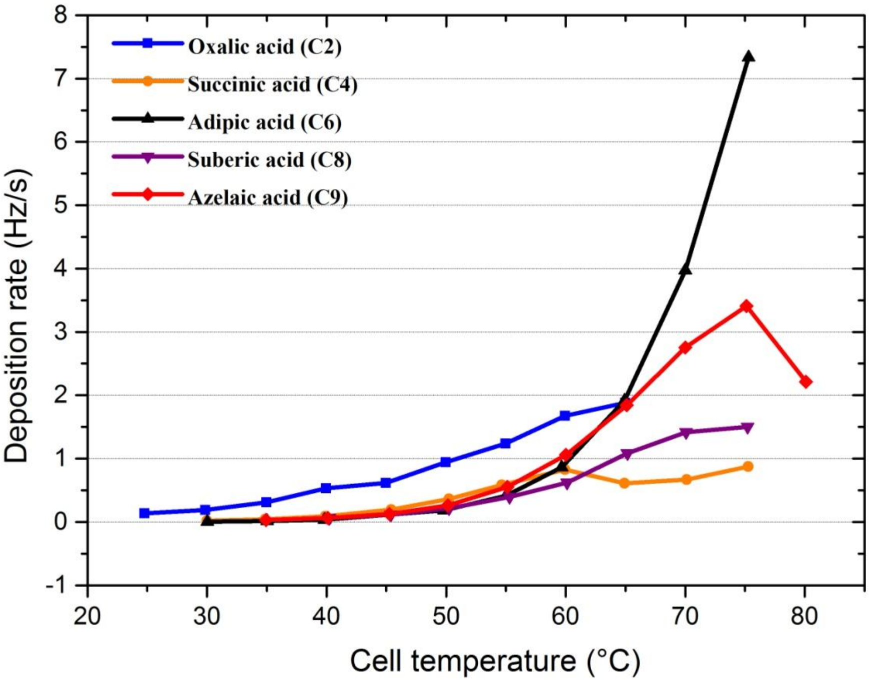

Figure 6.13. Deposition rates of dicarboxylic acids. Oxalic acid show high rates from 25°C while the deposition rates of samples with C≥6 start to be different from zero from 45-50°C (azelaic, suberic and adipic acids). In particular, adipic and azelaic acids show higher deposition starting to 60°C.

Table 6.7. Enthalpy of sublimation calculated from acid deposition rates measured in our experiment. Considering the succinic acid (bold highlighted values), when T_2 approaches T_L, the calculated enthalpy deviates from the previous work values whereas the temperature oscillations are ±0.5°C or larger produce an error ≥8 kJ mol^{-1} on the enthalpy of sublimation (underlined values). Instead, when two similar deposition rates (at two temperatures, e.g. 55-60 and 60-65°C, Azelaic and Suberic acid case, respectively) are used to calculate the enthalpy of sublimation, the error are larger than ~11 kJ mol^{-1} (italic values). Oxalic and succinic acids (weak lattice energies at low temperature) sublimate at smaller temperatures, in the range 25/30-55°C where the sublimation process was monitored. Otherwise, adipic and azelaic acid sublimate at larger temperatures. The temperature range is wide enough to calculate the enthalpy of sublimation but should be extended if the intent is to monitor the complete sublimation process (in particular for adipic acid, T≥75°C).

Acid	**$T_1 \pm \sigma_{T1}$(°C)**	**$T_2 \pm \sigma_{T2}$ (°C)**	**k_1 (mol cm^{-2} s^{-1})**	**k_2 (mol cm^{-2} s^{-1})**	**$\Delta H_{sub} \pm \sigma_{\Delta H}$(kJ mol^{-1})**
Oxalic	24.772±0.111	44.969±0.002	6.56×10^{-12}	3.01×10^{-11}	60.67±1.31
	29.843±0.105	44.969±0.002	9.15×10^{-12}	3.01×10^{-11}	64.35±0.64
	34.964±0.015	44.969±0.002	1.52×10^{-11}	3.01×10^{-11}	56.85±0.93
	24.772±0.111	49.962±0.075	6.56×10^{-12}	4.59×10^{-11}	63.15±1.34
	29.843±0.105	49.962±0.075	9.15×10^{-12}	4.59×10^{-11}	66.65±0.84
	34.964±0.015	49.962±0.075	1.52×10^{-11}	4.59×10^{-11}	62.40±1.07
	24.772±0.111	54.952±0.059	6.56×10^{-12}	6.04×10^{-11}	61.06±1.07
	29.843±0.105	54.952±0.059	9.15×10^{-12}	6.04×10^{-11}	63.44±0.60
	34.964±0.015	54.952±0.059	1.52×10^{-11}	6.04×10^{-11}	59.32±0.73
Succinic	34.85±0.02	45.42±0.68	1.59×10^{-12}	7.22×10^{-12}	117.93±4.36
	39.90±0.04	45.42±0.68	3.31×10^{-12}	7.22×10^{-12}	118.45±7.97
	34.85±0.02	50.22±0.02	1.59×10^{-12}	1.35×10^{-11}	116.61±3.32
	39.90±0.04	50.22±0.02	3.31×10^{-12}	1.35×10^{-11}	116.21±3.41
	29.98±0.02	54.64±0.02	8.01×10^{-13}	2.17×10^{-11}	111.88±4.15
	34.85±0.02	54.64±0.02	1.59×10^{-12}	2.17×10^{-11}	112.17±2.66
	39.90±0.04	54.64±0.02	3.31×10^{-12}	2.17×10^{-11}	110.27±2.47
	45.42±0.68	54.64±0.02	7.22×10^{-12}	2.17×10^{-11}	**105.14**±11.75
	50.22±0.02	54.64±0.02	1.35×10^{-12}	2.17×10^{-11}	**95.73**±3.47
Adipic	39.84±0.04	59.65±0.05	1.10×10^{-12}	2.60×10^{-11}	139.58±3.69
	49.82±0.04	59.65±0.05	5.47×10^{-12}	2.60×10^{-11}	142.90±3.06
	39.84±0.04	64.93±0.04	1.10×10^{-12}	5.78×10^{-11}	140.26±1.22
	49.82±0.04	64.93±0.04	5.47×10^{-12}	5.78×10^{-11}	142.95±1.86
	55.01±0.68	64.93±0.04	1.25×10^{-11}	5.78×10^{-11}	143.54±13.90
	59.65±0.05	64.93±0.04	2.59×10^{-11}	5.78×10^{-11}	142.99±4.98
	39.84±0.04	70.01±0.03	1.10×10^{-12}	1.20×10^{-10}	140.15±2.29
	49.82±0.04	70.01±0.03	5.47×10^{-12}	1.20×10^{-10}	142.14±1.22
	55.01±0.68	70.01±0.03	1.25×10^{-11}	1.20×10^{-10}	142.24±9.01
	59.65±0.05	70.01±0.03	2.59×10^{-11}	1.20×10^{-10}	141.34±2.18
Suberic	40.22±0.47	65.17±0.19	1.60×10^{-12}	2.76×10^{-11}	101.82±8.23
	45.39±0.10	65.17±0.19	2.89×10^{-12}	2.76×10^{-11}	103.61±3.22
	50.23±0.25	65.17±0.19	5.45×10^{-12}	2.76×10^{-11}	99.76±4.91
	55.30±0.01	65.17±0.19	9.98×10^{-12}	2.76×10^{-11}	**96.74**±4.09
	60.12±0.29	65.17±0.19	1.66×10^{-11}	2.76×10^{-11}	*__96.33__±13.29*
	40.22±0.47	60.12±0.29	1.60×10^{-12}	1.66×10^{-11}	103.11±10.83
	45.39±0.10	60.12±0.29	2.89×10^{-12}	1.66×10^{-11}	105.95±5.16
	50.23±0.25	60.12±0.29	5.45×10^{-12}	1.66×10^{-11}	101.44±8.59
	55.30±0.01	60.12±0.29	9.98×10^{-12}	1.66×10^{-11}	*97.15±10.62*
Azelaic	34.95±0.22	50.16±0.02	6.94×10^{-13}	6.09×10^{-12}	119.59±6.91

	40.13±0.26	50.16±0.02	1.48×10^{-12}	6.09×10^{-12}	120.24±8.27
	45.26±0.48	50.16±0.02	2.98×10^{-12}	6.09×10^{-12}	*126.42±20.11*
	40.13±0.26	55.14±0.27	1.48×10^{-12}	1.29×10^{-11}	124.70±8.06
	45.26±0.48	55.14±0.27	2.98×10^{-12}	1.29×10^{-11}	130.25±14.03
	50.16±0.02	55.14±0.27	6.09×10^{-12}	1.29×10^{-11}	*134.14±11.74*
	45.26±0.48	60.04±0.02	2.99×10^{-12}	2.48×10^{-11}	127.81±6.72
	50.16±0.02	60.04±0.02	6.09×10^{-12}	2.48×10^{-11}	128.53±1.86
	55.14±0.27	60.04±0.02	1.29×10^{-11}	2.48×10^{-11}	*122.65±10.71*

In table 6.8, the temperature range used is listed, as well as enthalpy results obtained in this study. A high accuracy has been obtained for succinic, adipic, and azelaic acid, i.e. within 1%, for Suberic acid, i.e. within 2% and within 5% for oxalic acid.

Table 6.8. Comparison of enthalpy of sublimation of dicarboxylic acids retrieved by different techniques (1=Booth 2009, 2=Granovskaya 1948, 3=Chattopadhyay and Ziemann 2005, 4=Bilde 2003, 5=Davies and Thomas 1960, 6a=Ribeiro da Silva 1999, 6b= Ribeiro da Silva 2001,7= de Wit 1983, 8=Albyn 2001, 9=Salo 2010). *ΔT(°C)* is the temperature range used to calculate the enthalpy of sublimation. The enthalpy values and corresponding errors reported for this work have been calculated as the weighted average. The anhydrous (A) and dehydrate (deh) forms of the Oxalic acid have been treated and the results for the enthalpy of sublimation have been reported.

Compound	P_{work} (mbar)	ΔT (°C)	ΔH_{sub} (kJ mol^{-1})	Reference	Technique
Oxalic	10^{-6}	25/55	$^{(deh)}$62.5±3.1	This work	QCM
	10^{-6}	30/60	$^{(A)}$75.0±19.0	1	KEMS
	--	20/50	$^{(deh)}$61.8	2	EM
	--	-22/54	$^{(deh)}$56.5	7	EM
	--	37/62	$^{(A)}$98.5	7	EM
Succinic	10^{-6}	30/55	113.3±1.3	This work	QCM
	10^{-6}	30/60	93.0±6.0	1	KEMS
	10^{-8}	7/29	119.5	3	TDPBMS
	10^{3}	17/41	138.0±11.0	4	TDMA
	10^{3}	99/128	117.5±3.3	5	EM
	10^{-7}	87/102	123.2±1.6	6b	KEM
Adipic	10^{-6}	40/70	141.6±0.8	This work	QCM
	10^{-6}	30/60	119.0±26.0	1	KEMS
	10^{-8}	12/34	146.2	3	TDPBMS
	10^{3}	17/41	154.4±6.0	4	TDMA
	10^{3}	86/133	129.2±1.0	5	EM
	10^{-7}	25/60	121.0±8.0	8	ASTM E-1559

Suberic	10^{-6}	40/75	101.4±1.9	This work	QCM
	10^{-8}	21/43	148	3	TDPBMS
	10^{3}	106/134	143±4	5	EM
	10^{3}	30/84	101±10	9	VTDMA
Azelaic	10^{-7}	35/60	124.2±1.2	This work	QCM
	10^{-8}	21/38	138	3	TDPBMS
	10^{3}	17/41	153±24	4	TDMA
	10^{-7}	95/113	155.8±1.6	6a	KEM

Thus, in order to demonstrate the high quality of our method and the validity of these results, the enthalpies of sublimation have been compared with the results obtained by previous works. In the comparison, the different boundary conditions (initial temperatures and working pressures) of the different procedures (Table 5.6): TDMA [Bilde 2003], Knudsen Effusion Mass-loss (KEM) [Ribeiro da Silva 1999], KEMS [Booth 2009], TDPBMS [Chattopadhyay and Ziemann 2005], the effusion method, EM [Davies and Thomas 1960, Granovskaya 1948], Volatility Tandem Differential Mobility Analyzer (VTDMA) [Salo 2010] and ASTM E-1559 Method B [Albyn 2001] have been taken into account.

The values of enthalpy of sublimation obtained in our experiments for succinic and adipic acids are within 5% of the enthalpy values reported by Chattopadhyay and Ziemann (2005), who present a Temperature Programmed Thermal Desorption Method (TDPBMS) where the particles were collected at -50°C in a vacuum chamber. Successively, by means of a heating process (2°C min^{-1}), the vapor pressure and evaporation rates of submicron particles were measured. This method use a modified Langmuir equation and the Clausius–Clapeyron equation, similar to our theoretical approach. The gap in the enthalpy results for Suberic acid are probably due measured vapor pressure performed at different vacuum pressure, i.e. 10^{-8} instead of 10^{-5}-10^{-6} mbar, which allows a different sample desorption process at low temperatures.

Our values are lower compared to those measured by Bilde (2003) (within 9% for the adipic acid), who demonstrate the capability of the tandem differential mobility analyser (TDMA) technique to measure the vapor pressures of submicron aerosol particles at solid-state structure. The results of evaporation rates were measured over the temperature range 17-41°C. In the TDMA technique, the major source of error was based on the sensitivity analysis (a conservative uncertainty and systematic errors were considered on vapor pressures).

A different method was used by Booth (2009), who directly measured the steady state vapor pressure using the Knudsen effusion mass spectrometry (KEMS) method with a solid sample. In Booth (2009), the working pressure and heating method of the sample was similar to ours: there was a temperature step of 5°C considering 10 min of stabilization time. The enthalpy obtained for adipic and succinic acids is smaller than that measured in this work and is larger than that for the oxalic acid. However, it should be noted that their measurements are affected by a large uncertainty; in particular, the errors obtained for oxalic acid (19 kJ mol^{-}

^{1}) are the result of the variation in the three calibration compounds used for that determination, whereas the high error on the adipic acid (26 kJ mol^{-1}) is the result of low pressures, resulting in decreased signal-to-noise ratio. Regarding the oxalic acid, as discussed above, it is highlighted that these authors measured the value of the α-orthorhombic anhydrous form and a difference from our results is expected. This difference is evident in de Wit (1983) results, where the analysis of the dehydrate and anhydrous form (prepared by a prolonged evacuation of the hydrate substance and vacuum sublimation) of the oxalic acid has been performed. The enthalpy of sublimation of oxalic acid, as listed in table 6.7, agrees within 5.5% of the average value obtained from the dehydrated results [de Wit 1983, Granovskaya 1948]. Instead, Ribeiro da Silva (1999, 2001) present Knudsen mass-loss effusion, a method similar to Booth (2009) in order to study the vapor pressures of crystalline dicarboxylic acids at much higher temperatures. The vapor pressures were calculated with a Langmuir equation, whereas the enthalpy of sublimation at the mean temperature was derived by the Clausius-Clapeyron equation.

Ribeiro da Silva (1999) results show larger values than ours (Tab. 6.8): 32 kJ mol^{-1} for azelaic acid [Ribeiro da Silva 1999] and 10 kJ mol^{-1} for succinic acid [Ribeiro da Silva 2001]. As stated by Bilde (2015) the enthalpy of sublimation values between the different experimental methods can differ by tens of kilojoules per mole. The results of Davies and Thomas (1960), who measured heat and entropy of sublimation by means of the effusion method at 1.013 bar pressure, are in agreement with our values, i.e. within 9.5% for adipic acid and within 4% for succinic acid even though shows a difference of 42 kJ mol^{-1} for suberic acid due to different temperature range used to obtained the enthalpy of sublimation (106-134°C instead of 40-65°C, this work).

Albyn (2001) used two different 15 MHz microbalances cooled at -42°C in a vacuum chamber to measure the deposition rates of adipic acid from 25 to 60°C. The enthalpy of sublimation measured by Albyn (2001) is 121.8 kJ mol^{-1} and shows a difference of 20 kJ mol^{-1} compared to our result (Tab. 6.8). This is probably due to the different set-up and measurement procedure, i.e. the microbalance's temperature of -42°C instead of -72°C (this work) and the distance between the sensing crystal and the sample of 20 cm instead of 2 cm (this work). The constant error of 8 kJ mol^{-1}, obtained with a temperature stability of ±0.5°C on the effusion cell [Albyn 2001], could be due to the re-evaporation of a minor portion of the deposited material. In this work, when the temperature stability is within ±0.5°C, the error does not exceed 5 kJ mol^{-1} (Tab. 6.7, oxalic, succinic and adipic acid). This improvement in the accuracy could be due to our increased gas flow of adipic molecules.

The enthalpy of sublimation measured by Salo (2010) is (101±10) kJ mol^{-1} is in good agreement with our results (Tab. 6.8). This is probably due to the similar temperature range used to calculate the enthalpy of sublimation even though the set-up and measurement procedure were different. In particular, the Volatility Tandem Differential Mobility Analyzer (VTDMA) technique (generally applied to focus the attention on the

SOA formation) has been used by Salo (2010) to study the dicarboxylic acids vapor pressures in the temperature range: 17-41°C. This technique uses the acid aerosol with selected particles from 80 to 110 nm (using the differential mobility analyzer, TSI 3071) and the Clausius-Clapeyron equation to obtain the enthalpy of sublimation (from the slope of the curve: *lnp vs. 1/T*). In Salo (2010), the experimental uncertainties are related to the flow rates and evaporative temperature while for ΔH_{sub}, the error stated is at the statistical 95% confidence level for the least-squares regression fit to the assumed linear Clausius-Clapeyron relationship.

Thus, main differences observed among the various examined works and enthalpy results are probably due to different temperature and pressures considered in the experiments and different forms of the sample (e.g. solid or aerosol), which produced different deposition rates and vapor pressures at each monitored temperature.

Data analysis has been performed excluding the set point with high temperature oscillations (adipic and succinic acids) which affects the deposition rates trend and the low flows of molecules at lower temperatures (e.g. 30–35°C, adipic acid case). As listed in Tab. 6.7, a temperature stability within ±0.5°C on the effusion cell causes errors on the enthalpies of sublimation lower than 4% for oxalic, adipic, and succinic acids (a better accuracy compared with Albyn 2001), whereas when the temperature stability is ±0.5°C or larger, the corresponding errors are larger than 10%. Thus, for each compound, we obtained several measurements of the enthalpy of sublimation (individually having a worse accuracy, Tab. 6.7) that allows the weight average value to be retrieved for the enthalpy of sublimation where the weight function (eq. 6.2) has been used. The weight average values show a better accuracy compared with the single enthalpy measurement, i.e. an accuracy of within 1% for succinic, adipic, and azelaic acids, within 2% for suberic acid and within 5% for oxalic and suberic acid (Tab. 6.8).

In Fig. 6.14 the enthalpy of sublimation of five dicarboxylic acids analysed in this work are compared with previous works. The behaviors of the enthalpies of sublimation are very similar and increase as the carbon chain number of the substance increases (i.e., for C_2 to C_6 trend). Indeed, the substances with a short carbon chain (oxalic and succinic acid) show a lower enthalpy of sublimation compared with the substances with a higher carbon chain (adipic and azelaic acids), which require a higher temperature to reach complete sublimation (larger than 60°C).

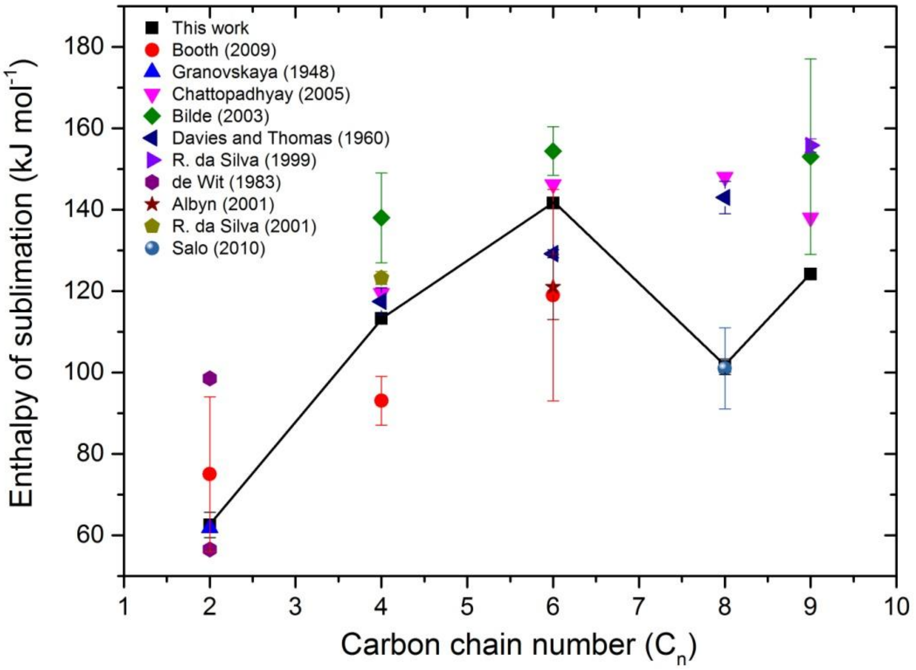

Figure 6.14. Comparison between the enthalpies of sublimation obtained with different methods and compounds (C_2, oxalic acid; C_4, succinic acid; C_6, adipic acid, C_8, suberic acid and C_9, azelaic acid, weight average values). The error bars available in literature are reported while the errors obtained in this work are included within the black square points. Different experimental conditions (temperature monitored and work pressure, Tab. 6.8) lead to diverging results: Booth (2009), Chattopadhyay and Ziemann (2005), R. da Silva (1999) in vacuum environments, Bilde (2003), Davies and Thomas (1960), Salo (2010) at atmospheric pressure. For oxalic acid are plotted the results for anhydrous and dehydrate forms [de Wit 1983, Booth 2009]. The black line connects the enthalpy values for the even-odd C number acid samples.

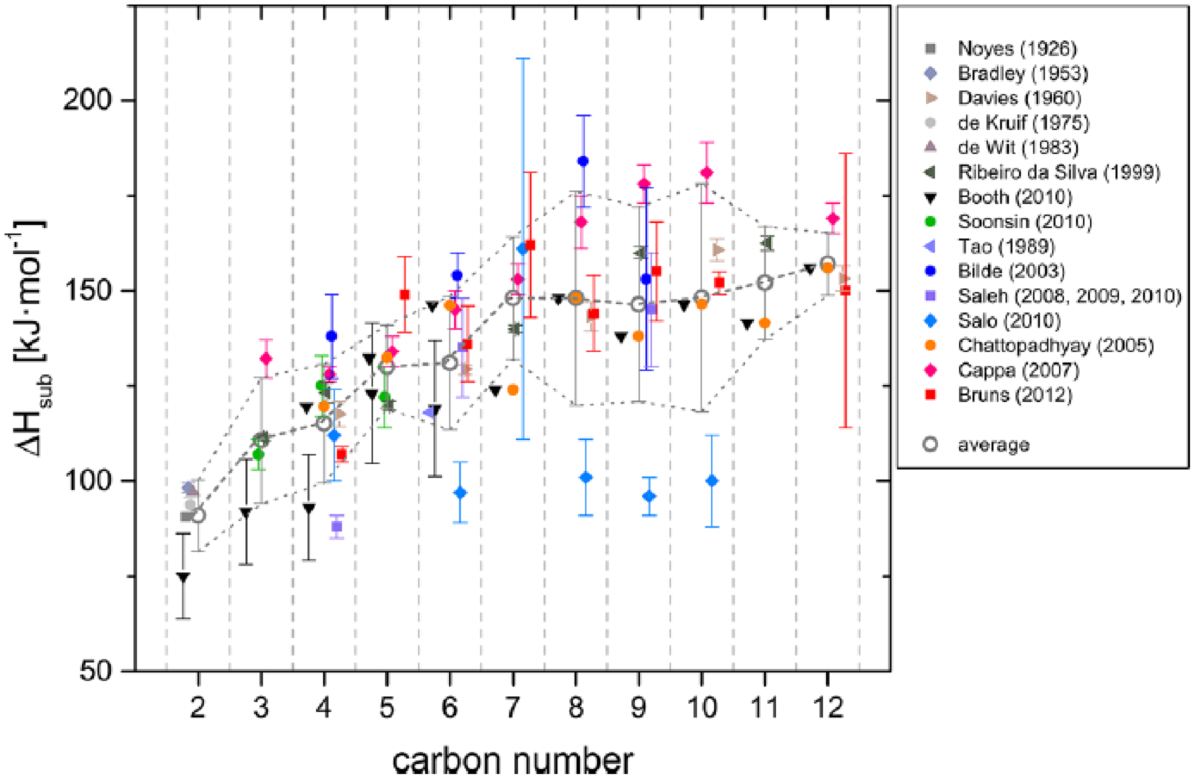

Figure 6.15. [Bilde 2015]. Enthalpies of sublimation (ΔH_{sub}) for straight-chain dicarboxylic acids as a function of the number of carbon atoms. Results from previous works are shown.

Furthermore, as reported by other studies, the dicarboxylic acid with an odd number of carbon atoms, has a lower sublimation enthalpy compared with dicarboxylic acids that have an even number of atoms [Booth 2009, Bilde 2003, Bilde 2015]. This behavior is based principally on the solid-state crystalline structure of the acids. In this work, the enthalpy alternation between the odd and even carbon chain dicarboxylic acid ($>C_5$) has been confirmed for three compounds: the enthalpy of sublimation of adipic acid (C_6) is higher than the sublimation enthalpy of azelaic (C_9) and suberic (C_8) acids of 17 and 41 kJ mol^{-1} (Fig. 6.14), respectively. Indeed, the Pimelic acid (C_7) (between the adipic and suberic acids, not analysed in this work) should have the enthalpy of sublimation higher than adipic (C_6) and suberic (C_8) acids [Bilde 2015] which confirm the enthalpy alternation [Fig. 6.14]. This behavior is confirmed also by the enthalpy of sublimation of adipic acid whose average value calculated by Bilde (2015), i.e. ~130 kJ mol^{-1} (142 kJ mol^{-1} in this work) is lower than the average value of pimelic acid, i.e. ~150 kJ mol^{-1} (Fig. 6.15).

The alternation in the enthalpy of sublimation has also been confirmed by the results of Bilde (2003) even though as explained by Booth (2009), the behavior of the enthalpy alternation is not always clear and it is not possible to say firmly that this effect can be observed.

6.7. TGA, EM results and comparison

The results obtained for the deposition rates (in $Hz\ s^{-1}$) and enthalpy of sublimation (in $kJ\ mol^{-1}$) with Langmuir and Van't Hoff equations using the Sensor Head 1 and Sensor Head 2 breadboards are listed in table 6.9 and table 6.10. In particular, the deposition rates obtained for adipic acid have been compared with contamination experiments performed with SH1 and deposition tests performed with SH2 using a QCM as mass attractor at low temperatures.

In table 6.9 are also listed the deposition rates obtained for adipic acid during the preliminary test (PT) with SH2 where the organic fluxes were lower than those calculated in the second attempt (Tab. 6.7, Par. 6.6), i.e. DP-SH2. Thus, the deposition rates obtained in the PT are similar to those obtained with the first and second Contamination Tests (CTI, CTII) and Saturation Test (ST) (light blue, yellow and grey highlighted values). These low rates are probably due to the setup configuration as described in subpar. 4.4.2. On the other hand, high deposition rates reordered on the second attempt show a reliable organic fluxes thanks to a distance between the sample and the crystal of 2cm (subpar. 6.4.2). In particular, the deposition rates (specially at 65 and 75°C, violet highlighted values in table 6.9) are comparable with those obtained at higher temperatures (90 and 100°C) in the saturation test (ST).

The enthalpy of sublimation results obtained for the adipic acid using different methods (EM and TGA) are listed in table 6.10. The Effusion Method (EM) performed with the effusion cell, was used during the second attempt (Tab. 6.7, Par. 6.6) while the Thermogravimetric Analysis (TGA) has been used during the CTII and ST. Langmuir (eq. 3.9) and Van't Hoff (eq. 3.10) equations have been used both with deposition data set of the second attempt (DP-SH2) to obtain the enthalpy of sublimation: the results are in agreement within 2.5%. Instead, the enthalpy of sublimation obtained using different methods (EM and TGA) and the same equation (Langmuir) are in agreement within 3.5%. The results obtained from EM and TGA methods demonstrates the possibility to obtain a good characterization of a pure substance (adipic acid in this case) by using a single crystal configuration (Tab. 6.10).

On the other hand, using the eq. 3.10 (Van't Hoff), five dicarboxylic acids have been characterized using a single crystal configuration (SH2 breadboard). The enthalpy of sublimation results compared with previous studies (Tab. 6.8, Par. 6.6) show an accuracy of within 1% for succinic, adipic, and azelaic acids, within 2% for suberic acid and within 5% for oxalic and suberic acid.

Table 6.9. Deposition rates in *Hz/s* of Preliminary Test (PT), Deposition Test of second attempt (DP-SH2), first and second Contamination Test (CTI, CTII) and Saturation Test (ST) are listed. The light blue highlighted values of PT are comparable (within 20%) with the CTI, CTII and ST while the deposition rates obtained considering a distance sample-QCM of 2 cm are comparable (within 20%) with ST deposition rates obtained at higher temperatures.

T_{cell} (°C)	*df/dt (Hz/s) CT I - SH1*	*df/dt (Hz/s) CT II - SH1*	*df/dt (Hz/s) ST - SH1*	*df/dt (Hz/s) DP - SH2*	*df/dt (Hz/s) PT - SH2*
40	0.025	0.012	0.005	0.037	0.020
45	--	--	--	--	0.073
50	0.098	0.047	0.524	0.182	0.053
55	--	--	--	0.416	0.150
60	0.219	0.109	0.187	0.863	0.250
65	0.288	--	--	1.919	0.312
70	0.414	0.194	0.431	3.972	0.430
75	0.642	--	--	7.330	--
80	--	0.396	0.671	--	--
90	--	0.785	1.755	--	--
95	--	--	2.122	--	--
100	--	2.194	6.150	--	--
120	--	--	35.032	--	--

Table 6.10. Enthalpy of sublimation results obtained with Effusion Method (EM) and Thermogravimetric Analysis (TGA). The enthalpy of sublimation results are the average values obtained from deposition rates data (DP tests, Tab. 6.7) and desorption rates data (ST and CT tests) in each temperature range listed. Using the Langmuir equation, the enthalpy of sublimation results are in agreement within 3.5%.

Adipic acid	*PT - SH2*	*DP - SH2*	*CT II- SH1 (3° cycle)*	*ST - SH1 (2° cycle)*	*ST - SH1 (3° cycle)*
$\Delta H_{sub} \pm \sigma_{\Delta H}$ **(kJ/mol)**	141.6±0.8	138.2±1.1	133.8±1.8	134.3±3.4	138.2±2.2
T_{range} **(°C)**	40-70	30-70	25-50	47-72	44-69
Method	EM	EM	TGA	TGA	TGA
Equation	Van't Hoff	Langmuir	Langmuir	Langmuir	Langmuir

Chapter 7. Conclusion

7.1. Calibration and experimental phase

The work here presented has been performed within the VISTA project framework, in particular regarding its application both to the Solar System's minor bodies space mission, and to the monitoring of space contamination produced by outgassing processes aboard satellites, spacecrafts and by thruster firing. Breadboards of VISTA Sensor Head 1 and Sensor Head 2 have been designed and developed. In particular, VISTA sensor heads have been tested for contamination monitoring (SH1) and to characterize some organic compounds present in terrestrial atmosphere (SH2). In this work, the main goals reached with SH1 (double crystal configuration) have been:

1. to measure the contamination of organic particles from outgassing processes in space environment (in the mass range: 5×10^{-9} to 7×10^{-4} g/cm^2, verified with saturation test);
2. to regenerate the crystals by means of the built-in heaters measuring the temperature directly on the crystal surface (with an accuracy of 0.1°C or better);
3. to characterize the contaminant source by means of TGA cycles (ΔT_{max} ~60°C) and calculating the vapor pressures (Pi) and the enthalpy of sublimation (ΔH_{sub}) using Langmuir and Clausius-Clapeyron equations.

On the other hand, the SH2 have been also tested using a single crystal configuration (a QCM). In this work, the main goal reached with SH2 have been:

1. to measure the deposition of volatiles at different temperature steps using an Effusion Method (EM) simulating the asteroidal/cometary environment;
2. providing a VOCs characterization, i.e. dicarboxylic acids, calculating the enthalpy of sublimation (ΔH_{sub}) and using Van't Hoff equation.

A first phase of the work was based on VOCs study in planetary atmospheres including their physical-chemical properties and their connections with the atmospheric aerosol sources. Simultaneously, a study of VOCs detection in space and contamination processes induced in space environment, i.e. surface erosion, weight loss, oxidation from different materials and their product, e.g. silicon, aluminum, magnesium has been realized. Successively, an in-depth study of Thermogravimetric Analysis (TGA) concept and the theory of thermochemical processes as well as a complete review for QCM sensors used for contamination in space (including the mechanical characteristics and the scientific results) has been performed. Thus, the main thermochemical parameters for VOCs characterization, i.e. deposition rates, vapor pressures and enthalpy of sublimation have been retrieved from deposition on PCM crystals and TGA measurements. Different organic compounds (dicarboxylic acids) identified in Earth atmospheric SOA and in meteorites (carbonaceous chondrites) as one of the main organic component [Andersen 2005, Briscoe 1993] have been selected to perform deposition processes and TGA cycles, i.e. reaching a complete characterization by means of SH1 breadboard and SH2 breadboard.

Two different laboratory set-up have been developed in order to verify the performance and capability of SH1 and SH2 to monitor the deposition process and to apply an Effusion Method for a pure compound characterization, as well as TGA cycles to characterize a contaminant source performing the crystal regeneration. A first laboratory phase was devoted to sensor heads calibration in vacuum and at low temperatures using one organic substance (adipic acid) while a second phase was devoted to a physical-chemical characterization of different VOCs present in Earth atmosphere SOA with SH2. Two different setup have been designed (by using SolidWorks Software) and assembled for SH1 and SH2 breadboards in order to obtain the deposition rates, the vapor pressures and the enthalpy of sublimation of the organic compounds analysed. By using TGA and deposition process (i.e. effusion method), it has been possible to calculate these thermochemical quantities for each compound.

An appropriate setup have been built for each sensor head.

In the first setup, the SH1breadboard (double crystal configuration, Par. 4.3) is positioned on a copper S-shape in contact with a cold finger while the effusion cell containing the contaminant (in the FOV of SH1) is heated up to the sublimation. A UI is realized with LabView software to manage SH1 and to monitor the experiment. Contamination tests and TGA cycles performed with adipic acid demonstrate the capability of VISTA-SH1 to monitor a contamination process and to characterized the contaminant by means of vapor pressure and enthalpy of sublimation.

In the second setup, the SH2 breadboard (single crystal configuration, Par. 4.4) is positioned on a copper L-shape in contact with a cold finger while the heating and cooling systems are managed by two external PIDs. The effusion cell and QCM are positioned in a sublimation micro-chamber while the sample is heated up to the sublimation. Deposition tests performed with the effusion method demonstrate the capability of VISTA-SH2 to characterize a pure compounds (dicarboxylic acids from C_2 to C_9) by means of deposition rates and enthalpy of sublimation.

7.2. Results and methods comparison

Tests performed with SH1 breadboard confirm the capability of the instrument to detect organic contaminants using TGA cycles in space environment. In order to reach these goals, a specific setup has been developed and tested with contamination (CT) and saturation tests (ST) at low temperatures and in vacuum environment. The SH1 experimental results have shown that:

- the organic deposition can be monitored from 25 to 120°C temperature steps (CT);
- the maximum detectable mass is 733 $\mu g\ cm^{-2}$ (ST);

- TGA cycles can be performed with built-in heaters (CT and ST);
- the vapor pressures from 25 to 72°C can be obtained for the contaminant source while the enthalpy of sublimation can be calculated with Langmuir and Clausius-Clapeyron equations (CT and ST);
- the average value obtained for vapor pressure: $P_{\text{this work}} = (2.7\times10^{-6})$ Pa is in agreement within two times the error bars with literature average value: $P_{\text{literature}} = (1.9\times10^{-5})$ Pa while the average value of the enthalpy of sublimation: $\Delta H_{\text{sub, this work}} = (136.5\pm1.2)$ kJ mol^{-1} is in agreement within 5% with $\overline{\Delta H}_{\text{sub, literature}} = (131\pm18)$ kJ mol^{-1} (Tab. 6.2).

Furthermore, a specific setup has been developed for SH2 breadboard to characterize different organic compounds presents in SOA terrestrial atmosphere using the effusion method. The experimental results have shown that:

- different pure organic compounds can be characterized from 25 to 80°C temperature steps using the QCM as mass attractor at -72°C;
- reliable deposition rates can be calculated by the frequency variation in time considering a distance between the organic sample and QCM of 2 cm (subpar. 6.4.2);
- a reliable enthalpy of sublimation can be obtained when $T_2 << T_{sub}$ and when the difference between T_1 and T_2 is at least 5°C (Tab. 6.7);
- a reliable enthalpy of sublimation can be obtained when two successive fluxes are not comparable;
- the enthalpy results (weight average values) show an accuracy of within 1% for succinic, adipic, and azelaic acids, within 2% for suberic acid and within 5% for oxalic and suberic acid and are in very good agreement with previous works (within 6% for adipic, succinic, and oxalic acid and within 11% or larger for azelaic and suberic acid) (Tab. 6.8).

The enthalpy of sublimation (in *kJ mol^{-1}*) results for adipic acid (the only compound analysed with TGA and EM methods) obtained with Langmuir (from linear fit: $\ln[dm/dt]T^{1/2}$ *vs. 1000/T)* and Clausius-Clapeyron equations (from linear fit: $\ln P$ *vs. 1000/T*) and with Van't Hoff equation ($\Delta H = R\left[\left(\frac{T_1T_2}{T_2-T_1}\right)\ln\left(\frac{k_1\sqrt{T_1}}{k_2\sqrt{T_2}}\right)\right]$) using SH1 and SH2 breadboards are listed in table 7.1. Two different method have been used to calculate the enthalpy of sublimation: TGA and EM. The Effusion Method (EM) performed with the effusion cell, was used during the preliminary test and during second attempt (enthalpy results in chapter 6) while the Thermogravimetric Analysis (TGA) has been used during the CTII and ST. Langmuir and Van't Hoff equations have been both used with deposition data set reported in chapter 6 to obtain the enthalpy of sublimation: the results are in agreement within 2.5%. Otherwise, the enthalpy of sublimation obtained using different methods (EM and TGA) and Langmuir equation are in agreement within 3.5%. The results obtained from EM and TGA methods demonstrates the possibility to obtain a good characterization for a pure substance (adipic acid in this case) using a single crystal configuration (Tab. 7.1).

Table 7.1. Enthalpy of sublimation results obtained with Effusion Method (EM) and Thermogravimetric Analysis (TGA). The enthalpy of sublimation results are the average values obtained from deposition rates data (DP tests, Tab. 6.7, Par. 6.6) and desorption rates data (ST and CT tests) in each temperature range listed. The deposition data set obtained with SH2 have been analysed both with Van't Hoff and Langmuir equations. The number of the cycles between brackets (CT and ST tests) are referred to TGA cycle.

Adipic acid	***DP - SH2***	***DP - SH2***	***CT II- SH1 (3° cycle)***	***ST - SH1 (2° cycle)***	***ST - SH1 (3° cycle)***
$\Delta H_{sub} \pm \sigma_{\Delta H}$ (kJ/mol)	141.6±0.8	138.2±1.1	133.8±1.8	134.3±3.4	138.2±2.2
T_{range} (°C)	40-70	30-70	25-50	47-72	44-69
Method	EM	EM	TGA	TGA	TGA
Equation	Van't Hoff	Langmuir	Langmuir	Langmuir	Langmuir

Five dicarboxylic acids have been analysed with single crystal configuration (SH2), aimed at characterizing a compound in a planetary environment. The obtained enthalpies of sublimation have been compared with literature values (Tab. 6.8). The results' accuracy is within 1% for succinic, adipic, and azelaic acids, within 2% for suberic acid and within 5% for oxalic and suberic acid. In table 7.2 are reported the average enthalpies of sublimation obtained in this work compared with literature values. Oxalic acid (dehydrate form), succinic and adipic are in agreement within 6% with previous works (Booth 2009, Granovskaya 1948, Chattopadhyay and Ziemann 2005, Bilde 2003, Davies and Thomas 1960, Ribeiro da Silva 2001, de Wit 1983, Albyn 2001, Salo 2010) whereas the suberic and azelaic acids are in agreement within 11% (Salo 2010, Chattopadhyay and Ziemann 2005).

Table 7.2. Comparison of enthalpy of sublimation of dicarboxylic acids retrieved by different techniques. The green values are the average enthalpy obtained from Booth (2009), Granovskaya (1948), Chattopadhyay and Ziemann (2005), Bilde (2003), Davies and Thomas (1960), Ribeiro da Silva (2001), de Wit (1983) and Albyn (2001) while the light blue values are obtained from Salo (2010) and Chattopadhyay and Ziemann (2005) for suberic and azelaic acids, respectively. These results are compared with the average values obtained in this work. Because of the standard deviation is not always reported in the literature, the errors have been not included in this table.

Organic compound	$\Delta H_{\text{sub, this work}}$ $(kJ\ mol^{-1})$	$\Delta H_{\text{sub, literature}}$ $(kJ\ mol^{-1})$
Oxalic	$^{(deh)}$62.5	$^{(deh)}$59.2
Succinic	113.3	118.2
Adipic	141.6	134.0
Suberic	101.4	101
Azelaic	124.2	138

7.3. Future perspectives

7.3.1. Laboratory Set-up improvements

In the future, in order to extend the temperature range of interest and the analysed compounds, the setup should be modified as follows (Fig. 7.1):

1. the organic source should be cooled at temperature lower than 25-30°C in order to study the deposition rates and vapor pressures at low temperatures;
2. a teflon guide can be applied to effusion cell containing the organic acids in order to have a well-defined molecules path;
3. the temperature control system (managed by LabVIEW core program) should be improved, by decreasing the temperature oscillation down to ±0.5°C and having a better stabilization at each temperature set point.

Besides, more organic acids should be analysed in the temperature range of interest. Some of these compounds are the odd-carbon number acids, i.e. malonic acid (C_3), glutaric acid (C_5), pimelic acid (C_7) and one more even-carbon number compound, i.e. sebacic acid (C_{10}). Analysing the dicarboxylic acids with odd-carbon number it will be also possible to study in depth the enthalpy of sublimation alternation discussed in Par. 6.6 between the even-odd compounds carbon number. Studying the compounds between C=2 to C=10 it will be possible to have a complete characterization (obtaining: P_i, ΔH_{sub}) for this class of compounds.

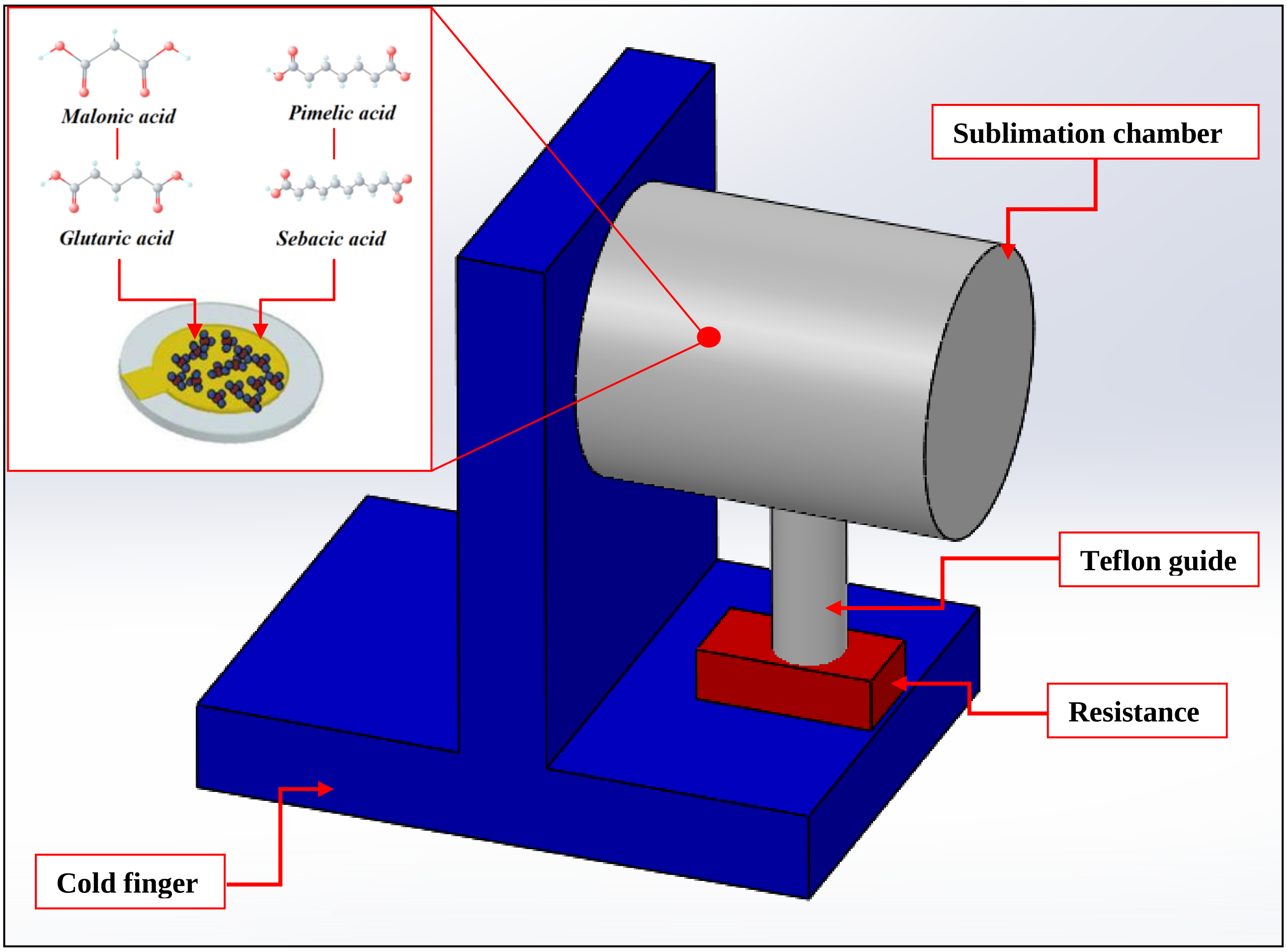

Figure 7.1. A simplified setup is shown. In particular, the cold finger can be modified (tip over T-shape) in order to cool the effusion cell surrounded by a teflon guide which aim to isolate the cell and redirect the flux on the sensing crystal. Inside the sublimation chamber, new compounds, i.e. malonic, glutaric, pimelic and sebacic acids will be analysed one at a time using a single crystal as mass attractor at low temperature, e.g. around -70°C. At that temperature the resistance can be switched on studying the deposition rates from -70°C to +30°C while the temperature range from +30 to +80/100 can be covered by the first setup configuration (described in chapter 4, Fig. 4.16).

Finally, the good capability of VISTA Sensor Head 1 to monitor a contamination process as well as the capability to obtain the typical thermochemical parameters (during a phase change from solid to gas), i.e. the vapor pressure, P_i and the enthalpy of sublimation, ΔH_{sub} from TGA tests have been verified. At the same time, the good capability of VISTA Sensor Head 2 to characterize organic compounds, i.e. five dicarboxylic acids present in the terrestrial atmospheric SOA, by means of deposition tests (effusion method) at low temperatures, has been demonstrated.

The CT and TGA and the compound characterization applied in this work using Sensor Head 1 and Sensor Head 2 will help a compound identification or a mix of them in a space or planetary environment and to monitor the contamination behaviour of particles and molecules caused by outgassing processes in space. VISTA instrument will surely help to know the properties of volatile material in the asteroidal regolith or cometary material by means of additional laboratory tests aimed to the next space mission scenarios (i.e. MarcoPolo-R, Akon, JEM, Castalia).

7.3.2. Technological transfer application

Generally, QCM’s technology and QCM-based devices have been applied in industrial, pharmaceutical, chemical fields and in the study of the terrestrial atmosphere. Most important QCM's applications include the metal deposition, chemical reaction monitors, electroactive polymers and corrosion studies. In particular, QCM's application for biomedical and industries fields are focused on the interaction between a substrate on the microbalance surface with a protein, DNA, sugar chain, lipid and enzyme (Biolin Scientific, Initium, Gamry instruments).

QCM's have been applied also for terrestrial atmosphere measurements [Effiong 2010] or for industrial processes to monitoring the assembly line and the possible risks induced by chemical substances, e.g. environmental assessment of a new drug [Elder 1997]. In the table 7.3 are described the applications and objectives that can be reached by VISTA.

Table 7.3. Application and objectives provided by VISTA in different research fields.

Application & Scientific Objectives	*Monitoring the volcanic activity*	*Monitoring gas and PM emission from vehicles*	*Evaluating the soil fertility*	*Monitoring the transition phase of the organic compounds*	*Monitoring the fine particulate*	*Monitoring the emissions of* waste-to-energy plant
1.	Monitoring gas and particulate in real time	Control the FAP efficiency	Quantify the organic matter inside a sample	Determination of vapor pressure for solid-liquid phase	Monitoring PM10 - PM2.5	Monitoring the combustion process
2.	Discrimination between PM2.5 and PM10	Control the gas emitted from the source	Quantify the water inside the sample	Revelation the toxicity of the substances	Reveal Nitrates	Monitoring the flue-gas emitted at different temperatures
3.	Monitoring gas emission dangerous for the human health	Detect the PM types	TGA cycles	Assessment of a new drugs	Measurement of suspended organic particulate	Control the emissions of the domestic boilers
4.		Monitoring the combustion process		Characterise each substance by its chemical-physical properties		Improving the efficiency of heating of domestic boilers

The VISTA adaptability to different environment make it a sensor which can be applied in different fields of research, e.g. urban, atmospheric farming business, pharmaceutical area etc. Thus, VISTA can be used to monitor:

1. *the gas and PM emission from vehicles*: the device should detect dangerous pollutants, i.e. carbon monoxide, CO, nitrogen oxide, NOx and fine particulate of different size (PM 2.5-10). Considering the high accuracy (0.01°C), the exactly combustion and the gaseous produced at each temperature can be monitored.

2. *the fine particulate (PM_{10}-$PM_{2.5}$) in the urban environment*: the sensor (which doesn't use the radioactive materials as used by Beta Attenuation Monitors, BAM) can be able to measure the volatile components as Nitrates and the suspended organic particulate. Furthermore, by using the built-in heaters, the sieve system (particulate filter) regeneration is possible increasing the time of operations.

3. *the geochemical parameters to forecast volcanic risk* : the device could be used to measure the solid particles such as the aerosol present (CO_2, SO_2, HCl, HF, H_2S, CH_4) in atmosphere after strong volcanic eruptions [Casadevall 1984] allowing the continuous measurement at high temperature of the gaseous component. The gas/dust ratio should be revealed in the depths of the craters and in the magmatic fireplaces.

3. *the soil fertility with TGA cycle:* considering the device accuracy and low mass of soil required, a good analysis (using TGA cycles) of the soils and sediments containing a large variety of organic material, i.e. sugars and carbohydrates and more complex proteins, fats, waxes, and organic acids can be obtained.

4. *the transition phase of the organic compounds (pharmaceutical area):* the organic compounds may be characterized at higher temperatures obtaining the vapour pressures, the sublimation/fusion/ evaporation enthalpy and entropy of the substances and analyzing the transitions phase new drugs for pharmaceutical industries [Freedman 2008].

5. the emissions of waste-to-energy plant and combustion processes for domestic use: the device can be useful to monitoring the substances in a wide range of temperatures, i.e. the combustion products in thermoelectric stations whose main constituents are the water vapour, nitrogen, carbon dioxide and oxygen and smaller amounts of CO, HCl, HF, HBr, HI, NOX, SO2, VOCs, PCDD/F, PCBs.

7.3.3. ESA-M5 Call: proposed missions application

VISTA instrument, able to monitor a contamination process and to characterized a compound using deposition rates and TGA cycles, has been included in the scientific payload of ESA-M5 proposed missions:

1. *MarcoPolo-M5*, which offers a unique opportunity to study the most primitive material (the first sample return mission to a primitive D-type asteroid) from a small body identified as 1993 HA;
2. *Joint Europa Mission (JEM)*, which aims at understanding Europa as a complex system responding to Jupiter system forcing, at characterizing the habitability of its potential biosphere, and search for life in its surface, sub-surface and exosphere;
3. *Akon Europa Penetrator*, which aims at searching biosignatures in near-surface material, at determining the internal structure of Europa and its dynamics and the existence and characteristics of a subsurface ocean, at characterizing the physical (e.g. radiation, thermal, magnetic, electrical, mechanical) and chemical environment of the near-surface region;
4. *Castalia*, whose main goals are to characterize a new Solar System family, the Main Belt Comets (MBCs) by in-situ investigation, to understand the physics of activity on MBCs, to directly detect water in the asteroid belt and measure D/H ratio to test if MBCs are a viable source for Earth's water and to use MBCs as tracers of planetary system formation and evolution.

The main scientific goals of VISTA for the proposed missions are:

a. to measure of the abundance of water and organics in the asteroid regolith (in-situ measurement), by heating the regolith disturbed during sampling that is deposited on the heating crystal (MarcoPolo-M5 mission);
b. to measure of possible cometary-like activity (in-orbit measurement), by measuring the dust and volatile flux emitted from the asteroid (MarcoPolo-M5 mission);
c. monitoring the sampling operations by measuring the flux of dust raised during sampling operations (MarcoPolo-M5 mission);
d. to discriminate between water ice and clathrate hydrates, by heating the QCM up to the decomposition temperature of clathrate hydrates (120-160 K) [Lunine and Shevchenko 1985] and to the sublimation temperature of water ice (200 K at a depth of 3 meters) [Weast 1980], and by recording the temperature at which mass loss due to heating occurs (JEM, Akon missions);
e. to measure the composition of non-ice materials, by heating a PCM up to the dehydration temperatures of possible Europa components, ranging in the interval 220-320 K [McCord 2001], by recording the temperature where mass loss due to heating occurs and by measuring the volatile/refractory abundance ratio (JEM, Akon missions);

f. to detect and measure the relative abundance of organics, by heating the PCM up to organics desorption (at about 230 K) [Chazallon 2004], and by measuring the mass difference before and after desorption (JEM, Akon missions).

The results obtained in this work make VISTA an useful instrument to monitor the contamination processes in space environment and for the study of planetary surfaces and atmospheres. VISTA is able to perform in-situ measurement and to accomplish several scientific objectives for the study of minor bodies of our Solar System. By using TGA and take advantages by deposition and desorption rates, it will be possible to study the deposition, sublimation and desorption processes of compounds obtaining the vapor pressures and the enthalpy of sublimation useful to their characterization. Moreover, the technological and scientific objectives reached in this work with TGA and EM methods, make VISTA a useful instrument which can be applied in different fields of research (e.g. terrestrial atmosphere, farming business, pharmaceutical area etc.) and for space mission applications (MarcoPolo, Akon, JEM and Castalia).

Chapter 8. Bibliography

Afeedy H. Y., Liebman, J. F., and Stein, S. E., *Phase change Data - NIST Chemistry Web Book*, NIST (National Institute of Standards and Technology) Standard Reference Database, n. 69, 2015. http://webbook.nist.gov

Albyn K. C., *Extension of the Enthalpy of Sublimation for Adipic Acid to Temperatures below 80°C*, J. Chem. Eng. Data, v. 46, p. 1415–1416, 2001

Albyn K. C., *Quartz Crystal Microbalance Operation and In Situ Calibration*, Report NASA/TM–213550, 2004

Air filters (industrial) information, GlobalSpec Engineering. http://www.globalspec.com

Andersen C.A., Haack, H., *Carbonaceous chondrites: tracers of the prebiotic chemical evolution of the Solar System*, International Journal of Astrobiology, vol. 4, Issue 1, pp. 13-17, 2005

Arnold G.S. and Hall D.F., *Contamination of optical surface*, Chemistry and Physics Laboratory, The Aerospace Corporation, Report N88-25400, 1988

AS DataBase List, *Chemical Book*. http://www.chemicalbook.com/CASDetailList_19500_EN.htm

Atkins P. and de Paula J., *Physical Chemistry for the Life Sciences*, II Ed., W.H. Freeman and Company, New York, United States, 2006

Aumont B., Szopa, S., and Madronich, S., *Modelling the evolution of organic carbon during its gas-phase tropospheric oxidation:development of an explicit model based on a self generating approach*, Atmos. Chem. Phys., v. 5, p. 2497–2517, 2005

Bacco D., *Studio della caratterizzazione chimica di composti organici polari nel particolato atmosferico,* PhD Thesis, University of Ferrara, 2010;

Bahl A. and Bahl B. S., *Advanced Organic Chemistry*, S. Chand & Co Ltd, Printed in India, Ram Nagar, New Delhi, ISBN-10: 8121935156, 2010.

Barthelmie R.J., *Secondary organic aerosols: formation potential and ambient data, S.C.* Pryor. Sci. Total Environ., v. 205, n.2-3, p. 167–178, 1997

Barucci M.A., Yoshikawa, M., Michel, P. and other 23 co-authors, *MarcoPolo-R near earth asteroid sample return mission*, Experimental Astronomy, v. 33, n. 2-3, p. 645-684, 2011

Benner S., C. Lorentson, P. Chen, S. Thomson , *Atomic Oxygen Erosion of a Graphic Coating on a TQCM Aboard the Return Flux Experiment*, Proc. SPIE, v. 3427, "Optical Systems Contamination and Degradation," pp. 168-177, 1998

Benson S. W., *Thermochemical Kinetics*, 2nd ed., John Wiley & Sons, New York, NY, 1017, 1968

Berry K., Sutter B., May A., Williams K., Barbee B.W., Beckman M. and Williams B., *OSIRIS-REx Touch-And-Go (TAG) Mission Design and Analysis*, 36th Annual AAS Guidance and Control Conference, Breckenridge, CO, United States, 2013

Bilde M., Svenningsson, B., Mønster, J., and Rosenørn, T., *Even-Odd Alternation of Evaporation Rates and Vapor Pressures of C3–C9 Dicarboxylic Acid,* Environ. Sci. Technol., v. 37, p. 1371-1378, 2003

Bilde M., Barsanti, K., Booth, M., Cappa, C. D., Donahue, N. M., Emanuelsson, E. U., McFiggans, G., Krieger, U. K., Marcolli, C., Topping, D., Ziemann, P., Barley, M., Clegg, S., Dennis-Smither, B., Hallquist, M., Hallquist, Å. M., Khlystov, A., Kulmala, M., Mogensen, D., Percival, C. J., Pope, F., Reid, J. P.,Ribeiro da Silva, M. A. V., Rosenoern, T., Salo, K., Soonsin, V. P., Yli-Juuti, T., Prisle, N. L., Pagels, J., Rarey, J., Zardini, A., A., and Riipinen, I., *Saturation Vapor Pressures and Transition Enthalpies of Low-Volatility Organic Molecules of Atmospheric Relevance: From Dicarboxylic Acids to Complex Mixtures*, Special Issue: 2015 Chemistry in Climate, Chem. Rev., v. 115, p. 4115-4156, 2015

Biolin Scientific, Q-SENSE (E1- E4 Module), 2016. http://www.biolinscie ntific.com/product/q-sense-sensors/

Booth A.M., Markus, T., McFiggans G., Percival C.J., Mcgillen M.R., and Topping D.O., *Design and construction of a simple Knudsen Effusion Mass Spectrometer (KEMS) system for vapour pressure measurements of low volatility organics*, Atmos. Meas. Tech., v. 2, p. 355–361, 2009

Booth A.M., Barley M.H., Topping D.O., McFiggans G., Garforth A., and Percival C.J., *Solid state and sub-cooled liquid vapour pressures of substituted dicarboxylic acids using Knudsen Effusion Mass Spectrometry (KEMS) and Differential Scanning Calorimetry*, Atmos. Chem. Phys., v. 10, p. 4879–4892, 2010

Briscoe J. F., Moore, C. B., *Determination of Formic and Acetic Acid in Chondritic Meteorites*, Meteoritics, v. 28, n. 3, p. 330, 1993

Brown S.S., Dubé W.P., Bahreini R., Middlebrook A.M., Brock1 C.A., Warneke C., de Gouw J.A. et al., *Biogenic VOC oxidation and organic aerosol formation in an urban nocturnal boundary layer: aircraft vertical profiles in Houston, TX*, Atmos. Chem. Phys., v. 13, p. 11317-11337, 2013

Bruckenthal E. A. and Singer R. B., *Spectral Effects of Dehydratation on Phyllosilicates*, Abstracts of the Lunar and Planetary Science Conference, v. 18, p. 135, 1987

Bruns E.A., Greaves J. and Finlayson-Pitts B.J., *Measurement of Vapor Pressures and Heats of Sublimation of Dicarboxylic Acids Using Atmospheric Solids Analysis Probe Mass Spectrometry*, J. Phys. Chem., v. 116, p. 5900-5909, 2012

Camredon M., Aumont B., Lee-Taylor J. and Madronich S., *The SOA/VOC/NOx system: an explicit model of secondary organic aerosol formation*, Atmos. Chem. Phys., v. 7, p. 5599-5610, 2007

Cappa C.D., Lovejoy E.R. and Ravishankara A.R., *Determination of Evaporation Rates and Vapor Pressures of Very Low Volatility Compounds: A Study of the C4-C10 and C12 Dicarboxylic Acids*, J. Phys. Chem. A., v. 111, p. 3099-3109, 2007

Casadevall T. J., Rose W.I.J., Fuller W.H., Hunt W.H., Woods D.C., Hart M.A., Moyers J.L., Chuan R.L., Friend J.P, *Sulfur dioxide and particles in quiescent volcanic plumes from Poas, Arenal, and Colima volcanos,* Costa Rica and Mexico, J. Geophys. Res., v. 89, p. 9633, 1984

Chattopadhyay S. and Ziemann, P. J., *Vapour Pressures of Substituted and Unsubstituted Monocarboxylic and Dicarboxylic Acids Measured Using an Improved Thermal Desorption Particle Beam Mass Spectrometry Method*, Aerosol Sci. Tech., v. 39, p. 1085–1100, 2005

Chazallon B., Lebrun N., Dhamelincourt P., Toubin C., Fosa C., *Micro-Raman Investigations of the Formaldehyde−Ice System*, J. Phys. Chem. B., v. 109, p. 432-439, 2005

Davies M. and Thomas G. H., *The lattice energies, infra-red spectra, and possible cyclization of some dicarboxylic acids*, T. Faraday Soc., v. 56, p. 185–192, 1960

de Chambure, D., Laine, R., van Katwijk, K., van Casteren, J., Glaude, P., *Status of the x-ray flight mirror production for the ESA XMM spacecraft*, Proc. SPIE, v. 3114, p. 113-124, 1997

De Segovia J.L., *Physics of outgassing, CERN European organization for nuclear research-reports-CERN*, p. 99-110, 1999

de Wit, H. G. M., Bouwstra, J. A., Blok, J. G., and de Kruif, C. G., *Vapor pressures and lattice energies of oxalic acid, mesotarticacid, phloroglucinol, myoinositol, and their hydrates*, J. Chem. Phys., v. 78, p. 1470-1475, 1983

Dirri F., Palomba E., Longobardo A., and Zampetti E., *Piezoelectric crystal Microbalance measurements of enthalpy of sublimation of C2–C9 dicarboxylic acids*, Atmos. Meas. Tech., v. 9, p. 1–14, 2016a

Dirri F., Palomba E., Longobardo A., and Zampetti E., *Measuring enthalpy of sublimation of volatiles by means of Piezoelectric Crystal Microbalances*, Origin of Life and Evolution of Biosphere, 2016b

EEA Report No 5/2014 on air quality in Europe, 2014. http://www.eea.europa.eu/publications/air-quality-in-europe-2014

Effiong E.B. and V. R. Morris, 24 January 2011, *Physical/Chemical Characterization of Trans-Atlantic Airborne Saharan Dust during the Aerosol and Ocean Science Expeditions (AEROSE)*, Washington State Convention Center, 13th Conference on Atmospheric Chemistry, 227

Elder J.P., *Sublimation Measurements of pharmaceutical compound by isothermal thermogravimetry*, Journal of Thermal Analysis, v. 49, p. 897-905, 1997

ELTRA GmbH Company, *TGA analyser Operation*. http://www.eltra.com/products/thermogravimetric-analyzer/tga-thermostep/

Measuring aerosol, Earth Observatory, NASA**, 2016.** http://earthobservatory.nasa.gov/Features/Aerosols/page5.php

EPA, *Technical Overview of Volatile Organic Compounds, 2016.* https://www.epa.gov/indoor-air-quality-iaq/technical-overview-volatile-organic-compounds

ESA Statement of Work, *Evaluation of an in-situ molecular contamination sensor for space use*, SRE-F/2013.033, 2013

EU Directive/2008/50 EC, of the European Parliament and of the Council of 21 May 2008 on ambient air quality, 2008. http://ec.europa.eu/environment/air/quality/legislation/existing_leg.htm

Fermo P., Piazzalunga A., Vecchi R., Valli G., Ceriani M., *A TGA/FT-IR study for measuring OC and EC in aerosol samples*, Atmos. Chemic. Phys., v. 6, p. 255-256, 2006

Freedman A., Kebabian, P. L., Ziman, Li, Robinson, W. A., and Wormhoudt, J. C., *Apparatus for determination of vapor pressures at ambient temperatures employing a Knudsen effusion cell and quartz crystal microbalance*, Meas. Sci. Technol., v. 19, 125102 (8p.), 2008

Gamry Instruments (eQCM), 2016. http://www.gamry.co m/

Garrett J. W., Glassford A.P.M. and Steakley J.M., *ASTM E 1559 Method for Measuring Material Outgassing/Deposition Kinetics*, 18th Space Simulation Conference, Baltimore, Maryland, 1994

Glassmeier K.H., Boehnhardt H., Koschny D., Kührt E., Richter I., *The Rosetta Mission: Flying Towards the Origin of the Solar System,* Space Science Review, V. 128, , n.1, p. 1–21, 2007

Gowen R.A.. Smith A., Fortes A. D. et al., *Penetrators for in situ subsurface investigations of Europa*, Advances in Space Research, v. 48, i. 4, p. 725-742, 2011

Grady M. M. and Wright I. P., *Elemental and Isotopic Abundances of Carbon and Nitrogen in Meteorites*, Space Science Reviews, v. 106, p. 231-248, 2003

Granovskaya A., *Izmereniemalykhdavlenii para privysokikhtemperaturakh. 1. davlenie para vismuta*, J. Phys. Chem. (USSR), v. 21, p. 967–968, 1948

Green B.D., *Satellite Contamination and Materials Outgassing Knowledgebase*, An Interactive Database Reference, NASA/CR-2001-210909, 2001

Halbout J., Mayeda T.K., Calyton R.N., *Carbon Isotoped and Light Element Abundances in Carbonaceous Chondrites*, 39, Earth and Planetary Science Letters, v. 80, p. 1-18, 1986

Hansen P.A., *An integrated approach for contamination control and verification for the Hubble Space Telescope first servicing mission*, SPIE, v. 2261, p. 10-21, 1994

Hatakeyama S. T., Tanonaka, T.,Weng, J., Bandow, H., Takagi, H., and Akimoto, H., *Ozone cyclohexene reaction in air: quantitative analyses of particulate products and the reaction mechanism*, Environ. Sci. Technol., v. 19, p. 935-942, 1985

Ho K.F., Lee S.C., Cao J.J., Kawamura K., Watanabe T., Cheng Y., Chow. J.C., *Dicarboxylic acids, ketocarboxylic acids and dicarbonyls in the urban roadside area of Hong Kong,* Atmospheric Environment, v. 40, p. 3030–3040, 2006

Inguimbert V., Duzellier, S., Siguier, J.M., Tighe, A., Van Eesbeek, M., *MEDET in flight experiment (material exposure and degradation experiment) description and first results,* Proc. of International Symposium on “SM/MPAC&SEED Experiment”, Tsukuba, Japan, 2008

INITIUM, *QCM Affinix Series*, 2016. http://www.initium20 00.com/en/

James J.T., T.F. Limero, H.J. Leano, J.F. Boyd, and P.A. Covington, *Volatile organic contaminants found in the habitable environment of the Space shuttle: STS-26 to STS-55*, Aviat. Space Environ. Med., v. 65, p. 851-857, 1994

Kawamura, K. and Keplan, I. R., *Organic compound in the rainwater of Los Angeles*, Environ. Sci. Technol., v. 17, p. 497-501, 1983

Kawamura K. and Ikushima, K., *Seasonal change in the distribution of dicarboxylic acid in the urban atmosphere*, Environ. Sci. Technol., v. 27, p. 2227–2235, 1993

Kawamura K., Imai, Y., and Barrie, L. A., *Photochemical Production and Loss of Organic Acids in High Arctic Aerosols During Long-Range Transport and Polar Sunrise Ozone Depletion Events*, Atmos. Environ., v. 39, p. 599–614, 2005

Kawamura K., Ono K., Tachibana E., Charrier B., Sempere R., Biogeosciences, *Distributions of low molecular weight dicarboxylic acids, ketoacids and α-dicarbonyls in the marine aerosols collected over the Arctic Ocean during late summer*, v. 9, p. 4725-4737, 2012

Kerminen V., Ojanen C., Pakkanen T., Hillamo R., Aurela M. and Merilainen J., *Low Molecular weight dicarboxylic acid in an urban and rural atmosphere*, J. Aerosol Sci., v. 31, p. 349–362, 2000

Kroll J. H. and Seinfeld J. H., *Representation of secondary organic aerosol laboratory chamber data for the interpretation of mechanisms of particle growth*, Environ. Sci. Technol., v. 39, p. 4159-4165, 2005

Kubota T., Hashimoto T., Kawaguchi J., Uo M. and Shirakawa K., *Guidance and Navigation of Hayabusa Spacecraft for Asteroid Exploration and Sample Return Mission*, *SICE-ICASE International Joint Conference*, Busan, p. 2793-2796, 2006

Ladji R., N. Yassaa, A. Cecinato, B.Y. Meklati., *Seasonal variation of particulate organic compounds in atmospheric PM_{10} in the biggest municipal waste landfill of Algeria*, Atmospheric Research, v. 86, n. 3-4, p. 249-260, 2007

Langmuir I., *The vapour pressure of metallic tugsten*, Phys. Rev., APS Journals, v. 2, p. 329–342, 1913

Levine I.R., *Physical Chemistry VI Edition*, Published by McGraw-Hill, 1978

Limbeck A., Puxbaum, H., Otter, L., and Scholes, M. C., *Semivolatile Behavior of Dicarboxylic Acids and Other Polar Organic Species at a Rural Background Site (Nylsvley, RSA),* Atmos. Environ., v. 35, p. 1853–1862, 2001

Longobardo A., Palomba, E., Bearzotti, A., Zampetti, E., Pantalei,S., Biondi, D., Saggin, B., Dirri, F., and Macagnano, A., *The MOVIDA instrument: measurement of volatile content and charging processes of the lunar dust*, 44th LPSC, abstract 2204, 2013

Lunine J. I. and Shevchenko D. J., Astrophysical Journal Supplement Series, v. 58, p. 493-531, 1985

McCord T. B., Orlando T.M., Teeter G., Hansen G.B., Sieger M.T., Petrick N.G., Keulen N.V., *Thermal and radiation stability of the hydrated salt minerals epsomite, mirabilite, and natron under Europa environmental conditions*, Jour. Geo. Res., v. 106, i. E2, p. 3311-3319, 2001

McKeown D, *Optical System Contamination and Degradation*, SPIE, v. 3427, p. 112-125, 1999

Milinevsky G., Y. Yatskiv, O. Degtyaryov, I. Syniavskyi, Y. Ivanov, A. Bovchaliuk, M. Mishchenko, V. Danylevsky, M. Sosonkin, and V. Bovchaliuk, *Remote sensing of aerosol in the terrestrial atmosphere from space: New missions*, Adv. Astron. Space Phys., v. 5, n. 1, p. 11-16, 2015

Miller E.R., *STS-2 Induced Environment contamination monitor (IECM)*, quick-look Report (NASA) , NASA TM- 82457, 1982

Miller E.R., *Induced Environment contamination monitor (IECM) - preliminary results from the SpaceLab1 flight*, NASA TM-86461, 1984

Mkoma S.L. and Kawamura K., *Molecular composition of dicarboxylic acids, ketocarboxylic acids, α-dicarbonyls and fatty acids in atmospheric aerosols from Tanzania, East Africa during wet and dry seasons*, Atmos. Chem. Phys., v. 13, p. 2235–2251, 2013

Mishchenko M., Geogdzhayev, I.V., Rossow W.B., Cairns B., Carlson B.E., Lacis A.A., Liu L., Travis L.D., *Long-term satellite record reveals likely recent aerosol trend*, *Science*, v. 315, p. 1543, 2007, DOI: 10.1126/science.1136709;

Morris V., Roldan L., Armstrong R. and Detres Y., *Size-Resolved Aerosol Mass and Aerosol Number Distributions During the NOAA Center for Atmospheric Sciences (NCAS) Trans-Atlantic Saharan Dust Aerosol and Oceanographic Science Expedition (AEROSE)*, 7th conference on atmospheric chemistry 2005
Atmospheric Aerosols: What Are They, and Why Are They So Important?, FS-1996-08-11-LaRC, NASA, 1996. https://www.nasa.gov/centers/langley/news/factsheets/Aerosols.html

Muraishi K. and Suzuki Y., *The thermal behaviour of dicarboxylic acids in various atmospheres*, Thermochimica Acta, Elsevier Science B.V., v. 232, p. 195-*20*, 1994

Narukawa M. and Kawamura K., *Distribution of dicarboxylic acids and carbon isotopic composition in aerosols from 1997 Indonesian forest fires*, Geophysical Research Letters, v. 26, n. 20, p. 3101-3104, 1999

National Research Council, *Methods for Developing Spacecraft Water Exposure Guidelines, Subcommittee on Spacecraft Water Exposure Guidelines*, Committee on Toxicology, Board on Environmental Studies and Toxicology, Commission on Life Sciences, Division on Earth and Life Studies, National Academies Press, 2000

Orchin M., Macomber, R. S., Pinhas, A. R., and Wilson, R. M., *Organometallic Chemistry, in: The Vocabulary and Concepts of Organic Chemistry*, Wiley-Interscience, Second Edition, John Wiley & Sons, Inc., Hoboken, NJ, USA, p. 01–900, 2005

Otto S., and coauthors, *Atmospheric radiative effects of an in situ measured Saharan dust plume and the role of large particles*, Atmos. Chem. Phys., n. 7, p. 4887-4903, 2007

Palomba E., Longobardo A., Zinzi A., Pantalei S., Macagnano A., Bearzotti A., Zampetti E., Biondi D., Saggin B. and Bellucci G., *VISTA for DREAMS-ExoMars 201*6, EPSC Abstract Vol. 6, EPSC-DPS2011-87, 2011

Palomba E., Longobardo A., Dirri F., Zinzi A., Biondi D., Zampetti E., Pantalei S., Saggin B., Bearzotti A., Macagnano A., Brucato J. R. and Keheyan Y., *VISTA: a thermogravimeter for the MarcoPolo-R Mission*, 39th COSPAR, Scientific assembly, Mysore, India, 2012

Palomba E., Longobardo , Dirri F., Zampetti E., Biondi D. , Saggin B., Bearzotti A., Macagnano A., *VISTA: A μ-Thermogravimeter for Investigation of Volatile Compounds in Planetary Environments*, Origin of Life and Evolution of Biosphere, v. 46, n. 2, p. 273-281, 2016

Pankow J. F., *An absorption model of gas/particle partitioning of organic compounds in the atmosphere*, Atmos. Environ., v. 28, p. 185–188, 1994

Patrick T.J, *Outgassing and the choice of materials for space instrumentation*, Vacuum, v. 23, p. 411-413, 1973

Peacock R.N., *Practical selection of elastomer materials for vacuum seals*, Journal of Vacuum Science & Technology, v. 17, p. 330, 1980

Peltzer E.T., Bada J.L., Schlesinger G., Miller S.L., *The chemical conditions on the parent body of the Murchison meteorite: some conclusions based on amino, hydroxy and dicarboxylic acids*, Adv. Space Res., v.4, p. 69-74, 1984

Petrucci R.H., Herring F.G., Madura J.D., Bissonnette C., *General Chemistry Principles & Modern Applications*., 9th Ed., Upper Saddle River, NJ: Pearson Prentice Hall, 2007

Pietrogrande M. C., Bacco, D., Visentin, M., Ferrari, S., and Poluzzi, V., *Polar organic marker compounds in atmospheric aerosol in the Po Valley during the Supersito campaigns – Part 1: Low molecular weight carboxylic acids in cold seasons*, Atmos. Environ., v. 86, p. 164–175, 2014

Prenni A. J., De Mott, P. J., Kreidenweis, S. N., and Sherman, D. E., *The effects of low molecular weight dicarboxylic acids on cloud formation*, J. Phys. Chem. US, v. 105, p. 11240-11248, 2001

Price D. M., *Vapour Pressure determination by Thermogravimetry*, Thermochimica Acta v. 367-368, p. 253-262, 2001

PubChem Database, *Dicarboxylic acids chemical properties*, 2016. https://pubchem.ncbi.nlm.nih.gov/

Puxbaum H., Rendl, J., Allabashi, R., Otter, L., and Scholes, M. C., *Mass balance of atmospheric aerosol in a South-African subtropical savanna (Nylsvley, May 1997)*, J. Geophys. Res., v. 105, n. 20, p. 697–706, 2000

Ray J. and McDow S., *Dicarboxylic acid concentration trends and sampling artifacts*, Atmospheric Environment, v. 39, p. 7906–7919, 2005

Remer L., Kleidman R.G., Levy R.C., Kaufman Y.J. et al., *An emerging aerosol climatology from the MODIS satellite sensors*, *Journal of Geophysical Research*, v. 113, D14S01, 2008

Remusat L., Le Guillou C., Rouzaud J.N., Binet L., Derenne S., Robert F., *Molecular Study of the Insoluble of Organic Matter of Kainsaz CO3 Carbonaceous Chondrites: Comparison with CI and CM IOM*, Meteoritics and Planetary Science, v. 43, i. 7, p. 1099-1111, 2008

Ribeiro da Silva, M. A. V., Monte, M. J. S., Ribeiro, J. R. *J., Vapour pressures and the enthalpies and entropies of sublimation of five dicarboxylic acids***,** v. 31, i. 8, p. 1093-1107, 1999

Ribeiro da Silva, M. A. V., Monte, M. J. S., and Ribeiro, J. R., *Thermodynamic study on the sublimation of succinic acid and of methyl- and dimethyl-substituted succinic and glutaric acids*, J. Chem. Thermodyn., v. 33, p. 23–31, 2001

Riipinen I., Koponen I. K., Frank G. P., Hyvaerinen, A.P., Vanhanen J., Lihavainen H., Lehtinen K. E. J., Bilde M., Kulmala, *Adipic and Malonic Acid Aqueous Solutions: Surface Tensions and Saturation Vapor Pressures*, M. J. Phys. Chem., v. 111, p. 12995, 2007

Rogge W.F., Monica A. Mazurek, Lynn M. Hildemann, Glen R. Cass, Bernd R.T. Simoneit, *Quantification of urban organic aerosols at a molecular level: Identification, abundance and seasonal variation*, Atmospheric Environment. Part A. General Topics, v. 27, p. 1309-1330, 1993

Rohrl A. and Lammel, G., *Low-Molecular Weight Dicarboxylic Acids and Glyoxylic Acid: Seasonal and Air Mass Characteristics,* Environ. Sci. Technol., v. 35, p. 95–101, 2001

Rozaini M.Z.H., *The Chemistry of Dicarboxylic Acids in the Atmospheric Aerosols, Atmospheric Aerosols, Regional Characteristics,* Chemistry and Physics, Dr. Hayder Abdul-Razzak (editor), InTech. http://www.intechopen.com/books/atmospheric-aerosols-regional-characteristics-chemistry-and-physics/the-chemistry-of-dicarboxylic-acids-in-the-atmospheric-aerosols

Russell C.T., Raymond C.A., *The Dawn Mission to Vesta and Ceres,* Space Science Review, v. 163, n. 1, p. 3–23, 2011

Saleh R., Walkerb J., Khlystov A., *Determination of saturation pressure and enthalpy of vaporization of semi-volatile aerosols: The integrated volume method,* Aerosol Science, v. 39, p. 876–887, 2008

Saleh R., Khlystov, A., *Determination of Activity Coefficients of Semi-Volatile Organic Aerosols Using the Integrated Volume Method,* Aerosol Sci. Technol., v. 43, p. 838, 2009

Saleh R., Khlystov A., Shihadeh, *Effect of Aerosol Generation Method on Measured Saturation Pressure and Enthalpy of Vaporization for Dicarboxylic Acid Aerosols,* Aerosol Sci. Technol., v. 44, p. 302-307, 2010

Salo K., JonssonÅsa, M., Andersson, P. U., and Hallquist, M., *Aerosol Volatility and Enthalpy of Sublimation of Carboxylic Acids*, J. Phys. Chem. A, v. 114, p. 4586–4594, 2010

Salt D., In: *Hy-Q Handbook of Quartz Crystal Devices*, Van Nostrand, UK, 1987

Salzen K. and Schlünzen K. H., *Simulation of the dynamics and composition of secondary and marine inorganic aerosol in the costal atmosphere*, J. Geophys. Res., v. 104, p. 30201–30217, 1999

Schuetzle D., Cronn D., Crittenden A.L., Charlson R.J.., Molecular composition of secondary aerosol and its possible origin, *Environmental Science and Technology*, v. 9, p. 838–845, 1975

Sephton M. A., *Organic Compounds in Carbonaceous Meteorites,* Nat. Prod. Rep., v. 19, p. 292-311, 2002

Serpaggi F., Luxbacher T., Cheetham A.K., Férey G., *Dehydration and Rehydration Processes in Microporous Rare-Earth Dicarboxylates: A Study by Thermogravimetry*, Thermodiffractometry and Optical Spectroscopy, J. Solid State Chem., v. 145, p. 580-586, 1999

Soares C.E. and Mikatarian R.R, *Mir Contamination Observations and Implications to the International Space Station*, Space Station External Contamination Control Requirements, NASA SSP 30426 Revision D, 1994

Soares C. E., Barsamian H., Rauer S., *Thruster plume induced contamination measurements from the PIC and SPIFEX flight experiments*, Proceedings of the 9th International Symposium on Materials in a Space Environment Noordwijk, The Netherlands, ESA SP-540, 2003

Sorooshian A., Varutbangkul V., Brechtel F. J., Ervens B., Feingold G., Bahreini R., Murphy S. M., Holloway J. S., Atlas E. L., Buzorius G., Jonsson H., Flagan R. C. and Seinfeld J. H., *Oxalic acid in clear and cloudy atmospheres: analysis of data from International Consortium for Atmospheric Research on Transport and Transformation 2004*, J. Geophys. Res., v. 111, D23S45, 2006

Stalder R. and Skogby H., *Hydrogen Incorporation in Enstatite,* European Journal of Mineralogy, v. 14, n. 6, p. 1139-1144, 2002

Stalport. F., Coll P., Cabane M., Person A., Gonzaléz R.N., Raulin F., Vaulay M.J., Ausset P., McKay C.P., Szopa C., Zarnecki J., *Search for past life on Mars: Physical and chemical characterization of minerals of biotic and abiotic origin: part 1 - Calcite*, Geophys. Res. Lett., 32, L23205, 2005

Stuckey W.K., *An Overview of the On-Orbit Contamination of the Long Duration Exposure Facility (LDEF)*, LDEF Materials Results for Spacecraft Applications, NASA CP-3257, pp. 533-539, 1993

Sundberg M, Malmqvist G., Magnusson A., El-Raghy T., *Alumina forming high temperature silicides and carbides*, Ceramics International, v. 30, i. 7, p. 1899-1904, ISSN 0272-8842, 2004

Tao Y. and McMurry P.H., *Vapor Pressures and Surface Free Energies of C14-C18 Monocarboxylic Acids and C5 and C6 Dicarboxylic Acids*, Environ. Sci. Technol., v. 23, p. 1519-1523, 1989

Tribble A.C., Peter A., Glassford M., Breault R.P., Pompea S.M., *Contamination control engineering design guidelines for the aerospace community*, Optical System Contamination V, and Stray Light and System Optimization, Proc. SPIE Vol. 2864, p. 4-15, 1996

Tsuda Y., Yoshikawa M., Abe M., Minamino H., Nakazawa S., *System design of the Hayabusa 2—Asteroid sample return mission to 1999 JU3*, Acta Astronautica, v.91, p.356-362,2013

Tyagi P., *Termochemistry,* Discovery Publishing Pvt. Ltd, 1st edition, New Delhi, 1–266, ISBN 10: 8183561403, 2006

Vanderzee C. E. and Westrum E. F., *Succinic Acid, heat capacities and thermodynamic properties from 5 to 328 K, an efficient drying procedure,* J. Chem. Thermodyn., v. 2, p. 681–687, 1970

Weast R.C., *CRC Handbook of Chemistry and Physics,* 61st Edition, Boca Raton, FL, CRC Press, 1980

WHO, *Indoor air quality: organic pollutants,* report on a WHO Meeting, Berlin, EURO Reports and Studies 111. Copenhagen, World Health Organization Regional Office for Europe, 1987

Williams B. G., Antreasian P. G., Bordi J. J. and Carranza E., *Navigation for NEAR Shoemaker: the first mission to orbit an asteroid,* Conference Paper, AAS/AIAA Astrodynamics Specialists Conference Quebec City, Quebec, Canada, 2001

Wilson C. F., Chassefière E., Hinglais E., Baines K. H., Balint T. S., Berthelier J.-J., Blamont J., Durry G., Ferencz C. S., Grimm R. E., Imamura T., Josset J.-J., Leblanc F., Lebonnois S., Leitner J. J., Limaye S. S., Marty B., Palomba E., Pogrebenko S.V., Rafkin S. C. R., Talboys D. L., Wieler R., Zasova L. V., and Szopa C., *The 2010 European Venus Explorer(EVE) mission proposal*, Exp. Astron., v. 33, p. 305–335, 2011

Wood B. E., Hall D.F., Lesho J.C., Dyer J.S., Uy O.M., Bertrand W.T., *Quartz crystal microbalance (QCM) flight measurements of contamination on the MSX satellite*, Proc. SPIE, 2864, 187-194, 1996

Wood B.E., Green B. D., Hall D.F., Uy O.M., Cain R.P., Galica G. A., Boies M.T. and Bertrand, W.T., *Update of the Midcourse Space Experiment (MSX) Satellite Measurements of Contaminant Films using QCMs*, Proceedings of SPIE v.4096, p. 1-10, 2000

Xu Y. and Zhang. J.S., *Understanding SVOCs*, ASHRAE Journal v.53, p.121-125, 2011

Yu Z. and Fraser M. P., *Polar organic compounds measured in fine particulate matter during TexAQS 2000*, Atmos. Environ., v. 38, p. 3253–3261, 2004

Appendix A - Publications

The **Published Papers** of the candidate during the PhD years are listed below.

1) **Dirri F.**, Palomba E., Longobardo A., Zampetti E., Biondi D., Boccaccini A., Pantalei S. and Zinzi A., *Measuring enthalpy of sublimation of volatiles by means of micro-thermogravimetry for the study of the water and organics in planetary environments*, MSAIS, v.26, p.133, 2014;
2) **Dirri F.,** Palomba E., Longobardo A. and Zampetti E., *Piezoelectric Crystal Microbalance measurement of enthalpy of sublimation of C2-C9 dicarboxylic acids*, Atmospheric Measurement and Techniques, v.9, p.655-668, 2016;
3) **Dirri F.,** Palomba E., Longobardo A. and Zampetti E, *Measuring enthalpy of sublimation of volatiles by means of piezoelectric crystal microbalance*, Origin of Life and Evolution of Biospheres, 2016.
4) Palomba E., Longobardo A., **Dirri F.,** Zampetti E., Biondi D., Saggin B., Bearzotti A., Macagnano A., *VISTA: a micro-thermogravimeter for investigation of volatile compounds on planetary environment*, Origin of Life and Evolution of Biospheres, v.46, p.273-281, 2016.

The contribution in Conference/Congress of the candidate during the PhD years are listed below.

1) **Dirri F.**, Palomba E., Longobardo A., Zampetti E., Biondi D., Boccaccini A., *Micro-thermogravimetry for planetary in-situ measurement*, European Planetary Science Congress, 413, 2014;
2) Palomba E., Zampetti E., Longobardo A., Biondi D., Saggin B., Boccaccini A., **Dirri F.**, *VISTA: a micro-Thermogravimeter to analyze condensable species in planetary atmospheres*, 40th COSPAR Scientific Assembly, 2014;
3) Palomba E., Longobardo A., **Dirri F.**, Zampetti E., Biondi D., Boccaccini A., Saggin B., Scaccabarozzi D., Bearzotti A., *VISTA, a micro-Thermogravimeter to measure water and organics content in planetary environments*, International Workshop on Instrumentation for Planetary Missions, 2014;
4) Longobardo A., Palomba E., **Dirri F.,** Biondi D., Zampetti E., Saggin B., Scaccabarozzi D., Bearzotti A., Macagnano A., *Measuring volatile content and charging processes of lunar dust: the MOVIDA μ-Thermogravimeter*, European Planetary Science Congress, 2014;
5) **Dirri F.**, Palomba E., Longobardo A., Zampetti E., Biondi D., Boccaccini A., *Micro-thermogravimetry: a miniaturized technique for in-situ measurement of volatiles in planetary environments*, XII Congresso Nazionale di Scienze Planetarie, 2015;

6) Palomba E., Longobardo A., **Dirri F.**, Biondi D., Bearzotti A., Zampetti E., Macagnano A., Saggin B., Scaccabarozzi D., *Characterization of lunar levitating dust and measurement of volatiles: the MOVIDA instrument,* European Lunar Symposium, 2015;
7) Palomba E., Longobardo A., **Dirri F.**, Biondi D., Boccaccini A., Saggin B., Scaccabarozzi D., Zampetti E., Macagnano A., Bearzotti A., *VISTA, a light and cheap sensor to measure volatile amount and dust deposition*, 11th Low-Cost Planetary Mission Conference, 2015;
8) Palomba E., **Dirri F.,** Longobardo A., Biondi D., Saggin B., Scaccabarozzi D., Zampetti E., *CAM: Contamination Assessment Microbalance,* Metrology for Aerospace 2016;
9) Palomba E., **Dirri F.,** Longobardo A., Galiano A., Biondi D., Boccaccini A., Zampetti E., Saggin B., Scaccabarozzi D., *VISTA: a miniaturized thermogravimeter to detect planetary dust and volatiles*, 3rd International Workshop on Instrumentation for Planetary Missions 2016;
10) Palomba E., Longobardo A., **Dirri F.,** Biondi D., Boccaccini A., Galiano A., Zampetti E., Saggin B., Scaccabarozzi D., *VISTA, a thermogravimeter to measure dust and volatile from Dydimos*, AIM Science Meeting, 2016;
11) Longobardo A., **Dirri F.,** Palomba E., Berthoud L., Holt J., Pottage T., Bridges J., Vrublevskis J., Bennett A., Smith C., Russell S., *Basic requirements for packaging and transporting returned extra terrestrial samples from landing sites to curation facility*, European Astrobiology Network Association, 2016;
12) **Dirri F.**, Palomba E., Ferrari M., Longobardo A., Rotundi A., *A combined FE-SEM/EDS and μ-IR analysis of CM, CI and CV chondrites for next sample return missions*, European Astrobiology Network Association, 2016;
13) **Dirri F.**, Palomba E., Ferrari M., Longobardo A., Rotundi A., *A combined FE-SEM/EDS and μ-IR analysis of Carbonaceous Chondrites, analogue of the next returned asteroid samples*, 48th Division for Planetary Sciences - 11th European Planetary Science Congress 2016;
14) Ferrari M., **Dirri F.**, Palomba E., Longobardo A., Rotundi A., *FE-SEM/EDS and μ-IR combined analysis of HED meteorites in relation to infrared spectra of Vesta-like asteroids*, 48th Division for Planetary Sciences - 11th European Planetary Science Congress, 2016;
15) **Dirri F.**, Palomba E., Longobardo A., Biondi D., Boccaccini A., Zampetti E., Saggin B., Scaccabarozzi D., Tortora A., Nanni A., Alves J., Tighe A., *Monitoring contamination due to materials outgassing by QCM-based sensors*, 41st COSPAR Scientific Assembly, 2016.

The Technical Reports realized during the PhD years, which describe the test plans, test activities and results are listed below.

- Palomba E., ..**Dirri F.** et al., *Survey of existing QCM technologies*, CAM 2014;
- Palomba E., ..**Dirri F.** et al., *Test Plan*, CAM 2014;
- Palomba E., ..**Dirri F.** et al., *Compliance Matrix*, CAM 2014;
- **Dirri F.** et al., *BB Test Report*, CAM, 2015;
- **Dirri F.** et al., *EM Test Plan*, CAM, 2015;
- Palomba E., ..**Dirri F.** et al., *EM Manufacture Plan*, CAM 2015;
- Palomba E., ..**Dirri F.** et al., *EM Model detailed design report*, CAM 2015;
- **Dirri F.** et al., *BB Test Report*, CAM, 2015;
- Palomba E., ..**Dirri F.** et al., *Progress Report 3*, CAM 2015;
- **Dirri F.** et al., *EM Model Functional Testing Report*, CAM, 2016;
- **Dirri F.** et al., *EM Model Functional Testing Report (I Ad.)*,CAM, 2016;
- Palomba E., ..**Dirri F.** et al., *Final Report*, CAM 2016;
- Longobardo A., **Dirri F.** et al., *Transport to Curation Facility*, EURO-CARES, 2016.

Appendix B - Scientific and Technological Projects

During the PhD course (years 2014-2016), the scientific and technological projects performed by the candidate are listed below.

1) **VISTA Project** (Volatile In-Situ Thermogravimeter Analyser). This project aims to develop a Thermogravimeter (a Piezoelectric Crystal Microbalance and the related Proximity Electronics) proposed for MarcoPolo-R Mission, to perform the in-situ measurements of volatile compounds in planetary environments. *Position held*: test manager for the test planned for VISTA Breadboard and data analysis manager, managing for design e trade-off activities for the Breadboard of the instrument and for the definition of the technical and scientific requirements.

2) **CAM Project** (Contamination Assessment Microbalance). This project has been developed in collaboration with Institute for Space Astrophysics and Planetology (IAPS-INAF), the Institute of Atmospheric Pollution Research (IIA-CNR), Politecnico di Milano and Kayser Italia and aims to monitor the contamination induced from spacecraft materials during in-orbit space missions for the next ESA payloads. *Position held*: test manager and data analysis manager, collaborator for the design e trade-off activities for the Breadboard e Engineering Model of the instrument and for the definition of the technical and scientific requirements.

3) **PRIN-INAF Project**. The project: "Composition and origin of Dark and Bright materials on Vesta", was developed in collaboration between Institute for Space Astrophysics and Planetology (IAPS-INAF), Università di Lecce and "Sapienza Università di Roma" and aimed to investigate the origin and composition of dark material deposits on Vesta and their relation with the bright deposits and the “average” material. *Position held*: test manager for the laboratory analysis on planetary analogue samples (i.e. meteorites).

4) **EURO-CARES Project** (European Curation of Astromaterials Returned from Exploration of Space): is a three year, multinational project, funded under the European Commission's Horizon2020 research programme to develop a roadmap for a European Sample Curation Facility (ESCF) for precious samples returned from Solar System exploration missions to asteroids, Mars, the Moon, and comets. the project is carried out in close cooperation between six different European countries and represent 14 different institutions: Natural History Museum, London, UK (NHM); National Institute for Astrophysics, Italy (INAF); Naturhistorisches Museum Wien, Vienna, Austria (NHMW); Muséum National d’Histoire Naturelle, Paris, France (MNHN); Centre de Biophysique Moléculaire, Orléans, France (CBM); Centre de Recherches Pétrographiques et Géochimiques, Nancy, France (CRPG); Thales Alenia Space UK, Bristol, UK (TAS); Open University, Milton Keynes, UK (OU),

Deutsches Zentrum für Luft - und Raumfahrt, Cologne, Germany (DLR); University of Leicester, Leicester, UK (LEI); Public Health England, Soulsbury, UK (PHE); Dipartimento di Scienze della Terra, Università di Pisa, Italy (Pisa); Senckenberg Gesellschaft für Naturforschung, Frankfurt, Germany (SENCK); Université Libre de Bruxelles, Brussels, Belgium (ULB). *Position held*: collaborator for the design and materials definition of the Transportation Box used for samples transportation and containment of planetary samples.

The developed instrument during the CAM Project (one of the main projects developed and managed during the PhD course) has been awarded with: ***"Innovation Award"*** at "WIRE16 Workshop on Business, Research and Economics" (http://wire16.frascatiscienza.it/wire16/i-premi.html), organized and promoted by Frascati Scienza, from Frascati municipality and from European Commission and from ESA-ESRIN (http://www.media.inaf.it/2016/06/20/wire16-microbilancia/).